



UCGE Reports

Number 20252

Department of Geomatics Engineering

**INS-Assisted High Sensitivity GPS Receivers for
Degraded Signal Navigation**

(URL: <http://www.geomatics.ucalgary.ca/research/publications/GradTheses.html>)

by

Guojiang Gao

February 2007



UNIVERSITY OF CALGARY

INS-Assisted High Sensitivity GPS Receivers for Degraded Signal Navigation

by

Guojiang Gao

A THESIS

SUBMITTED TO THE FACULTY OF GRADUATE STUDIES
IN PARTIAL FULFILMENT OF THE REQUIREMENTS FOR THE
DEGREE OF DOCTOR OF PHILOSOPHY

DEPARTMENT OF GEOMATICS ENGINEERING

CALGARY, ALBERTA

FEBRUARY, 2007

© Guojiang Gao 2007

ABSTRACT

This thesis proposes a novel architecture for ultra-tight integration of a High Sensitivity Global Positioning System (HSGPS) receiver with an Inertial Navigation System (INS), to address the issue of GPS tracking and positioning in degraded signal environments. By enhancing signal tracking loops in receivers through the use of optimal controllers/estimators and aiding from external sources such as INS, the capabilities of the GPS receiver can be enhanced to provide positioning in urban canyon and indoor environments. The proposed approach is distinct from the commonly used ultra-tightly coupled GPS/INS approaches, and includes different tracking enhancement technologies used in typical HSGPS receivers, multi-channel co-operated GPS receivers and the current ultra-tightly coupled GPS/INS methods.

The proposed method in this thesis consists of three signal tracking loop types, namely conventional sophisticated Delay Lock Loops (DLL) and Phase Lock Loops (PLL) for all individual tracking channels, external INS aiding loops and multi-channel co-operated tracking loops, namely COOP loops. The signal tracking strategy is described, with specific focus on the role of COOP loops in the proposed ultra-tightly coupled GPS/INS. Furthermore, the effect of inertial measurement unit (IMU) quality and the effect of receiver oscillator noise and coherent integration time on weak signal tracking are also analyzed.

To perform ultra-tight integration, an INS simulator is developed, and static and dynamic field tests are simulated to analyze the system performance. The test results

show that the proposed INS-aided GPS receiver can track the incoming weak GPS signals down to a C/N₀ of 15 dB-Hz without carrier phase locked, or 25 dB-Hz with carrier phase locked. When there are multiple strong GPS signals in view, the other weak signals can be tracked down to 15 dB-Hz with carrier phase locked.

ACKNOWLEDGEMENTS

This thesis would not have been possible without the assistance and support of the following people:

My son, Jamie Jianxing Gao, I would like to dedicate my thesis to you, my wonderful son, although you cannot understand it at the moment.

My wife, minmin Lin, You have been by my side for all of the good times and the more frustrating times. I don't know what I would do without you.

My father, who freely gave everything he had to support and encourage me for many, many years.

To my supervisor, Professor Gérard Lachapelle, thank you for giving me encouragement, insight, guidance, and patience all the time.

To all my colleagues and classmates in the PLAN group, without your support, this process would have been much more difficult. I thank you for everything you have done. Special thanks to Dr. Mark Petovello, Mr. Saurabh Godha, Mr. Rob Watson, Dr. Debo Sun and many others in the department.

TABLE OF CONTENTS

APPROVAL PAGE	ii
ABSTRACT	ii
ACKNOWLEDGEMENTS	iv
TABLE OF CONTENTS.....	v
LIST OF TABLES	viii
LIST OF FIGURES.....	ix
LIST OF SYMBOLS, ABBREVIATIONS AND NOMENCLATURE	xiii
Chapter One: Introduction	1
1.1 BACKGROUND	1
1.1.1 Urban Canyon and Indoor Positioning.....	1
1.1.2 Positioning Technologies for Degraded GPS Signal Navigation	3
1.2 LIMITATIONS OF PREVIOUS WORK	5
1.2.1 High Sensitivity Global Positioning System (HSGPS).....	5
1.2.2 Assisted Global Positioning System (AGPS).....	6
1.2.3 Cellular Network Based Solutions Using Cellular Phone Signals	7
1.2.4 Optimal Estimator-Based GPS Receiver.....	7
1.2.5 External Sensor Assisted GPS Receivers with Optimal Estimators	9
1.3 THESIS OBJECTIVES AND CONTRIBUTIONS	11
1.4 THESIS ORGANIZATION	14
Chapter Two: GPS Receiver Limitation under Weak Signal Conditions.....	17
2.1 GPS L1 RECEIVER TRACKING STRATEGY	18
2.1.1 Overview of GPS Receiver Tracking.....	18
2.1.2 Features of Correlated GPS Signals.....	22
2.2 DESIGN OF GPS RECEIVER CODE DELAY LOCKED LOOP (DLL)	29
2.2.1 Code Delay Locked Loop Architecture	30
2.2.2 DLL Discriminator and Normalization.....	31
2.2.3 Selection of Loop Filter for DLL.....	37
2.2.4 DLL Tracking Errors	39
2.3 DESIGN OF GPS RECEIVER FREQUENCY LOCKED LOOP (FLL)	42
2.3.1 Transition from Acquisition to FLL	42

2.3.2 Cross-Product Discriminator for Fine FLL	42
2.3.3 FLL Tracking Errors	44
2.4 DESIGN OF RECEIVER PHASE LOCKED LOOPS.....	49
2.4.1 PLL Discriminator and Normalization	50
2.4.2 Design of FLL-Assisted PLL	53
2.4.3 PLL Tracking Errors	55
2.5 HIGH SENSITIVITY GPS RECEIVER FOR WEAK SIGNAL NAVIGATION	60
2.5.1 High Sensitivity GPS (HSGPS) Overview.....	61
2.5.2 Navigation Data Wipe off	61
Chapter Three: GPS/INS Ultra-Tight Integration Overview	64
3.1 INTRODUCTION TO GPS/INS INTEGRATION.....	64
3.2 OVERVIEW OF GPS/INS ULTRA-TIGHT INTEGRATION	68
3.3 COMPARISON OF DIFFERENT KALMAN FILTERS	71
3.3.1 Loosely Coupled Kalman Filter.....	72
3.3.2 Tightly Coupled Kalman Filter.....	74
3.3.3 Ultra-Tightly Coupled Kalman Filter	75
3.3.4 Performance Comparison of Different Kalman Filters	75
Chapter Four: A Novel Design of INS Assisted GPS Receiver for Degraded GPS Signal Navigation.....	79
4.1 TOP-LEVEL ARCHITECTURE OF HSGPS RECEIVER WITH INS AIDING ...	80
4.2 DESIGN OF INS AIDING LOOPS	83
4.3 DESIGN OF INDIVIDUAL FLL/PLL/DLL LOOPS	85
4.3.1 Determination of Integration Time for Individual FLL/PLL/DLL Loops	86
4.3.2 Design of Individual FLLs	88
4.3.3 Design of Individual PLLs	91
4.3.4 Design of Individual DLLs	96
4.4 DESIGN OF MULTI-CHANNEL COOP TRACKING LOOPS	98
Chapter Five: Development of Testing Tools.....	106
5.1 DEVELOPMENT OF GPS FRONT END	106
5.2 DEVELOPMENT OF INS SIMULATOR	110
Chapter Six: System Testing and Analysis	114

6.1 TEST SETUP	114
6.2 STATIC TESTS	116
6.2.1 Static Test Description	118
6.2.2 Static Test Results and the Analysis	124
6.2.3 Static Tests Summary	155
6.3 DYNAMIC TESTS.....	156
6.3.1 Scenario 1: Direction Change Test	157
6.3.2 Scenario 2: Linear Motion Test	164
6.3.3 Dynamic Test Summary	171
6.4 COMPARISON OF INS-ASSISTED AND STANDARD GPS RECEIVERS....	172
6.4.1 Test Results and Analysis of Static Test	172
6.4.2 Test Results and Analysis of Dynamic Test	177
6.4.3 Summary.....	180
Chapter Seven: Conclusions and Recommendations	181
7.1 CONCLUSIONS	183
7.2 RECOMMENDATIONS FOR FUTURE WORK.....	185
References.....	188
Appendices.....	193

LIST OF TABLES

Table 1.1 Characteristics of Degraded GPS Signal Environments	2
Table 1.2 HSGPS Characteristics Under Attenuated Signals	6
Table 1.3 The Characteristics of Optimal Estimator Tracking Method under Attenuated Signals	9
Table 1.4 Characteristics of INS-Assisted GPS Navigators under Attenuated Signals	11
Table 2.1 Characteristics of Different Loop Filters	38
Table 2.2 $C/N_0 = 15$ dB-Hz, Early/Late Discriminator	41
Table 2.3 FLL Thermal Noise Frequency Jitter with Different Parameters.....	45
Table 2.4 PLL Thermal Noise with Different Parameters.....	55
Table 2.5 PLL Dynamic Stress Error	57
Table 2.6 PLL Allan Oscillator Phase Noise with Different Parameters	59
Table 6.1 Simulated INS Parameters.....	117
Table 6.2 Receiver Parameters Adopted in Different Scenarios.....	123
Table 6.3 Receiver Parameters Adopted in FPLL/COOP Methods.....	124
Table 6.4 Parameters Adopted in Three Receivers	139
Table 6.5 Tracking Result Statistics of Different Receivers when the Incoming Signal is 15 dB-Hz.....	140

LIST OF FIGURES

Figure 2.1 Architecture of GPS Signal Tracking Loops.....	20
Figure 2.2 Architecture of PLL-Assisted DLL	21
Figure 2.3 PRN Code Autocorrelation Function.....	26
Figure 2.4 Signal Amplitude Attenuation over Doppler Frequency Error and Integration Time I	28
Figure 2.5 Signal Amplitude Attenuation over Doppler Frequency Error and Integration Time II.....	28
Figure 2.6 The Architecture of Delay Locked Loop (DLL)	30
Figure 2.7 Processing Gains after Discriminator Normalization.....	36
Figure 2.8 Discriminator Products after Normalization	36
Figure 2.9 Discriminator Corrections with Respet to Carrier Phase Error.....	52
Figure 2.10 Architecture of a Second-Order FLL-Assisted Third-Order PLL	54
Figure 3.1 Architecture of Loosely, Tightly and Ultra-Tightly Coupled GPS/INS.....	65
Figure 3.2 Ultra-Tightly Coupled GPS/INS with Loosely, Tightly or Ultra-Tightly Coupled Kalman Filter.....	69
Figure 3.3 Two Different Architectures of Current Ultra-Tightly Coupled GPS/INS.....	71
Figure 4.1 Proposed Architecture of Ultra-Tightly Coupled GPS/INS.....	81
Figure 4.2 Signal Power Loss with Respect to Integration Time	86
Figure 4.3 Individual Frequency Locked Loop Scheme	88
Figure 4.4 Phase Tracking Error for a Digital FLL under a 15 dB-Hz Signal.....	91
Figure 4.5 Individual Phase Locked Loop Scheme.....	92
Figure 4.6 The Architecture of the FLL-Assisted PLL in One Tracking Channel	93
Figure 4.7 Phase Tracking Error for a Digital PLL under a 15 dB-Hz Signal.....	95
Figure 4.8 Phase Tracking Error for a Digital PLL under the Signal of 15 dB-Hz (Oscillator Phase Noise Ignored).....	96
Figure 4.9 Externally Aided DLL Tracking Errors under a 15 dB-Hz Signal.....	98

Figure 4.10 Cooperated (COOP) Tracking Module Architecture.....	99
Figure 4.11 The Architecture of a Velocity-Assisted Position Tracking Loop along the East Direction.....	105
Figure 5.1 Relationship between GPS Front End and Software Receiver	107
Figure 5.2 Structure of the GPS IF Data Collection System	108
Figure 5.3 GPS IF Data Collection System Used for Software Receiver Testing & Validation During Simulation and Field Tests	109
Figure 5.4 INS Simulator Architecture.....	110
Figure 5.5 INS Simulator Interface	111
Figure 6.1 INS-assisted HSGPS Receiver Test Setup.....	116
Figure 6.2 INS Simulator Set-up.....	117
Figure 6.3 Static Test Scenarios.....	119
Figure 6.4 Simulated INS Velocity Errors.....	120
Figure 6.5 Estimated C/N ₀ of FLL-Assisted PLL Tracking	125
Figure 6.6 Estimated C/N ₀ of COOP Tracking	126
Figure 6.7 Carrier Phase Errors Estimated by FLL-Assisted PLL Method.....	127
Figure 6.8 Carrier Phase Errors Estimated by COOP Method	128
Figure 6.9 FLL-Assisted PLL Tracking Method Horizontal Velocity Errors	128
Figure 6.10 COOP Tracking Method Horizontal Velocity Errors.....	129
Figure 6.11 FLL-Assisted PLL Tracking Method Vertical Velocity Errors	129
Figure 6.12 COOP Tracking Method Vertical Velocity Errors	130
Figure 6.13 FPLL+COOP Tracking Method Estimated C/N ₀	132
Figure 6.14 FPLL+COOP Method Carrier Phase Tracking Errors.....	133
Figure 6.15 Carrier Doppler Tracked by FPLL and COOP Methods Separately in FPLL+COOP Method	134
Figure 6.16 FPLL+COOP Tracking Horizontal Velocity Errors.....	136

Figure 6.17 FPLL+COOP Tracking Vertical Velocity Errors.....	136
Figure 6.18 Total Carrier Phase Errors of Receiver One.....	141
Figure 6.19 Estimated C/N _o of PLL+COOP Tracking	142
Figure 6.20 FPLL+COOP Carrier Phase Tracking Errors.....	143
Figure 6.21 Carrier Doppler Tracked by FPLL and COOP Methods Separately in the FPLL+COOP Approach.....	143
Figure 6.22 Total Carrier Phase Errors of FPLL+COOP Receiver with INS Aiding	144
Figure 6.23 FPLL+COOP Tracking Horizontal Velocity Errors.....	144
Figure 6.24 FPLL+COOP Tracking Vertical Velocity Errors.....	145
Figure 6.25 Estimated C/N _o of PLL+COOP Tracking	146
Figure 6.26 FPLL+COOP Carrier Phase Tracking Errors.....	147
Figure 6.27 Carrier Doppler Tracked by FPLL and COOP Methods	147
Figure 6.28 Total Carrier Phase Errors of the FPLL+COOP Receiver with INS Aiding	149
Figure 6.29 FPLL+COOP Tracking Horizontal Velocity Errors.....	149
Figure 6.30 FPLL+COOP Tracking Vertical Velocity Errors.....	150
Figure 6.31 Estimated C/N _o of PLL+COOP Tracking	151
Figure 6.32 FPLL+COOP Carrier Phase Tracking Errors.....	151
Figure 6.33 Carrier Doppler Tracked by FPLL and COOP Methods	152
Figure 6.34 Total Carrier Phase Errors of FPLL+COOP Receiver with INS Aiding	152
Figure 6.35 FPLL+COOP Tracking Horizontal Velocity Errors.....	154
Figure 6.36 FPLL+COOP Tracking Vertical Velocity Errors.....	154
Figure 6.37 Dynamic Test Trajectory.....	158
Figure 6.38 Dynamic Test Velocity	159
Figure 6.39 Simulated Signal Power Variations	159
Figure 6.40 Dynamic Test INS Velocity Errors.....	160
Figure 6.41 Estimated C/N _o of PLL+COOP Tracking	161

Figure 6.42 FPLL+COOP Carrier Phase Tracking Errors.....	162
Figure 6.43 Total Carrier Phase Errors of FPLL+COOP Receiver with INS Aiding	162
Figure 6.44 FPLL+COOP Tracking Horizontal Velocity Errors.....	163
Figure 6.45 FPLL+COOP Tracking Vertical Velocity Errors.....	163
Figure 6.46 The Vehicle Trajectory in WGS-84 Coordinate Frame	165
Figure 6.47 Linear Dynamic Test Vehicle Trajectory.....	165
Figure 6.48 Dynamic Test INS Velocity Errors.....	166
Figure 6.49 Estimated C/N ₀ of PLL+COOP Tracking	167
Figure 6.50 FPLL+COOP Carrier Phase Tracking Errors.....	167
Figure 6.51 Total Carrier Phase Errors of FPLL+COOP Receiver with INS Aiding	168
Figure 6.52 FPLL+COOP Tracking Horizontal Velocity Errors.....	168
Figure 6.53 FPLL+COOP Tracking Vertical Velocity Errors.....	169
Figure 6.54 Satellite 07 C/N ₀ During Static Test	175
Figure 6.55 Satellite 07 PLL Carrier Phase Errors During Static Test	175
Figure 6.56 Satellite 07 Total Carrier Phase Errors During Static Test	176
Figure 6.57 Horizontal Velocity Errors During Static Test.....	176
Figure 6.58 Satellite 07 Total Carrier Phase Errors of PLL-Only Receiver with INS Aiding in Static Test	177
Figure 6.59 Satellite 07 C/N ₀ in Dynamic Test.....	178
Figure 6.60 Satellite 07 PLL Carrier Phase Errors in Dynamic Test	178
Figure 6.61 Satellite 07 Total Carrier Phase Errors in Dynamic Test.....	179
Figure 6.62 Satellite 07 Horizontal Velocity Errors in Dynamic Test	179

LIST OF SYMBOLS, ABBREVIATIONS AND NOMENCLATURE

Symbol	Definition
A	Signal amplitude
B'	Discriminator gain
B_n	Noise bandwidth of loop filter
CA	C/A PRN code
C / N_o	Carrier-to-Noise ratio
D	Navigation data bit
H	Observation matrix
I	In-phase component
M_E	Sampling number in pre-detection integration time
N_0	Noise power density
Q	Quadra-phase component
$R(\delta\tau)$	PRN code self-correlation function
T	Pre-detection Integration Time
T_c	PRN code chip interval
b_a	Accelerometer bias
b_g	Gyro bias
f_D	Code Doppler
f_L	L1 frequency
f_e	FLL Dynamic stress error
Δf	Doppler error
$\tau, \delta\tau$	Code time delay and code time delay misalignment
ω_L, ω_D	Carrier frequency and carrier Doppler
ω_{IF}	Intermediary frequency
ω_n	Natural frequency of loop filter
ω_{nf}	FLL national frequency
ω_{np}	PLL national frequency
ϕ_0	Initial carrier phase
θ_T, θ_A	Accumulated carrier phase error and Allan deviation oscillator phase noise
δ	Correlator spacing
$\sigma_{FLL, t}, \sigma_{PLL, t}$	$1-\sigma$ FLL thermal noise frequency jitter and $1-\sigma$ PLL thermal phase noise

Abbreviation and Nomenclature	Definition
AGPS	Assisted Global Positioning System
AOA	Angle Of Arrival
CPLF	Carrier Phase Loop Filter
DLL	Delay Locked Loop
DMA	Direct Memory Access
FLF	Frequency Loop Filter
FLL	Frequency Locked Loop
GPS	Global Positioning System
HSGPS	High Sensitivity Global Positioning System
LBS	Location based services
LOS	Line-Of-Sight
IF	Intermediate Frequency
IMU	Inertial Measurement Unit
INS	Inertial Navigation System
LOS	Line Of Sight
MEMS	Micro-Electro-Mechanical System
NCO	Numerically Controlled Oscillator
OCXO	Oven Compensated Crystal Oscillator
PIT	Pre-detection Integration Time
PLF	Position Loop Filter
PLL	Phase Locked Loop
P-PLL	Pull-Phase Locked Loop
PRN	Pseudo-Random-Noise
PVT	Position, Velocity, and Time
RAIM	Receiver Autonomous Integrity Monitoring
RMS	Root Mean Square
SNR	Signal-to-Noise Ratio
Std	Standard deviation
TCXO	Temperature Compensated Crystal Oscillator
TDOA	Time Difference Of Arrival
TOA	Time Of Arrival
TTFF	Time To First Fix
XO	Crystal Oscillator
ZUPT	Zero velocity UPdaTe

Chapter One: Introduction

1.1 Background

Given the broad application of positioning and navigation systems, such as wireless location of cell phones for emergencies, automobile positioning for en-route guidance, commercial aircraft positioning for transport and others, extensive research, especially that related to GPS and INS, is being conducted to enhance these systems.

Although standard GPS technologies have met most positioning requirements for Line-Of-Sight (LOS) navigation, they display limits in indoor applications and are not applicable to highly attenuated signal environments due to the weak signal power, multipath, and other limitations (e.g. MacGougan 2003). Location-based services, on the other hand, such as the E112 (Europe) and E911 (U.S.), call for navigation capability in degraded signal environments, for example, in urban canyons and indoors (e.g. Lachapelle & Kuusniemi 2003). In these types of environment, the GPS signals are 10-30 dB lower than normal values (Van Diggelen & Abraham 2001, Klukas et al 2004). Thus, standard GPS technologies are not suited for these applications.

1.1.1 Urban Canyon and Indoor Positioning

The standard downtown environments that contain many large buildings are considered urban canyons. They are characterized by signal masking, multipath, and echo-only signals due to the presence of skyscrapers and other high-rise buildings. In

these environments, signal attenuation and strong specular reflections constitute various sources of signal degradation. Environmental variables such as height of buildings, reflective characteristics of buildings' walls, orientation of city streets, and construction material used for skyscrapers can attenuate GPS signals. For auto navigation in downtowns, multipath and echo-only signals are the sources of interference. They change quickly and behave randomly due to the movement of vehicles (MacGougan 2003).

The indoor environment is characterized by varying levels of signal attenuation from all directions. Windows and doors, for example, sometimes provide clear signal propagation. Environmental variables, which pollute Line of Sight (LOS) signals, include the number of building levels; types of building materials for roofs, walls, floors, and ceilings; the availability of windows for unobstructed signal sources; and the availability of reflected signals (MacGougan 2003). The characteristics of degraded GPS signal environments are summarized in Table 1.1.

Table 1.1 Characteristics of Degraded GPS Signal Environments

	Signal Fading	Multipath signal	Platform Dynamics	Receiver Size Required
Urban Canyon Auto navigation	10-30 dB*	Strong, high frequency	Moderate	Moderate
Indoor personal positioning	20-30 dB*	Strong, low frequency	Low	Small

*: See reference (Van Diggelen & Abraham 2001)

1.1.2 Positioning Technologies for Degraded GPS Signal Navigation

In order to meet the government requirements in E911 and E112, High Sensitivity Global Positioning System (HSGPS), Assisted Global Positioning System (AGPS), and cellular network-based solutions which use cellular phone signals, have been developed recently (e.g. Klukas et al 2000).

HSGPS receivers are a class of receivers that display significantly higher acquisition/tracking sensitivity in comparison to standard receivers. Typical HSGPS receivers are designed for weak signal acquisition/tracking using coherent and non-coherent integration, over periods longer than 20 ms in the latter case. Since non-coherent integration is not sensitive to Doppler mismatch between the incoming and the local replicate signal, HSGPS does not require precise user Doppler information, as coherent integration times do not exceed 20 ms (e.g. Van Diggelen & Abraham 2001).

Due to the squaring processing loss, non-coherent integration for weak signal acquisition/tracking is not as effective as coherent integration. As a result, assisted-GPS has been developed to enable the use of long coherent integration by providing the navigation message, timing information, almanac, and approximate position through alternate communications channels. This assistance allows coherent integration intervals longer than 20 ms (e.g. Karunananayake et al 2004).

Cellular network based solutions including Time Of Arrival (TOA), Time Difference Of Arrival (TDOA) and Angle Of Arrival (AOA) methods are similar to GPS in methodology. Due to the hearability problem and non-line-of-sight errors, positioning solutions of cellular network-based method are not accurate in both urban canyons and indoor environments (e.g. Ma 2003).

Besides the above positioning technologies, GPS receiver enhancement with external aiding information, namely user Doppler, has been proposed recently to meet positioning and navigation requirements in degraded GPS signal environments. By aiding signal tracking loops in receivers with external sensors (e.g., INS, radars, odometers or even cellular phones), external sensor-aided GPS receivers, such as deeply integrated GPS/INS receivers, can track incoming weak signals that are 10-30 dB lower than standard technologies. As a result, it can project a strong light beam into the “indoor darkness” (Chiou et al. 2004).

Furthermore, even when there are no external aiding sensors available, a similar method derived from external sensor-aided GPS receiver can be used to improve receiver tracking sensitivity. This class of technology regularly is referred to as optimal estimator-based GPS receiver or deeply integrated GPS navigators with optimal estimators (Gustafson & Dowdle 2000, Psiaki & Jung 2002). In this class of receivers, optimal estimators are used to fuse all channel measurements and then estimate code phase, carrier phase, Doppler shift, rate of change of Doppler shift, data bit sign, etc.

1.2 Limitations of Previous Work

Many GPS receiver technologies mentioned above have been developed recently in order to realize personal/auto navigation in degraded signal environments. It seems, however, that current technologies cannot completely meet indoor navigation requirements. The limitations of these technologies are discussed below.

1.2.1 High Sensitivity Global Positioning System (HSGPS)

Personal/auto navigation in signal fading environments has partly led to the development of high sensitivity GPS receivers. With the ability to track weak signals by increasing coherent/non-coherent integration time, HSGPS offers higher availability and wider applicability compared to standard GPS. HSGPS, however, is associated with higher noise levels and multiple measurement fault sources. Its performance is also limited by factors such as receiver clock stability, navigation message bit length, user dynamics and so on. Moreover, many field tests (Lachapelle & Kuusniemi 2003) illustrate that current HSGPS cannot meet all of the requirements in weak signal conditions. The assessment of HSGPS performance in weak signal navigation is summarized in Table 1.2.

Table 1.2 HSGPS Characteristics Under Attenuated Signals

Items	Rating	Description (Van Diggelen & Abraham 2001)
Tracking Sensitivity	Good	15-25 dB Gain, sometimes not enough for indoor positioning
Acquisition Sensitivity	Bad	Long TTFF, not enough processing gain available for signal acquisition
Re-acquisition Ability	Bad	For the long integration time, re-acquisition is time-consuming.
Data Output Frequency	Fair	The long integration time limits the data output rate.
Positioning Accuracy	Fair	Degraded by multipath signal and frequency/phase variation
Carrier phase output	Bad	Limited benefit on PLL tracking, hard to output carrier phase measurement
Dynamic response	Bad	Used mainly for low dynamic users. In some commercial applications, it is not vital.
Receiver Size	Small	No need for any other hardware. Can be realized in GPS software
Power Cost	Low	No other hardware required, so no additional power cost
Augment by AGPS	Good	Needs wireless data link

1.2.2 Assisted Global Positioning System (AGPS)

In order to speed signal acquisition and decrease the Time To First Fix (TTFF), AGPS has been introduced in recent years. By providing the receiver with helpful information (e.g., the satellite ephemeris, frequency shift, and so on) via a wireless network, AGPS technology can estimate the satellite Doppler ahead of time. Thereby it can dramatically reduce the required frequency/delay search space, and therefore TTFF. However, since AGPS can only increase acquisition sensitivity up to 10 dB, in practice, it

has to work with HSGPS to enhance GPS signal acquisition (Van Diggelen & Abraham 2001).

1.2.3 Cellular Network based Solutions Using Cellular Phone Signals

Cellular network based solutions, including Time Of Arrival (TOA), Time Difference Of Arrival (TDOA) and Angle Of Arrival (AOA), are similar to GPS in methodology (e.g. Klukas 1997). For the hearability problem and non-line-of-sight errors, positioning solutions of Cellular Network-based method are not accurate in both urban canyon and indoor environments.

Furthermore, since cellular base stations may not be available in some areas of country, e.g. suburban areas, it is impossible to provide users with positioning solutions anywhere in the world only by using cellular phone signals. In order to obtain positioning capability anywhere at any time, both standard GPS and Cellular phone based methods would be required, which would lead to complex systems.

1.2.4 Optimal Estimator-Based GPS Receiver

An optimal estimator-based GPS receiver aims at obtaining more signal tracking processing gain than regular technologies. The first approach of the deeply integrated GPS-based navigator is the Vector Delay Locked Loop (VDLL) technique proposed by Parkinson & Spilker (1996). Gustafson & Dowdle (2000), in turn, utilized optimal estimation techniques to track (estimate) code phase, carrier phase, Doppler shift, rate of change of Doppler shift, carrier amplitude and data bit sign by fusing all channel

measurements. Zhodzishsky & Yudanov (1998), on the other hand, introduced a COOP tracking architecture design, which fuses information from the tracking channels to track (estimate) code phase, carrier phase, Doppler shift, rate of change of Doppler shift, carrier amplitude and data bit sign, with variances of the estimate states. This entire optimal estimation-based receiver is called deeply integrated GPS-based navigator with optimal estimators (Gustafson & Dowdle 2000, Zhodzishsky & Yudanov 1998, Psiaki & Jung 2002).

Compared with the above GPS receiver augmentation technologies, the integrated optimal estimators bring very significant processing gain to the GPS signal tracking loops and make possible the tracking on GPS carrier phase under attenuated signal environments (Gustafson & Dowdle 2000, Psiaki & Jung 2002).

For decades, GPS receivers have been designed and developed employing classical control theory which is consistent with modern digital communication theory. Optimal estimator-based GPS receiver enhancements, however, improve receiver performance based on modern control theory, and, thus, can result in a revolution in GPS receiver design. Nevertheless, the optimal estimator-based method still cannot meet the requirements for urban canyon and indoor navigation completely. Table 1.3 shows its characteristics under attenuated signals.

Table 1.3 The Characteristics of Optimal Estimator Tracking Method under Attenuated Signals

Items	Rating	Description (Gustafson & Dowdle 2000, Zhodzishsky & Yudanov 1998)
Tracking Sensitivity	Fair	15-25 dB Gain, not enough for fading GPS signal positioning
Acquisition Sensitivity	Good	Information obtained from acquired signals may be used to speed acquisition processing of the other signals, especially in hot starts
Re-acquisition Ability	Good	Re-acquisition of unlock channels will be aided by other locked channels.
Data Output Rate	Fair	The Kalman filter in tracking loops cannot be performed with a high recursive rate.
Positioning Accuracy	Good	The best performance can be achieved in fading signal environments for its optimal nature.
Carrier phase output	Good	By enhancing PLLs, this method can output phase observations and reduce/avoid cycle slips.
Dynamic response	Fair	It can meet the requirements for most commercial low-dynamics applications.
Receiver Size	Small	No need for any other hardware Can be realized in GPS receiver software
Power Cost	Low	No other hardware required, so no additional power cost
Anti-multipath Ability	Bad	Channels affect each other when fused, multipath signals in environments pollute the filter estimation and, thus, degrade this technology.*

(*: If a strong echo-only signal is received by a standard receiver, the latter still works but with a poor positioning accuracy. For a receiver with an optimal estimator, however, it might lose lock on all channels because of the echo-only signal, and, thus, does not work at all.)

1.2.5 External Sensor Assisted GPS Receivers with Optimal Estimators

In order to enhance the anti-multipath ability, obtain sufficient processing gain for indoor navigation, and increase signal tracking reliability and availability simultaneously, external sensors such as INS, radars, odometers or even cellular phones (enhanced by cellular network-based positioning technologies) can be used to aid GPS navigators via

optimal estimators. Ultra-tight integration of GPS and inertial navigation systems has recently received considerable attention for precision positioning/navigation in attenuated signal environments. In an INS-assisted GPS receiver (also called ultra-tightly coupled GPS/INS or GPS/INS deep integration), an external INS is used to provide receiver dynamics information so as to allow the GPS receiver to achieve very long coherent integration to track weak signals (Soloviev & Graas 2004). INS reduces the receiver dynamics uncertainty and, thus, enables the GPS receiver to track an incoming weak signal that is 20-30 dB lower than normal (Beser & Alexander 2002, Soloviev & Graas 2004, Kreye & Eissfeller 2000, Sennott 1997). Table 1.4 displays the characteristics of an INS-assisted GPS navigator with optimal estimators under attenuated signals.

Table 1.4 also shows that an INS-assisted GPS receiver is far superior to any of the other positioning technologies introduced above and, therefore, offers the greatest potential for meeting GPS navigation and positioning requirements under attenuated signals. In INS-assisted GPS receivers, velocity aiding from INS enhances the GPS Phase Lock Loops (PLL) , which are the weakest loops among the GPS signal tracking loops. Furthermore, full navigation capability, including carrier phase output under attenuated signals, is preserved in INS-assisted GPS receivers. This availability of accurate carrier phase measurements is deemed necessary for many high-accuracy applications, such as mobile mapping in urban areas, and indoor surveys with GPS.

Table 1.4 Characteristics of INS-Assisted GPS Navigators under Attenuated Signals

Items	Rating	Description (Soloviev & Graas 2004, Soloviev & Gunawardena 2004)
Tracking Sensitivity	Excellent	20-30 dB gain, enough for numerous GPS degraded signal positioning applications
Acquisition Sensitivity	Excellent	Measurements from an aligned INS and the information from acquired signals may be used together to speed acquisition, especially in hot starts.
Re-acquisition Ability	Excellent	Re-acquisition of channels will be aided by INS measurements and other locked channels.
Data Output Rate	Excellent	Using INS aiding, output rate can be above 100 Hz with a Kalman filter running at a low recursive rate.
Positioning Accuracy	Excellent	INS solution can help with blunder detection and noise compression (by using long-time integration).
Carrier phase output	Excellent	Assisted by INS, this method can output precise phase observation and avoid/reduce cycle slips.
Dynamic response	Excellent	Used for both low and high dynamic users and thus in both commercial and military applications.
Receiver Size	Moderate/Big	A good size under Ultra-tight integration for MEMS IMU
Power Cost	Moderate/High	Additional external sensor needed, so more power is required
Anti multipath Ability	Excellent	Assisted by INS, the deeply integrated navigator can detect multipath signals and directly track weak LOS signals in urban canyon and indoor environments.

1.3 Thesis Objectives and Contributions

Given the ultimate goal of improving GPS-based navigation in weak signal environments, this thesis expands upon the previous research and focuses on GPS receiver enhancement for weak-signal navigation and introduces an INS-aided high sensitivity GPS receiver.

This thesis aims to achieve the following objectives:

1. *To Investigate a Deeply Coupled GPS/INS System to Design a Novel INS-Assisted GPS Receiver for GPS Weak Signal Navigation.* This project starts with the exploration of the mechanism of GPS/INS deep integration. Then, the advantages and disadvantages of present deep integration architectures under attenuated signals are analyzed. Finally, based on system overall investigation, a novel design of an INS-assisted GPS receiver for weak signal navigation is presented. This new system integrates many GPS receiver enhancement approaches implemented in high sensitivity GPS receivers, optimal estimator-based GPS receivers, and current GPS/INS ultra-tightly integrated systems.

2. *To Develop a High Sensitivity GPS Receiver with Optimal Estimator to Assess GPS-Only Receiver Performance Under Attenuated Signals.* With the ultimate goal of developing an INS-assisted GPS receiver for degraded GPS signal navigation, an optimal estimator-based high sensitivity GPS-only receiver is first developed. Work to be performed later will aim to modify the receiver for external INS aiding. This GPS-only receiver adopts some receiver enhancement technologies for both HSGPS receivers and optimal estimator-based receivers. It is used to assess GPS-only receiver performance under attenuated signals.

3. *To Develop an INS-Assisted GPS Receiver under Attenuated Signals to Assess Receiver Tracking Capability with INS Aiding.* Based on the above optimal estimator-based GPS-only receiver, an INS-aiding loop is added into the receiver. Using this INS-assisted GPS receiver, receiver tracking capability with different levels of dynamics is evaluated. This evaluation will facilitate the understanding of required Doppler accuracy, as well as help to determine the grade of aiding inertial sensors.

4. *To Develop Testing Tools Including a GPS Front End and an INS Simulator to Test Performance of The INS Assisted GPS Receiver.* These testing tools are developed in this project to test receiver performance.

The major contributions of this thesis are:

1. A detailed analysis of critical parameters involved in GPS receiver design for weak signal tracking;

2. The design and test of a novel INS-assisted HSGPS receiver for degraded GPS signal navigation;

3. Characterization of benefits and limitations of integrating different quality IMUs with GPS receivers for weak signal navigation;

4. The development and verification of testing tools: A GPS front end and an INS simulator.

1.4 Thesis Organization

This thesis is organized in seven chapters as follows:

In Chapter 1, GPS signal characteristics in urban canyons or indoor environments are described. Then, the limitations of three main GPS receiver technologies including HSGPS, AGPS and cellular network-based solutions are discussed. Next, this chapter presents the methodology and limitations of optimal estimator-based GPS receivers. Finally, the current research related to INS-aided GPS receivers is discussed and followed by the objectives and contributions.

Chapter 2 starts from an overview of the design of current GPS L1 receivers. After an introduction of GPS signal features, this chapter presents all the important parameters in the design of the various tracking loops, including carrier phase tracking loops and code delay tracking loops. Chapter 2 also presents a study of HSGPS receivers designed especially for weak signal navigation. This chapter further discusses some effective receiver enhancement approaches, such as very long coherent integration intervals and navigation data wipe off. The emphasis is placed on the limiting factors of high sensitivity processing gain under degraded signals.

As the fundamental contribution of this thesis, the research discussed in Chapter 2 outlines the system design for the GPS portion of an INS-assisted high sensitivity GPS receiver. The deep understanding of GPS theory in this chapter and the theory of GPS/INS deep integration introduced in Chapter 3 will help readers to study the main contribution of this thesis, which is shown in Chapters 4 and 6.

In Chapter 3, INS-assisted GPS receivers using the GPS/INS ultra-tight integration method are introduced and compared to the GPS/INS loosely/tightly integrated receivers. Then, this chapter examines present architectures of GPS/INS ultra-tight integration. The focus is on the methodologies and limitations of present GPS/INS deep integration systems and their applications in degraded GPS signal environments.

Chapter 4 presents the main contribution of this thesis. First, the chapter proposes a novel design of an INS-assisted high sensitivity GPS receiver for degraded GPS signal navigation. After an introduction of the top-level design of this INS-assisted GPS receiver, the details and advantages of this novel architecture are presented. Finally, Chapter 4 describes the module design in greater detail including external INS aiding Loops, internal individual receiver tracking loops and multi-channel COOP tracking loops, which bridge the external INS aiding loops and internal receiver signal tracking loops.

Chapter 5 describes the testing tools developed by the author in order to test algorithms and approaches. First, the chapter introduces a GPS front end including front end design and its testing. In addition, an INS simulator is outlined in this section since it is used for several types of tests in the subsequent study.

Chapter 6 illustrates post-mission results of the integrated system for GPS weak signal navigation. Specifically, receiver tracking threshold with different quality IMUs, position accuracy during INS aiding, as well as overall system reliability are investigated. At last, based on the result analysis, the assessment of the INS assisted GPS receiver is outlined.

Chapter 7 discusses conclusions from this research and makes recommendations for future work.

Chapter Two: GPS Receiver Limitation under Weak Signal Conditions

Given the topic ‘INS-assisted high sensitivity GPS for degraded GPS signal navigation’, this research consists of the following two objectives: 1) to investigate and develop a well-designed high sensitivity GPS receiver with effective tracking performance under weak signal environments; and 2) to investigate and further improve receiver tracking capability under weak signal environments with Inertial Navigation System (INS) aiding.

In order to achieve the first objective, this chapter answers the following three questions, which represent the theoretical basis for this research:

1. What kinds of signal tracking strategies are being used in GPS receivers?
2. What are the most important sets of receiver parameters affecting signal tracking for a software-based GPS receiver, especially in weak signal environments?
3. Even with the best set of receiver parameters, what is the limitation of a GPS receiver under weak signals?

This chapter starts with an overview of GPS receiver tracking approaches. Then, it presents a thorough analysis of the design of receiver tracking loops including the code Delay Locked Loop (DLL), Frequency Locked Loop (FLL), and carrier Phase Locked Loop (PLL). Finally, the chapter discusses how to tune receiver tracking parameters for effective weak signal tracking. The research outlined in this chapter and Chapter 3 contribute to the fundamental design of the INS-assisted GPS receiver prototype developed in this thesis.

2.1 GPS L1 Receiver Tracking Strategy

After the signals broadcasted by satellite arrive at the receiver antenna, the signal located in RF frequency band is first down-converted to the Intermediate Frequency (IF) band in the RF module of the receiver, and then signal acquisition is preformed by the receiver baseband processor to do the Doppler and code removal roughly. After signal down conversation and acquisition, the GPS IF signal is sent into the signal tracking loops for carrier phase and code delay coherent tracking to recover the incoming signal accurately (Kaplan 1996).

2.1.1 Overview of GPS Receiver Tracking

GPS signal tracking loops include the code Delay Locked Loop (DLL) and carrier Phase Locked Loop (PLL). Figure 2.1 shows the architecture of the GPS baseband signal tracking loops. These two loops normally work in parallel: The DLL replicates the incoming code to wipe off the Pseudo-Random-Noise (PRN) code. At the same time, the

PLL replicates the incoming carrier phase and remove the carrier from the incoming signal.

Because of the navigation data bits modulated on GPS signal, the PLL usually uses a Costas loop, which is insensitive to 180° data bit reversal (Kaplan 1996). The disadvantage of using the Costas tracking loop is that there is a 6 dB tracking-sensitivity loss as compared to a Pull-Phase Locked Loop (P-PLL) (Julien 2005). For this reason, the PLL is more sensitive to environment noise, interference and jamming, as compared to DLL. In GPS signal tracking, it is always the PLL that first loses lock, and then the DLL loses lock since the receiver cannot correctly replicate the incoming signal carrier phase (Kaplan 1996).

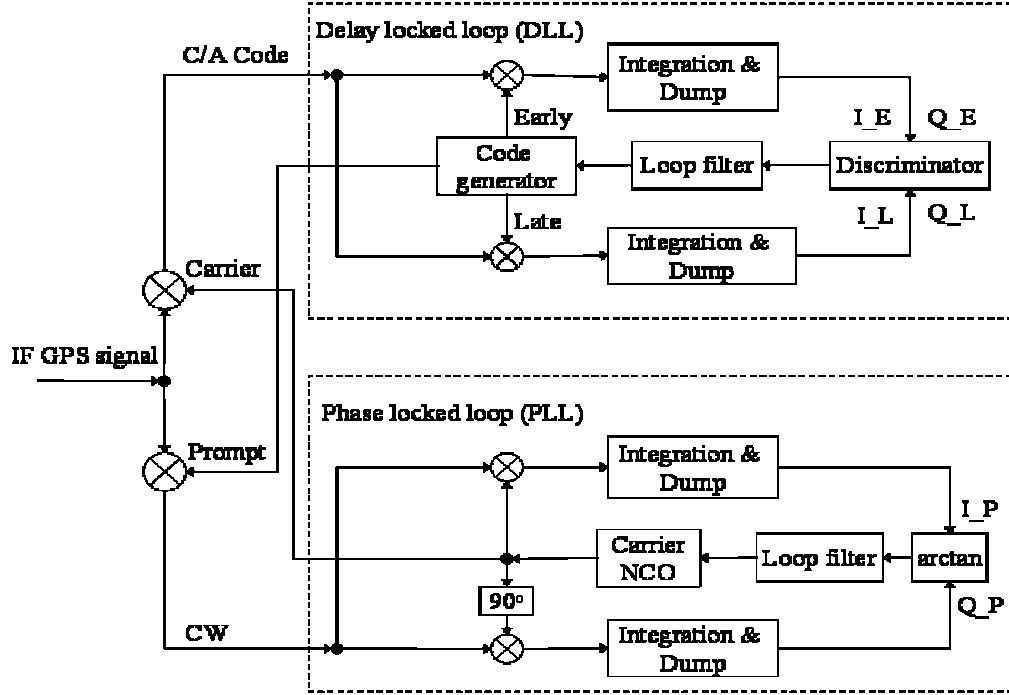


Figure 2.1 Architecture of GPS Signal Tracking Loops

Since the C/A code is modulated on the carrier wave, the code Doppler can be computed using the carrier Doppler as:

$$Doppler_{carrier} = \frac{f_{carrier}}{f_{code}} \times Doppler_{code} = 1540 \times Doppler_{code} . \quad (2.1)$$

To improve the accuracy of the DLL, a PLL-assisted DLL architecture is regularly used in GPS signal tracking, as shown in Figure 2.2. Based on Equation (2.1), the carrier Doppler from the PLL is divided by a factor of 1540 and then fed into the code generator for code tracking (Kaplan 1996).

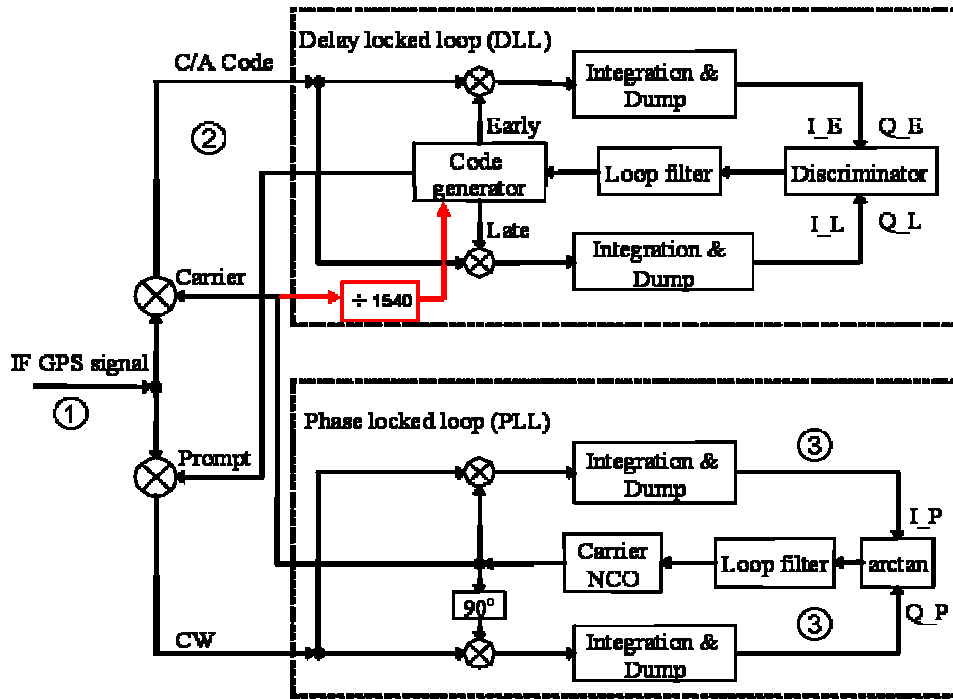


Figure 2.2 Architecture of PLL-Assisted DLL

Since external aiding from the carrier loop is applied to compensate for most of code tracking errors and therefore improve DLL tracking performance, DLLs here only need to correct some insignificant errors, such as initial tracking errors, the rate of change of the ionosphere or differences in code, and multipath. These residual variations are normally small and change very slowly with time in open-sky environments. Thus, the DLL loop bandwidth can be significantly reduced to an order of 0.05 to 1 Hz, depending on the application. With external aiding from the carrier loop, the pre-detection time can be extended dramatically based on the Doppler aiding accuracy (Kaplan 1996). In personal/vehicle navigation applications in weak signal environments, the mulitpath error might be very large and change very quickly. Fortunately, with INS aiding, it is possible

for the INS-assisted GPS receiver to track on LOS signal directly and avoid tracking the rapidly changed multipath signals.

Carrier tracking loops can be divided into two classes: Phase Locked Loops (PLL) to track the incoming carrier phase and Frequency Locked Loops (FLL) to track the incoming carrier frequency. Now a GPS receiver usually uses a FLL-assisted PLL for carrier tracking. FLL generates the uncorrelated local carrier wave whose frequency is the same as the incoming signal, but whose phase can be different with the incoming signal, while PLL generates the correlated local carrier wave whose frequency and phase are both the same as the incoming signal. Compared to a FLL, a PLL provides more accurate carrier phase measurements but tends to lose track under adverse situations. The FLL-assisted PLL design takes advantage of the robustness of FLL and the accuracy of PLL (Kaplan 1996).

2.1.2 Features of Correlated GPS Signals

The incoming GPS signal can be expressed as follows (Raquet 2004):

$$r(t) = A \cdot D \cdot CA((1 + \frac{f_D}{f_L})t - \tau) \cdot \cos((\omega_L + \omega_D)t + \phi_0) \quad , \quad (2.2)$$

where A is the signal amplitude, D is navigation data bit, CA is the C/A pseudo-random code, f_D is the code Doppler and f_L is the C/A chip rate on L1 frequency. τ is the code delay which is the distance from the satellite to the receiver in units of time, e.g, seconds.

ω_L and ω_D are carrier frequency and carrier Doppler.

After the frequency down conversion and carrier phase wiping off, the output signals shown in Figure 2.2 are as follows (Raquet 2004):

$$\begin{aligned} I_2 &= I_1 \cos(\omega_{ref} t) + Q_1 \sin(\omega_{ref} t) = \frac{A}{\sqrt{2}} \cdot D \cdot CA((1 + \frac{f_D}{f_L})t - \tau) \cdot \cos((\omega_{IF} + \omega_D - \omega_{ref})t + \phi_0) \\ Q_2 &= Q_1 \cos(\omega_{ref} t) - I_1 \sin(\omega_{ref} t) = \frac{A}{\sqrt{2}} \cdot D \cdot CA((1 + \frac{f_D}{f_L})t - \tau) \cdot \sin((\omega_{IF} + \omega_D - \omega_{ref})t + \phi_0) , \end{aligned} \quad (2.3)$$

where ω_{IF} is the intermediate frequency which is down-converted from the L1 frequency, ω_{ref} is the frequency of local replica, ϕ_0 represents the initial carrier phase and

$$\begin{aligned} I_1 &= \frac{A}{\sqrt{2}} \cdot D \cdot CA((1 + \frac{f_D}{f_L})t - \tau) \cdot \cos((\omega_{IF} + \omega_D)t + \phi_0) \\ Q_1 &= \frac{A}{\sqrt{2}} \cdot D \cdot CA((1 + \frac{f_D}{f_L})t - \tau) \cdot \sin((\omega_{IF} + \omega_D)t + \phi_0) . \end{aligned} \quad (2.4)$$

In some commercial GPS receivers, there is only an in-phase (I_1) component output from the front end and the quadra-phase (Q_1) component is not available. Equation (2.3) then becomes:

$$\begin{aligned}
I_2 = I_1 \cos(\omega_{ref} t) &= \frac{1}{2} \cdot \frac{A}{\sqrt{2}} \cdot D \cdot CA((1 + \frac{f_D}{f_L})t - \tau) \cdot \cos((\omega_{IF} + \omega_D - \omega_{ref})t + \phi_0) \\
&\quad + \frac{1}{2} \cdot \frac{A}{\sqrt{2}} \cdot D \cdot CA((1 + \frac{f_D}{f_L})t - \tau) \cdot \cos((\omega_{IF} + \omega_D + \omega_{ref})t + \phi_0) \\
&\approx \frac{1}{2} \cdot \frac{A}{\sqrt{2}} \cdot D \cdot CA((1 + \frac{f_D}{f_L})t - \tau) \cdot \cos((\omega_{IF} + \omega_D - \omega_{ref})t + \phi_0) \text{ (after low pass filter)} \\
Q_2 = -I_1 \sin(\omega_{ref} t) &= \frac{1}{2} \cdot \frac{A}{\sqrt{2}} \cdot D \cdot CA((1 + \frac{f_D}{f_L})t - \tau) \cdot \sin((\omega_{IF} + \omega_D - \omega_{ref})t + \phi_0) \\
&\quad + \frac{1}{2} \cdot \frac{A}{\sqrt{2}} \cdot D \cdot CA((1 + \frac{f_D}{f_L})t - \tau) \cdot \sin((\omega_{IF} + \omega_D + \omega_{ref})t + \phi_0) \\
&\approx \frac{1}{2} \cdot \frac{A}{\sqrt{2}} \cdot D \cdot CA((1 + \frac{f_D}{f_L})t - \tau) \cdot \sin((\omega_{IF} + \omega_D - \omega_{ref})t + \phi_0) \text{ (after low pass filter)}
\end{aligned}$$

(2.5)

In Equation (2.5), it is clear that the quadra-phase (Q_2) component is the negative of the product of the incoming signal I_1 and the local carrier.

After a low pass filter, Equations (2.3) and (2.5) are almost the same, except for a factor of 0.5 in Equation (2.5). Equation (2.3), which is for the more general case, will be used for future analysis.

In Figure 2.2, after signal correlation and dumping, one can write (Raquet 2004)

$$\begin{aligned} I_3 &= \frac{A}{\sqrt{2}} M_E D R(\delta\tau) \frac{\sin(\pi\Delta f T)}{\pi\Delta f T} \cos(\pi\Delta f T + \phi_0) \\ Q_3 &= \frac{A}{\sqrt{2}} M_E D R(\delta\tau) \frac{\sin(\pi\Delta f T)}{\pi\Delta f T} \sin(\pi\Delta f T + \phi_0) \end{aligned}, \quad (2.6)$$

where T is the Pre-detection Integration Time (PIT), $\delta\tau$ is the code delay misalignment, M_E is the sampling number in T , and $R(\delta\tau)$ is the PRN code self-correlation function and expressed as

$$R(\delta\tau) = \begin{cases} 1 - \frac{(L+1)}{LT_c} |\delta\tau| & (|\delta\tau| \leq T_c) \\ -\frac{1}{L} & (T_c < |\delta\tau| < (L-1)T_c) \end{cases} \approx \begin{cases} 1 - \frac{1}{T_c} |\delta\tau| & (|\delta\tau| \leq T_c) \\ 0 & (T_c < |\delta\tau| < (L-1)T_c) \end{cases}, \quad (2.7)$$

where L is the chip numbers of the PRN C/A code (1023). T_c is the PRN code chip interval.

Equation (2.6) shows clearly the four main factors which limit the Signal-to-Noise Ratio (SNR):

1. Incoming Signal power A : a weak incoming signal will decrease tracking sensitivity.
2. Navigation data bit D : the unknown nature of navigation data will limit the coherent integration time.

3. Code-delay misalignment $\delta\tau$: A code-delay alignment error will decrease the signal power after de-spreading, with the power loss characterized by the function $R(\delta\tau)$. Figure 2.3 illustrates the signal degradation due to code-delay misalignment $\delta\tau$.
4. Doppler error Δf : the tracking difference between the local replica carrier frequency and the incoming carrier frequency will lead to signal power loss when doing coherent integration. The loss is characterized by the function $\frac{\sin(\pi\Delta f T)}{\pi\Delta f T}$ and is illustrated in Figure 2.4 and Figure 2.5.

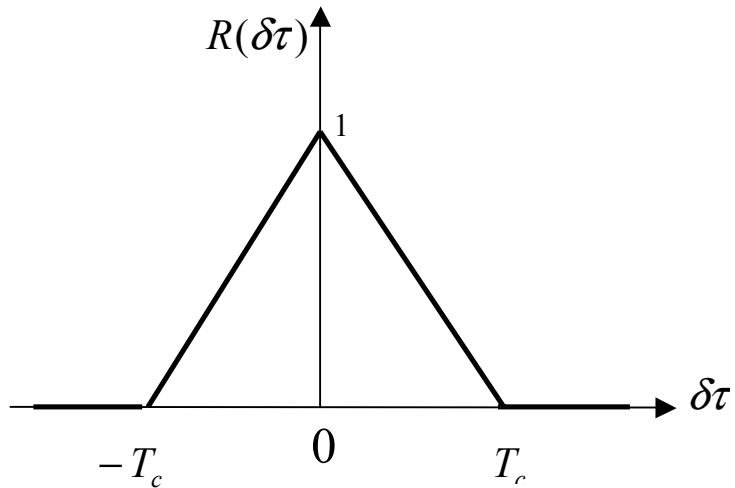


Figure 2.3 PRN Code Autocorrelation Function

Figure 2.4 and Figure 2.5 show two plots of the signal amplitude attenuation due to Doppler frequency error and integration time. As shown in both figures, to decrease the signal power loss characterized by the function $\frac{\sin(\pi\Delta f T)}{\pi\Delta f T}$, both the Doppler frequency error and integration time should keep small. However, from Equation (2.6), it is clear that a shorter integration time will lead to a small value of M_E and thus decrease the accumulated signal power, which is not desired. Therefore, there is a balance in choosing the integration time for weak signal tracking.

There are several reasons that might lead to the mismatch (Δf) of the incoming Doppler with the local replica, namely satellite motion, receiver dynamics, oscillator instability, etc. In previous research (Watson 2005), the contributions of propagation effects were shown to be negligible for stationary receivers, contributing up to a 0.01 Hz random error, and up to a 0.13 Hz constant bias, although average values are expected to be lower. These random errors are insignificant until reaching or exceeding a full 10 s of coherent integration. In summary, the only significant factors likely to limit coherent integration for stationary receivers are the errors in the receiver oscillator. If the oscillator under test is proved capable of supporting coherent integration of up to 10 s, at which point satellite oscillator errors and propagation errors might become factors, this assumption can be re-evaluated. So, in all these factors, receiver dynamics and oscillator instability are the two most important error sources.

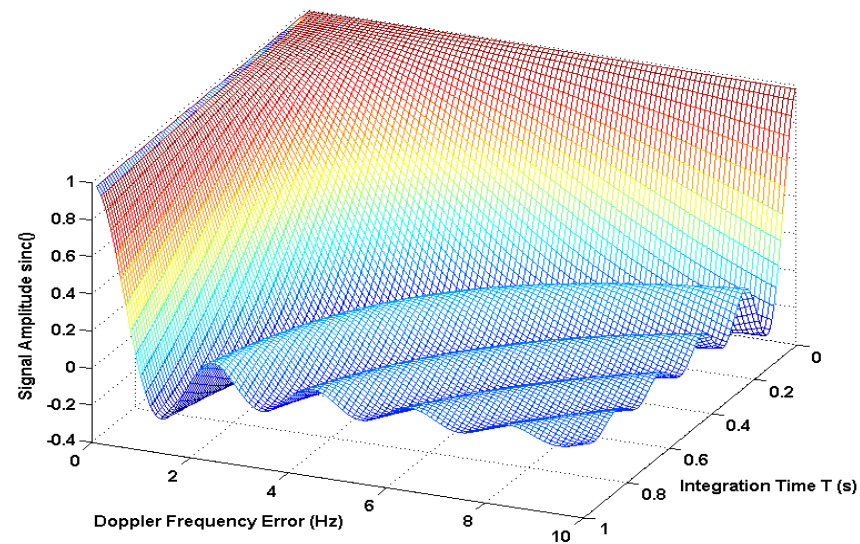


Figure 2.4 Signal Amplitude Attenuation over Doppler Frequency Error and Integration Time I

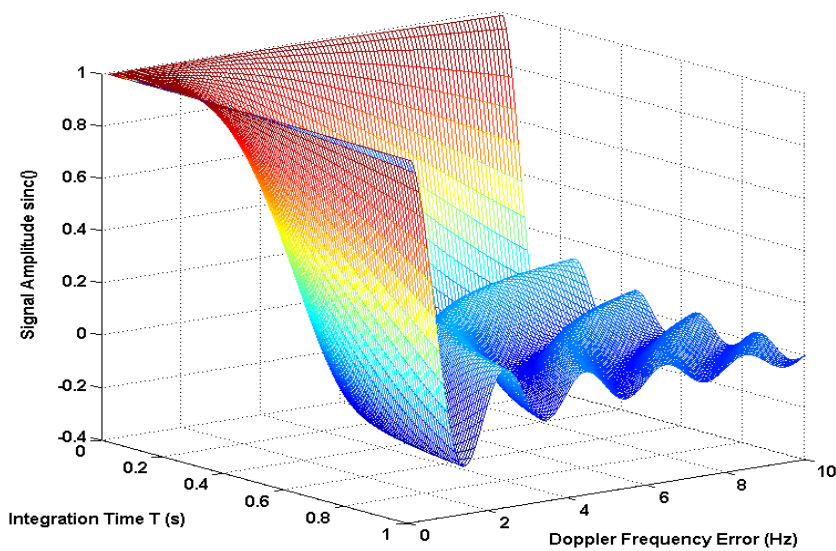


Figure 2.5 Signal Amplitude Attenuation over Doppler Frequency Error and Integration Time II

These four limiting factors in weak signal tracking are analyzed in greater detail later in this chapter.

Besides the limiting factors outlined above, multipath and cross-correlation are the other two important factors that must be considered carefully in HSGPS receiver design (MacGougan 2003). These two topics, however, are outside of the scope of this research and are not discussed in this thesis.

2.2 Design of GPS Receiver Code Delay Locked Loop (DLL)

Starting with an introduction of DLL architecture, this section analyzes three commonly used DLL discriminators in terms of their processing gain and normalization effects. The research's emphasis is to find a discriminator capable of achieving the highest discriminator gain and the widest phase error pull-in range in degraded signal environments.

Next, effects of loop filters on signal tracking are discussed, with the focus on the analysis of loop characteristics, e.g. tracking error pull-in/pull-out range, loop pull-in time, loop natural frequency and so on. Last, DLL tracking errors are investigated, and a set of proper receiver parameters affecting signal tracking is chosen in order to provide the proposed INS-assisted GPS receiver with an effective tracking performance from the GPS side.

2.2.1 Code Delay Locked Loop Architecture

The architecture of a DLL is shown in Figure 2.6.

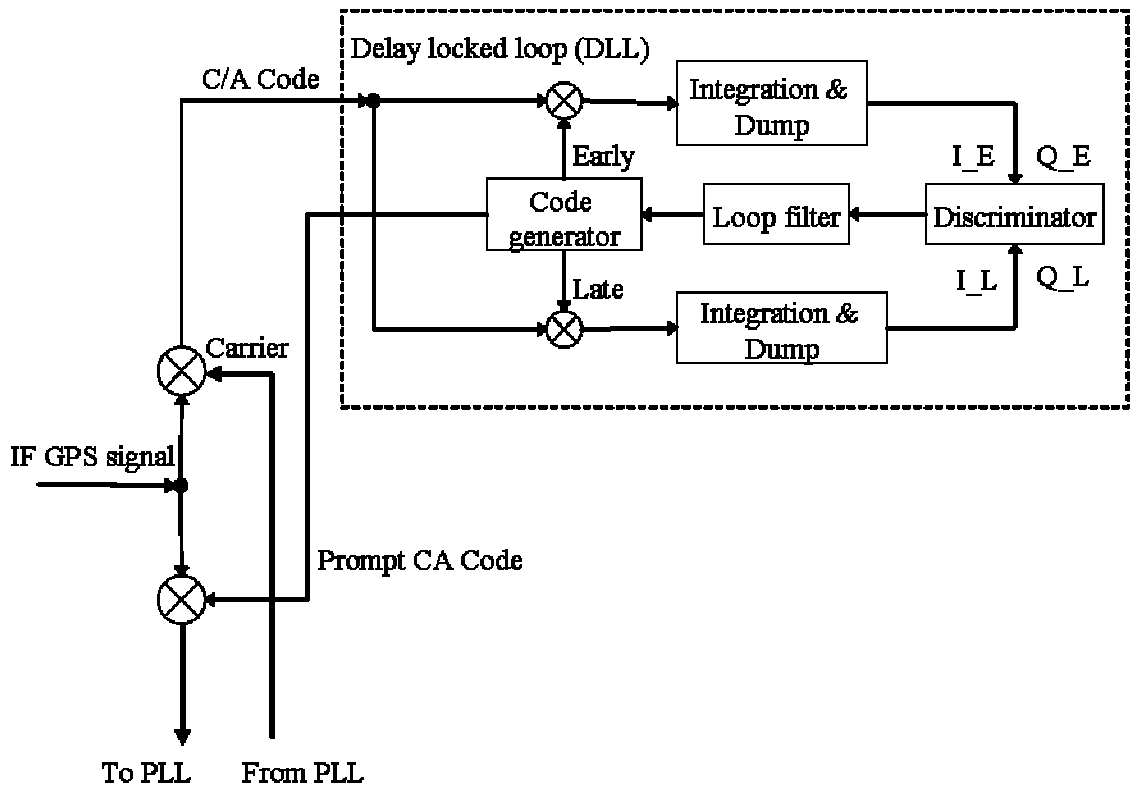


Figure 2.6 The Architecture of Delay Locked Loop (DLL)

Using Equation (2.6), I_E , Q_E , I_L , and Q_L in Figure 2.6 can be written as follows (Raquet 2004):

$$\begin{aligned}
I_E &= \frac{A}{\sqrt{2}} \cdot M_E \cdot D \cdot R(\delta\tau - \delta) \cdot \frac{\sin(\pi\Delta fT)}{\pi\Delta fT} \cdot \cos(\pi\Delta fT + \phi_0) \\
Q_E &= \frac{A}{\sqrt{2}} \cdot M_E \cdot D \cdot R(\delta\tau - \delta) \cdot \frac{\sin(\pi\Delta fT)}{\pi\Delta fT} \cdot \sin(\pi\Delta fT + \phi_0) \\
I_L &= \frac{A}{\sqrt{2}} \cdot M_E \cdot D \cdot R(\delta\tau + \delta) \cdot \frac{\sin(\pi\Delta fT)}{\pi\Delta fT} \cdot \cos(\pi\Delta fT + \phi_0) \\
Q_L &= \frac{A}{\sqrt{2}} \cdot M_E \cdot D \cdot R(\delta\tau + \delta) \cdot \frac{\sin(\pi\Delta fT)}{\pi\Delta fT} \cdot \sin(\pi\Delta fT + \phi_0)
\end{aligned} \tag{2.8}$$

where δ is correlator spacing.

2.2.2 DLL Discriminator and Normalization

In order to obtain the best DLL performance under weak signal tracking, the discriminator and its normalization algorithm with the highest processing gain are selected herein. Three well-known DLL discriminators proposed by Kaplan (1996) are:

$$\begin{aligned}
B_1(\delta\tau) &= (I_E - I_L)I_P + (Q_E - Q_L)Q_P \\
B_2(\delta\tau) &= (I_E^2 + Q_E^2) - (I_L^2 + Q_L^2) \\
B_3(\delta\tau) &= \sqrt{I_E^2 + Q_E^2} - \sqrt{I_L^2 + Q_L^2}
\end{aligned} \tag{2.9}$$

Substituting Equation (2.8) into (2.9) yields

$$\begin{aligned}
B_1(\delta\tau) &= (I_E - I_L)I_P + (Q_E - Q_L)Q_P \\
&= \left(\frac{A}{\sqrt{2}}M_E D \frac{\sin(\pi\Delta fT)}{\pi\Delta fT}\right)^2 [R(\delta\tau - \delta) - R(\delta\tau + \delta)]R(\delta\tau) \\
B_2(\delta\tau) &= (I_E^2 + Q_E^2) - (I_L^2 + Q_L^2) \\
&= \left(\frac{A}{\sqrt{2}}M_E D \frac{\sin(\pi\Delta fT)}{\pi\Delta fT}\right)^2 [R(\delta\tau - \delta)^2 - R(\delta\tau + \delta)^2] \\
B_3(\delta\tau) &= \sqrt{I_E^2 + Q_E^2} - \sqrt{I_L^2 + Q_L^2} \\
&= \left(\frac{A}{\sqrt{2}}M_E D \frac{\sin(\pi\Delta fT)}{\pi\Delta fT}\right)[R(\delta\tau - \delta) - R(\delta\tau + \delta)]
\end{aligned} \tag{2.10}$$

Assuming that

$$A_{dis} = \frac{A}{\sqrt{2}}M_E D \frac{\sin(\pi\Delta fT)}{\pi\Delta fT} \tag{2.11}$$

and inserting Equations (2.7) and (2.11) into (2.10), when $|\delta\tau| \leq \delta$, yields

$$\begin{aligned}
B_1(\delta\tau) &= (I_E - I_L)I_P + (Q_E - Q_L)Q_P \\
&= A_{dis}^2 [R(\delta\tau - \delta) - R(\delta\tau + \delta)]R(\delta\tau) \\
&= A_{dis}^2 [2\delta\tau(1 - |\delta\tau|)] \\
B_2(\delta\tau) &= (I_E^2 + Q_E^2) - (I_L^2 + Q_L^2) \\
&= (A_{dis})^2 [R(\delta\tau - \delta)^2 - R(\delta\tau + \delta)^2] \\
&= (A_{dis})^2 [4\delta\tau - 4\delta\tau\delta]
\end{aligned} \tag{2.12}$$

$$\begin{aligned}
B_3(\delta\tau) &= \sqrt{I_E^2 + Q_E^2} - \sqrt{I_L^2 + Q_L^2} \\
&= A_{dis} [R(\delta\tau - \delta) - R(\delta\tau + \delta)] \\
&= A_{dis} [2\delta\tau]
\end{aligned}$$

The discriminator gain is defined as the slope of B at $\delta\tau = 0$. So the processing gains of the three discriminators are:

$$\begin{aligned} B'_1(\delta\tau = 0) &= A_{dis}^2 \cdot [2] \\ B'_2(\delta\tau = 0) &= A_{dis}^2 \cdot [4 - 4\delta] \quad . \\ B'_3(\delta\tau = 0) &= A_{dis} \cdot [2] \end{aligned} \tag{2.13}$$

Equation (2.13) shows clearly that the discriminator gain of discriminators 1 and 3 is independent of the correlator spacing δ . The gain for discriminator 2 increases when correlator spacing δ decreases. When $\delta = 0.25$ chip, $B'_2(\delta\tau = 0) = 3 \cdot A_{dis}^2$. When $\delta = 0.1$ chip, $B'_2(\delta\tau = 0) = 3.6 \cdot A_{dis}^2$. In section 2.2.4 it is suggested that Narrow Correlator™ spacing is preferred in order to reduce multipath and thermal noise, so discriminator 2 is selected to maximize the processing gain.

Signal power in urban canyons or indoor environments might change very quickly due to receiver motion or signal masking due to the presence of buildings. In order to remove the effect of signal power swing on signal tracking, the GPS signal sign for code tracking in DLL should be normalized. In this research, three normalization algorithms are presented below. Please note, only the discriminator 2 is analyzed herein:

$$\begin{aligned}
 Norm_1(\delta\tau) &= \frac{B2}{(I_E^2 + Q_E^2) + (I_L^2 + Q_L^2)} = \frac{(I_E^2 + Q_E^2) - (I_L^2 + Q_L^2)}{(I_E^2 + Q_E^2) + (I_L^2 + Q_L^2)} \\
 Norm_2(\delta\tau) &= \frac{B2}{(I_p^2 + Q_p^2)} = \frac{(I_E^2 + Q_E^2) - (I_L^2 + Q_L^2)}{(I_p^2 + Q_p^2)}, \\
 Norm_3(\delta\tau) &= \frac{B2}{SNR \frac{M_E N_0}{T_s}} = \frac{(I_E^2 + Q_E^2) - (I_L^2 + Q_L^2)}{SNR \frac{M_E N_0}{T_s}}
 \end{aligned} \tag{2.14}$$

where T_s is the sample period, M_E is the number of samples accumulated during the integration time T and N_0 is the noise power density.

Instead of using $\frac{M_E N_0}{T_s}$ for the normalization method 3 in Equation (2.14), one can de-spread the incoming GPS signal with PRN 37 to estimate the noise power; PRN 37 is reserved for ground testing and is not being broadcasted by any GPS satellite. This approach was adopted in the first generation software GPS receiver GNSS_SoftRxTM developed by Ma & Lachapelle (2004).

Inserting Equation (2.8) into (2.14) yields

$$\begin{aligned}
 Norm_1(\delta\tau) &= \frac{2\delta\tau - 2\delta\tau\delta}{1 - 2\delta + \delta^2 + \delta\tau^2} \\
 Norm_2(\delta\tau) &= \frac{4\delta\tau - 4\delta\tau\delta}{1 - 2|\delta\tau| + \delta\tau^2} \\
 Norm_3(\delta\tau) &= 4\delta\tau - 4\delta\tau\delta
 \end{aligned} \tag{2.15}$$

So the gain of discriminator 2 after normalization is

$$\begin{aligned}
 B'_{norm1}(\delta\tau = 0) &= \frac{2 - 2\delta}{1 - 2\delta + \delta^2} \\
 B'_{norm2}(\delta\tau = 0) &= 4 - 4\delta \\
 B'_{norm3}(\delta\tau = 0) &= 4 - 4\delta
 \end{aligned} \tag{2.16}$$

Figure 2.7 shows the processing gains after discriminator normalization. From this figure, it is clear that the processing gain of normalized discriminator 2 and 3 increases when correlator spacing δ decreases. The processing gain of normalized discriminator 1, however, decreases when the correlator spacing δ decreases.

Figure 2.8 shows the normalized discriminator output as a function of the code delay error. In Figure 2.8, 0.1/0.25/0.5 chips of correlator spacing are used, respectively. It is clear that, when the correlator spacing is 0.1 or 0.25 chip, the normalization method 2 yields the best discriminator performance. When the correlator spacing is 0.5 chip, the normalization method 2 is somewhat worse than method 1. From Figure 2.7, however, it is known that the use of normalization method 1 will yield a smaller discriminator gain if a narrower correlator spacing is used. So, it is clear that normalization method 2 provides the best performance if a narrow correlator spacing is required.

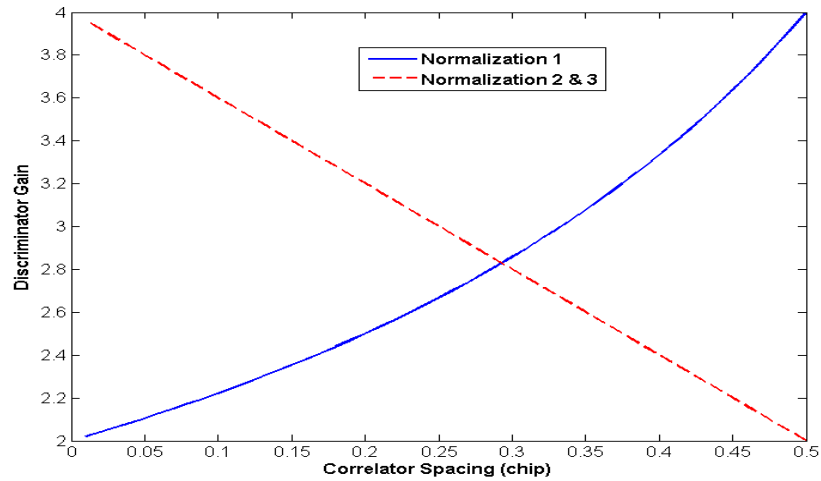


Figure 2.7 Processing Gains after Discriminator Normalization

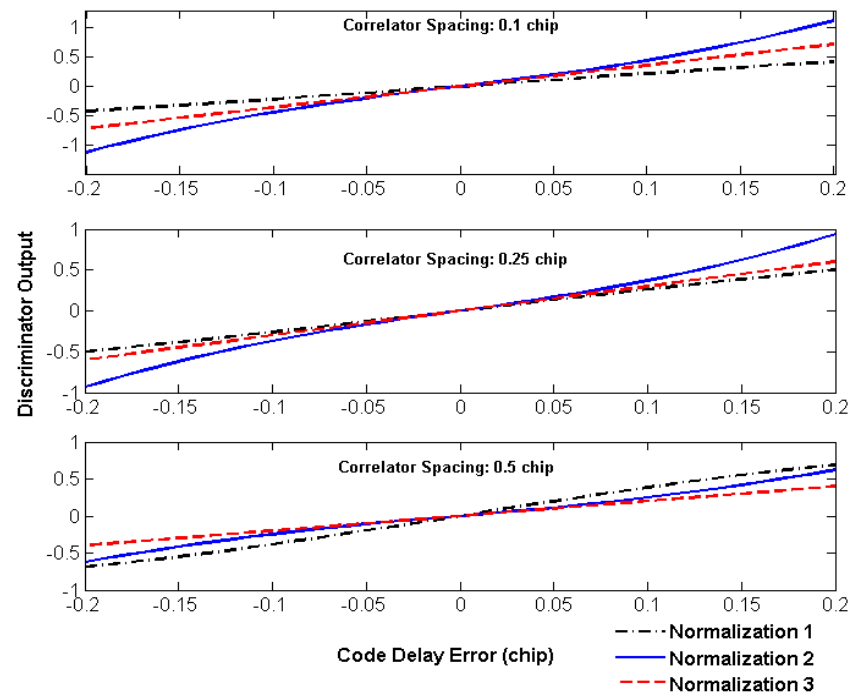


Figure 2.8 Discriminator Products after Normalization

In conclusion, it is suggested to use a normalized Early-Minus-Late discriminator for code tracking. The track arm of the correlator can be set 1/2 chip (or less) early of the late arm. The normalized discriminator is given by

$$B(\delta\tau) = \frac{(I_E^2 + Q_E^2) - (I_L^2 + Q_L^2)}{(I_P^2 + Q_P^2)} . \quad (2.17)$$

i.e., when the loop is locked, the track arm will be nominally 1/4 chip (or less) early and the late arm 1/4 chip (or less) late of the actual.

2.2.3 Selection of Loop Filter for DLL

Appendix A derives the closed-loop transfer function for signal tracking loop systems and illustrates the relationship between the loop characteristics and loop filter parameters. Table 2.1 summarizes the characteristics of different loop filters (Kaplan 1996).

Table 2.1 Characteristics of Different Loop Filters

Loop Order	Noise Bandwidth	Typical Filter Values	Steady-State Error
1	$\frac{\omega_n}{4}$	$B_n = 0.25\omega_n$	$R_e = \frac{dR}{dt}$
2	$\frac{\omega_n(1 + \alpha_2^2)}{4\alpha_2}$	$\alpha_2 = 1.414$ $B_n = 0.53\omega_n$	$R_e = \frac{dR^2}{dt^2}$
3	$\frac{\omega_n(\alpha_3 b_3^2 + \alpha_3^2 - b_3)}{4(\alpha_3 b_3 - 1)}$	$\alpha_3 = 1.1$ $b_3 = 2.4$ $B_n = 0.7845\omega_n$	$R_e = \frac{dR^3}{dt^3}$

For a second-order system, as shown in Equation (A.11), (A.12) and (A.13) in Appendix A, the Pull-in range $\Delta\omega_P$, Pull-in time T_P (from $\Delta\omega_0$) and Pull-out range $\Delta\omega_{P0}$ are

$$\frac{4\sqrt{2\xi\omega_n K_\phi K_0 - \omega_n^2}}{\pi}, \frac{\pi^2 \Delta\omega_0^2}{16\xi\omega_n^3} \text{ and } 1.8\omega_n(\xi + 1),$$

respectively. In order to design a stable control system with wider pull-in/pull-out ranges and a shorter pull-in time, a higher loop natural frequency ω_n is preferred. It is the same with a first-order or third-order system. However, Table 2.1 shows that the same natural frequency ω_n will lead to different noise bandwidth B_n . When the natural frequency ω_n is

the same, a first-order system will yield the narrowest noise bandwidth and a third-order system will yield the widest noise bandwidth. It is well known that the narrower noise bandwidth that a DLL adopts, the less thermal noise the receiver will output. So, in loop filter design, although a higher order system normally provides better steady-state error performance, as shown in Table 2.1, a lower order system usually provides shorter response time, better system stability and less thermal noise.

2.2.4 DLL Tracking Errors

DLL tracking error sources consist mostly of thermal noise, multipath and receiver dynamics (Kaplan 1996).

In order to suppress the DLL tracking error caused by multipath, a narrow correlator technology can be used to minimize this kind of error by reducing the correlator spacing, which, when multiplied by the reflected signal coefficient, bounds the maximum multipath envelope (e.g. Raquet 2004). As for the receiver dynamic stress error, because the PLL-aided DLL design efficiently decreases the dynamic of DLL to as small as less than 0.1 Hz, the dynamic stress error can be ignored (Kaplan 1996).

The last and most important portion of DLL tracking error caused by thermal noise is (Kaplan 1996)

$$\sigma_{\text{t}_{\text{DLL}}} = \sqrt{\frac{2\delta^2 B_n}{C/N_o} [2(1-\delta) + \frac{4F\delta}{T \cdot C/N_o}]} , \quad (2.18)$$

where δ is the correlator spacing between early and prompt or prompt and late, B_n is the noise bandwidth, C/N_o is the carrier-to-noise ratio in unit of dB-Hz, and T is the pre-detection integration time. F is a DLL discriminator factor and has a value of 1 for an early/late discriminator or a value of 0.5 for a dot discriminator. With Equation (2.18), Table 2.2 lists the tracking errors with nine combinations of different parameter combinations when the C/N_o is 15 dB-Hz. Please note that, the thermal noise listed in Table 2.2 is theoretical value. In real applications, the thermal noise will be a little bit larger, since the low pass filter in tracking loops can not be designed perfectly.

The first three combinations use the same correlator spacing and pre-detection integration time. The difference is that different noise bandwidths are used to study the effect of noise bandwidth on the DLL tracking error. In combination 3, 4 and 5, the correlator spacing parameter is tested for the same purpose. Combinations 5, 6 and 7 are used to investigate the pre-detection integration time. From the results of combinations 1 to 3, one can see that decreasing the noise bandwidth can significantly decrease the DLL thermal noise error. Decreasing correlator spacing, as shown in combination 3 to 5, can also decrease the thermal noise error. It can however decrease the DLL tracking threshold simultaneously. Combinations 4 and 5 show that the DLL tracking capability is only improved marginally when the correlator spacing is decreased from 0.2 chips to 0.1 chips. Increasing pre-detection integration time in combination 5 to 7 can also decrease thermal noise. When the integration time is above 0.1 s, however, the improvement is very limited.

Table 2.2 C/N_o = 15 dB-Hz, Early/Late Discriminator

Group No.	Noise Bandwidth (Hz)	Correlator Spacing (chip)	Pre-detection Integration Time (s)	Tracking Threshold (chip)	Thermal Noise (chip)
1	1	0.5	0.02	0.167	0.715
2	0.5	0.5	0.02	0.167	0.506
3	0.1	0.5	0.02	0.167	0.226
4	0.1	0.2	0.02	0.067	0.067
5	0.1	0.1	0.02	0.033	0.029
6	0.1	0.1	0.1	0.033	0.024
7	0.1	0.1	1	0.033	0.022
8	0.1	0.1	0.1	0.033	0.024
9	0.05	0.1	0.1	0.033	0.017

From the above analysis, the following strategies can be used in order to choose the proper DLL parameters:

1. A noise bandwidth must be as narrow as possible
2. A moderate pre-detection integration time must coincide with the narrow noise bandwidth
3. A narrow correlator spacing must be used in order to enhance tracking performance in multipath environments

In Table 2.2, Combinations 8 and 9 show the two sets of proper DLL parameters for weak signal tracking that are used in this research.

2.3 Design of GPS Receiver Frequency Locked Loop (FLL)

2.3.1 Transition from Acquisition to FLL

After signal acquisition, the accuracy of carrier frequency is a few hundred Hertz, depending on the width of frequency search bin used in signal acquisition. From Equations (A.11) and (A.13) in Appendix A, it is clear that the pull-in and pull-out ranges are both at the same level of a few Hertz, assuming that the natural frequency of FLL loop filters is a few Hertz.

In order to bridge the acquisition and FLL, a so-called two-step strategy is applied regularly: a FLL is initially achieved by using a coarse tracking discriminator, e.g. four-quadrant frequency discriminator (Mitel 1998). Then a fine discriminator, such as a cross-product discriminator, is used for fine carrier tracking, followed by a low-pass loop filter to remove the high frequency portion of the incoming noise.

Another method called analytic frequency refinement presented by Ma & Lachapelle (2004) achieves the objective by refining the frequency from the acquisition stage. Only the fine FLL is needed. This method is used in the software receiver GNSS_SoftRxTM (Ma & Lachapelle 2004).

2.3.2 Cross-Product Discriminator for Fine FLL

The Cross-Product Discriminator for fine FLL can be represented as:

$$\delta f_i = (NormI_{i-1} \cdot NormQ_i - NormI_i \cdot NormQ_{i-1}) sign(NormI_{i-1} \cdot NormI_i + NormQ_i \cdot NormQ_{i-1}) , \quad (2.19)$$

where, $NormI$ and $NormQ$ are the normalized I and Q components of the GPS signal and, there are $NormI = D \cos(\phi)$ and $NormQ = D \sin(\phi)$.

Rearranging Equation (2.19) leads to

$$\begin{aligned} \delta f_i &= (NormI_{i-1} \cdot NormQ_i - NormI_i \cdot NormQ_{i-1}) sign(NormI_{i-1} \cdot NormI_i + NormQ_i \cdot NormQ_{i-1}) \\ &= D_{i-1} \cdot D_i \cdot \sin(\phi_i - \phi_{i-1}) \cdot sign(D_{i-1} \cdot D_i \cdot \cos(\phi_i - \phi_{i-1})) \\ &= D_{i-1} \cdot D_i \cdot \sin(\phi_i - \phi_{i-1}) \cdot sign(D_{i-1} \cdot D_i) \\ &= |D_{i-1} \cdot D_i| \cdot \sin(\phi_i - \phi_{i-1}) \propto (\phi_i - \phi_{i-1}) \end{aligned} . \quad (2.20)$$

Equation (2.20) shows that the cross-product discriminator is proportional to the frequency difference between the incoming and local signal replica.

As discussed in Section 2.1.1, the FLL has a lower tracking threshold as compared to a PLL. Therefore, it keeps lock on the incoming signal after the PLL has lost lock. This occurs often in urban canyons or indoor environments where the signal power is very low.

To decode the navigation data bit from a FLL directly when the PLL has lost lock, a three-step strategy is discussed in Appendix B.

2.3.3 FLL Tracking Errors

In a FLL, the dominant sources of frequency errors are thermal noise, frequency jitter and dynamic stress. Kaplan (1996) argues that the FLL tracking threshold is 90° in one pre-detection integration time T . This threshold is also shown clearly in Figure C.1 in Appendix C. The rule-of-thumb for the FLL tracking threshold is as follows:

$$3\sigma_{FLL} = 3\sigma_{FLL,t} + f_e \leq \frac{90}{360T} = \frac{0.25}{T} , \quad (2.21)$$

where $\sigma_{FLL,t}$ is 1- σ thermal noise frequency jitter, and f_e is the dynamic stress error in the FLL tracking loop.

2.3.3.1 FLL Thermal Noise

The major error source comes from the FLL tracking loop jitter due to thermal noise, which can be expressed as (Kaplan 1996):

$$\sigma_{FLL,t} = \frac{1}{2\pi T} \sqrt{\frac{4FB_n}{C/N_o} \left(1 + \frac{1}{TC/N_o}\right)} \text{ (Hz)} , \quad (2.22)$$

where

$F = 1$ for a high C/N_o

$= 2$ near the threshold.

Based on Equation (2.22), Table 2.3 lists the FLL frequency jitter with seven combinations of different parameter combinations.

Table 2.3 FLL Thermal Noise Frequency Jitter with Different Parameters

Group No.	Noise Bandwidth (Hz)	Pre-detection Integration Time (s)	C/N_o (dB-Hz)	Thermal Noise (Hz)	Tracking Error Threshold (Hz)
1	10	0.001	15	1446	83
2	5	0.001	15	1022	83
3	1	0.001	15	457	83
4	1	0.01	15	16	8.3
5	1	0.1	15	0.9	0.8
6	1	1	15	0.08	0.08
7	1	0.1	20	0.4	0.8

In Table 2.3, the first three combinations use the same C/N_o values and pre-detection integration time intervals. The difference is that different noise bandwidths are adopted to study the effect of noise bandwidth on the FLL thermal noise jitter. In Combinations 3, 4, 5 and 6, the pre-detection integration time is tested for the same purpose. From the results of Combinations 1 to 3, one can observe that decreasing the noise bandwidth can significantly decrease the FLL thermal noise error. Increasing pre-detection integration time as shown in Combinations 3 to 6 can also decrease the thermal noise error. It can however also decrease the FLL tracking threshold simultaneously.

Finally, combination 7 demonstrates that a combination of 1-Hz noise bandwidth and 0.1 s pre-detection integration time can safely lock GPS signal as low as 20 dB-Hz. This combination is used in this work for the proposed receiver.

2.3.3.2 Receiver Dynamics and Resulting Dynamic Stress Error

In Section 2.1.2, it was stated that receiver dynamics and oscillator instability are the two most important error sources of Doppler Error Δf . That error is caused by receiver dynamics affecting the signal tracked in two ways: it changes the signal's amplitude characterized by the function $\frac{\sin(\pi\Delta f T)}{\pi\Delta f T}$ and the signal's phase characterized by the sinusoid function $\sin(\cdot)$.

The signal power loss caused by the Doppler error is illustrated in Figure 2.4 and Figure 2.5. Because of Δf , the Pre-detection Integration Time (PIT) used in signal tracking cannot be long to avoid further signal power losses. Nevertheless, when an external system can accurately sense the receiver's dynamics, the system, e.g. INS, can be used to assist the receiver significantly to decrease the Doppler error caused by receiver dynamics and, therefore, increase Pre-detection Integration Time (PIT) to achieve much higher tracking sensitivity.

Receiver dynamics not only decrease the signal power, but also affect the phase rotation rate of the signal. This change is characterized with the sinusoid function

$\sin(\pi\Delta f T + \phi_0)$ shown in Equation (2.6). In the frequency domain, the existing Doppler error Δf means that the central frequency of the incoming signal is shifted from 0 Hz to Δf Hz. Therefore, the signal tracking loop bandwidth must be larger than Δf . It is known that a wide bandwidth loop filter allows more thermal noise coming into the tracking loops and, thus, leads to lower SNR. Furthermore, in the case of digital carrier phase tracking loops, in order to sufficiently limit the phase rotation during the pre-detection integration time, a small Doppler error Δf is required to use the longer coherent integration time T . This limitation can be written as:

$$\Delta\phi = 360 \times \Delta f \times T \leq 90^\circ. \quad (2.23)$$

Besides Equation (2.23), receiver dynamics also introduce a dynamic stress error. When the GPS receiver is not used for high dynamic applications or if there is external aiding information available to compensate for receiver dynamics, the FLL dynamic stress error can be ignored.

2.3.3.3 Oscillator Instability and Resulting Oscillator Frequency Jitter

The clock error caused by receiver oscillator instability can be divided into turn-on bias, in-run drift, and remaining colored noise components, the latter being characterized by the Allan Variance (Alban et al. 2003). Although oscillator performances for long averaging time are significantly different for different oscillators such as Crystal Oscillators (XO), Temperature Compensated Crystal Oscillators (TCXO), Oven Controlled Crystal Oscillators (OCXO) and Atomic oscillators, the stability performance

of crystal quartz oscillators is the same or better than that of atomic standards for short averaging time periods. For example, the Allan standard deviation of a low-cost quartz crystal oscillator over 0.1s or 1 s is typically between 10^{-9} and 10^{-10} (Raquet 2004). Nevertheless, this parameter over longer time periods decreases to 10^{-4} to 10^{-6} , namely 100 ppm to 1 ppm.

As discussed in Section 2.1.2, oscillator instability is another major source of Doppler error Δf . Its effects on carrier phase tracking are placed into two combinations: the reference oscillator vibration and Allan deviation-induced frequency jitter. For a regular commercial receiver, the FLL tracking error caused by the reference oscillator is small and can be ignored (Kaplan 1996).

However, for a digital GPS receiver, besides the above small errors, there is additional frequency noise caused by oscillator instability. Similar to Equation (2.23), the accumulated carrier phase error θ_T in the pre-detection integration time of a FLL has to be taken care of carefully in order to ensure that it is under the tracking threshold of 30° .

$$\theta_T = 360 \times \sigma_A(\tau) \cdot f_L \cdot T \leq 30^\circ , \quad (2.24)$$

where, $\sigma_A(\tau)$ is the root of Allan variance of the receiver oscillator for the short-term gate time τ .

2.3.3.4 Total FLL Tracking Error in a Digital FLL

Based on the above analysis, the total FLL tracking error in a digital FLL can be written as follows:

$$3\sigma_{FLL} = \Delta f_d \cdot T + 3 \cdot \sqrt{\sigma_{FLL,t}^2 + (\sigma_A \cdot f_L)^2} \cdot T + f_e \cdot T \leq \frac{90}{360} = 0.25. \quad (2.25)$$

Comparing Equation (2.25) with Equation (2.21), it is clear that the FLL tracking error in a digital FLL is larger than the theoretical error in a continuous system.

2.4 Design of Receiver Phase Locked Loops

Depending on different discriminators used in the PLLs, there are two classes of PLLs: pure PLLs and Costas PLLs. Costas PLLs adopt discriminators, which are insensitive to 180° bit reversals. Costas PLLs, however, suffer 6 dB tracking-sensitivity loss when compared to pure PLLs (Kaplan 1996). If there were no 50-Hz navigation data modulated on the signal, a pure PLL would be more effective than Costas PLLs in terms of processing gain. Thus, pure PLLs will be used with the GPS L5 and Galileo frequencies, thanks to the presence of dataless pilot signals. The existence of the navigation bits however, makes Costas PLL necessary for L1 signal tracking.

Therefore, in AGPS, since navigation data bits can be obtained from outside sources, pure PLLs are recommended in these applications. Furthermore, in this study, the author proposes two new FLL algorithms that can achieve an additional 6 dB

sensitivity gain in theory as compared to the gain achieved by traditional FLLs. Thus, they are more suitable for these applications. More details about these FLLs can be found in Appendix C.

In this section, four commonly used PLL discriminators are analyzed in terms of their processing gain and normalization effects. Also, PLL thermal noise, oscillator phase noise and dynamic stress errors are analyzed in order to select carefully the best performance set of parameters including correlator spacing, pre-detection integration time, and filter order.

2.4.1 PLL Discriminator and Normalization

As shown in Equation (2.6), the incoming GPS signal after integration and dump is written as

$$\begin{aligned} I_P &= \frac{A}{\sqrt{2}} M_E DR(\delta\tau) \frac{\sin(\pi\Delta f T)}{\pi\Delta f T} \cos(\pi\Delta f T + \phi_0) \\ Q_P &= \frac{A}{\sqrt{2}} M_E DR(\delta\tau) \frac{\sin(\pi\Delta f T)}{\pi\Delta f T} \sin(\pi\Delta f T + \phi_0) \end{aligned} \quad (2.26)$$

The following four PLL discriminators are frequently used (Kaplan 1996):

$$\begin{aligned}
D(1) &= \frac{\text{sign}(I_p) \cdot Q_p}{\sqrt{I_p^2 + Q_p^2}} \\
D(2) &= \frac{2 \cdot I_p \cdot Q_p}{I_p^2 + Q_p^2} \\
D(3) &= \frac{Q_p}{I_p} \\
D(4) &= \text{ATAN}\left(\frac{Q_p}{I_p}\right)
\end{aligned} \tag{2.27}$$

Assuming a phase error bound of $-90^\circ \leq \phi_i = \pi \Delta f_i T + \phi_0 \leq 90^\circ$, and inserting Equation (2.26) into (2.27) yields

$$\begin{aligned}
D(1) &= \frac{\text{sign}(I_p) \cdot Q_p}{\sqrt{I_p^2 + Q_p^2}} = \sin(\phi_i) \\
D(2) &= \frac{2 \cdot I_p \cdot Q_p}{I_p^2 + Q_p^2} = \sin(2\phi_i) \\
D(3) &= \frac{Q_p}{I_p} = \text{TAN}(\phi_i) \\
D(4) &= \text{ATAN}\left(\frac{Q_p}{I_p}\right) = \phi_i
\end{aligned} \tag{2.28}$$

Their discriminator gains are

$$\begin{aligned}
D(1)' &= \cos(\phi_i) \Big|_{\phi=0} = 1 \\
D(2)' &= 2 \cdot \cos(\phi_i) \Big|_{\phi=0} = 2 \\
D(3)' &= \frac{1}{\cos(\phi_i)^2} \Bigg|_{\phi=0} = 1 \\
D(4)' &= 1
\end{aligned} \tag{2.29}$$

Figure 2.9 shows the four discriminator products as a function of the carrier phase errors.

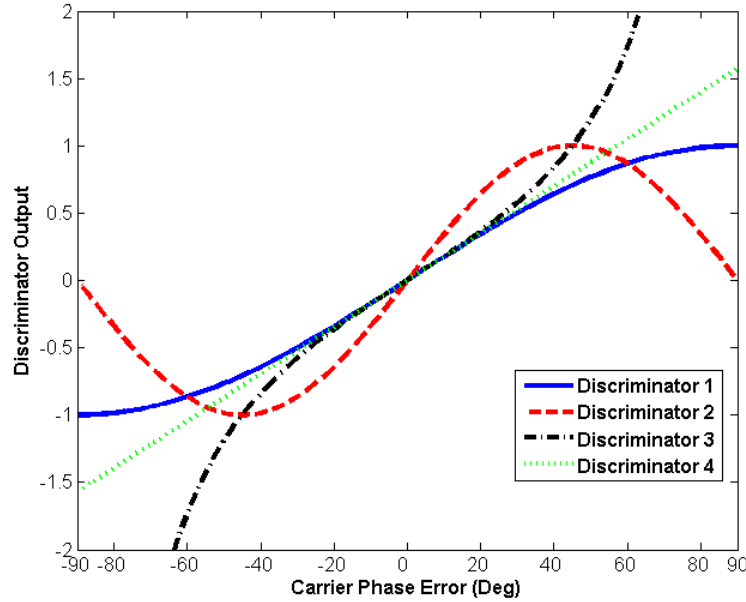


Figure 2.9 Discriminator Corrections with Respect to Carrier Phase Error

From Figure 2.9, one can see that the two-quadrant arctangent discriminator D(4) has a balanced performance for both high and low SNR situations. Its processing gain is not dependent on its carrier phase error input. The dot product discriminator D(2) shows good performance when the phase error is in the range of $\pm 45^\circ$. The red line in Figure 2.9 shows a slope of close to 2 at the centre while others are 1. With the phase error increasing, however, the performance of D(2) decreases quickly. For this reason, the tracking threshold of PLL is normally set 45° (or 15° for 1σ).

$D(1)$ and $D(2)$ are normalized discriminators as presented in Equation (2.28).

When the C/N_0 is very low, the thermal noise will distort the discriminator slope during normalization. When the incoming signal is very weak, the thermal noise included in the signal becomes significant so that the signal power used to perform discriminator normalization changes to

$$P = (I + n_I)^2 + (Q + n_Q)^2 \approx (I^2 + Q^2) + (n_I^2 + n_Q^2) \neq (I^2 + Q^2), \quad (2.30)$$

where n_I and n_Q are the in-phase (I), and quadra-phase (Q) thermal noise.

Therefore, in weak signal environments, how to normalize signal sign properly in DLL/FLL/PLL is a major issue and will affect the tracking sensitivity significantly (Julien 2005).

In order to avoid the normalization under weak signal tracking, the two-quadrant arctangent discriminator $D(4)$ is chosen as the PLL discriminator of the receiver prototype in this study.

2.4.2 Design of FLL-Assisted PLL

Although a FLL cannot provide the carrier phase as accurately as a PLL, it offers superior dynamic performance, robustness and insensitivity to interference in comparison to a PLL. It is very common to use a FLL-assisted PLL strategy (Kaplan 1996). This section discusses how to design a FLL-assisted PLL.

Refer to Appendix A, for a second-order FLL-assisted third-order PLL, the loop output can be written as

$$y_i = (2y_{i-1} - y_{i-2}) + (\omega_{np}^3 T^2 + a_3 \omega_{np}^2 T + b_3 \omega_{np}) DP_i - (a_3 \omega_{np}^2 T + 2b_3 \omega_{np}) DP_{i-1} + (b_3 \omega_{np}) DP_{i-2}, \quad (2.31)$$

$$+ (\omega_{nf}^2 T^2 + a_2 \omega_{nf} T) DF_i - (a_2 \omega_{nf} T) DF_{i-1}$$

where ω_{np} is the PLL nominal frequency, ω_{nf} is the FLL nominal frequency, DP is the PLL discriminator output and DF is the FLL discriminator output.

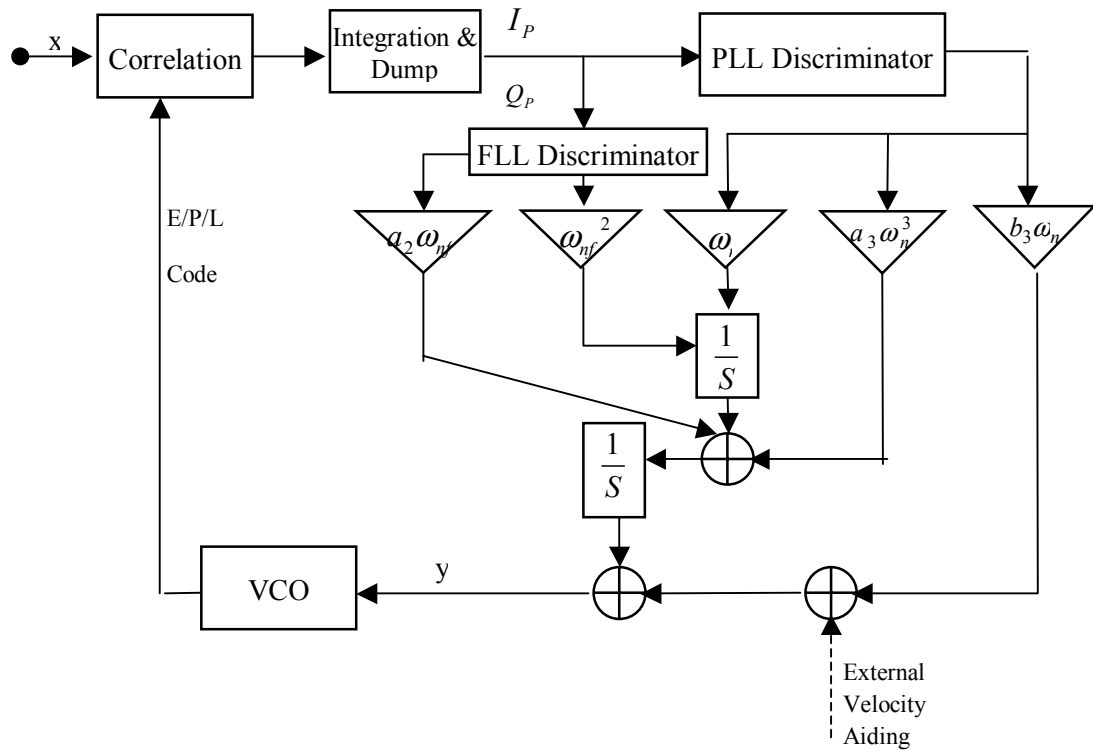


Figure 2.10 Architecture of a Second-Order FLL-Assisted Third-Order PLL

Similarly, for a first-order FLL-aided second-order PLL, the output can be expressed as

$$y_i = y_{i-1} + (T\omega_{np}^2 + a_2\omega_{np})DP_i - (a_2\omega_{np})DP_{i-1} + (\omega_{nf}T)DF_{i-1} . \quad (2.32)$$

2.4.3 PLL Tracking Errors

The dominant tracking error sources of a PLL are thermal noise, oscillator phase noise and dynamic stress error (Kaplan 1996).

2.4.3.1 PLL Thermal Noise

The PLL thermal noise is (Kaplan 1996)

$$\sigma_{PLL_t} = \frac{360}{2\pi} \sqrt{\frac{B_n}{C/N_o} \left(1 + \frac{1}{2TC/N_o}\right)} \text{ (deg)} . \quad (2.33)$$

Table 2.4 PLL Thermal Noise with Different Parameters

Group No.	Noise Bandwidth (Hz)	Pre-detection integration time (s)	C/N _o (dB-Hz)	Dynamics Uncertainty (degree)	Thermal Noise (degree)
1	10	0.001	15	0.18	132.1
2	5	0.001	15	0.18	93.4
3	1	0.001	15	0.18	41.8
4	1	0.01	15	1.8	16.4
5	1	0.1	15	18	11.0
6	1	0.02	15	3.6	13.6
7	1	0.02	20	3.6	6.4

In order to study the effect of different parameters on PLL thermal noise, Table 2.4, which is based on Equation (2.33), gives the PLL thermal noise for seven different parameter combinations. In Table 2.4, the Doppler error $\Delta f = 0.5$ Hz is used.

In this table, the first three combinations use the same Carrier-to-Noise ratio (C/N_o) and pre-detection integration time. The difference is that different noise bandwidths are adopted to study the effect of noise bandwidth on the PLL thermal noise. In Combinations 3, 4 and 5, the pre-detection integration time is tested for the same purpose. From the results of Combinations 1 to 3, it is clear that the most efficient approach to decrease the PLL thermal noise is to decrease the noise bandwidth. The choice of noise bandwidth however, is restricted by receiver dynamics uncertainty and, thus, cannot be decreased endlessly. Increasing pre-detection integration time, as shown in combinations 3 to 5, also can decrease the thermal noise error. Unfortunately, since digital tracking loops are normally used in a receiver, when the pre-detection integration time is increased, receiver dynamics uncertainty in the integration time increases and leads to an unacceptably high phase error.

If the receiver dynamics uncertainty is 0.1 m/s or 0.5 Hz, a reasonable set of parameters for the PLL is 1 Hz bandwidth and 20 ms integration time, which are shown as Combinations 6 and 7 in Table 2.4. When this set of parameters is used, the lowest signal that can be tracked safely is 20 dB-Hz.

2.4.3.2 Receiver Dynamics and Resulting Dynamic Stress Error

As discussed in section 2.3.3.2 and illustrated in Equation (2.23), the effect of a Doppler error Δf on PLL tracking is as follows:

$$\Delta\phi = 360 \times \Delta f \times T . \quad (2.34)$$

Besides Equation (2.34), receiver dynamics also introduce a dynamic stress error. Table 2.5 shows the dynamic stress error, namely the PLL steady-state error. The PLL steady-state error depends on both the loop order and receiver dynamics. In order to decrease the dynamic stress error, the first important task is to determine the level of dynamics and the kind of dynamics the receiver is experiencing, e.g., is the vehicle moving smoothly with high acceleration and small jerk? Or is one dealing with an aircraft wing vibrating with small acceleration and high jerk?

Table 2.5 PLL Dynamic Stress Error

Loop order	Steady-state error
1	$R_e = \frac{dR}{dt} = 0.25 \frac{dR}{B_n}$
2	$R_e = \frac{dR^2}{dt^2} = 0.2809 \frac{dR^2}{B_n^2}$
3	$R_e = \frac{dR^3}{dt^3} = 0.4828 \frac{dR^3}{B_n^3}$

2.4.3.3 Oscillator instability and Resulting Oscillator Phase Noise

As discussed in Section 2.1.2, oscillator instability is another major source of Doppler error Δf . Its effects on carrier phase tracking are placed into two combinations: vibration induced oscillator phase noise and Allan deviation-introduced oscillator phase noise. For a regular commercial receiver, Allan deviation oscillator phase noise is the primary oscillator noise (Kaplan 1996).

Allan deviation oscillator phase noise θ_A can be expressed as

$$\theta_A = a \frac{\sigma_A(\tau) f_L}{B_n} \text{ (deg)} \quad (2.35)$$

where, a is the scale factor, with $a=144$ for a second-order loop and $a=160$ for a third-order loop, $\sigma_A(\tau)$ is the root of Allan variance for the short-term gate time τ , which is equal to $\frac{1}{B_n}$, B_n is the noise bandwidth of the PLL loop filter, and f_L is the L1 frequency.

For a digital PLL, and as per Equation (2.24), the accumulated carrier phase error θ_T in the pre-detection integration time interval has to be taken care of carefully in order to ensure that it is under the tracking threshold of 15° :

$$\theta_T = 360 \times \sigma_A(\tau) \cdot f_L \cdot T \leq 15^\circ \quad (2.36)$$

Table 2.6 PLL Allan Oscillator Phase Noise with Different Parameters

Group No.	Noise Bandwidth (Hz)	The Root of Allan Variance	Pre-detection Integration Time (s)	Allan Deviation Oscillator Phase Noise θ_A (degree)	Accumulated Oscillator Phase Noise θ_T (degree)
1	10	10^{-10}	0.001	2.52	0.06
2	5	10^{-10}	0.001	5.04	0.06
3	1	10^{-10}	0.001	25.21	0.06
4	1	10^{-9}	0.001	250.21	0.06
5	5	10^{-10}	0.001	5.04	0.06
6	5	10^{-10}	0.01	5.04	0.57
7	5	10^{-10}	0.1	5.04	5.67

In order to analyze the effect of different parameters on the PLL Allan oscillator phase noise, Table 2.6 lists that noise for seven combinations of parameter combinations. In this table, the first three combinations use the same oscillator Allan variance and pre-detection integration time. The difference is that different noise bandwidths are adopted to study the effect of noise bandwidth. In Combinations 3 and 4, different oscillator Allan variances are tested for the same purpose. Combinations 5, 6 and 7 are used to investigate the effect of parameter pre-detection integration time intervals. From the results of combinations 1 to 4, one sees that PLL oscillator phase noise increases when noise bandwidth decreases or oscillator Allan variance increases. Increasing the pre-detection integration time interval as shown in combinations 5 to 7 does not affect the PLL Allan oscillator phase noise. A longer integration time, however, will lead to higher

accumulated oscillator phase noise in a digital GPS receiver and this will increase PLL tracking errors caused by oscillator instability.

In conclusion, combination 7 gives a set of balanced receiver parameters.

2.4.3.4 Total PLL Tracking Error in a Digital PLL

Based on the above analysis, the total PLL tracking error in a digital PLL can be summarized as follows:

$$\sigma_{PLL} = \Delta f \cdot T \cdot 360 + \sqrt{\sigma_{PLL_t}^2 + (\sigma_A \cdot f_L \cdot T)^2 + \theta_A^2} + \frac{\theta_e}{3} , \quad (2.37)$$

where, Δf is the Doppler error, σ_{PLL_t} is the PLL thermal noise, θ_A is Allan deviation oscillator phase noise and θ_e is PLL dynamic stress error.

2.5 High Sensitivity GPS Receiver for Weak Signal Navigation

This section presents a thorough study of HSGPS, followed with a discussion of the navigation data wiping off. This data wipe off technology is used in the prototype INS-assisted HSGPS receiver proposed in the sequel.

2.5.1 High Sensitivity GPS (HSGPS) Overview

HSGPS is a receiver that can increase processing gain beyond standard levels to receive and measure weak GPS signals. Typical HSGPS implementations rely on non-coherent integration over periods longer than 20 ms (Watson 2005). Coherent integration time cannot be very long due to the unknown navigation data bit reversal, user dynamics uncertainty and oscillator-induced frequency noise. Nevertheless, some technologies such as AGPS (Karunananayake et al 2004), GPS receiver self-prediction, and external-aiding can somewhat deal with this limit.

In this research, the objective is to improve receiver tracking performance independent of AGPS. Therefore, only GPS receiver self-prediction and external-aiding are studied. Proposed by Zhodzishsky & Yudanov (1998), the strategy of self-prediction algorithms is to model receiver dynamics and oscillator behaviour and estimate the receiver Doppler and oscillator errors at current time based on current and previous measurements. Besides self-prediction, aiding information from external resources, such as Inertial Navigation Systems (INS), can also be used to measure the receiver dynamics and calibrate GPS oscillator errors. With the external aiding information from INS, the integration time can be increased substantially (e.g. Gao & Lachapelle 2006).

2.5.2 Navigation Data Wipe off

Due to the squaring loss that occurs in non-coherent integration, coherent integration is preferable for weak signal tracking. In order to achieve longer than 20 ms

coherent integration, the navigation data bit should be removed, thus the expression “wiped off”. Knowledge of the navigation data bits is very useful when performing the data wipe off for continuous carrier phase tracking.

AGPS technology relies on a base station to provide navigation data. Therefore, it may lead to a complex two-way communication system (Karunananayake et al 2004). A novel energy-based bit detection approach that extracts the navigation data from the incoming signal on-line (Soloviev & Gunawardena 2004) advances the traditional AGPS technique. This algorithm searches for the bit combination for every 20 ms segment of integration time to maximize signal energy over the tracking integration interval. For example, if the very long coherent integration time is 0.1 s, then there are 5 unknown 20-ms-length data bits. For the binary navigation data, the total number of possible bit combinations is 2^5 . Thus, the signal energy must be evaluated for 32 different bit combinations. In these 32 combinations, the bit combination that maximizes the signal energy is selected (Soloviev & Gunawardena 2004).

Although the algorithm provides receivers an approach to wipe off navigation data bit without external aiding, Gao & Lachapelle (2006) concluded that this energy-based bit detection will not perform efficiently if the signal is lower than -157 dBm. This approach presumes that the right bit combination is that which maximizes the signal energy over the tracking integration interval. For example, the Signal-to-Noise Ratio

(SNR) after 20 ms of integration should be above zero. This yields a limitation of -157 dBm for this approach, as given by

$$C = N_0 B \text{ SNR}_{I20} = (-204) + 10 \cdot \log_{10}\left(\frac{1000}{20}\right) + 0 = -157 \text{ (dBm)} , \quad (2.38)$$

where, SNR_{I20} is the signal-to-noise ratio after 20 ms coherent integration, N_0 is the environmental thermal noise and $N_0 = -204 \text{ dBm}$.

Equation (2.38) illustrates that an incoming signal lower than -157 dBm will fail the assumption implied in this algorithm and, hence, the energy-based bit detection approach.

Chapter Three: GPS/INS Ultra-Tight Integration Overview

3.1 Introduction to GPS/INS Integration

Inertial Navigation Systems (INS) have long been used in navigation and guidance. Two of their major disadvantages are the initial alignment and the positioning degradation as a function of time. In contrast, GPS does not need an external input for initialization, and its positioning accuracy is not affected by mission length or time since update. However, GPS positioning accuracy depends on GPS signal strength and availability. As a consequence, GPS positioning accuracy varies considerably in different applications and environments.

Previous research has shown that integrating INS with GPS can leverage the advantages of each positioning system (e.g. Petovello 2003, Godha & Cannon 2005). The advantages of GPS/INS integration, relative to either GPS or INS alone, can be summarized as follows:

1. A high data rate of complete navigation solution including position velocity and attitude.
2. Superior short-term and long-term positioning accuracy.

3. Improved availability.

4. Smoother trajectories.

5. Greater integrity.

Based on different data fusion strategies, GPS/INS integrated systems can be divided into three types: loosely coupled GPS/INS, tightly coupled GPS/INS, and ultra-tightly coupled GPS/INS (Gautier et al. 2003, Alban et al. 2003). Figure 3.1 shows the architectures of the three different GPS/INS integration schemes.

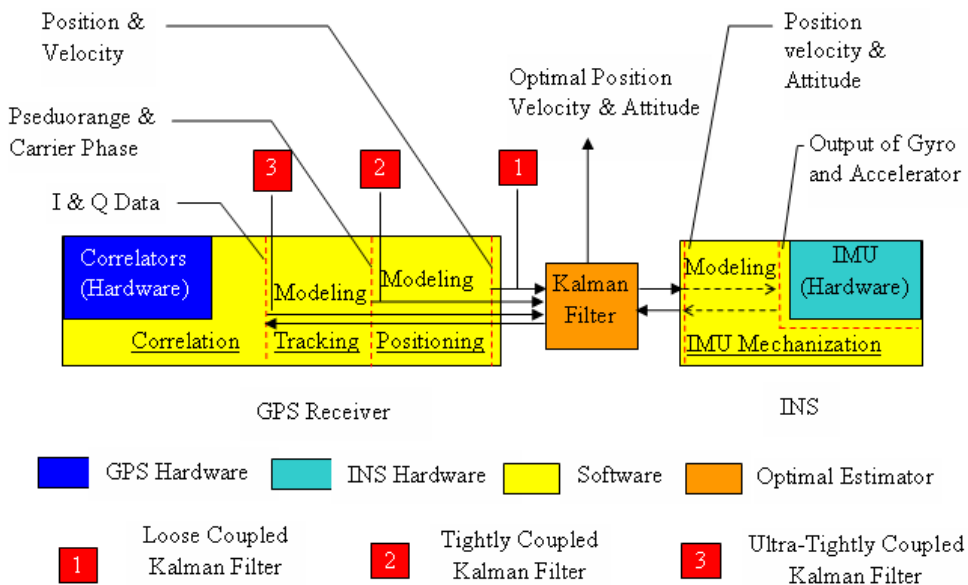


Figure 3.1 Architecture of Loosely, Tightly and Ultra-Tightly Coupled GPS/INS

The strategy of loosely and tightly coupled GPS/INS integration is based on optimal estimation theory and generally can be summarized into two steps: 1) Initialize the INS system with GPS data and, if possible, any other positioning information about the INS. The initial processing is called INS alignment; 2) Calibrate and compensate INS errors online with GPS data and then estimate an optimal positioning solution with both GPS data and INS data. The ultra-tightly coupled GPS/INS approach does one more operation, namely the measurements from the INS are fed back into the receiver to decrease GPS signal tracking errors and, in the process, enhance GPS positioning performance.

The difference between a loosely or tightly coupled GPS/INS and an ultra-tightly coupled one is that in the case of the former, GPS assists INS and significantly improves INS positioning performance. INS, however, does nothing to aid GPS signal tracking. In the latter, while GPS assists INS, the improved INS measurements are fed back to the receiver to improve signal tracking capability.

Chapter 2 argues that, for a stand-alone GPS receiver, the Doppler error caused by receiver dynamics degrades receiver's tracking capability significantly. In the case of GPS/INS ultra-tight receivers, the numerically controlled oscillator (NCO) receives its Doppler error corrections not only from within the channel, but also from the INS. The additional measurements from the INS remove the dynamics, which is the receiver velocity along the LOS direction, from the GPS signal and, consequently helps keep the receiver's tracking loop in lock. The assistance from the INS provides ultra-tight

receivers better tracking capability, higher positioning accuracy, and greater integrity and availability.

In loosely or tightly coupled GPS/INS for applications such as vehicle navigation in urban canyons or personal indoor positioning, the GPS receiver frequently loses lock on weak incoming signals. Therefore, the INS in this type of application may have to bridge significant GPS data gaps on some or all satellites. When the GPS solution is not available, INS error will increase over time so that positioning performance of the integrated system will still deteriorate over time at a rate that will be a function of the INS characteristics. In many scenarios, however, an ultra-tightly coupled GPS/INS system will be able to track much weaker GPS signals continuously because of INS aiding. Thus, the INS can be constantly corrected by GPS measurements, which can be made available at a rate superior to once per second. As a result, positioning performance is higher than loosely or tightly coupled systems, especially in weak signal environments or situations where receiver dynamics are very high (Gautier et al. 2003).

In commercial applications, Micro-Electro-Mechanical System (MEMS) based Inertial Measurement Units (IMU) are preferred in GPS/INS systems due to their low cost, low power-cost and smaller sizes. Unfortunately, the positioning performance of MEMS-based IMU is so poor that INS error increases to an unacceptable level in just a few seconds without feedback from GPS. In vehicle navigation and personal positioning in urban canyons or indoors, GPS/INS with MEMS-based IMU cannot meet the requirements of positioning availability, integrity, accuracy, and continuity (e.g. Nassar

2005, Niu 2005). In order to improve the positioning performance, many approaches have been proposed, such as utilizing constraints of vehicle/person motion (Godha & Cannon 2005), applying novel self-learning estimation methods (Abdel-Hamid 2005), etc. In all these approaches, GPS/INS ultra-tight integration is far superior to any other methods and, consequently, is receiving more and more attention.

3.2 Overview of GPS/INS Ultra-Tight Integration

It is well known that loosely or tightly coupled GPS/INS is defined depending on what kind of Kalman filter is adopted in the system. A loosely coupled GPS/INS system uses a GPS/INS Kalman filter that receives Position, Velocity, and Time (PVT) solutions from the GPS receiver. A tightly coupled GPS/INS system has a Kalman filter whose input data from the GPS side are raw measurements such as pseudorange, carrier phase, and carrier Doppler. Researchers agree with the definition of a ultra-tightly coupled Kalman filter, which uses I and Q components of GPS signals as the input data from the GPS side. In real life conditions, an ultra-tightly coupled GPS/INS, however, is commonly regarded as a system, in which INS assists GPS for GPS signal tracking.

Based on the type of Kalman filter used, existing ultra-tightly coupled GPS/INS systems can be divided into three different classes, namely (1) loosely coupled Kalman filter-based ultra-tight integration; (2) tightly coupled Kalman filter-based ultra-tight integration, and (3) ultra-tightly coupled Kalman filter-based ultra-tight integration. Figure 3.2 summarizes the different architectures. The integration algorithms include two sides, namely:

1) Both GPS measurements and INS measurements are fed into a GPS/INS Kalman filter in order to yield the best solution for navigation. Besides, the Kalman filter also estimates INS errors (e.g., INS attitude alignment errors, accelerometer biases, and gyro drifts) and GPS errors (e.g., clock biases, clock drifts and signal dynamics errors).

2) The estimation results from the Kalman filter are sent back to INS and GPS. Thus, the positioning solution plus the INS errors are fed back to the INS for its alignment and calibration, and the positioning solution plus the GPS errors are fed back to the receiver for signal tracking enhancements.

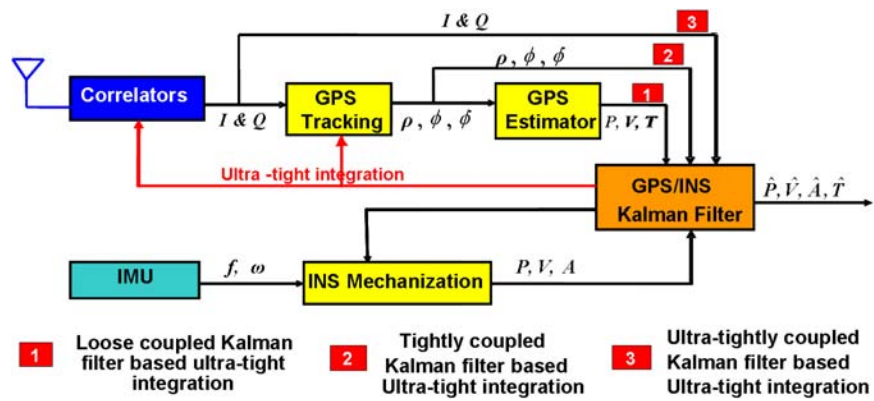


Figure 3.2 Ultra-Tightly Coupled GPS/INS with Loosely, Tightly or Ultra-Tightly Coupled Kalman Filter

Figure 3.3 shows two specific architectures for INS-assisted GPS receivers described by Gautier (2003) and Gustafson & Dowdle (2000), respectively.

The first architecture of the INS-assisted GPS receiver shown in Figure 3.3(a) is based on a loosely or tightly coupled integration scheme. All individual PLLs and DLLs are inside the receiver. The Kalman filter utilizes either raw measurements or processed positions and velocities from the receiver in order to update the INS periodically. The updated INS information is then used to predict the phase and Doppler measurements, which are used as aiding inside the receiver. Thus, based on the type of measurements used for updating the INS, these strategies can be classified as loosely coupled Kalman filter-based ultra-tight integration or tightly coupled Kalman filter-based ultra-tight integration. In the second architecture shown in Figure 3.3(b), however, an ultra-tightly coupled Kalman filter is used in the place of the conventional in-receiver PLL and, in some cases, even the DLLs. This filter operates directly on in-phase (I) and quadra-phase (Q) components. This integration strategy is referred to as ultra-tightly coupled Kalman filter-based ultra-tight integration.

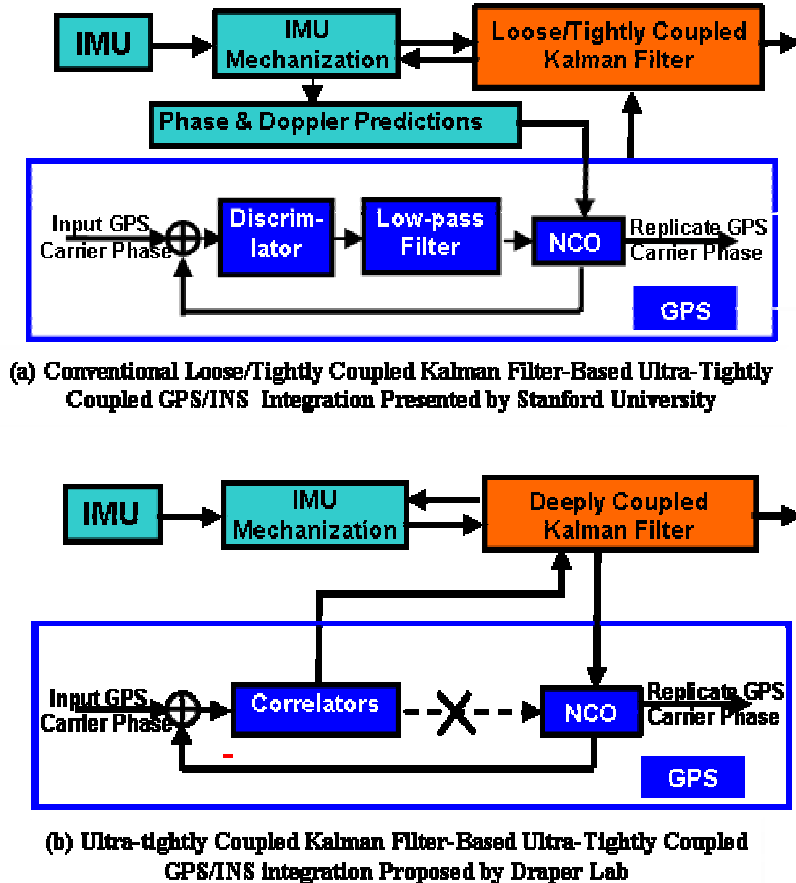


Figure 3.3 Two Different Architectures of Current Ultra-Tightly Coupled GPS/INS

3.3 Comparison of Different Kalman Filters

The main difference among the three architectures of ultra-tightly coupled GPS/INS, as shown in Figure 3.2, is that different GPS measurements are used and different Kalman filters are adopted in these systems. In this section, an overview of

different Kalman filters is presented and followed by a performance comparison of these filters.

3.3.1 Loosely coupled Kalman Filter

When INS (or GPS) uses its measurements to determine the position, INS sensor component errors (or GPS sensor component errors) affect positioning calculation and lead to positioning errors. By modeling the relationship between sensor errors and positioning errors, a Kalman filter can estimate and recover the INS sensor errors (or GPS sensor errors) from the positioning errors. The basic model for a loosely coupled Kalman filter is:

$$\dot{X} = AX + W \quad (3.1)$$

and

$$Z = HX + V. \quad (3.2)$$

Equation (3.1) and Equation (3.2) are the system model and observation model, respectively. In these equations, X is the state vector, defined as

$$X = [X_{INS} \quad X_{IMU_ERROR} \quad X_{GPS}], \quad (3.3)$$

Equation (3.3) shows clearly that the state vector (X) includes three parts: INS states (X_{INS}), IMU sensor error states (X_{IMU_ERROR}) and GPS states (X_{GPS}). These states are listed as follows:

$$X_{INS} = [\delta L \ \delta \lambda \ \delta H \ \delta V_E \ \delta V_N \ \delta V_U \ \phi_E \ \phi_N \ \phi_U], \quad (3.4)$$

where, $\delta L \ \delta \lambda \ \delta H$ are INS position errors in longitude, latitude and height, respectively. $\delta V_E \ \delta V_N \ \delta V_U$ are INS velocity errors along the east, north and up directions in local level frame, respectively. $\phi_E \ \phi_N \ \phi_U$ are INS attitude misalignments along the east, north and up directions in local level frame.

$$X_{GPS} = [T_{bias} \ T_{drift}], \quad (3.5)$$

where, T_{bias} is the GPS receiver clock bias and T_{drift} is the GPS receiver clock drift.

$$X_{IMU_ERROR} = [\varepsilon_x \ \varepsilon_y \ \varepsilon_z \ S_{g_x} \ S_{g_y} \ S_{g_z} \ \nabla_x \ \nabla_y \ \nabla_z \ S_{a_x} \ S_{a_y} \ S_{a_z}], \quad (3.6)$$

where, $\varepsilon_x \ \varepsilon_y \ \varepsilon_z$ are gyro drifts along X, Y, Z axes in the INS body frame. $S_{g_x} \ S_{g_y} \ S_{g_z}$ are gyro scale factors along X, Y, Z axes in the INS body frame. $\nabla_x \ \nabla_y \ \nabla_z$ are accelerometer biases along X, Y, Z axes in the INS body frame and $S_{a_x} \ S_{a_y} \ S_{a_z}$ are accelerometer scale factors along X, Y, Z axes in the INS body frame.

Z is the measurement vector (or observation vector) that can be written as

$$Z_{Loose} = [\delta P^n \ \delta V^n] = [(P_{GPS}^n - P_{INS}^n) \ (V_{GPS}^n - V_{INS}^n)], \quad (3.7)$$

where, P_{GPS} and P_{INS} are GPS position and INS position, respectively. V_{GPS} and V_{INS} are GPS velocity and INS velocity, respectively. The super-script n represents the local level frame.

More details on the other variables, such as the transition matrix A and observation matrix H , can be found in Appendix D.

3.3.2 Tightly Coupled Kalman Filter

In a tightly coupled Kalman filter, GPS measurements are changed from the positioning solution (PVT) to raw measurements including pseudorange, carrier phase, and carrier Doppler. The following measurement vector adopted by Godha & Cannon (2005) only uses pseudorange (ρ) and carrier Doppler ($\dot{\rho}$):

$$Z_{Tight} = \begin{bmatrix} \delta\rho_1 & \delta\dot{\rho}_1 \\ \vdots & \vdots \\ \delta\rho_n & \delta\dot{\rho}_n \end{bmatrix} = \begin{bmatrix} \rho_{GPS,1} - \rho_{INS,1} & \dot{\rho}_{GPS,1} - \dot{\rho}_{INS,1} \\ \vdots & \vdots \\ \rho_{GPS,n} - \rho_{INS,n} & \dot{\rho}_{GPS,n} - \dot{\rho}_{INS,n} \end{bmatrix}, \quad (3.8)$$

where the subscript n represents the number of GPS satellites tracked by the receiver.

Figure 3.1 shows clearly that a mathematical model can be derived to represent the relationship between the positioning solution and GPS raw measurements. Therefore,

just updating the observation matrix H and the corresponding observation noise matrix V will be the only tasks in transforming a loosely coupled Kalman filter into a tightly coupled Kalman filter.

3.3.3 Ultra-Tightly Coupled Kalman Filter

Similarly to the design of a tightly coupled Kalman filter, in order to update a loose or tightly coupled Kalman filter into an ultra-tightly coupled Kalman filter, the new measurements are used. They include the GPS signal I and Q components and the corresponding H and V in the measurement model of a Kalman filter. The concept of an ultra-tightly coupled Kalman filter has been proposed by several authors (e.g. Gustafson & Dowdle 2000, Beser & Alexander 2002, Soloviev & Gunawardena 2004, Babu 2005). Unfortunately, as to this date, there is no standard mathematical model for an ultra-tightly coupled Kalman filter.

In Appendix D, the author presents a model suitable for ultra-tightly coupled Kalman filter.

3.3.4 Performance Comparison of Different Kalman Filters

The above introduction to loosely, tightly, and ultra-tightly coupled Kalman filters shows that the only difference among these filters is the input measurements from the receiver. Figure 3.1 shows that mathematic models can be used to bridge GPS measurements at different stages. Therefore, although these new architectures offer more flexibility for filter design, from the point of view of information theory, the performance

of these filters must be theoretically the same. Also the estimation accuracies must be on the same level. This concept is best illustrated by an analogy of water in a river. Although water looks very different at higher, lower, and lowest points of a river, the volume of water is the same at all these points. Therefore, adopting different kinds of Kalman filter cannot improve the positioning performance of GPS/INS integrated systems significantly. This is the case for line-of-sight environments, where a tightly coupled Kalman filter will not provide significant improvements in an integrated system performance as compared to a loosely coupled filter.

However, although the information from the observations will not be lost in the transition from ultra-tight to tight and to loose integration at the end, the information presented in the observation noise does get lost. For example, after the pseudorange noise is transferred from the measurement domain to the position domain and becomes position noise, even the original measurement noise is uncorrected in the measurement domain; the noise will become correlated in position domain. A Kalman filter is built up using the least-squares estimation criteria. It is known that least-squares estimation guarantees an optimal solution assuming the input noises are uncorrelated. Since in the loose case where we know the input, noise is clearly correlated, there is no guarantee that the solution is optimal. Furthermore, unlike the characteristics of signals, adding one noise with the other noise or subtracting one noise from the other will both increase noise value. Therefore, more operations one implements on the noise, the higher the noise level one might get. For these reasons, a tightly coupled Kalman filter will still be slightly better

than a loosely coupled one in the same situation, although this improvement is likely marginal in most cases.

For an ultra-tightly coupled GPS/INS system, the NCOs (and the tracking loops in general) in the GPS receiver are usually not concerned with state covariance, but only with the "actual" state values. The level of "noise" in the states of the involved GPS/INS Kalman filter (reflected in the covariance matrix) will influence whether the signal can be tracked (or not), but will not affect the implementation of the tracking loop per se. As such, the different state covariance in a loosely, tightly or ultra-tightly coupled Kalman filter will not affect the signal tracking in the receiver, so much as it is simply unnecessary for the tracking loop to continue.

Different Kalman filters have different advantages and disadvantages, and, thus, are suitable for different applications. This is due to application constraints and the fact that it is difficult to ensure correct systematic and statistical models for a specific system in real applications. For example, when a receiver operates in line-of-sight environments, loosely coupled Kalman filter can provide a simple and stable system with good positioning accuracy. In urban canyon environments, however, a tightly coupled Kalman filter yields better performance when the number of received satellite signals is less than four. In the design of a GPS/INS integration scheme, many people simply use off-the-shelf products. They normally do not know what kind of signal processing is implemented in the receiver and are not familiar with the statistics of GPS measurement noise after GPS signal processing. Signal processing worsens when a receiver is in urban

canyons or indoors where it suffers multipath, cross-correlation, signal blockage, etc. In this kind of applications, using ultra-tightly coupled Kalman will be easier for the designer since people are more familiar with the statistics of GPS I and Q measurements and their noise.

In conclusion, this chapter presented an overview of ultra-tightly coupled GPS/INS systems. It also showed that there are two tasks pertaining to the design and development of this system:

1. Adopting a suitable Kalman filter to correct the INS solution online for both navigation and receiver aiding.
2. Enhancement of the receiver in weak signal tracking environments by applying external INS aiding information.

In this chapter, the first task has been discussed from a system design point of view. Considerations and design details for the second task will be presented in Chapter 4.

Chapter Four: A Novel Design of INS Assisted GPS Receiver for Degraded GPS Signal Navigation

Most of the research conducted in ultra-tight GPS/INS integration has focused on adapting three different integration strategies. They include loosely, tightly and ultra-tightly coupled Kalman filters. As discussed in Chapter 3, although these architectures offer better system flexibility, just adopting different kinds of Kalman filters may not improve the positioning performance of GPS/INS integrated systems significantly.

Furthermore, there are some specific limitations in present architectures. The first limitation is that the receiver tracking capability is sensitive to IMU quality. For reliable aiding from INS, 1 cm/s velocity accuracy along LOS direction is required from the INS solution (Soloviev and Gunawardena 2004), which demands a high quality IMU. The second limitation is that before the integrated system moves to attenuated signal environments, it has to be initialized in line-of-sight environments, which includes GPS-only receiver initial acquisition and INS initial alignment. Furthermore, the accuracy estimation of a Kalman filter relies on the assumption of correct stochastic modeling of both system and measurement errors, which may not be possible in severe urban canyon environments. For vehicle navigation in urban canyons, GPS measurement's faults such as those caused by multipath or echo-only signals are very significant. Also, the errors in

IMU measurements may not be compensated effectively, which ultimately degrades the receiver tracking performance.

A novel INS- assisted GPS receiver approach is proposed herein to overcome some of the limitations of current INS-assisted GPS receivers. In this new architecture, a technique based on multi-channel co-operated tracking, namely COOP tracking (Zhodzishsky & Yudanov 1998), is proposed to estimate/track the predicted Doppler error caused by INS errors and, thus, further improve the receiver tracking performance.

4.1 Top-Level Architecture of HSGPS Receiver with INS Aiding

The architecture of the proposed integration system is shown in Figure 4.1. The ultra-tightly integrated system used the software receiver GNSS_SoftRxTM (Ma & Lachapelle 2004) as a starting point. The proposed strategy includes three loops. The first loop includes the conventional loosely or tightly coupled Kalman filter, which predicts the user Doppler based on information from the INS. In this study, a loosely coupled Kalman filter is suggested. This loop provides external Doppler aiding and clock error correction from the INS. In order to decrease the effects of INS positioning errors on receiver Doppler prediction and receiver clock error compensation, a COOP loop is used as the second loop to estimate the carrier Doppler error and receiver clock error caused by INS position and velocity errors. Thus, the INS and COOP loops function together in order to provide a nearly perfect reference for receiver dynamics and receiver clock errors. Since receiver dynamics is removed from the signal, long coherent/non-coherent integration time for individual PLLs and DLLs becomes possible, which constitutes the

third loop of the proposed architecture. Thus, the PLL/DLL loops track the difference between the incoming and the local signals, which have been compensated by INS and COOP loops.

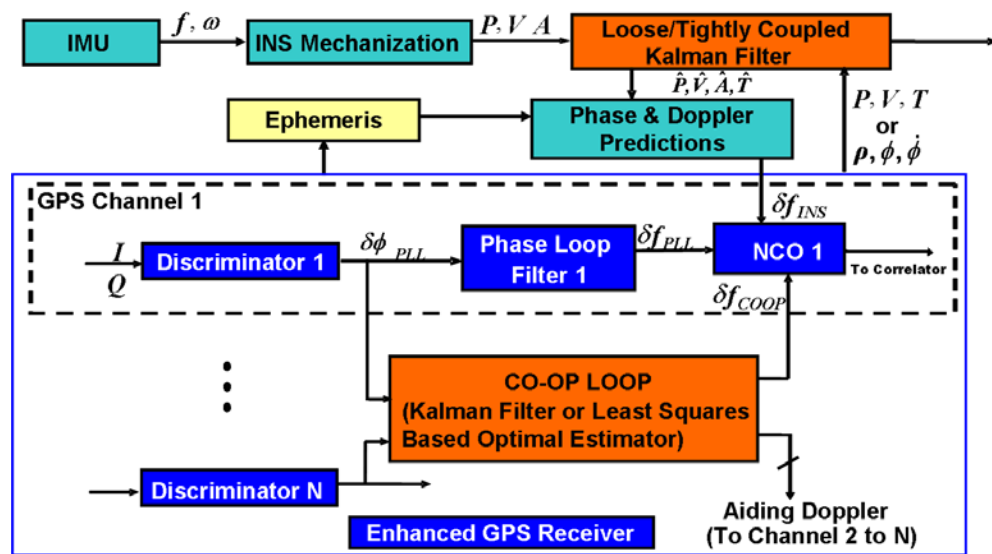


Figure 4.1 Proposed Architecture of Ultra-Tightly Coupled GPS/INS

The characteristics and advantages of this system can be summarized as follows:

1. As presented in Chapter 2, a HSGPS receiver is developed, based on the GNSS_SoftRx™ software by optimizing parameterization and employing data wipe off technology for long coherent integration. This HSGPS/INS structure enables initialization in a weak signal environment.

2. To provide INS aiding to the GPS receiver, the loosely/tightly coupled GPS/INS software SAINTTM developed by Petovello (2003) is suggested to handle INS measurements and provide a corrected INS solution for receiver aiding.
3. The multi-channel co-operated tracking loop tracks the weak signals and eliminates the effects of INS errors. The design of this estimator is discussed later in Section 4.4.
4. All individual DLL/PLLs are different from those of ultra-tightly coupled GPS/INS systems, which adopt ultra-tightly coupled Kalman filters for signal tracking. So all sophisticated individual DLL/PLLs in receivers are used in this design and they are combined with INS aiding loops and COOP loops to track both strong and weak signals.
5. Since INS is mainly used in this approach to provide receiver dynamics information, any other sensors such as odometers or radars can replace INS sensors to provide user Doppler measurements for the enhanced receiver. This provides an effective capability to re-configure the software receiver to suit various aiding hardware.

4.2 Design of INS Aiding Loops

In a loosely or tightly coupled GPS/INS for vehicle navigation in urban canyons, the receiver frequently loses lock on incoming signals. Therefore the INS in this kind of integrated system must be able to accommodate GPS outages for relatively long periods, e.g over 30 s. In an ultra-tightly coupled GPS/INS, however, the receiver can track weak GPS signals continuously because of INS aiding. Thus, the INS is constantly corrected by GPS measurements which are typically available every 1 s. Consequently, the maximum INS prediction duration may be limited to 1 s in many common operation scenarios. This implies that a low-cost Micro Electro-Mechanical System (MEMS) IMU might be acceptable for ultra-tightly coupled GPS/INS.

Considering that GPS measurements ($\rho, \phi, \dot{\phi}, C/N_{\circ}$) and solution (P, V, T) usually are available in ultra-tightly coupled systems, a loosely coupled GPS/INS Kalman filter is suggested for the present prototype. Its function is to calibrate/correct INS errors online with GPS measurements. The loosely/tightly coupled GPS/INS software SAINTTM can realize this function. Receiving GPS and INS measurements from both receiver and INS, SAINTTM can accurately estimate the position and velocity and feed them back into the receiver as aiding information.

For the INS involved in the prototype, its velocity error caused by sensor errors in 1 s can be estimated by velocity error signatures, as follows (Scherzinger 2004):

$$\begin{aligned}\delta V &= b_a t = b_a \\ \delta V &= -\frac{1}{6} g b_g t^2 = -\frac{1}{6} g b_g,\end{aligned}\tag{4.1}$$

where δV is the velocity error, b_a is the accelerometer bias, b_g is the gyro bias, g is the gravity, and t is the time interval.

With COOP loops, which will be discussed in Section 4.4, the effects of an INS position and velocity errors on the receiver Doppler prediction and clock error compensation will be limited. Therefore, the accuracy for aiding velocity need not be accurate to 1 cm/s level any more, as pointed out by Soloviev and Gunawardena (2004) as necessary for these kinds of systems. In this research, the velocity error of 0.1 m/s is simulated for the Doppler aiding accuracy, which makes it feasible to use a lower grade IMU quality with an accelerometer bias of 10 milli G (mg) or a gyro bias of 3.4°/s.

In actual applications, a velocity error of 0.1 m/s in 1 s can be achieved with most low cost MEMS IMU available today, such as the Crista IMU from Cloud Cap Technology (Godha & Cannon 2005). The in-run gyro biases and accelerometer biases of this IMU are about 0.3 °/s and 2.5 mg, respectively. However, the 0.1 m/s velocity error is available usually after the INS is well aligned with GPS measurements and the vehicle's motion contains sufficient dynamics to make all the INS error states observable. In the static case or where the vehicle motion does not contain enough dynamics to ensure observability, the accuracy of the Doppler information from the INS may be of

poor quality. A particular concern is the poorly observable states of azimuth and azimuth gyro bias. If the estimates of these states are of poor quality, the velocity error provided by a MEMS-based INS in still can be much larger than 0.1 m/s. It should also be noted that, the vehicle dynamics that needs to be estimated and removed by the INS is not limited to line of sight velocity but all motion. For example, an erroneous estimate of azimuth can result in dynamics errors due to “phase wind-up” effects (Tetewsky & Mullen 1996, Don et al. 2005).

Furthermore, when a low cost MEMS-based INS is involved in an INS-assisted GPS receiver, because of the very low accuracy and very poor stability of IMU sensors, the INS velocity error might present jumps or blunders. These huge errors will induce a big problem in INS-assisted GPS receiver. Plus the observability issue of GPS/INS Kalman filter discussed above, MEMS-based INS/GPS ultra-tight integration is still a big challenge.

4.3 Design of Individual FLL/PLL/DLL Loops

In the prototype INS-assisted GPS receiver, FLL-assisted PLLs are used for carrier phase tracking, and then the carrier phase replica is implemented to aid the code phase DLL.

4.3.1 Determination of Integration Time for Individual FLL/PLL/DLL Loops

Given that the carrier wavelength is about 19 cm, a 0.1 m/s velocity error obtained by an INS will lead to a maximum Doppler error of 0.5 Hz along a given LOS vector. The resulting signal power loss over the total integration time due to this phenomenon has been discussed in Section 2.12 and presented in Figure 4.2. Figure 4.2 also shows that a 1-s coherent integration time may result in a power loss of approximately 4 dB.

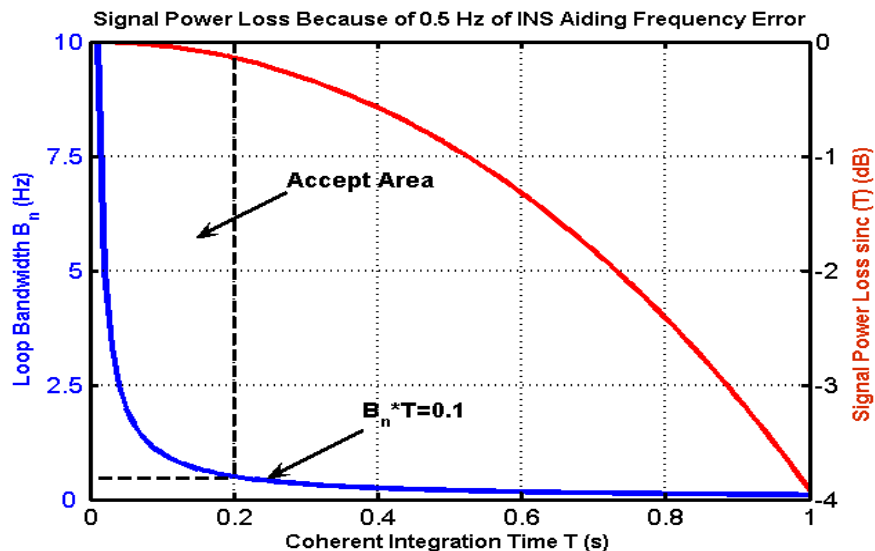


Figure 4.2 Signal Power Loss with Respect to Integration Time

The design of receiver tracking loops, which utilizes continuous update approximation, is discussed in detail by Kaplan (1996). Stephens and Thomas (1995) have shown that, when the product of loop bandwidth (B_n) and coherent integration time (T_{coh}) is much greater than 0.1, the continuous update approximation does not hold any

more. Since the Doppler uncertainty from INS aiding is 0.5 Hz, as shown in Figure 4.2, coherent integration time must be shorter than 0.2 s to satisfy $B_n \times T_{coh} \ll 1$ or $B_n \times T_{coh} < 0.1$.

Section 2.4.3.3 has discussed oscillator instability and its effects on PLL tracking. In theory, since the clock noise described by its Allan variance is characteristically coloured noise, it can be modeled, and, thus, partly estimated in the GPS/INS Kalman filters. If the coloured noise is modeled perfectly, the part of the clock noise that is not estimated will be limited to white noise, which can be regarded as thermal noise and easily handled by the receiver tracking loops. To simplify the filter design, the Allan clock noise is dealt with as white noise in most applications, and, thus, will not be estimated (Brown & Hwang 1992). As a consequence, the Allan clock noise has to be dealt with in conventional signal tracking loops in receivers and thus will limit the coherent integration time of these tracking loops (Kaplan 1996). For the correlated clock noise, most of its energy is located in the low frequency band in frequency domain. Therefore, when loop filters with narrow bandwidths try to get rid of the noise in the signal, most of the clock noise passes through these low-pass filters, since it is mixed with the GPS signal in the low frequency band in spectrum. However, the energy of the white clock noise spreads out evenly in the whole frequency domain, therefore, a low-pass filter can efficiently distinguish GPS signal from the white clock noise and block most of the clock noise in signal tracking loops. In weak signal navigation, the effect of the correlated clock noise on signal tracking may be one of the most limiting factors.

In consideration of the above factors, a maximum coherent integration time of 100 ms is chosen for the purposes of this study.

4.3.2 Design of Individual FLLs

The individual FLL scheme is shown in Figure 4.3. After acquisition, the signal is transferred to the FLLs for frequency tracking. At first, analytic frequency refinement is implemented to find the acquired signal frequency. Then, a second-order FLL is used for fine frequency tracking. This FLL adopts a cross-product discriminator. In frequency tracking, the FLL lock indicator is visited periodically to check if the signal frequency has been locked. If this occurs, the receiver moves to the PLL tracking stage. Otherwise, the receiver calls upon the FLL-based navigation data decoder to recover the navigation data bit.

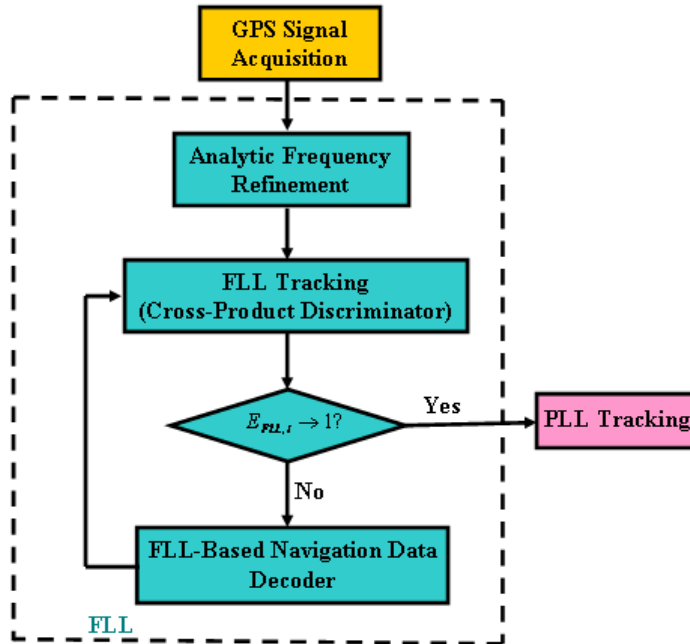


Figure 4.3 Individual Frequency Locked Loop Scheme

The frequency obtained from acquisition is refined analytically before input into the FLLs (Ma & Lachapelle 2004). The FLL uses the following cross-product discriminator that is discussed in Equation (2.20):

$$\delta f_i = (NormI_{i-1} \cdot NormQ_i - NormI_i \cdot NormQ_{i-1}) sign(NormI_{i-1} \cdot NormI_i + NormQ_i \cdot NormQ_{i-1}) \cdot \dots \quad (4.2)$$

The carrier lock indicator involved in this FLL is as follows (Ma & Lachapelle 2004):

$$E_{FLL,i} = |I_i I_{i-1} + Q_i Q_{i-1}| = |\cos[\pi T(\Delta f_i - \Delta f_{i-1})]|. \quad (4.3)$$

Appendix B describes how to decode the navigation data bits only with FLL measurements. This kind of design is helpful for GPS positioning in attenuated signal environments where the PLLs lose lock frequently because of weak signals.

As discussed in Section 2.3.3, the limitation of the phase tracking error for a digital FLL is as follows:

$$3\sigma_{FLL} = \Delta f_d \cdot T + 3 \cdot \sqrt{\sigma_{FLL,t}^2 + (\sigma_A \cdot f_L)^2} \cdot T + f_e \cdot T \leq \frac{90}{360} = 0.25. \quad (4.4)$$

With INS aiding, FLL dynamic stress errors can be ignored. The above equation therefore be rewritten as

$$\sigma_{FLL} = \frac{\Delta f_d}{3} \cdot T \cdot 360 + \sqrt{\sigma_{FLL,t}^2 + (\sigma_A \cdot f_L)^2} \cdot T \cdot 360 \leq 30^\circ. \quad (4.5)$$

To perform very long coherent integration over the 20 ms limit, a navigation data wiping off technology is used in this prototype receiver. This data wipe off algorithm was introduced in Section 2.5.2. The section also illustrates that the incoming signal must be above -157 dBm (equal to 17 dB-Hz) in order to implement the algorithm effectively.

Due to the above reason, Figure 4.4 shows the phase tracking error (1σ) for a digital FLL when the incoming signal power is 15 dB-Hz, which is 2 dB lower than the 17 dB-Hz limit given by the wipe off approach. The Doppler error is $\Delta f_d = 0.5 \text{ Hz}$, and the Allan standard deviation of the receiver oscillator is $\sigma_A = 1.0 \times e^{-10}$. In Section 4.3.1, it is concluded that a suitable coherent integration time should not be over 0.1 s. Therefore, pre-detection integration times between 0 to 0.1 s are examined.

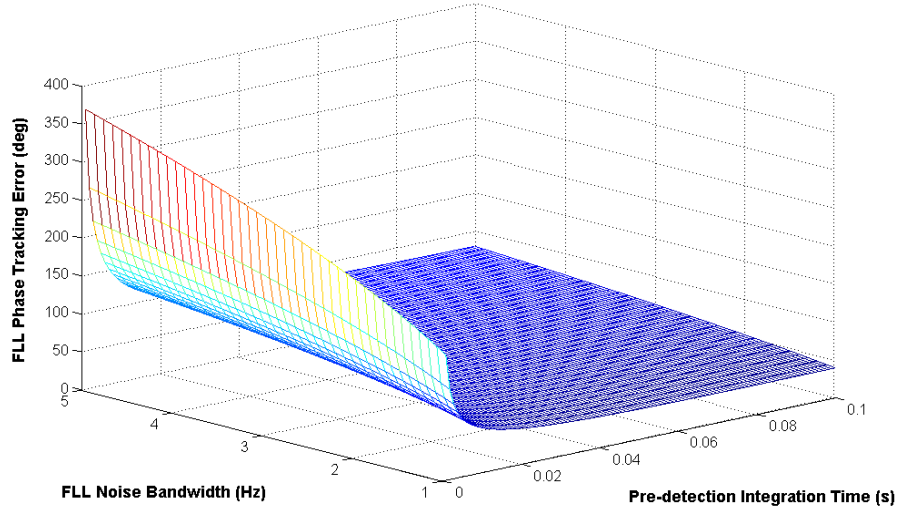


Figure 4.4 Phase Tracking Error for a Digital FLL under a 15 dB-Hz Signal

Based on Figure 4.4, the FLL parameters are chosen as 1 Hz of noise bandwidth and 0.1 s of pre-detection integration time interval.

4.3.3 Design of Individual PLLs

The PLL scheme is shown in Figure 4.5. When the signal frequency is locked by the FLLs, the signal is transferred to the PLLs for carrier phase tracking.

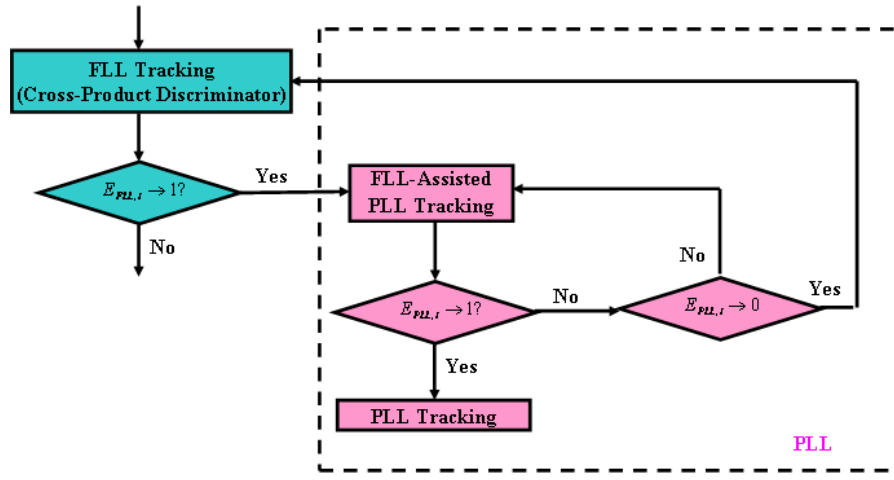


Figure 4.5 Individual Phase Locked Loop Scheme

The carrier phase tracking strategy consists of three steps:

- 1) When the FLL lock detector $E_{FLL,i} \rightarrow 1$, apply the FLL-assisted PLLs for phase tracking.
- 2) When the PLL lock indicator $E_{PLL,i} \rightarrow 1$, convert FLL-assisted PLLs into pure Costas PLLs.
- 3) When the PLL lock indicator $E_{PLL,i} \rightarrow 0$, the PLLs lose lock, and go back to FLL tracking.

According to Section 2.4, the ATAN discriminator D_i and carrier-phase lock indicator $E_{PLL,i}$ are used for the PLLs:

$$D_i = \text{ATAN}\left(\frac{Q_{P,i}}{I_{P,i}}\right) = \phi_i \quad (4.6)$$

and

$$E_{PLL,i} = \frac{I_i^2 - Q_i^2}{I_i^2 + Q_i^2} = \cos(2\phi_i). \quad (4.7)$$

Considering that the external INS aiding has removed most of receiver dynamics, first-order FLL-assisted second-order PLLs are used here for carrier phase tracking. Figure 4.6 illustrates the architecture of the FLL-assisted PLL in one tracking channel.

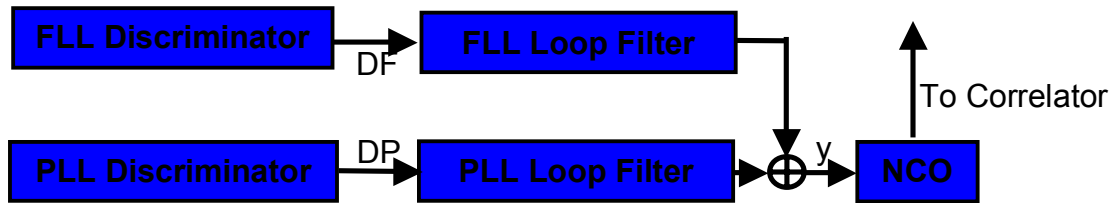


Figure 4.6 The Architecture of the FLL-Assisted PLL in One Tracking Channel

Therefore, the output is

$$y_i = y_{i-1} + (T\omega_{np}^2 + a_2\omega_{np})DP_i - (a_2\omega_{np})DP_{i-1} + (\omega_{nf}T)DF_{i-1}, \quad (4.8)$$

where, y_i is the combined output of loop filters at epoch i . DP and DF are the products of PLL and FLL discriminators, respectively.

As discussed in Section 2.4.3, the phase tracking error for a digital PLL is as follows:

$$\sigma_{PLL} = \Delta f_d \cdot T \cdot 360 + \sqrt{\sigma_{tPLL}^2 + (\sigma_A \cdot f_L \cdot T)^2 + \theta_A^2} + \frac{\theta_e}{3} . \quad (4.9)$$

With INS aiding, the PLL dynamic stress error is negligible and Equation (4.9) can be rewritten as

$$\sigma_{PLL} = \Delta f_d \cdot T \cdot 360 + \sqrt{\sigma_{tPLL}^2 + (\sigma_A \cdot f_L \cdot T)^2 + \theta_A^2} . \quad (4.10)$$

Figure 4.7 shows the phase tracking error ($1\ \sigma$) for a digital PLL when the incoming signal power is 15 dB-Hz. The Doppler error is $\Delta f_d = 0.5\ Hz$ and the Allan standard deviation of receiver oscillator is $\sigma_A = 1.0 \times e^{-10}$.

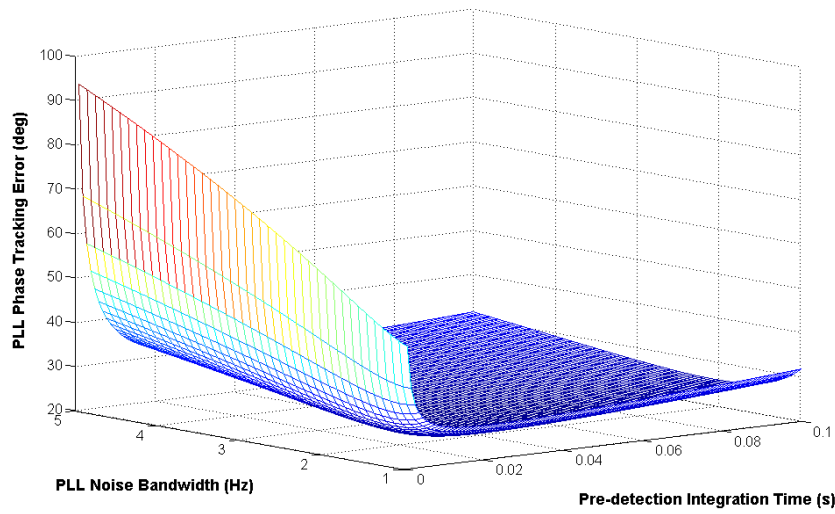


Figure 4.7 Phase Tracking Error for a Digital PLL under a 15 dB-Hz Signal

In order to demonstrate how the PLL thermal noise varies with integration time and noise bandwidth, the phase tracking error ($1\ \sigma$) is shown in Figure 4.8 with the effect of the Allan deviation oscillator phase noise ignored:

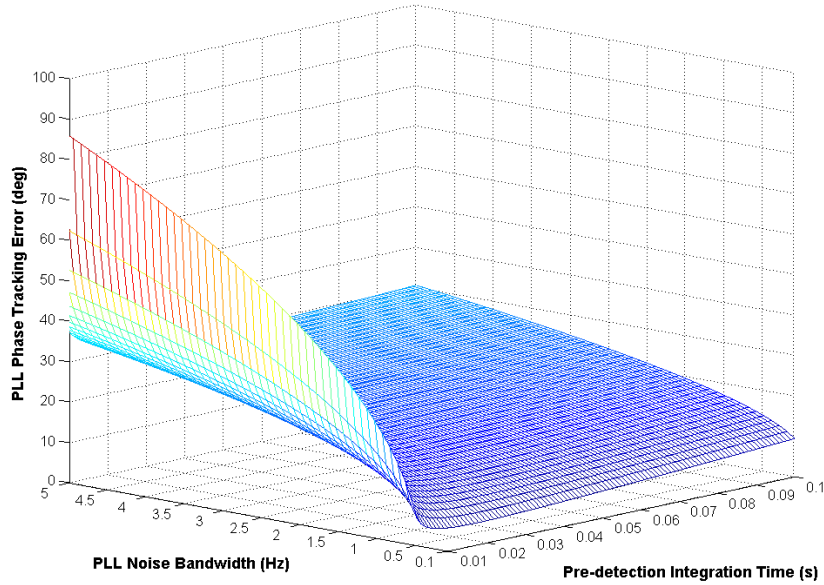


Figure 4.8 Phase Tracking Error for a Digital PLL under the Signal of 15 dB-Hz (Oscillator Phase Noise Ignored)

Based on Figure 4.7 and Figure 4.8, the PLL parameters are chosen as 0.2 Hz for the noise bandwidth and 0.1 s for the pre-detection integration time.

4.3.4 Design of Individual DLLs

With PLL-aiding and INS-aiding, the receiver dynamics left in the DLLs is negligible. Therefore, either second-order DLLs or first-order DLLs can be adopted here for code tracking. In this study, second-order DLLs are designed for the prototype receiver.

As discussed in Section 2.2.2 and Appendix A, the discriminator used in DLL is

$$D_{\text{DLL}}(\delta\tau) = \frac{(I_E^2 + Q_E^2) - (I_L^2 + Q_L^2)}{(I_p^2 + Q_p^2) \cdot B'(\delta\tau = 0)}. \quad (4.11)$$

Please note that B' is the discriminator gain:

$$B'(\delta\tau = 0) = 4 - 4\delta, \quad (4.12)$$

where δ is the correlator spacing.

According to Table 2.1, the product of a second-order DLL loop filter is

$$y_i = y_{i-1} + (\omega_n^2 T + a_2 \omega_n) x_i - (a_2 \omega_n) x_{i-1}, \quad (4.13)$$

where, x_i and y_i are products of the discriminator and the loop filter at epoch i , respectively.

For externally aided DLLs, the tracking error sources consist mostly of thermal noise. As discussed in Section 2.2.4, the DLL thermal noise can be estimated with the following equation:

$$\sigma_{t\text{DLL}} = \sqrt{\frac{2\delta^2 B_n}{C/N_0} [2(1-\delta) + \frac{4F\delta}{T \cdot C/N_0}]}. \quad (4.14)$$

The DLL thermal noise ($1\ \sigma$) is illustrated in Figure 4.9, where the incoming signal power is 15 dB-Hz and the correlator spacing 0.1 chip.

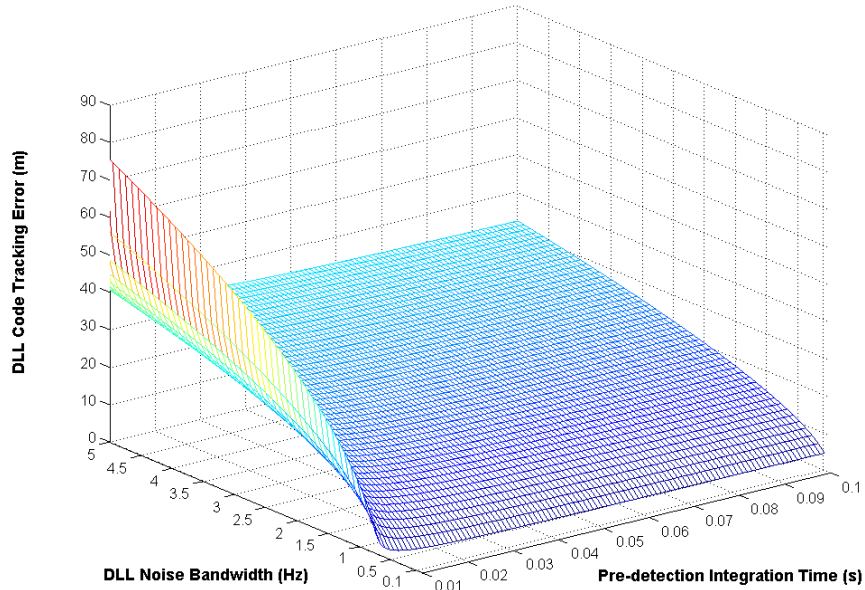


Figure 4.9 Externally Aided DLL Tracking Errors under a 15 dB-Hz Signal

Based on Figure 4.9, the DLL parameters selected for the prototype receiver are 0.1 Hz noise bandwidth, 0.1 chip for the correlator spacing, and 0.1 s for the pre-detection integration time.

4.4 Design of Multi-Channel COOP Tracking Loops

As discussed in Chapter 2, DLLs are always more robust than PLLs and have lower tracking thresholds. As the weakest portion of signal tracking, PLLs are enhanced with external INS measurements to improve their robustness and sensitivity in weak signal navigation.

Figure 4.10 shows the modular design of the multi-channel co-operated tracking loops, also referred to as COOP tracking loops. The basic strategy of COOP tracking is to project signals from the channel domain to the position domain and then try to track/estimate signals in the position domain. After low-pass filters, the signals are projected back to the channel domain for Doppler removal.

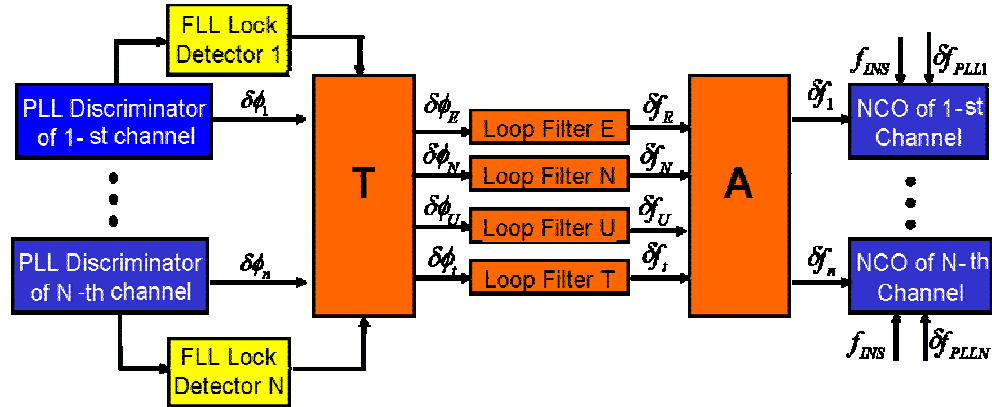


Figure 4.10 Cooperated (COOP) Tracking Module Architecture

The carrier-phase based pseudorange can be expressed by the following equation:

$$\rho_\phi = (N + \phi)\lambda = A(X_{sat} - X_{rec}) + \varepsilon, \quad (4.15)$$

where N is the integer ambiguity, ϕ is the carrier phase, A is the directional cosine matrix (or called geometry matrix), and X_{sat} and X_{rec} are the satellite and receiver positions, respectively.

The first-order term of Equation (4.15) can be written as:

$$\lambda\delta\phi = A\delta X_{rec} + \varepsilon, \quad (4.16)$$

where $\delta\phi$ is the carrier phase tracking error, δX_{rec} includes the receiver position and clock-offset difference between the true value and the nominal value provided by the INS solution. δX_{rec} represents the receiver position error caused by INS errors.

As shown in Figure 4.1, it is assumed that satellite motion is compensated in the INS-aided loops. So its effect on pseudoranges is ignored in the above equation. In Figure 4.10,

$$\begin{aligned} T &= T^n = C_e^n T^e \\ A &= A^n = A^e C_n^e, \end{aligned} \quad (4.17)$$

where the super-script n and e represent the Local-Level frame (LLF) and Earth-Centered Earth-Fixed (ECEF) frame, respectively. C is a rotation matrix and A is the direction cosine matrix. T is the transfer matrix and defined as follows (Zhodzishsky & Yudanov 1998):

$$T^n = \left((A^n)^T C_\phi^{-1} (A^n) \right)^{-1} (A^n)^T C_\phi^{-1}. \quad (4.18)$$

In the above equation, C_ϕ is a weighted matrix, which can be determined by either PLL lock detectors or FLL lock detectors. In this study, FLL lock detectors (E_{FLL}) are used as follows:

$$E_{FLL,i} = |I_i I_{i-1} + Q_i Q_{i-1}| = |\cos[\pi \cdot T \cdot (\Delta f_i - \Delta f_{i-1})]| , \quad (4.19)$$

where, I, Q are the I and Q components of the signals and Δf is the Doppler tracking error. The subscript i represents the $i-th$ epoch. The reason why E_{FLL} is chosen to determine C_ϕ will be discussed later in this section.

The COOP loop can be based on either a least-squares estimation method or on a Kalman filter. In this study, the least-squares method is used. Least-squares estimation is an effective optimal estimation method in GPS measurement processing, especially when measurement redundancy is high. Many blunder detection algorithms such as Receiver Autonomous Integrity Monitoring (RAIM) are in fact based on least-squares estimation, provided redundant measurements are available. Herein, the principle “using optimal estimator in GPS positioning fully to utilize measurement redundancy”, is put forward from the measurement processing domain into the GPS baseband signal processing domain, which leads to the COOP tracking method. COOP loops allow a GPS receiver to do signal tracking based on the multi-channel vector tracking approach (Petovello & Lachapelle 2006). Furthermore, based on measurement redundancy, blunder detection algorithms and adaptive estimation methods now can be realized at the signal processing stage rather than at the measurement processing stage.

Today, there are some 30 GPS satellites available. Other GNSS (GALILEO and GLONASS) are available or becoming available. GPS receivers can receive 6-10 or more

satellites simultaneously. There is no doubt that, in future, a GNSS receiver will track a much higher number of GNSS satellites.

Unfortunately, traditional receivers track every satellite signal independently so lock on one satellite does not help to track any other satellites. For this reason, although receiving more and more satellite signals leads to greater redundancy in GPS measurement processing, it is useless in signal tracking. COOP tracking implemented in this study, however, is different from this scalar-tracking method since it is a vector-based tracking approach. Therefore, it can receive more satellites and achieve more effective tracking performance. In field applications, especially in urban canyons and indoor environments, a receiver receives multiple strong and weak signals at the same time. With COOP tracking, the lock on the strong satellite signals will aid significantly in tracking other weak signals and, thus, will improve receiver positioning performance.

In Figure 4.10, the measurement noise $n_{\delta\phi_i}$ ($i = 1, 2, \dots, N$) before the module T is the difference between the measured carrier phase $\delta\phi_i$ ($i = 1, 2, \dots, N$) and the true carrier phase $\delta\phi_{i,true}$ ($i = 1, 2, \dots, N$). The variance of $n_{\delta\phi_i}$ is:

$$\begin{aligned}\sigma_{n_{\delta\phi_i}}^2 &= \boldsymbol{\varepsilon}^T \boldsymbol{\varepsilon} = (\delta\phi_i - \delta\phi_{i,true})^T \cdot (\delta\phi_i - \delta\phi_{i,true}) \\ &= (\delta\phi_i - A \cdot \delta\phi_j)^T (\delta\phi_i - A \cdot \delta\phi_j) \\ &\approx (\delta\phi_i - A \cdot \hat{\delta\phi}_j)^T (\delta\phi_i - A \cdot \hat{\delta\phi}_j) = \hat{\boldsymbol{\varepsilon}}^T \hat{\boldsymbol{\varepsilon}},\end{aligned}\quad (4.20)$$

$(i = 1, 2, \dots, N; \quad j = E, N, U, T)$

where $\delta\phi_i$ is the carrier phase measurement from the PLL discriminator and $\delta\phi_j$ is the state vector yielding three-dimensional positions and time. A is the direction cosine matrix. ε and $\hat{\varepsilon}$ are the true value and the estimation of measurement errors, respectively.

The state noise $n_{\delta\phi_j}$ ($j = E, N, U, T$) after module T is the difference between the estimated state $\delta\phi_j$ ($j = E, N, U, T$) and the true state $\delta\phi_{j,true}$ ($j = E, N, U, T$). Based on least-squares theory, after $\delta\phi_j$ is re-projected back to the signal channel domain through the matrix A , the measurement variance of $n_{\delta\phi_j}$ changes to:

$$\begin{aligned}\sigma_{n_{\delta\phi_i}}^2 &\approx (\hat{\delta\phi}_i - A \cdot \hat{\delta\phi}_{j,true})^T \cdot (\hat{\delta\phi}_i - A \cdot \hat{\delta\phi}_{j,true}) \\ &= \frac{\hat{\varepsilon}^T C_{\delta\phi_i}^{-1} \hat{\varepsilon}}{\nu},\end{aligned}\tag{4.21}$$

where, $C_{\delta\phi_i}^{-1}$ is the variance-covariance matrix of phase measurements $n_{\delta\phi_i}$ and ν is the measurement redundancy ($\nu = N - 3$).

After comparing Equation (4.20) with Equation (4.21), it becomes evident that, when the COOP receiver tracks more than four satellites, the channel noise $n_{\delta\phi_i}$ after module A in Figure 4.10 is smaller than the channel noise $n_{\delta\phi_i}$ after the PLL discriminators. The more satellite signals are received, the lower the tracking noise is.

The main portion of the noise located in different tracking channels is thermal noise and thus can be regarded as channel-independent white noise. However, from equation (4.21), it is known that the state noise $n_{\delta\phi_j}$ ($j = E, N, U, T$) in position domain is no longer independent noise: although $n_{\delta\phi_j}$ is still uncorrelated in frequency domain, it now becomes correlated in position domain and the correlation function is determined by the directional cosine matrix A. For this reason, when the noise in one tracking channel is very intense, which means Signal-to-Noise Ratio (SNR) is very small, the large noise in this channel will spread into other tracking channels after the COOP operation shown in Figure 4.10. As a result, although the average noise level of the receiver will go down after the COOP tracking, for some channels, it may increase.

Test results discussed in Chapter 6 illustrates that, because signals affect each other in the COOP loop, COOP tracking is more suitable in carrier Doppler tracking rather than carrier phase tracking. For this reason, four velocity-assisted position loop filters are adopted along the east, north, up and time directions in a COOP loop. Figure 4.11 shows the architecture of a velocity-assisted position tracking loop along the east direction. In this study, all four loop filters in the COOP loop are identical and thus adopt the same set of loop parameters. However, the four tracking channels may have different LOOP parameters if it is necessary (e.g., if the receiver only has horizontal motion, the vertical loop filter can use more stringent parameters). For the same reason, FLL lock detectors E_{FLL} rather than PLL lock detectors are used to determine C_ϕ in Figure 4.10. As shown in Equation (4.18), signals whose frequencies can not be tracked by the

receiver will be ignored in signal transition through the matrix T, and therefore will not affect COOP tracking.

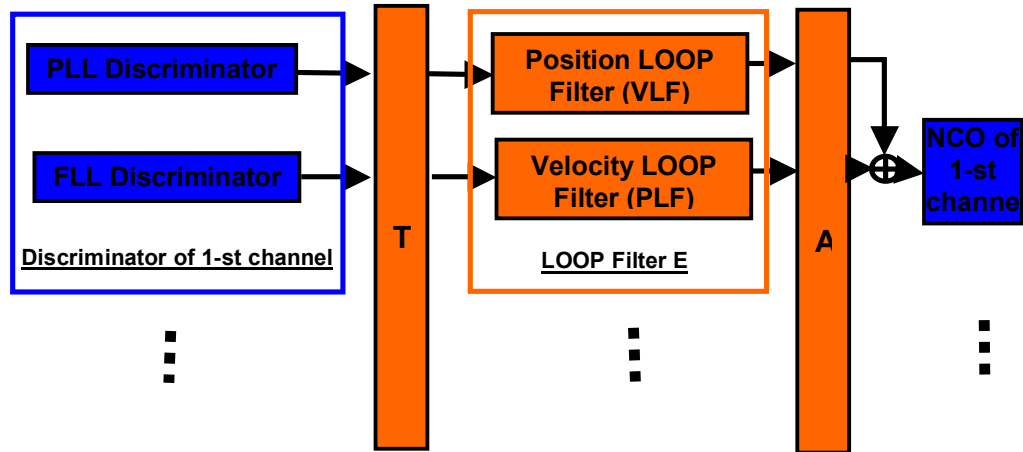


Figure 4.11 The Architecture of a Velocity-Assisted Position Tracking Loop along the East Direction

Since COOP loops suppress the PLL thermal noise, a wide noise bandwidth and a short integration time can be adopted in the COOP loops to tolerate a lower quality receiver oscillator. The COOP loop parameters used in the prototype are a 3-Hz bandwidth for position loop filter, a 1-Hz bandwidth for velocity loop filter and a 20-ms coherent integration time.

Chapter Five: Development of Testing Tools

A software-based GPS receiver was assembled, as shown in Chapter 4. In order to conduct testing and qualification of this receiver, a GPS front end is proposed to collect live GPS signals. In future, this model can be used further for field tests of ultra-tightly coupled GPS/INS. Also, an INS simulator is designed to provide INS measurements and positioning solutions for simulation testing of the GPS/INS ultra-tight integration.

5.1 Development of GPS Front End

To collect live GPS IF data for software receiver testing and qualification, a GPS IF data collecting system, referred to as a front end, is implemented.

Figure 5.1 presents the architecture of the IF data collection system and how it is used to test the software receiver.

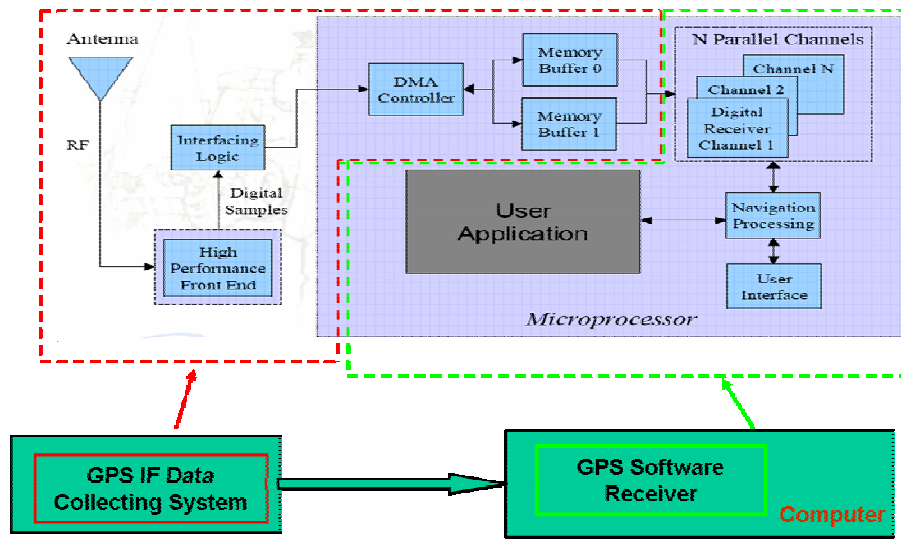


Figure 5.1 Relationship between GPS Front End and Software Receiver

In Figure 5.1, the portion in the red box is the front end, and the part in the light-green box is the software receiver. The IF data collection system includes an antenna, a high performance front end, a logic interface, Direct Memory Access (DMA), and memory buffers 0 and 1.

The architecture of the IF data collection system developed herein is presented in Figure 5.2. This system includes three parts: a commercial GPS front end GP2015, a NI-DAQ data collection card PCI-6534, and a data collection software, all running in a common computer. To collect live data, a GPS antenna is also required. The function of the logic interface and DMA controller, as indicated in Figure 5.1, is implemented in the NI-DAQ data collection card.

As illustrated in Figure 5.2, data collection software adopts double-buffered data transition technology to transfer GPS signal continuously from the dual memory buffers 0 and 1 in the NI-DAQ card to a common PC. The yellow box represents the common PC that runs the data collection software.

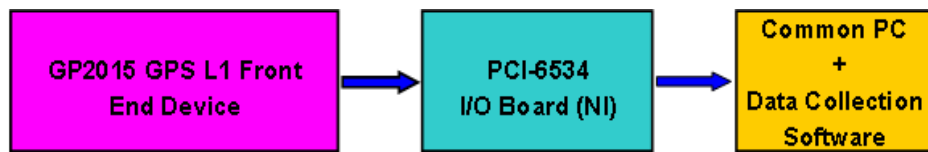


Figure 5.2 Structure of the GPS IF Data Collection System

In the GPS data collection system, the incoming RF signal is first converted down to IF frequency and sampled into digital signals by the GP2015 front end. Next, the digital IF signal is transferred to the common PC by the PCI-6534 data collection card. At last, the data collection software is used to receive the data and save it to the PC hard drive.

The system uses a NovAtel AllstarTM receiver as its front end. Therefore, this system not only provides GPS IF data as the input signal for a software receiver, but also yields GPS measurements (e.g., pseudorange, carrier phase, etc.), and GPS solutions (e.g., position, velocity, etc.). During the software receiver testing and validation, these GPS measurements and solutions are used as reference. Figure 5.3 illustrates how the

GPS IF data collection system is used for the software receiver testing and qualification in both simulation and field tests.

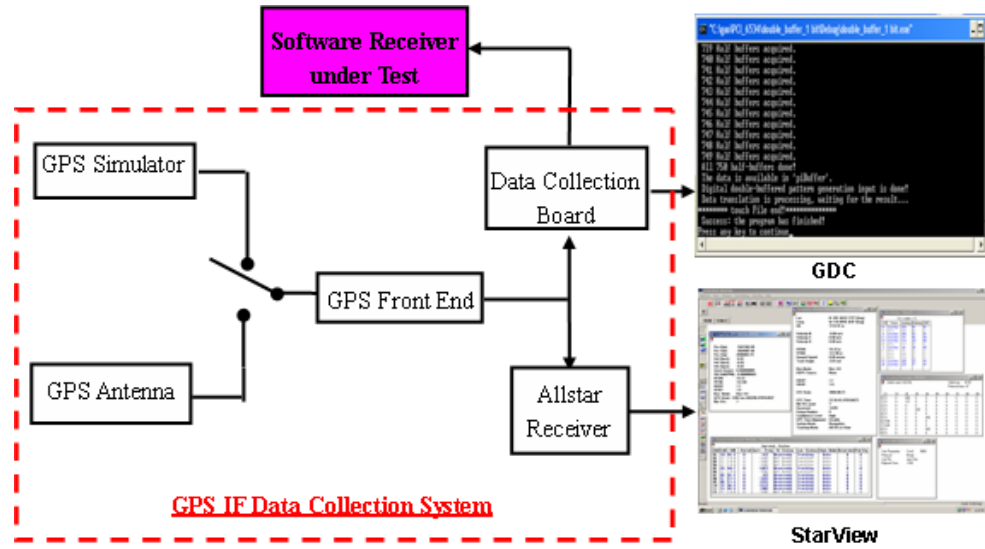


Figure 5.3 GPS IF Data Collection System Used for Software Receiver Testing & Validation During Simulation and Field Tests

Using the GPS IF data collection system, this study examined if the software receiver can correctly track the incoming signals and then yields the right positioning solution. For this purpose, several benchmark tests were conducted when the receiver was in stationary, medium dynamic and high dynamic situations. These benchmark tests validated that the receiver was designed properly, and its functions such as tracking and positioning operated correctly.

For more information about the design details of the GPS IF data collection system and the testing and validation of software receiver with this system, please refer to Appendix E.

5.2 Development of INS Simulator

In order to provide INS measurements in the simulation tests for the study of GPS/INS ultra-tight integration, an INS simulator called INS_Sim was also developed. Figure 5.4 and Figure 5.5 illustrate the architecture and the interface of the INS simulator, respectively.

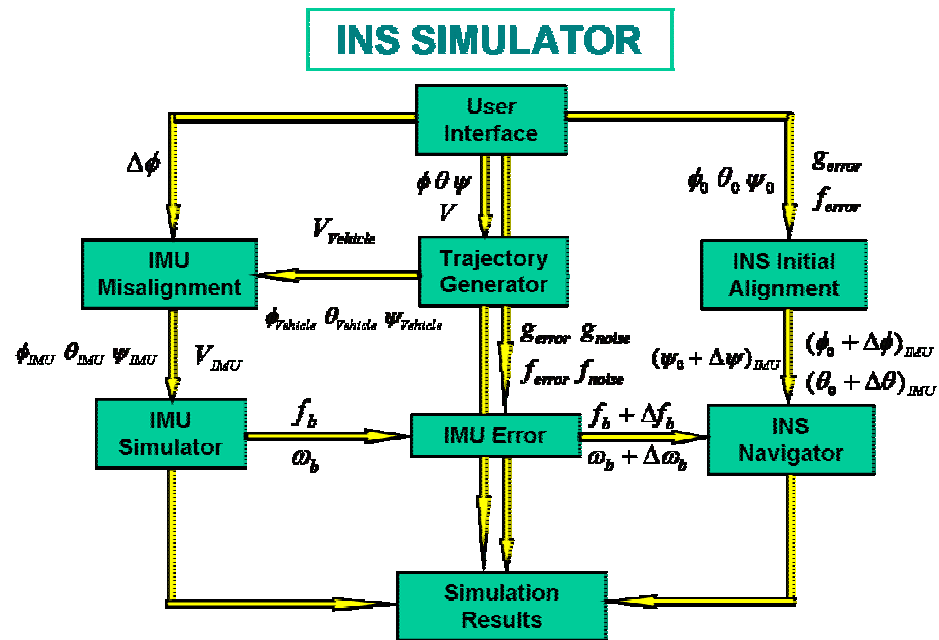


Figure 5.4 INS Simulator Architecture

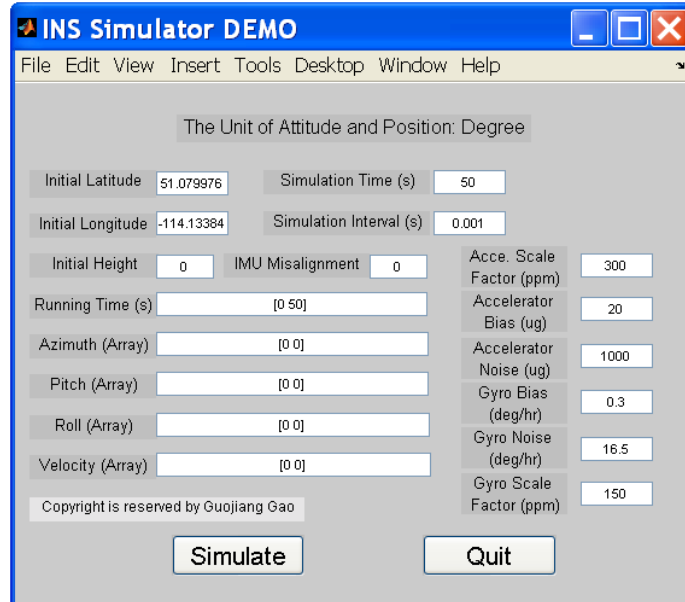


Figure 5.5 INS Simulator Interface

Figure 5.4 shows that INS_Sim includes eight modules. The functions of each module are as follows:

1. User Interface: This module is designed to input IMU and vehicle trajectory parameters for INS simulation.
2. Trajectory Generator: This module generates the vehicle trajectory over the specified simulation time with the required sampling rate.
3. IMU Simulator: This module simulates IMU and generates error-free IMU gyro and accelerometer measurements.

4. IMU Error Generator: This module simulates IMU errors and generates gyro and accelerometer measurements with errors.
5. IMU Misalignment: Because of INS mounting errors between the vehicle body frame and the IMU body frame, the vehicle attitude generated by the trajectory generator does not equal the attitude of the IMU mounted in the vehicle. An attitude rotation is achieved to calculate the correct IMU attitude parameters.
6. INS Initial Alignment: In default mode, the INS is assumed to align in Zero velocity UPdaTe (ZUPT). Thus, the INS alignment errors can be determined based only on the simulated gyro drifts and accelerometer biases.
7. INS Navigator: Based on input IMU measurements, this module calculates the position and attitude of the vehicle by using mechanization equations in the wander angle frame.
8. Simulation Result demonstrator: In this module, all simulation results are presented in ten different figures.

The simulator INS_Sim provides the following data:

- 1) Reference position, velocity, and attitude.

- 2) INS position, velocity, and attitude.
- 3) INS trajectory.
- 4) IMU raw measurements with and without IMU sensor errors.

For INS simulator testing and qualification, several benchmark tests were conducted, including static test, linear motion test, circle motion test, and “S” shaped trajectory test.

Specifics of the design and qualification of the INS simulator can be found in Appendix F.

Chapter Six: System Testing and Analysis

Based on the prototype INS-assisted high sensitivity GPS receiver described in the previous chapters, GPS/INS ultra-tight integration is tested and analyzed herein. First, the test setup is introduced. Next, both static and dynamic tests are performed in order to investigate the functions, roles and performances of different components of INS-assisted GPS receiver, namely, the INS-aided loops, the COOP loops, and the individual FLL-assisted PLLs. Following a detailed analysis of the mechanism of GPS/INS ultra-tight integration, an effective tracking strategy based on the results of the static and dynamic tests is proposed for GPS/INS integration. Finally, a performance comparison is conducted between a standard GPS receiver without INS aiding and the INS-assisted GPS receiver.

6.1 Test Setup

Both static and dynamic tests have been conducted on the GPS/INS ultra-tight integration system. Static tests included scenarios in which a GPS receiver was tracking strong and weak signals at the same time, as well as weak signals with the same power. These static tests presumed that the GPS receiver was under assessment in the simplest signal dynamics environment possible. These tests yielded a minimum receiver dynamics

impact on signal tracking. Based on these tests, the performances and the assumed roles of individual PLLs, COOP loops, and PLL+COOP loops in an INS-assisted GPS receiver were studied separately. In order to validate conclusions drawn on the basis of the static tests when the receiver was in high dynamics situations, dynamic tests were then conducted. The scenarios adopted were the same as those in static tests, with the addition of dynamics.

In this study, the effect of clock noise caused by the GPS receiver oscillator stability in signal tracking, namely, the Allan deviation oscillator phase noise, is outside of the scope of this research and, thus, is not considered in the tests. In order to limit the receiver clock error in tests, clock errors were set to zero in the simulated tests.

For simulating the incoming GPS IF signal and IMU measurements, the GPS simulator GPSIF_SimTM, developed by Dong et al (2004), and the INS simulator INS_Sim were used. These measurements were fed into the prototype INS-assisted GPS receiver as input data, as shown in Figure 6.1.

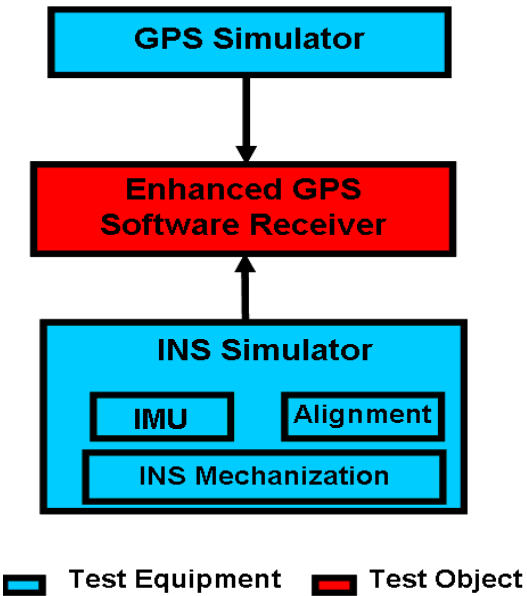


Figure 6.1 INS-assisted HSGPS Receiver Test Setup

6.2 Static Tests

For the static tests, GPS ephemeris at 19:27, July 06, 2000 was chosen for the signal simulations. At that time, seven satellites were visible from the test position (51° , -114°), and both the GDOP and HDOP were less than 2 during the test period. The PRNs visible were 04, 05, 07, 09, 17, 24 and 30.

The error characteristics of the IMU data simulated were similar to those of a tactical grade HG1700 IMU. Figure 6.2 and Table 6.1 show the INS_Sim parameters used. Refer to Petovello(2003), the simulation assumed that the INS had been initialized with GPS measurements. Therefore, the accelerometer and gyro bias residuals were

limited to approximately $20 \mu\text{g}$ and $0.3^\circ/\text{hr}$, respectively. The IMU noise bandwidth was held at about 10 Hz so that the gyro noise was equal to $16.5^\circ/\text{hr}$. Both the pitch and roll alignment errors were set to 0.01° , and the heading alignment error was set to 0.05° .

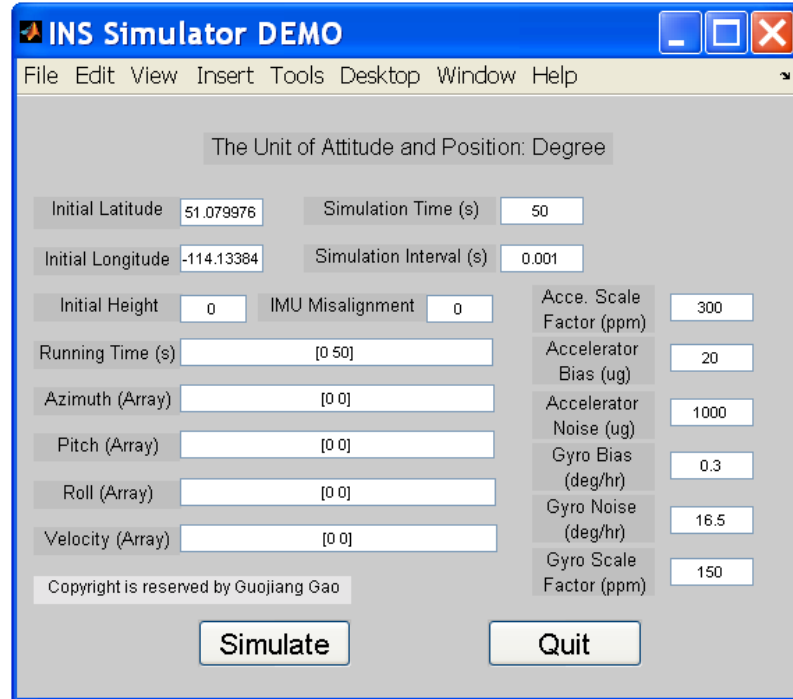


Figure 6.2 INS Simulator Set-up

Table 6.1 Simulated INS Parameters

	Accelerometer	Gyro
Scale Factor	300 ppm	150 ppm
Bias Residual	$20 \mu\text{g}$	$0.3^\circ/\text{hr}$
Random Noise	$1000 \mu\text{g}$	$5.5^\circ/(hr \cdot \sqrt{\text{Hz}})$

6.2.1 Static Test Description

Four different scenarios were examined. As shown in Figure 6.3, in these four static tests, the total duration of the data collection was the same and equalled to 50 s. During the first 14 s, the system initialization was performed in the same manner as they were performed in all four tests. Then, from 14 to 50 s, the INS output, which is the user velocity and position from INS, were fed to the GPS receiver in order to assist GPS signal tracking. In order to simplify the analysis of the tests, the INS operated in stand-alone mode for this 36 s aiding period, so that it continued to accumulate errors.

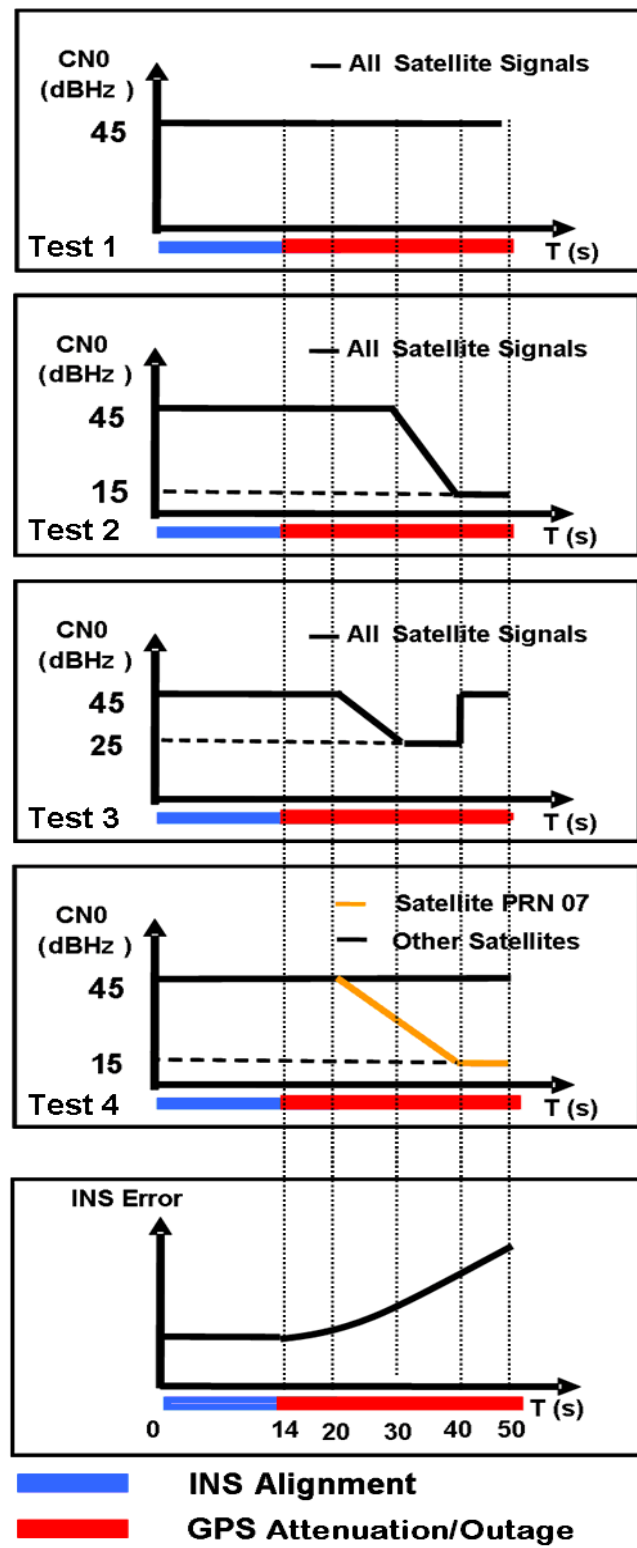


Figure 6.3 Static Test Scenarios

The simulated INS velocity errors are shown in Figure 6.4. It can be concluded that, at the 50-s point, the INS velocity errors grew to a level of 0.1 m/s in each component, which is similar to the velocity accuracy available from a MEMS IMU during 1 s in the integrated GPS/INS system (e.g., Godha & Cannon 2005). Figure 6.4 also shows that the INS velocity error increased slowly with time, although the cumulated error reached a large value (0.1 m/s) at the end of the test. The INS errors have low frequency content. In contrast to GPS errors, their time growth is somewhat smooth.

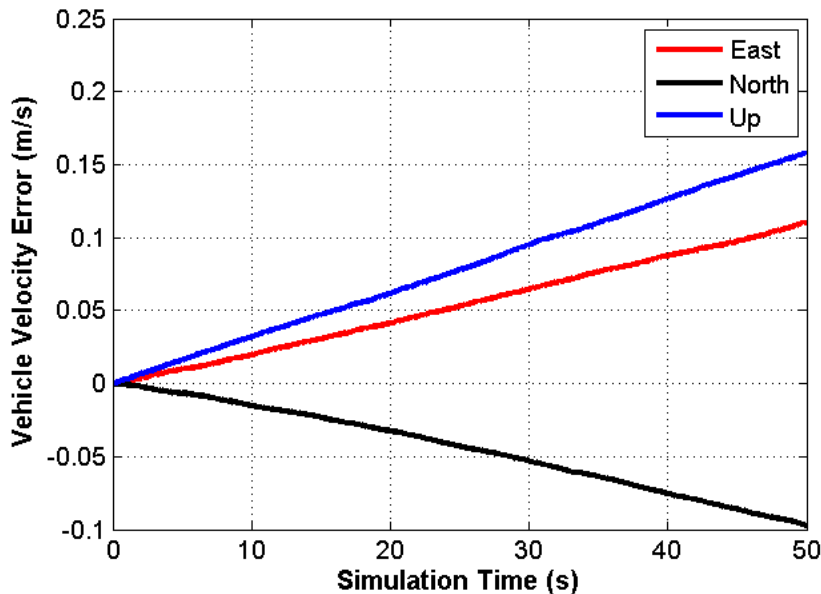


Figure 6.4 Simulated INS Velocity Errors

As shown in Figure 6.3, four different GPS scenarios were designed, namely:

Scenario 1: The GPS simulator outputted strong GPS signals (45 dB-Hz) for all satellites for the full test period of 50 s.

Scenario 2: The GPS simulator output strong GPS signals (45 dB-Hz) for all satellites during the first 30 s. During the next 10-s period, the signal power was gradually reduced to 15 dB-Hz, where it remained constant for the rest of the test.

Scenario 3: The power of all signals was held at 45 dB-Hz during the first 20 s. The power was then reduced to 25 dB-Hz during the period of 20 s to 30 s where it stayed for the next 10 s. Then, it increased back to 45 dB-Hz for the last 10 s (40 s to 50 s interval).

Scenario 4: The GPS simulator outputted strong GPS signals (45 dB-Hz) for all satellites, except for PRN 7. As illustrated in yellow in Figure 6.3, the signal power of satellite PRN 7 was 45 dB-Hz during the first 20-s period and then decreased to 15 dB-Hz during the next 20-s period. During the last 10-s period, its signal power held at 15 dB-Hz.

The above four test scenarios were designed to analyze the performance and roles of individual PLLs, COOP loops, and PLL+COOPs in the INS-assisted GPS receiver. The emphasis in every test was different as follows:

In Scenario 1, an independent FLL-assisted PLL (FPLL) and an independent COOP loop were adopted respectively in order to track the incoming signal in the INS-assisted GPS receiver. The test results were used to assess the performance of each tracking method and analyze their differences.

In Scenario 2, the COOP+FPLL combination tracking approach was used to track the incoming weak signal. In this scenario, the incoming signal was degraded to a low power level of 15 dB-Hz in order to assess the tracking threshold of the combination tracking method for both the code-delay and carrier phase signals.

In Scenario 3, the tracking performance of the new method COOP+FPLL on the incoming carrier phase was further investigated, particularly when the power of the incoming signal changed drastically with time and exhibited sharp jumps in signal strength.

In Scenario 4, the impact of strong satellite signals on weak signal tracking was studied. In this scenario, the power of satellite PRN 7 was decreased to 15 dB-Hz while that of other satellites remained at a normal open sky level. Test results illustrate how effectively strong satellite signals in view can help DLLs and PLLs maintain lock on satellite PRN 7.

The receiver parameters used in INS-assisted HSGPS receiver for each scenario are summarized in Table 6.2. This receiver uses the COOP+FPLL combination tracking approach and the involved parameters are: in FPLL, Carrier Phase Loop Filter (CPLF) and Frequency Loop Filter (FLF) noise bandwidths, FPLL coherent integration time and non-coherent integration times; in COOP, Position Loop Filter (PLF) and Velocity Loop Filter (VLF) noise bandwidths, and COOP coherent integration time and non-coherent integration times.

Table 6.2 Receiver Parameters Adopted in Different Scenarios

Adopted Receiver Parameters	Scenario One	Scenario Two	Scenario Three	Scenario Four
PLF Noise Bandwidth of COOP (Hz)	5	1.2	1.0	3
VLF Noise Bandwidth of COOP (Hz)	2	0.8	0.5	1
CPLF Noise Bandwidth of FPLL (Hz)	1	0.2	0.2	0.2
FLF Noise Bandwidth of FPLL (Hz)	0.5	0.1	0.1	0.1
Coherent Integration Time of COOP (ms)	20	20	20	20
Non-Coherent Integration Times of COOP	1	1	1	1
Coherent Integration Time of FPLL (ms)	100	100	100	100
Non-Coherent Integration Times of FPLL	10	10	10	10

6.2.2 Static Test Results and the Analysis

6.2.2.1 Scenario 1 Test Results and Analysis

Figure 6.5 to Figure 6.12 show the tracking results of both single FPLL and COOP loops for this scenario. The same receiver parameters, as shown in Table 6.3, are used for both tracking methods. These parameters include a 5-Hz noise bandwidth of Carrier Phase Loop Filter (CPLF) for FPLL or Position Loop Filter (PLF) for COOP, a 2-Hz noise bandwidth of Frequency Loop Filter (FLF) for FPLL or Velocity Loop Filter (VLF) for COOP, and a 20 ms coherent integration time. In the test, previous experience was used to empirically choose these parameters for this comparison. In reality, a standard GPS receiver in static situations typically uses these parameter values. In both cases, FPLL or COOP is first utilized in order to track the incoming signals. Then, after the receiver starts to output position solutions, which means the ephemeris is ready at that time, the INS solution is fed to the receiver through INS-aided loops.

Table 6.3 Receiver Parameters Adopted in FPLL/COOP Methods

CPLF/PLF Bandwidth (Hz)	FLF/VLF Bandwidth (Hz)	Coherent Integration Time (ms)	Non-Coherent Integration Times
5	2	20	1

In all figures in this chapter, PLL bandwidth represents the bandwidth of either carrier phase loop filter for FPLL or position loop filter for COOP. Similarly, FLL

bandwidth in all figures means the bandwidth of either frequency loop filter for FPLL or velocity loop filter for COOP.

Figure 6.5 and Figure 6.6 show the C/N₀ of satellite PRN 07, tracked by the single FPLL and COOP methods, respectively. It is clear that both FPLL and COOP methods can track the incoming signal independently. Figure 6.6 shows that COOP tracking can be used as a primary method for GPS signal tracking.

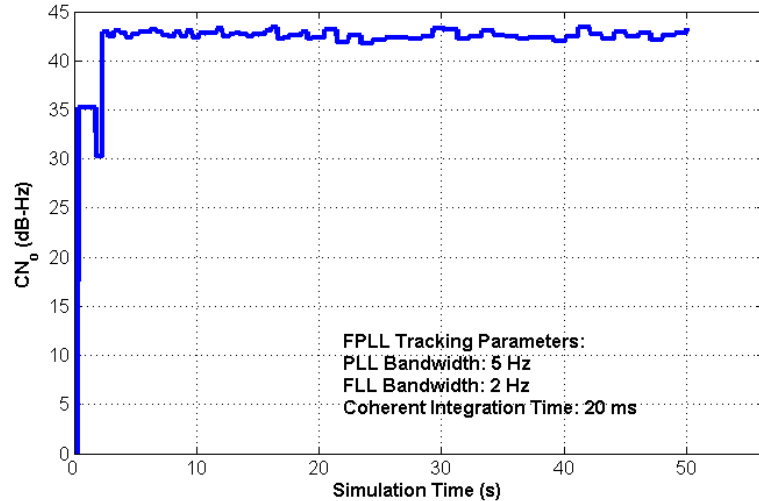


Figure 6.5 Estimated C/N₀ of FLL-Assisted PLL Tracking

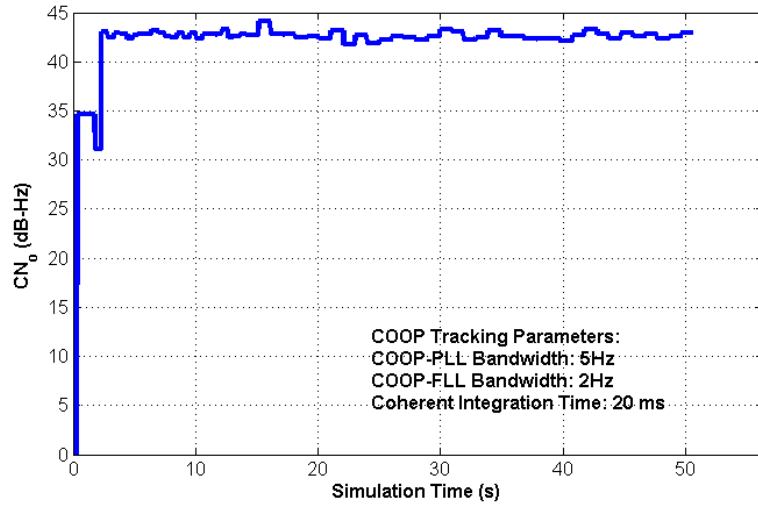


Figure 6.6 Estimated C/N₀ of COOP Tracking

Figure 6.7 and Figure 6.8 show the output of the phase discriminators in both FPLL and COOP methods. The discriminator output represent the estimated carrier phase errors tracked by the receivers. From these figures, it is obvious that the COOP discriminator product includes systematic noise after INS errors are added to the GPS receiver after the 14-s point. The PLL discriminator product appears as white noise. Furthermore, the carrier phase tracking errors of the COOP method in Figure 6.8 are larger than the PLL errors in Figure 6.7.

COOP tracking is a vector-tracking method. The COOP receiver allows received signals to aid each other to improve signal tracking performance. In other words, it means that signals affect each other through COOP loops. Figure 6.8 shows that a significant frequency error remains after signal correlation and integration. This error shown as the product of COOP discriminator can not be compensated very well after using the COOP loop. Although COOP is supposed to perform more effectively and yield lower thermal

noise as discussed in Chapter 4, unfortunately, this advantage cannot be realized if the incoming frequency cannot be tracked effectively. The following test results in the position domain illustrate that the COOP method is more suitable in tracking the incoming carrier frequency rather than the carrier phase. This method can achieve higher carrier tracking accuracy as compared to the FLL-assisted PLL method.

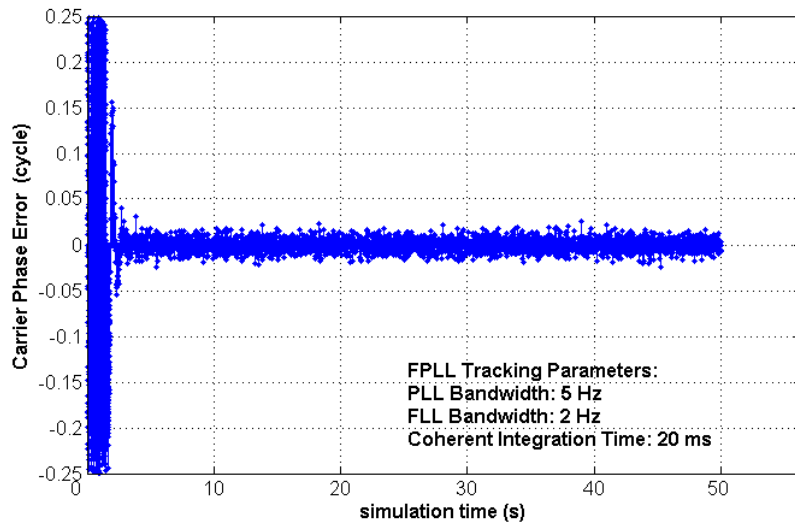


Figure 6.7 Carrier Phase Errors Estimated by FLL-Assisted PLL Method

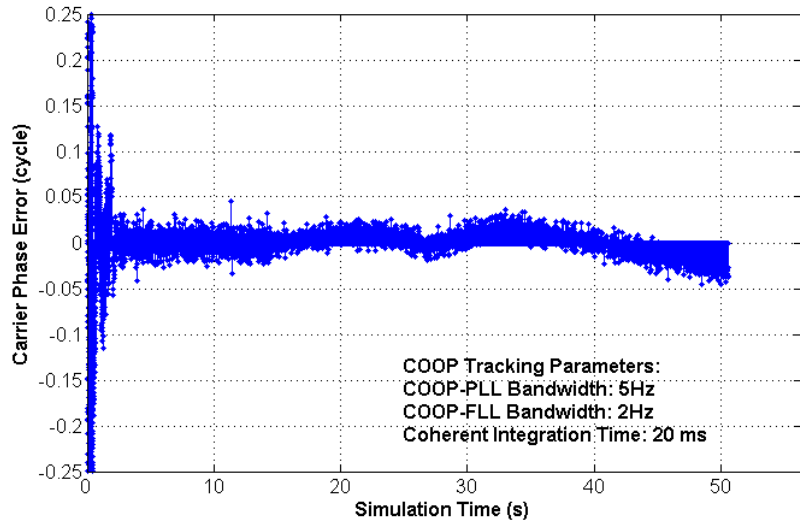


Figure 6.8 Carrier Phase Errors Estimated by COOP Method

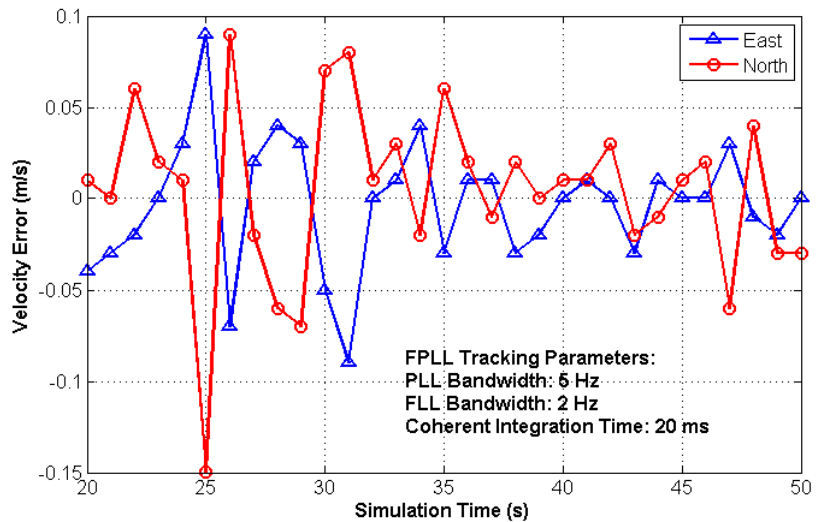


Figure 6.9 FLL-Assisted PLL Tracking Method Horizontal Velocity Errors

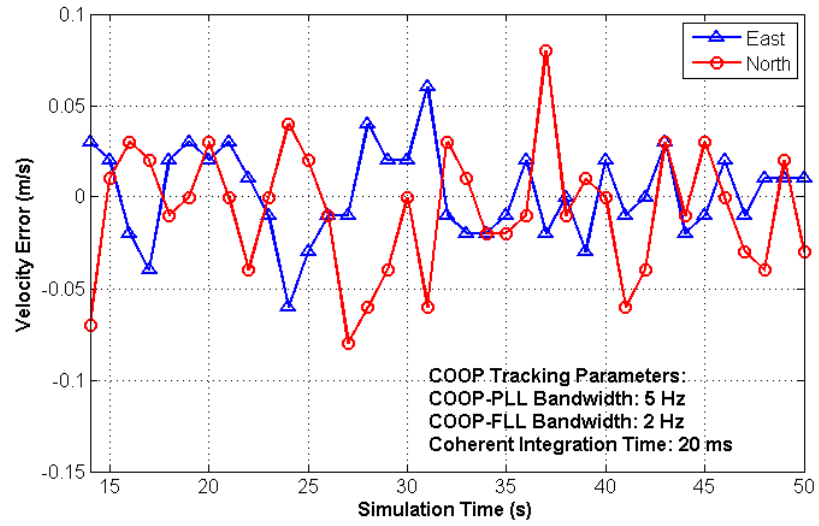


Figure 6.10 COOP Tracking Method Horizontal Velocity Errors

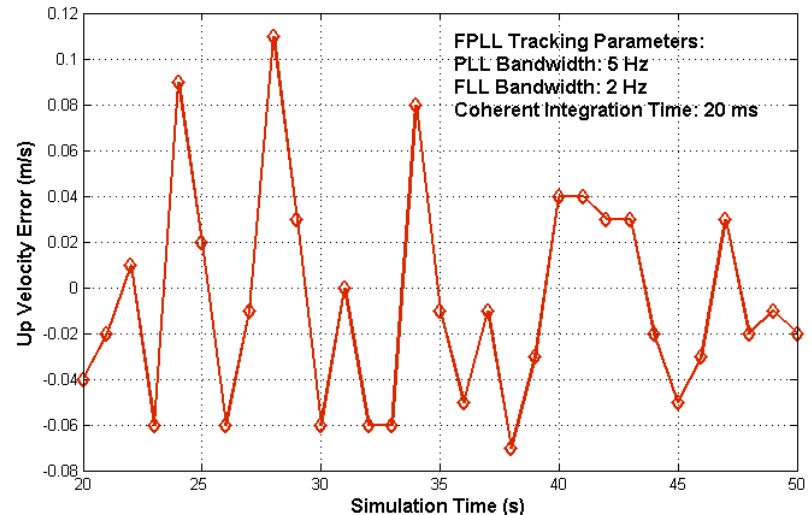


Figure 6.11 FLL-Assisted PLL Tracking Method Vertical Velocity Errors

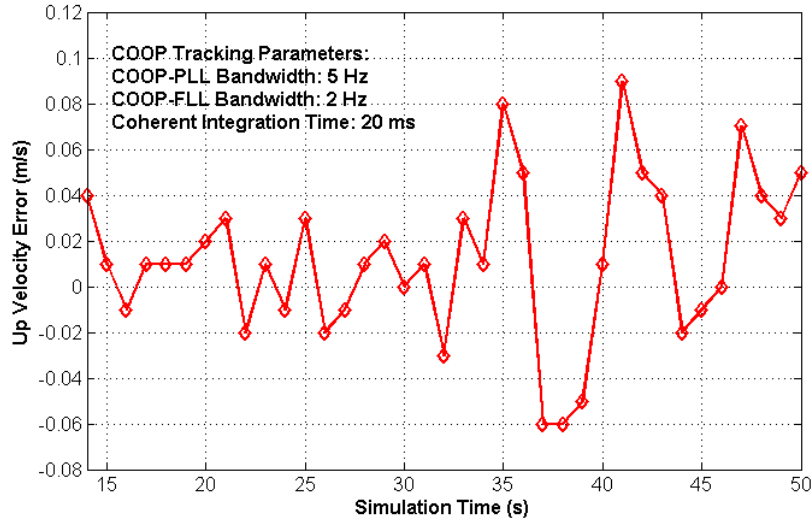


Figure 6.12 COOP Tracking Method Vertical Velocity Errors

Figure 6.9 to Figure 6.12 show the tracking results in positioning domain, given by both the FPLL and COOP methods. Since INS is used mainly to aid carrier phase tracking loops in this thesis, only the velocity solutions are examined.

As stated previously, in Figure 6.9 and Figure 6.11, FLL-assisted PLLs spend the first 20 s in order to perform frame synchronization and receive the broadcasting time of the GPS signal from the Z counter, which is available in navigation data. After the latter is received, the receiver continues to output position solutions from the 20-s point onward. However, as shown in Figure 6.10 and 6.12, it only takes the COOP method 14 s to perform the system initialization. The COOP method outputs the position 6 s earlier, as compared to the FLL-assisted PLL method.

After checking the tracking state, this study concludes that, for the FLL-assisted PLL method, there are four tracking channels that start to lock the carrier phase only after 20 s, and are in a bit and frame synchronization stage. With the COOP method, the same four channels start to lock on the carrier phase and finish bit and frame synchronization at the 14-s point. Since a receiver needs the Z counting in navigation data to calculate pseudoranges and yield position solutions, and since the navigation data can only be decoded when the tracked signal is synchronized with navigation bit and frame, the receiver with the FLL-assisted PLLs (or COOP) has to wait 20 s (or 14 s) to output position results.

The position results show that COOP can rapidly lock on the incoming carrier and finish the bit and frame synchronization faster than the FPLL method, since the COOP method is a vector-based tracking method. Therefore, the first tracked signal can assist in tracking other signals and lead to better tracking performance as compared to the speed of scale tracking.

Test results also show that the velocity accuracy achieved by the COOP method is better than that of the FPLL method, which implies that the COOP receiver suffers lower thermal noise. The velocity standard deviation (Std) with COOP tracking is 0.025 m/s, 0.035 m/s, and 0.035 m/s in the East, North and Up dimensions, respectively. With the FPLL methods, these values increase to 0.035 m/s, 0.048 m/s, and 0.047 m/s, respectively. This phenomenon is consistent with the theoretical analysis presented in Chapter 4.

In order to estimate the COOP and FPLL method performances when they are used together, the test was repeated with the INS+FPLL+COOP tracking method. In this test, PLF noise bandwidth in the COOP method was 5 Hz, VLF bandwidth in the COOP method was 2 Hz, and the coherent integration time was 20 ms. FLP and CPLF noise bandwidths in the FPLL method were 0.5 Hz and 1 Hz, respectively, and the coherent integration time was 100 ms. The GPS receiver utilizing the FPLL+COOP approach used first the COOP and FPLL methods simultaneously in order to track incoming signals. Then, after the receiver started to output position solutions, which meant that the ephemeris was ready at that time, the INS solution was fed into the receiver through INS-aiding loops.

Figure 6.13 to Figure 6.17 show the test results of the receiver with the FPLL+COOP approach.

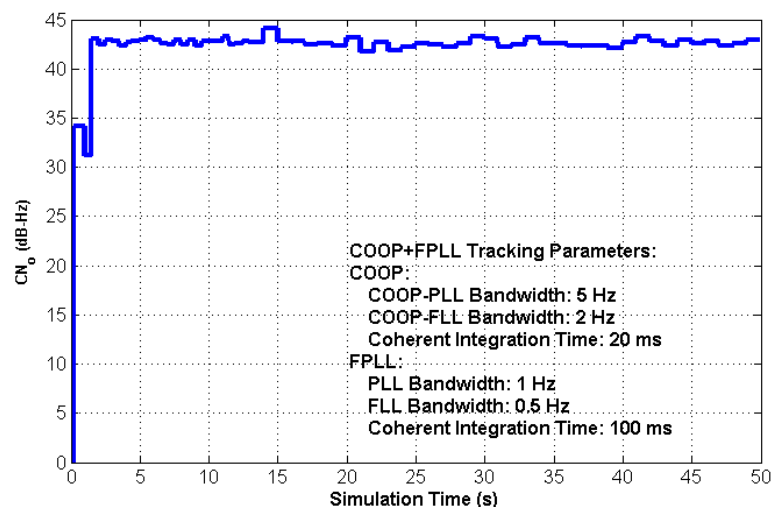


Figure 6.13 FPLL+COOP Tracking Method Estimated C/N_₀

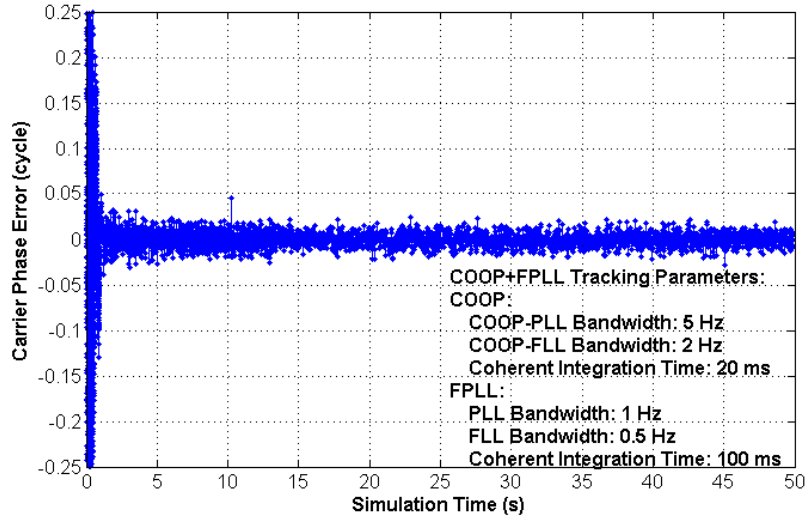


Figure 6.14 FPLL+COOP Method Carrier Phase Tracking Errors

Figure 6.13 and Figure 6.14 show that, as compared to the COOP method, the FPLL+COOP method yields better tracking performance. After FPLL aiding, the carrier phase tracking errors in Figure 6.14 do not include systematic errors any more. From the 14-s point onward, when the INS errors are added to the receiver, the carrier phase errors are obviously smaller than the COOP tracking errors shown in Figure 6.8. This phenomenon is explained in Figure 6.15.

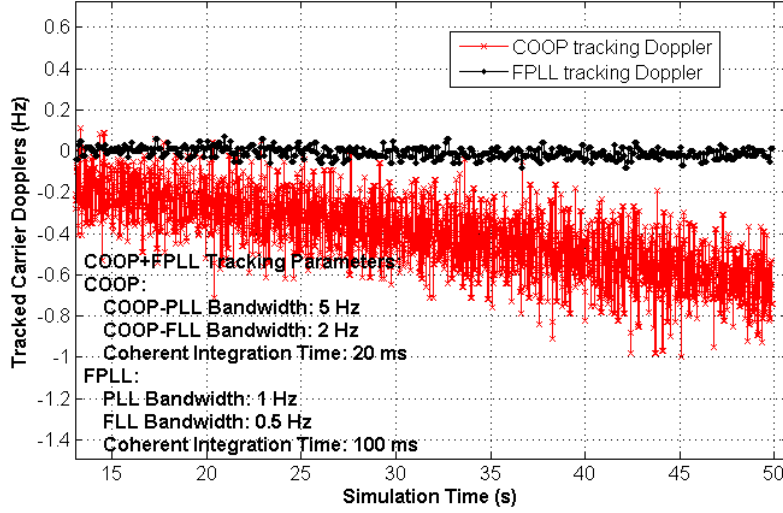


Figure 6.15 Carrier Doppler Tracked by FPLL and COOP Methods Separately in FPLL+COOP Method

In Figure 6.15, the red and black lines represent the carrier Doppler tracked by the COOP and FPLL methods at the same time. With the FPLL+COOP method, the FLL bandwidth used in the FPLLs is very narrow, namely 0.5 Hz, and the integration time is very long, i.e., 100 ms. Therefore, the carrier frequency tracking capability enhancement by FPLL is very low: very long integration and very narrow noise bandwidth average the dynamics of carrier phase and render the FPLL insensitive to the change of carrier frequency. In Figure 6.15, it is evident that the COOP method tracks the carrier Doppler very effectively, despite the error induced by INS aiding as shown in Figure 6.4. Since COOP tracking compensates for INS aiding errors, COOP+INS aiding provides a nearly perfect reference for receiver dynamics. Therefore, the carrier Doppler tracked by FPLLs is around zero, and FPLLs are used mainly for carrier phase tracking. Thus, FPLLs contribute significantly to carrier phase tracking accuracy enhancement in the

FPLL+COOP method. Figure 6.15 also shows clearly that the roles of the COOP and FPLL methods are different in a FPLL+COOP receiver: the COOP and FPLL methods are used to deal with carrier frequency and carrier phase tracking, respectively.

The velocity errors of the COOP+FPLL approach in Figure 6.16 and Figure 6.17 are smaller than the corresponding errors of the COOP approach as indicated in Figure 6.10 and Figure 6.12. The improvement, however, is not significant. The standard deviation of the velocity with the FPLL+COOP approach is 0.020 m/s, 0.023 m/s and 0.027 m/s in the East, North and Up dimensions, respectively.

The velocity accuracy depends on the accuracy of Doppler measurements. As discussed above, the FPLLs in the FPLL+COOP approach are used to track the carrier phase only. The improved tracking accuracy of the carrier phase by FPLLs does not benefit significantly velocity determination.

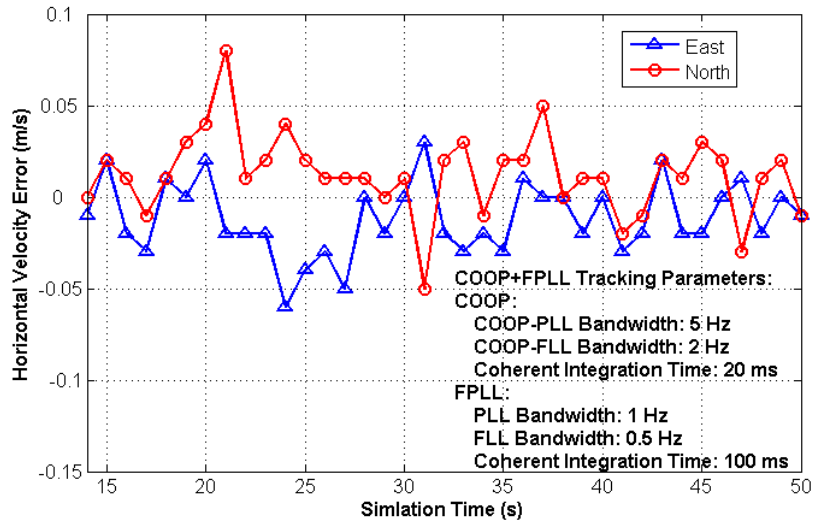


Figure 6.16 FPLL+COOP Tracking Horizontal Velocity Errors

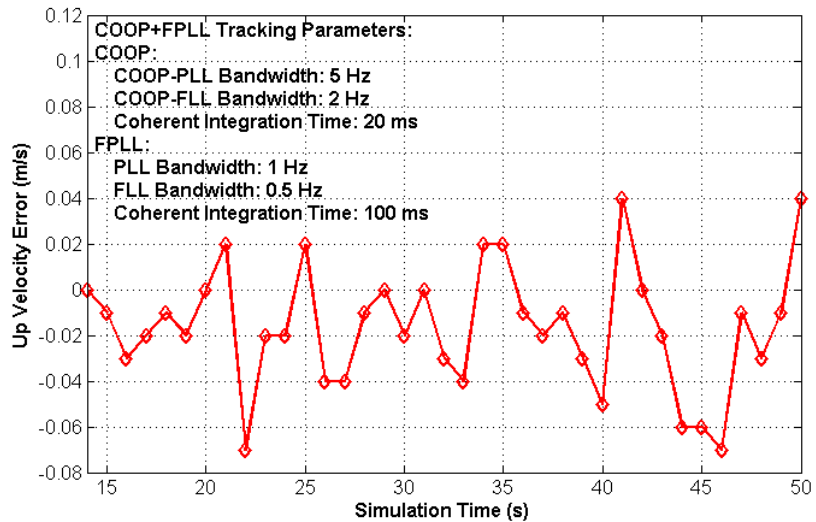


Figure 6.17 FPLL+COOP Tracking Vertical Velocity Errors

6.2.2.2 Scenario 2 Test Results and Analysis

In this test, the signal power of all satellites plummeted to 15 dB-Hz after the 30-s point, and then remained near 15 dB-Hz during the last 10-s period, as shown in Figure 6.3.

To find a set of receiver parameters that achieve the best signal tracking performance, different combinations of receiver tracking parameters are examined. These special parameter combinations were selected based on previous experience. The same approach was used to get the optimal receiver parameters for the INS-assisted GPS receiver in all other tests shown in later of this chapter. Table 6.5 illustrates the statistics of the last 10-second tracking results of three different receivers. As shown in Figure 6.19, the signal power in the last 10-second test was kept on 15 dB-Hz. Parameters adopted in three receivers in Table 6.5 are listed in Table 6.4: Receiver one used very narrow noise bandwidths for both COOP and FPLL, with a very long FPLL integration time, namely, 2 s. In receiver two, wider noise bandwidth and shorter integration time were adopted. However, compared to those used in a standard receiver, these parameters were still very stringent. Receiver three used a set of parameters which can also be used in a standard GPS-only receiver in static situations. As shown in Figure 6.20 and Figure 6.21, the estimated carrier phase error and COOP tracking Doppler in Table 6.5 are the receiver PLL discriminator output and the carrier Doppler tracked by the COOP, respectively. The standard derivations of these two observations are used in Table 6.5 to assess carrier phase tracking performance of the three receivers.

As illustrated in Table 6.5, when receiver parameters become more and more stringent from receiver three to receiver one, the standard deviation of the carrier Doppler tracked by COOP is smaller and smaller, which means COOP can track the incoming signal more and more accurately. From Table 6.5, one can also see that the 15 dB-Hz signal is locked in the entire test and all three receivers can output reasonable velocity solutions. Based on test results of Table 6.5, it is evident that: while the adopted receiver parameters vary in a large range, the INS-assisted HSGPS receiver presents very stable performance in both phase and code tracking.

In Table 6.5, receiver one illustrates the best performance, however, in the entire 50-second test of receiver one, as shown in Figure 6.18, the tracked carrier phase of satellite PRN 07 by receiver one presents cycle slips from the 24-second point onward. Although carrier phase tracked by receiver two or receiver three also presents cycle slips, these cycle slips will not appear until 40-second point onward. As conclusion, receiver two presents the best tracking performance in this test and its parameters are: 1.2 Hz of PLF noise bandwidth and 0.8 Hz of VLF noise bandwidth in COOP, 0.2 Hz of CPLF noise bandwidth and 0.1 Hz of FLF noise bandwidth in FPLL, 20 ms of coherent integration time in COOP, and 100 ms of coherent integration time and 10 times of non-coherent integration in FPLL.

In order to compute measurement errors, the “true” reference carrier phase is provided with the test results received from scenario 1 where all satellite signals stay at 45 dB-Hz. This measurement reference is also used in the remaining static tests.

Please note that, because of different receiver dynamics, different levels of signal power, etc, the optimal receiver parameters and the range of suitable parameters for the INS-assisted HSGPS receiver may change from one case to another.

In dynamic situations, a narrower range of suitable receiver parameters is expected in signal tracking. With INS aiding, the signal dynamics can be compensated and thus decreased into a low level, as compared to a standard GPS-only receiver. However, the remaining signal dynamics, which is mainly induced by INS velocity estimate error, is expected larger when the receiver is in dynamic situations. The reasons are: 1) INS velocity error induced by accelerometer or gyro's scale factors will increase in high dynamic situations. 2) The change of receiver attitude in dynamics will lead to jerks in INS aiding Doppler and thus affect the signal tracking significantly. These possible issues of signal tracking in dynamic situations in theory are observed in tests, as shown in later of this chapter.

Figure 6.19 to Figure 6.24 show the test results of the receiver two in the entire 50-second test.

Table 6.4 Parameters Adopted in Three Receivers

Adopted Receiver Parameters	Receiver One	Receiver Two	Receiver Three
PLF Noise Bandwidth of COOP (Hz)	0.2	1.2	3
VLF Noise Bandwidth of COOP (Hz)	0.6	0.8	1

CPLF Noise Bandwidth of FPLL (Hz)	0.1	0.2	0.2
FLF Noise Bandwidth of FPLL (Hz)	0.05	0.1	0.1
Coherent Integration Time of COOP (ms)	20	20	20
Non-Coherent Integration Times of COOP	1	1	1
Coherent Integration Time of FPLL (ms)	100	100	100
Non-Coherent Integration Times of FPLL	20	10	10

Table 6.5 Tracking Result Statistics of Different Receivers when the Incoming Signal is 15 dB-Hz

Observation Name	Receiver One	Receiver Two	Receiver Three
Estimated Carrier Phase Error Std on Satellite PRN 07 (cycle)	0.029	0.030	0.030
COOP Tracking Doppler Std on Satellite PRN 07 (Hz)	0.4	1.3	1.9
Estimated C/N _o Mean on Satellite PRN 07 (dB-Hz)	17.9	17.8	17.8
Estimated C/N _o Std on Satellite PRN 07 (dB-Hz)	3.1	3.2	3.1
Horizontal Velocity Error Mean (m/s)	0.21	0.38	0.40
Horizontal Velocity Error Std (m/s)	0.16	0.23	0.30
Vertical Velocity Error Mean (m/s)	-0.10	0.23	0.14
Vertical Velocity Error Std (m/s)	0.24	0.50	0.79

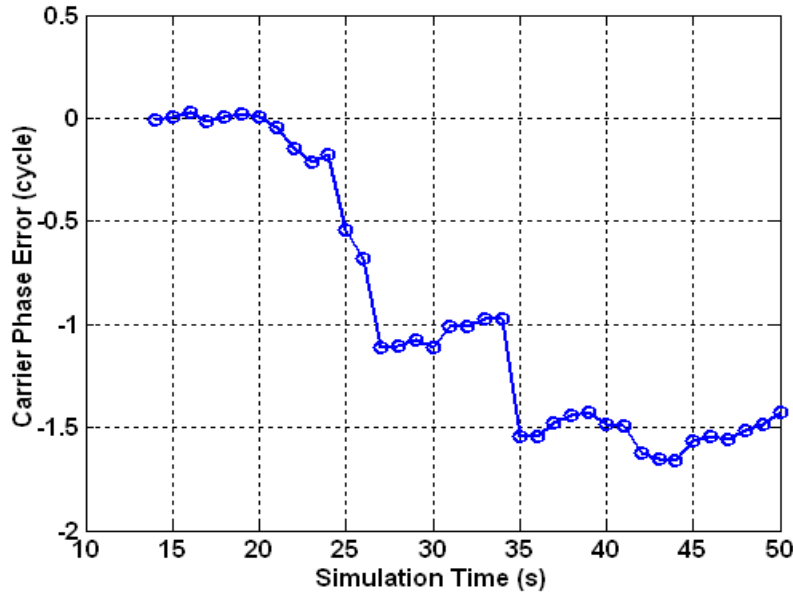


Figure 6.18 Total Carrier Phase Errors of Receiver One

Figure 6.19 shows the SNR of satellite PRN 07 tracked by the FPLL+COOP receiver. It is obvious that the INS-assisted HSGPS receiver can track the incoming signal as low as 15 dB-Hz. However, when the signal power is low, the estimation method used to calculate SNR is not as accurate as in the case when the signal power is strong.

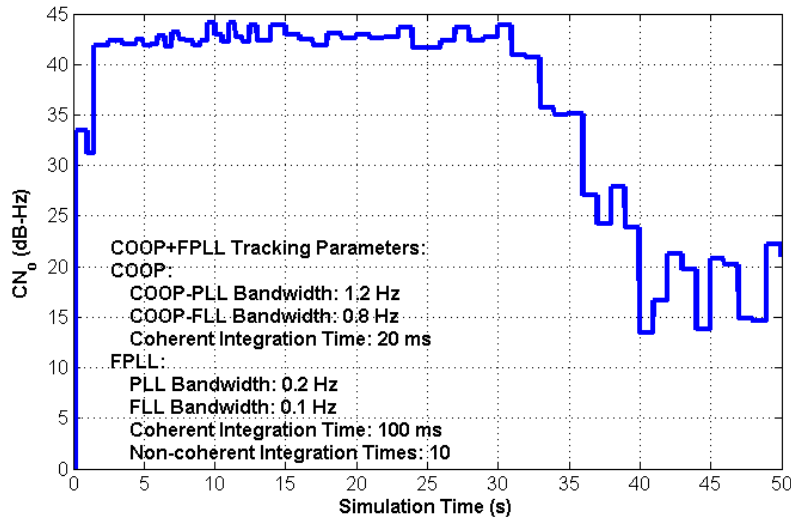


Figure 6.19 Estimated C/N_₀ of PLL+COOP Tracking

Figure 6.20 and Figure 6.21 show the carrier phase tracking errors of satellite PRN 07 in the FPPLL+COOP receiver. During the entire 50-s period, the receiver tracks the incoming carrier phase without a frequency bias. So, the phase error appears as thermal noise. The carrier phase error increases suddenly after the 38-s point. This jump implies that the COOP loop lost lock on the incoming carrier frequency. Therefore, the carrier phase tracked by the FPPLL is very noisy. However, as shown in Figure 6.20, although carrier phase errors are significant after the 38-s point, most of the errors are below 0.25 cycles, i.e. 90° . It means that the receiver still continues to track the incoming carrier phase, although cycle slips may occur.

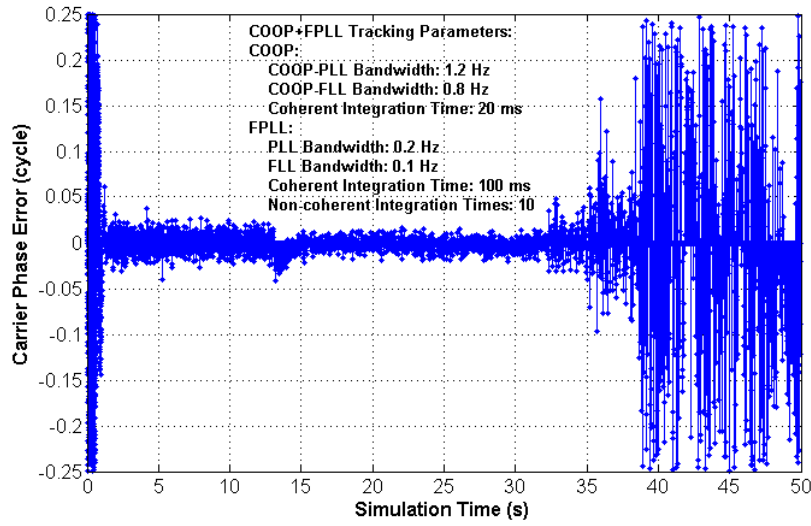


Figure 6.20 FPLL+COOP Carrier Phase Tracking Errors

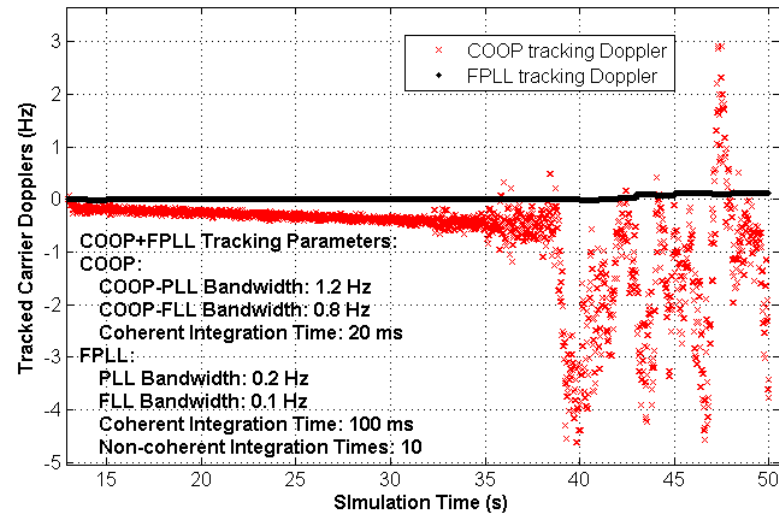


Figure 6.21 Carrier Doppler Tracked by FPLL and COOP Methods Separately in the FPLL+COOP Approach

Figure 6.22 shows the total carrier phase error of satellite PRN 07 in the FPLL+COOP receiver. From Figure 6.22 , one can see that the carrier phase is tracked

for the entire 50-s period. During the first 40 s, the carrier phase error is very small. After the 40-s point, although the carrier phase is tracked most of the time, cycle slips result due to frequency tracking errors.

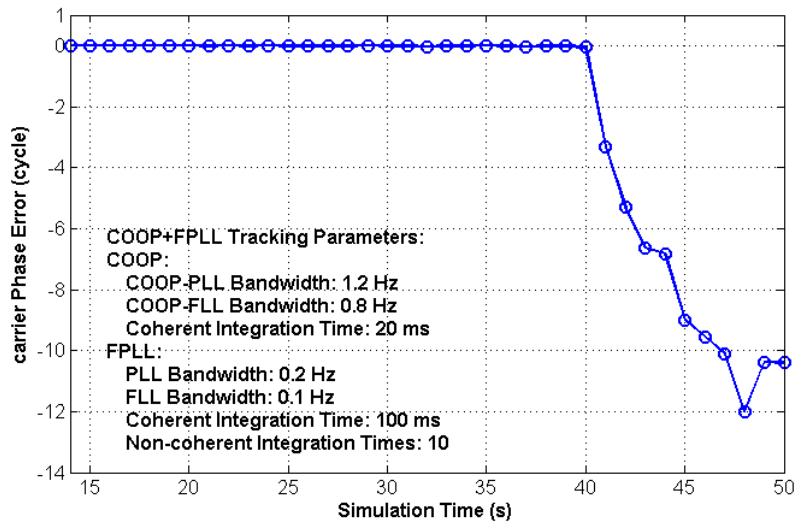


Figure 6.22 Total Carrier Phase Errors of FPLL+COOP Receiver with INS Aiding

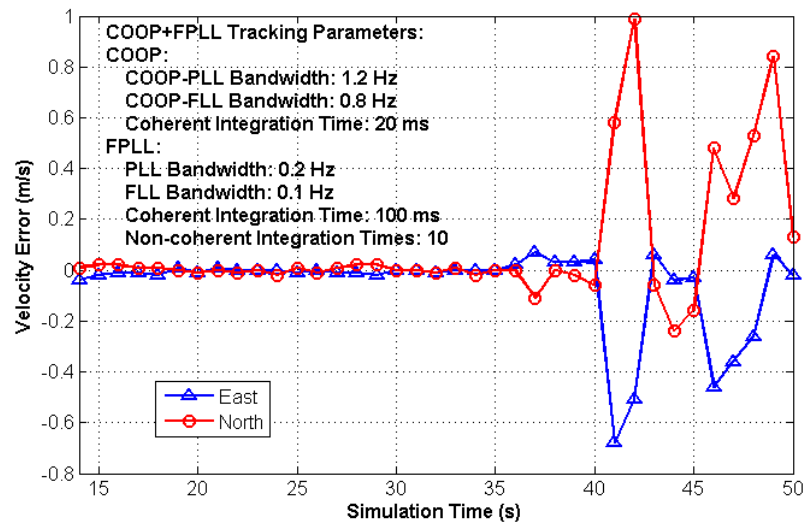


Figure 6.23 FPLL+COOP Tracking Horizontal Velocity Errors

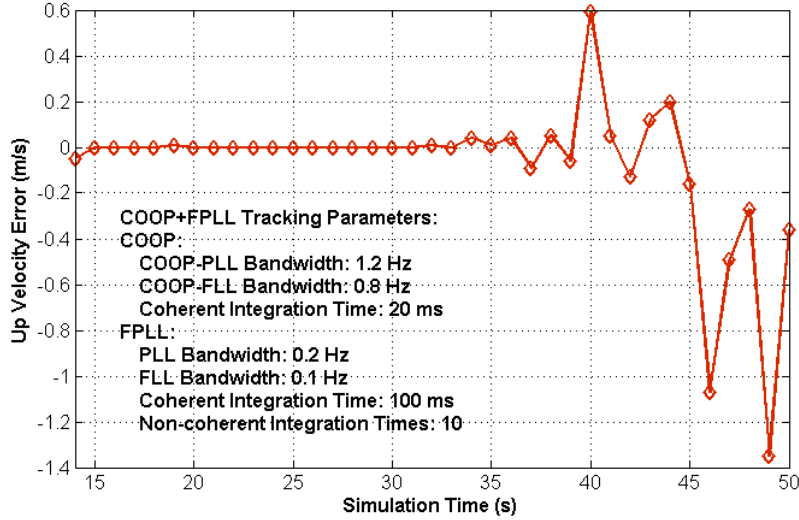


Figure 6.24 FPLL+COOP Tracking Vertical Velocity Errors

Figure 6.23 and Figure 6.24 show the horizontal and vertical velocity errors of the FPLL+COOP receiver, respectively. It is apparent that, before the COOP loop loses lock, the velocity errors are very small. After the COOP loop loses lock, the velocity errors increase significantly. When the carrier frequency is locked, the accuracy of the measured velocities stays at the same level until the incoming signal power decreases to 21 dB-Hz at the 38-s point.

6.2.2.3 Scenario 3 Test Results and Analysis

Figure 6.25 to Figure 6.30 show the test results of this FPLL+COOP receiver scenario. In this test, the signal power of all satellites dropped to 25 dB-Hz after the 20-s point, and held at 15 dB-Hz for 10 s (from the 30-s to the 40-s point). During the last 10 s period, the signal power of all satellites increased again to 45 dB-Hz. The receiver

parameters that presented the best tracking performance in this test were: PLF noise bandwidth in the COOP method was 1 Hz, VLF bandwidth in the COOP method was 0.5 Hz, the coherent integration time was 20 ms, the FLF and CPLF noise bandwidths in the FPLLs were 0.1 Hz and 0.2 Hz, respectively, and the coherent and non-coherent integration times were 100 ms and 10, respectively.

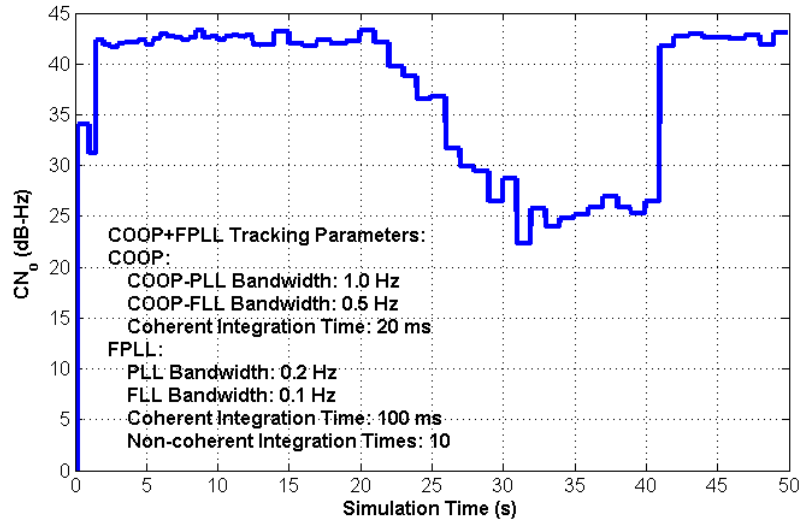


Figure 6.25 Estimated C/N_0 of PLL+COOP Tracking

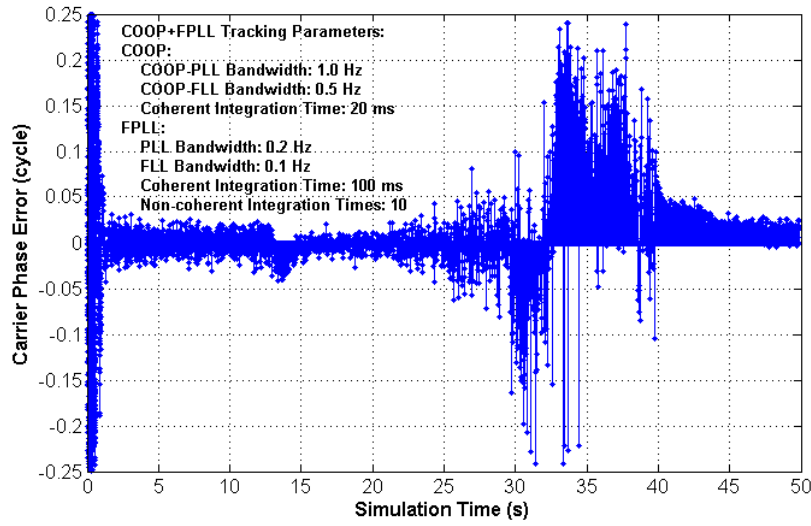


Figure 6.26 FPLL+COOP Carrier Phase Tracking Errors

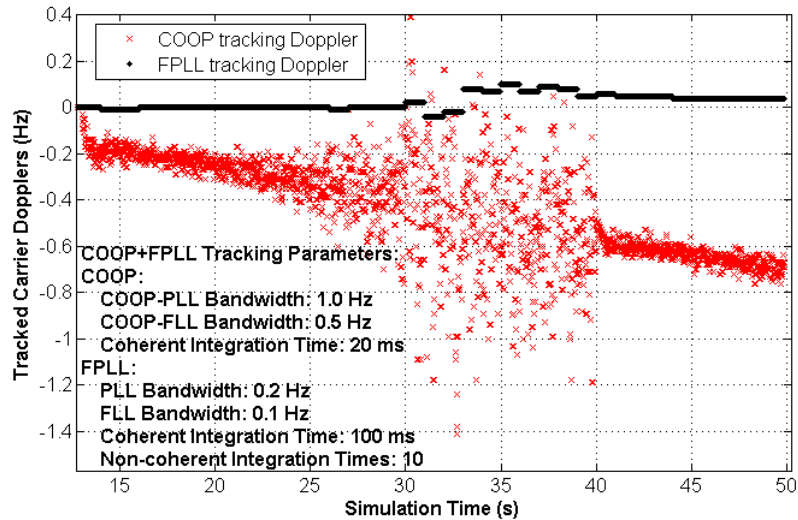


Figure 6.27 Carrier Doppler Tracked by FPLL and COOP Methods

Figure 6.25 to Figure 6.27 show the tracking results of satellite PRN 07 in the FPLL+COOP receiver. From these figures, one can conclude the following: 1) both the carrier frequency and carrier phase of the incoming signal can be locked in the INS-

assisted GPS receiver, although the tracking accuracy is very low when the signal power is approximately 25 dB-Hz. This conclusion is further confirmed by the test results in the measurement domain, as seen in Figure 6.28, 2) when a weak signal turns into a strong signal, the COOP loop can respond to this change quickly and can track the carrier frequency of the incoming signal accurately and without delay. However, there might be a frequency bias after the COOP adjusts the tracking frequency. Figure 6.26 shows a frequency bias resulting from the FPLLs after the 40-s point. Therefore, the mean of the carrier phase error after the 40-s point is not zero, as shown in Figure 6.26.

Figure 6.28 shows the total carrier phase errors of satellite PRN 07 in the FPLL+COOP receiver. As mentioned in Section 6.2.2.1, the “true” reference carrier phase is provided with test results obtained from scenario 1. The figure shows that carrier phase was locked during the entire 50-s period. Although the phase error is large when the signal power is 25 dB-Hz between the 30-s and the 40-s points, no cycle slip occurs. After the signal power reverts to 45 dB-Hz, the carrier phase error decreases immediately to a very small level.

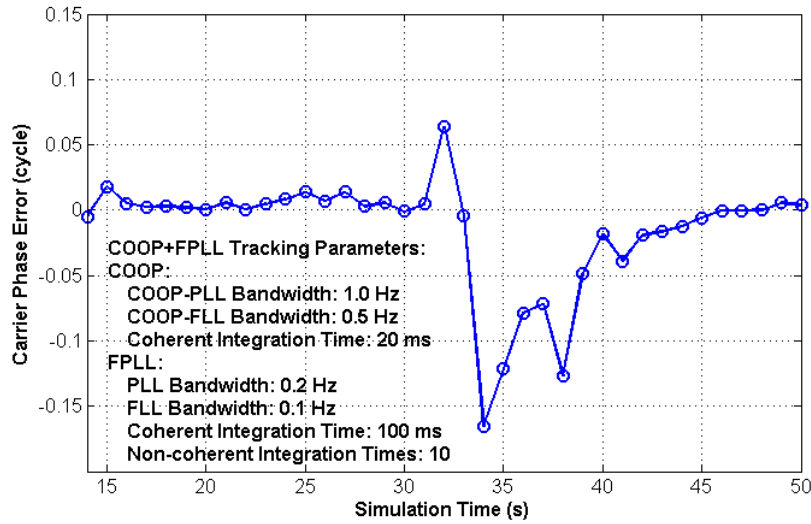


Figure 6.28 Total Carrier Phase Errors of the FPLL+COOP Receiver with INS Aiding

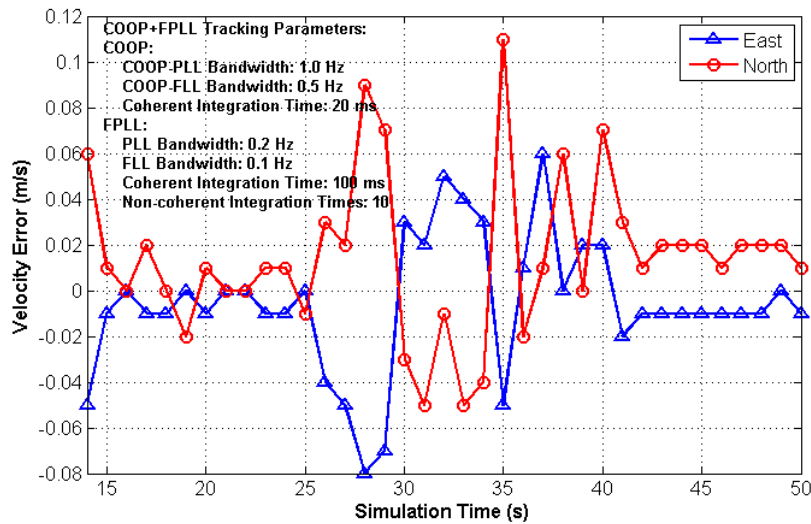


Figure 6.29 FPLL+COOP Tracking Horizontal Velocity Errors

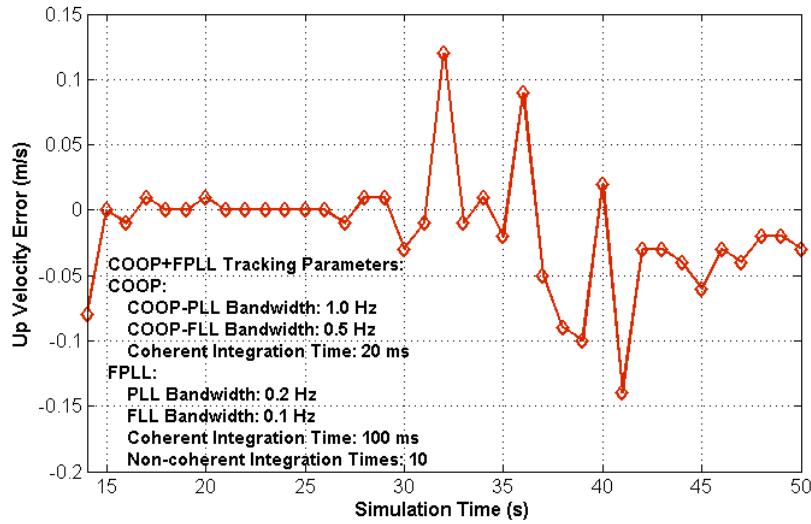


Figure 6.30 FPLL+COOP Tracking Vertical Velocity Errors

Figure 6.29 and Figure 6.30 show the horizontal and vertical velocity errors of the FPLL+COOP receiver. Although the signal power diminishes to 25 dB-Hz in the middle of the test, the velocity accuracy of INS-assisted GPS receiver remains at an acceptable level and is below 0.05 m/s (1σ).

6.2.2.4 Scenario 4 Test Results and Analysis

Figure 6.31 to Figure 6.36 show the test results of the FPLL+COOP receiver for this scenario. Only satellite signal PRN 07 dropped to 15 dB-Hz, step by step, from the 20-s point to the 40-s point, and then remained at that level for the last 10 s, while all other satellite signals were at 45 dB-Hz for the entire test period. The receiver parameters that presented the best tracking performance in this test were as follows: PLF noise bandwidth in the COOP method was 3 Hz, VLF bandwidth in the COOP method was 1 Hz, the

coherent integration time was 20 ms, the FLF and CPLF noise bandwidths in the FPLLs were 0.1 Hz and 0.2 Hz, respectively, and the coherent and non-coherent integration times were 100 ms and 10, respectively.

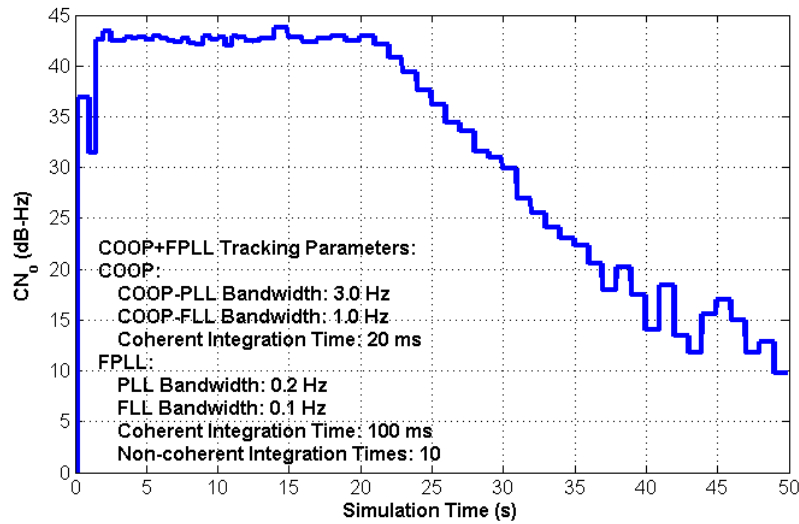


Figure 6.31 Estimated C/N_₀ of PLL+COOP Tracking

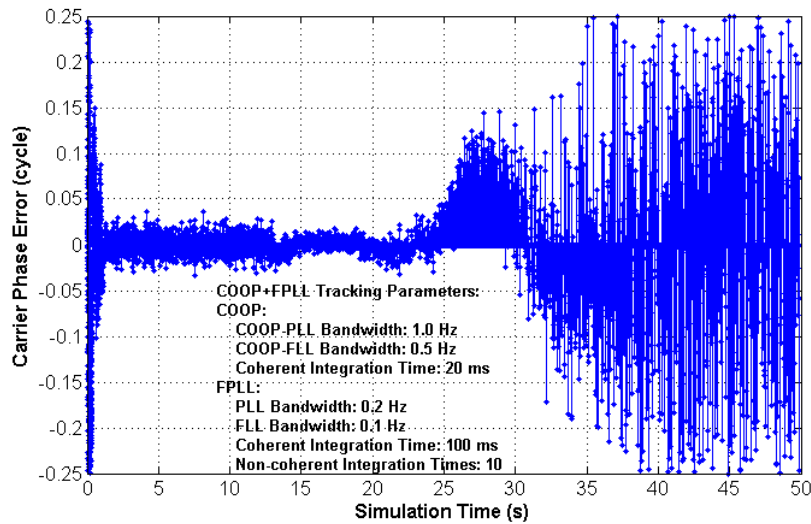


Figure 6.32 FPLL+COOP Carrier Phase Tracking Errors

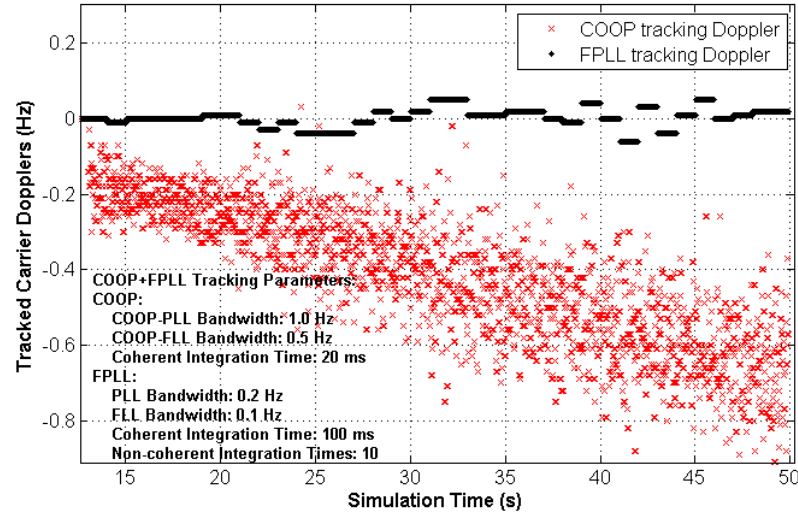


Figure 6.33 Carrier Doppler Tracked by FPLL and COOP Methods

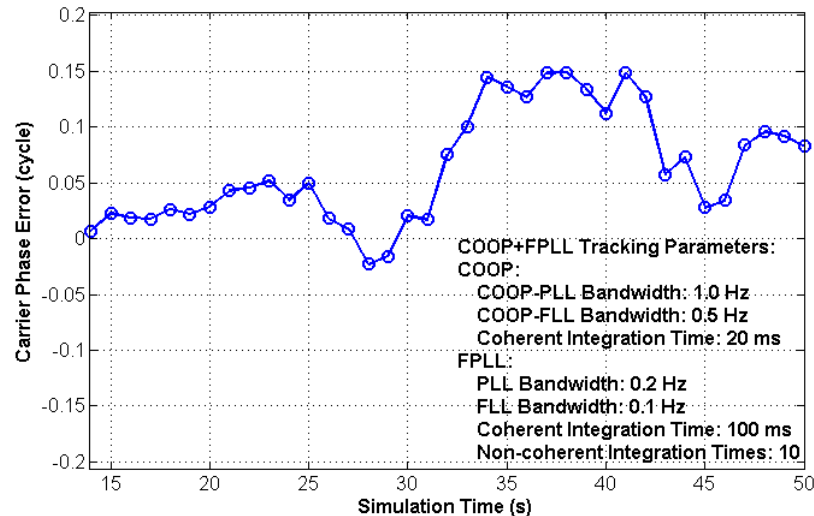


Figure 6.34 Total Carrier Phase Errors of FPLL+COOP Receiver with INS Aiding

Figure 6.31 to Figure 6.34 show the tracking results of satellite PRN 07 in the FPLL+COOP receiver. From these Figures, it can be discerned that, although the signal

power of satellite PRN 7 is attenuated from 45 dB-Hz to 15 dB-Hz during the last 30-s period, the INS-assisted GPS receiver still can track the satellite with carrier phase locked.

Figure 6.33 shows the carrier Doppler tracked by the FPLL and COOP methods. Although the signal power of satellite PRN 07 is degraded to 15 dB-Hz during the last 10-s period, the carrier Doppler is tracked by the COOP method very effectively. The residual carrier Doppler tracked by the FPLLs is close to zero and appears as white noise. If one compares Figure 6.33 and Figure 6.21 (Scenario 2), it is evident that, since the receiver is obtaining other strong signals, except satellite PRN 07, these strong signals assist the tracking of weak signals in the COOP approach. Therefore, COOP performance in tracking weak signals is improved considerably because of the existence of these strong signals.

Furthermore, if one compares Figure 6.34 with Figure 6.22, it is clear that the carrier phase is locked for the entire period of scenario 4, while the receiver suffers cycle slips when signal power is low (15 dB-Hz) in scenario 2. This improvement is achieved due to the assistance of tracked strong signals through the COOP loops.

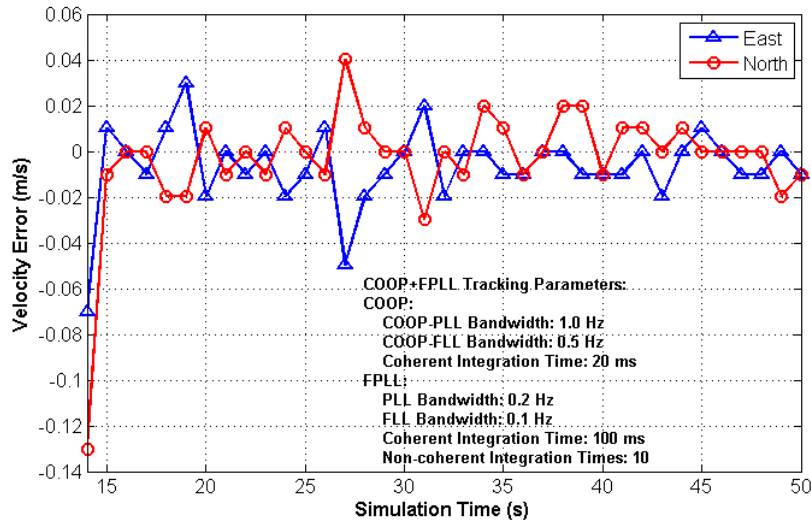


Figure 6.35 FPLL+COOP Tracking Horizontal Velocity Errors

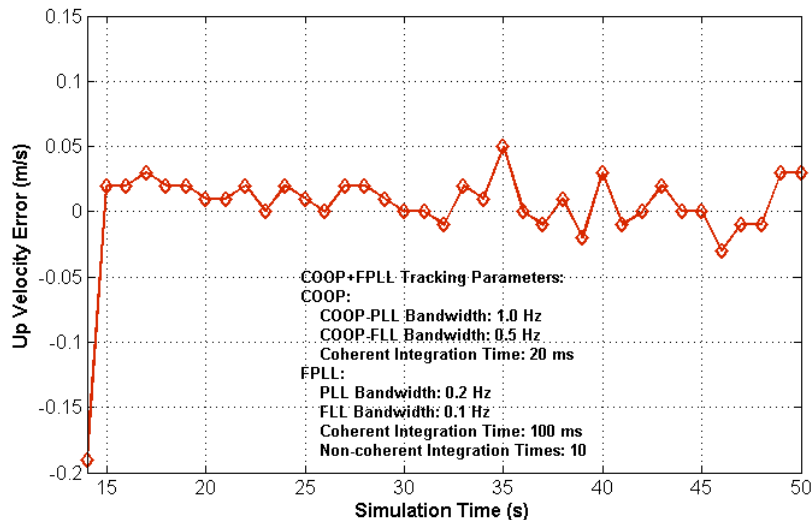


Figure 6.36 FPLL+COOP Tracking Vertical Velocity Errors

Figure 6.35 and Figure 6.36 show the horizontal and vertical velocity errors of the FPLL+COOP receiver. Although the signal power of satellite PRN 07 plummets to 15 dB-Hz during the last 30 s of the test, it does not affect the solution. The velocity

accuracy of the INS-assisted GPS receiver is not degraded by the weak signal and remains at the same level of about 0.02 m/s (1σ) during the entire test.

6.2.3 Static Tests Summary

Based on the above four tests and their analyses, the following conclusions can be drawn:

1. When the INS solution is available, an effective weak signal tracking strategy can be summarized into three steps: 1) by applying the INS aiding loops introduced in Chapter 4, the INS solution can be used to remove most receiver dynamics uncertainty. Therefore, the COOP and FPLL methods can work in a very narrow tracking range where the carrier Doppler is close to zero, 2) then, the small carrier Doppler is located in the pull-in range of the COOP tracking loop so that the COOP loop can track the residual carrier Doppler effectively. Today, there are always 6 to 10 satellites in view. Since the COOP method is a vector-based tracking method, it yields significantly better tracking performance for real applications as compared to the performance of conventional FPLLs, especially in weak signal environments such as urban canyons and indoors, 3) since the COOP method tracks the residual carrier Doppler, the FPLLs can be used to track only the carrier phase whose frequency is very close to zero. As discussed in Chapter 2, for a digital FLL/PLL, a zero Doppler error will significantly decrease the carrier phase tracking error, and, therefore, increase the FLL/PLL tracking sensitivity.

2. The combined FPLL and COOP tracking method presented here has been shown to track signals as low as 15 dB-Hz. When the signal power is above 22-23 dB-Hz, this method can lock on the incoming carrier phase, and provide accurate carrier phase measurements. When the signal is lower than 22 dB-Hz but higher than 15 dB-Hz, the method can track the incoming carrier phase most of the time, although cycle slips may occur. With assistance from strong signals, the receiver can track weak signals as low as 15 dB-Hz with carrier phase locked.
3. Although the INS errors increase rapidly with time during a GPS outage, as shown in Figure 6.4, the INS solution errors change very smoothly. Such smoothly increasing INS errors can be easily tracked by the COOP method and, therefore, will not affect signal tracking significantly. Even if the INS solution errors are as large as 0.1 m/s, the INS-assisted GPS receiver can track GPS signals that are 30 dB lower than LOS signals with acceptable accuracy.

6.3 Dynamic Tests

In order to validate the conclusions arrived at by conducting the static tests on the INS-assisted GPS receiver, this study implemented two dynamic tests. In these tests, two different trajectories were simulated. One was an “S” shaped trajectory used to simulate a receiver submitted to direction changes. In the other trajectory, the vehicle moved in a straight line with different accelerations in order to simulate a linear motion.

6.3.1 Scenario 1: Direction Change Test

6.3.1.1 *Test Description*

The receiver trajectory and the velocities simulated in this dynamic test are shown in Figure 6.37 and Figure 6.38, respectively. During the first 20 s, the vehicle moved east, with a velocity of 100 m/s. During the next 30 s, the vehicle followed a “S” shaped trajectory, with an angular rate of change of 6 °/s.

The change of signal power in the test can be seen in Figure 6.39. As with static test scenario 3, the signal power was reduced simultaneously from 45 dB-Hz to 25 dB-Hz during the period from 20 s to 30 s. Then, the power level for all signals remained at 25 dB-Hz from 30 s to 40 s, and then increased to 45 dB-Hz during the last 10 s.

The parameters for the INS simulator were the same as those used in the static tests. The INS velocity errors are shown in Figure 6.40. The receiver parameters that presented the best tracking performance and therefore used in this test were: PLF noise bandwidth in the COOP loops of 3 Hz, VLF bandwidth of 1 Hz in the COOP loops, a coherent integration time of 20 ms; FLF and CPLF noise bandwidths in FPLLS of 0.2 Hz and 0.4 Hz, respectively, and coherent and non-coherent integration times of 100 ms and 10, respectively.

In the above tests, including dynamic and static tests, the best set of receiver tracking parameters varies from one test to another, because of different signal dynamics, different

levels of signal power, etc. However, these changes are very little: the optimal noise bandwidth of phase loop filter in FPLL varies from 1 Hz to 3 Hz in all tests, while the optimal noise bandwidth of position loop filter in COOP keeps around 0.2-0.4 Hz. Compared to those values used in a standard GPS receiver in different dynamic situations, the optimal noise bandwidth of the INS-assisted GPS receive changes very little. In a standard GPS receiver, the noise bandwidth of PLL is regularly from 1-3 Hz in a static case to 20 Hz in a moderate-dynamics case. The reason for the improvement that one see in INS-assisted GPS receiver is that, because of INS aiding, most of signal dynamics has been measured by the INS and then compensated in receiver tracking loops.

The other parameters were kept the same as in the case of the static tests.

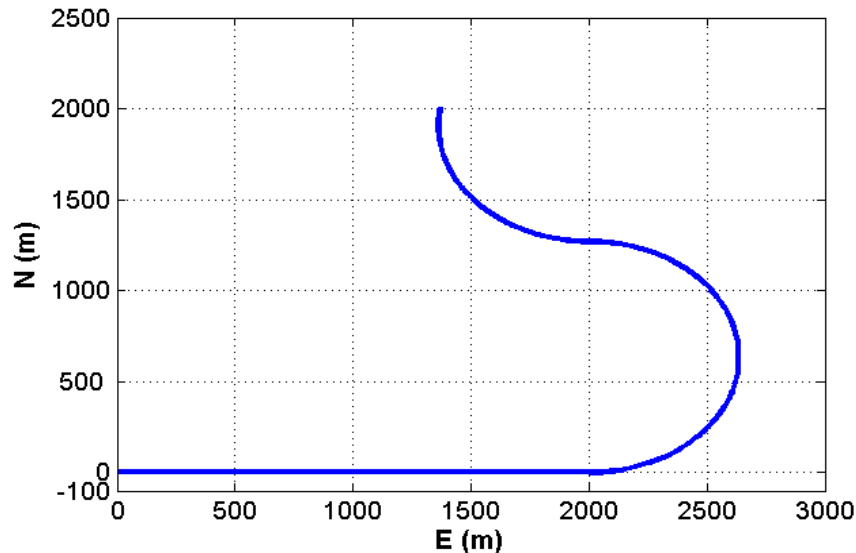


Figure 6.37 Dynamic Test Trajectory

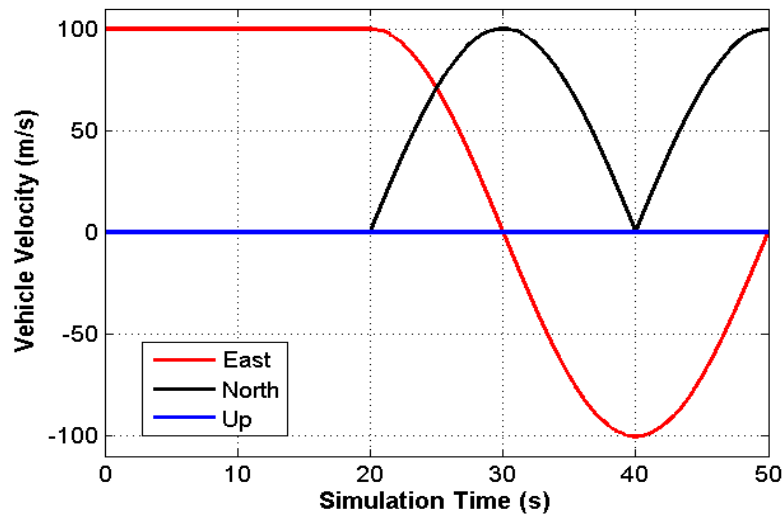


Figure 6.38 Dynamic Test Velocity

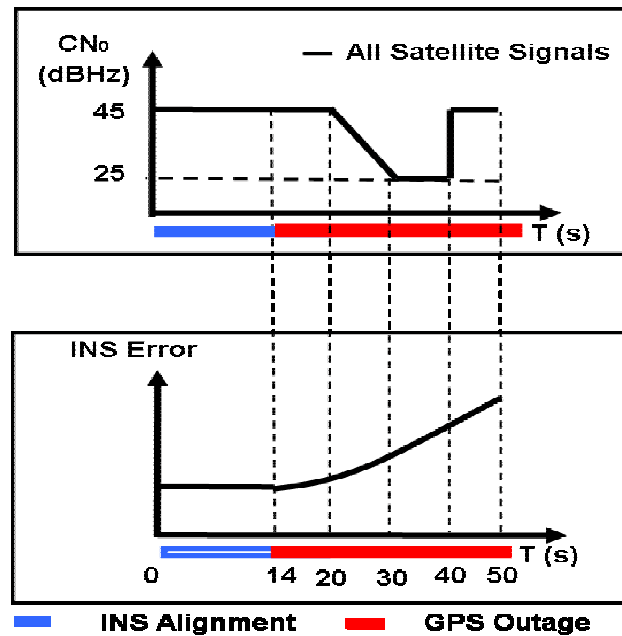


Figure 6.39 Simulated Signal Power Variations

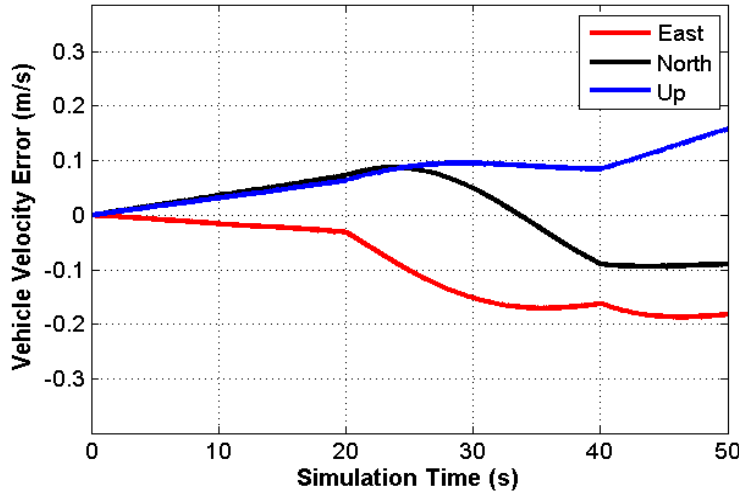


Figure 6.40 Dynamic Test INS Velocity Errors

6.3.1.2 Dynamic Scenario 1 Test Results and Analysis

Figure 6.41 to Figure 6.45 show the test results of the FPLL+COOP receiver for this dynamic test. The test scenario is very similar with static test scenario 3, except for the vehicle motion and thus different receiver parameters adopted for better tracking performance in dynamic situations.

Figure 6.41 to Figure 6.43 show the tracking results of satellite PRN 07 in the FPLL+COOP receiver, and Figure 6.44 and Figure 6.45 show the horizontal and vertical velocity errors of the FPLL+COOP receiver, respectively. The “true” reference of the carrier phase used for the computation of the carrier phase errors in Figure 6.42 was determined by performing another test where all satellite signals were uniformly held at 45 dB-Hz.

When one compares the test results of Figure 6.25 to Figure 6.30 for scenario 3 of the static test with the corresponding dynamic test figures, it is evident that all conclusions arrived at for static test apply for the dynamic test. The tracking strategy used in the INS-assisted GPS receiver is very successful. Although receiver dynamics is very high in this case, after INS aiding, the remaining carrier Doppler is considerably lower and changes very smoothly, as shown in Figure 6.40. Therefore, the signal tracking performance of the INS-assisted GPS receiver does not suffer when the receiver dynamics is very high. When the signal power is higher than 25 dB-Hz, the carrier phase of the incoming signal can be locked, and the velocity accuracy of the receiver is acceptable.

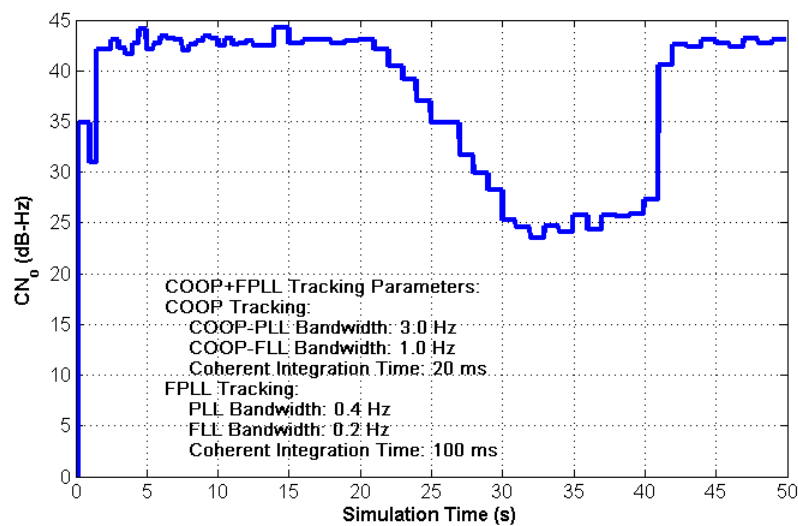


Figure 6.41 Estimated C/N₀ of PLL+COOP Tracking

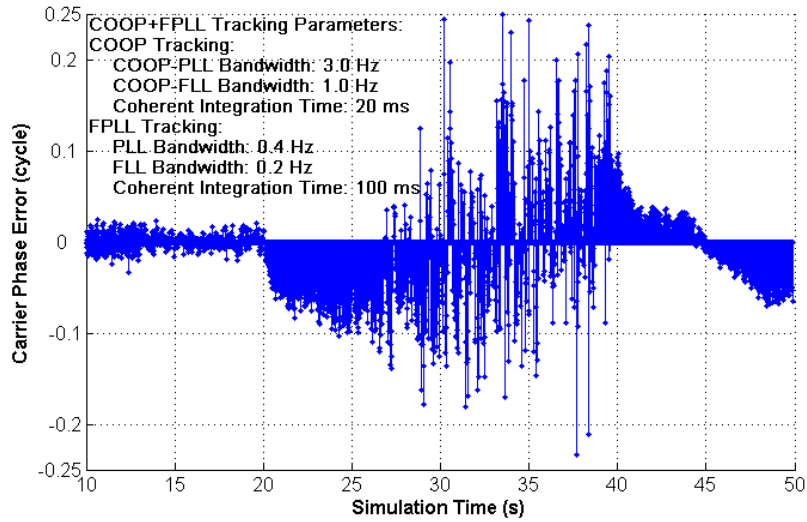


Figure 6.42 FPLL+COOP Carrier Phase Tracking Errors

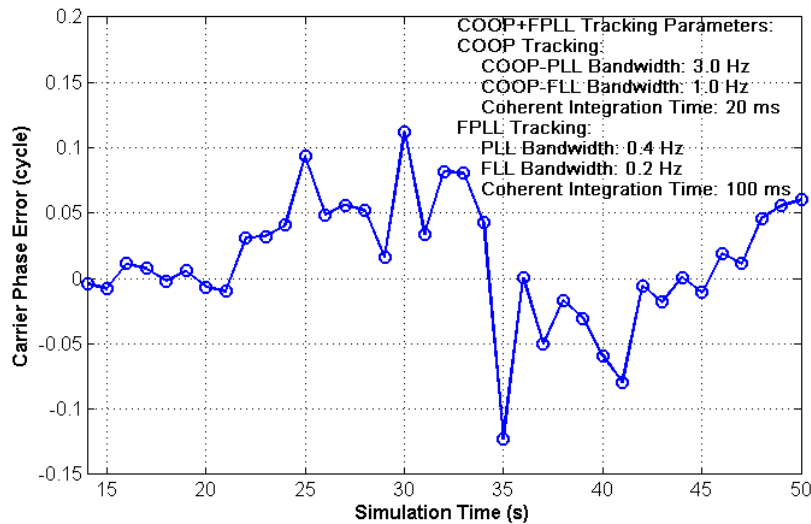


Figure 6.43 Total Carrier Phase Errors of FPLL+COOP Receiver with INS Aiding

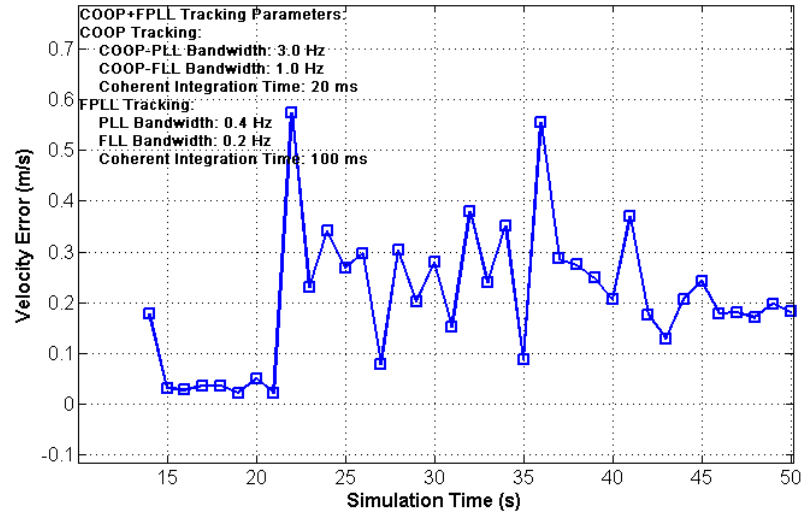


Figure 6.44 FPLL+COOP Tracking Horizontal Velocity Errors

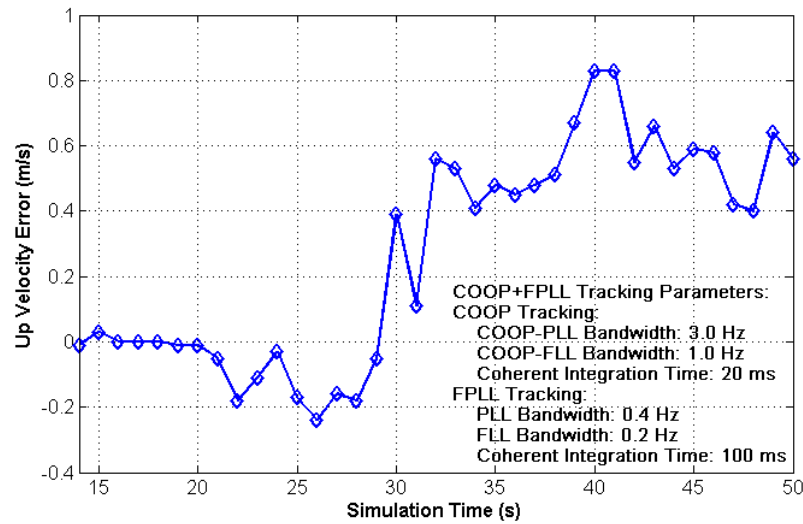


Figure 6.45 FPLL+COOP Tracking Vertical Velocity Errors

6.3.2 Scenario 2: Linear Motion Test

6.3.2.1 *Test Description*

This test was conducted in order to examine the receiver performance when it was in a linear motion. The receiver trajectory and the velocities simulated for this test are presented in Figure 6.46 and Figure 6.47. The receiver was stationary in the first 20 s. Then, the receiver moved straight toward east during the next 15 s, with a linear acceleration of 20 m/s^2 . During the last 15 s, the vehicle slowed down along the east direction, with a negative linear acceleration of 20 m/s^2 .

The signal power change in the linear motion test was the same as the one in static test scenario 2. In this test, the signal power of all satellites decreased to 15 dB-Hz after 30 s and remained approximately at that level during the next 10 s.

The INS simulator parameters were the same as those used in the angular motion test. The INS velocity errors are shown in Figure 6.48. The receiver parameters that presented the best tracking performance and therefore used in this test were: PLF noise bandwidth of 6 Hz in the COOP loops; VLF bandwidth of 3 Hz in the COOP loops, a coherent integration time of 20 ms, FLF and CPLF noise bandwidths of 1 and 2 Hz, respectively, in the FPLLs, and a coherent integration time of 100 ms for the FPLLs.

The other parameters were the same as those in the case of the angular motion test.

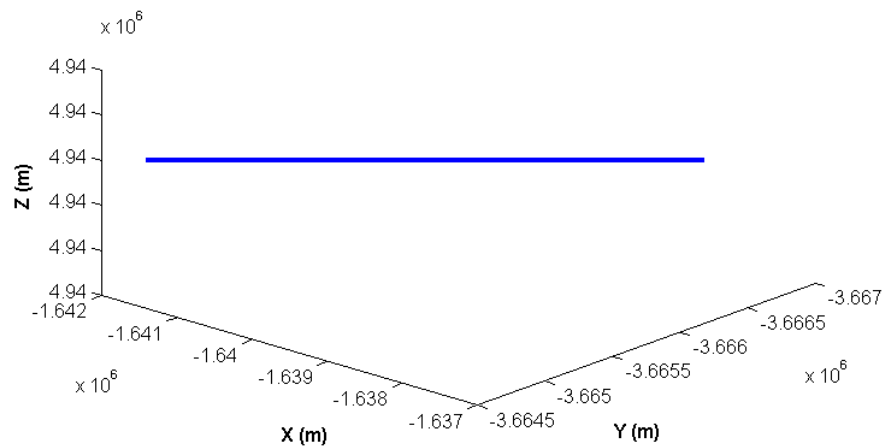


Figure 6.46 The Vehicle Trajectory in WGS-84 Coordinate Frame

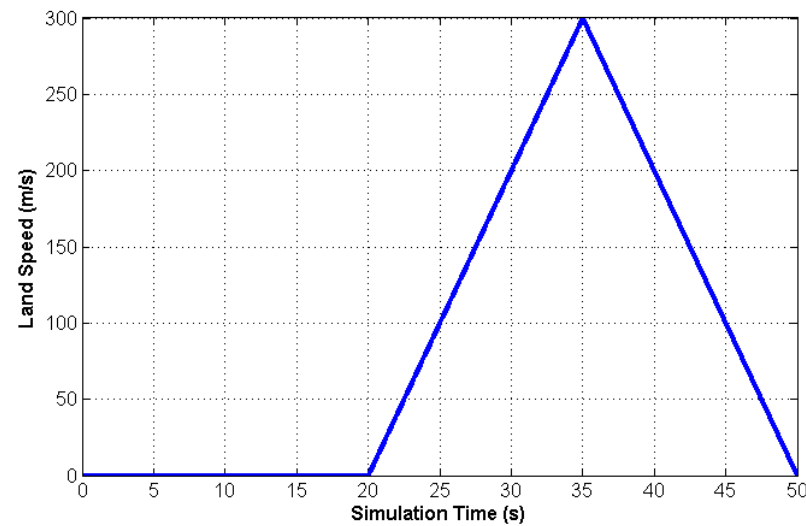


Figure 6.47 Linear Dynamic Test Vehicle Trajectory

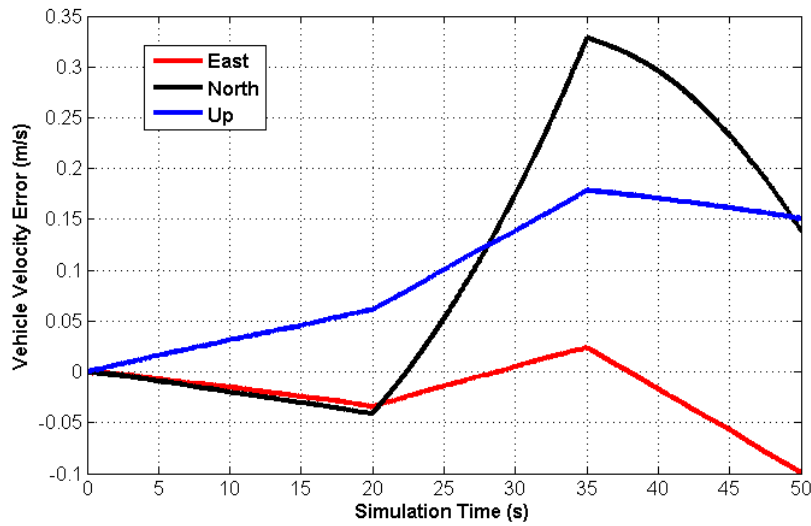


Figure 6.48 Dynamic Test INS Velocity Errors

6.3.2.2 Dynamic Scenario 2 Test Result and Analysis

Figure 6.49 to Figure 6.53 show the test results of the FPLL+COOP receiver for this dynamic test. The test scenario is the same as for static test scenario 2, except for the vehicle motion.

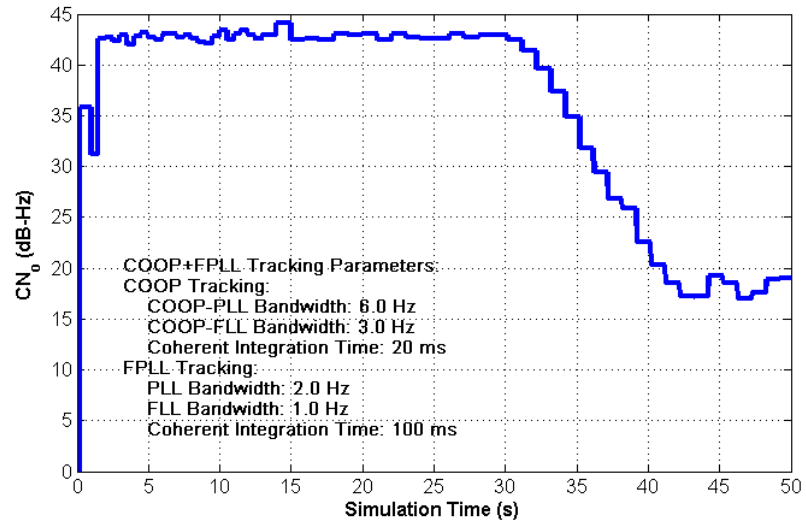


Figure 6.49 Estimated C/N_0 of PLL+COOP Tracking

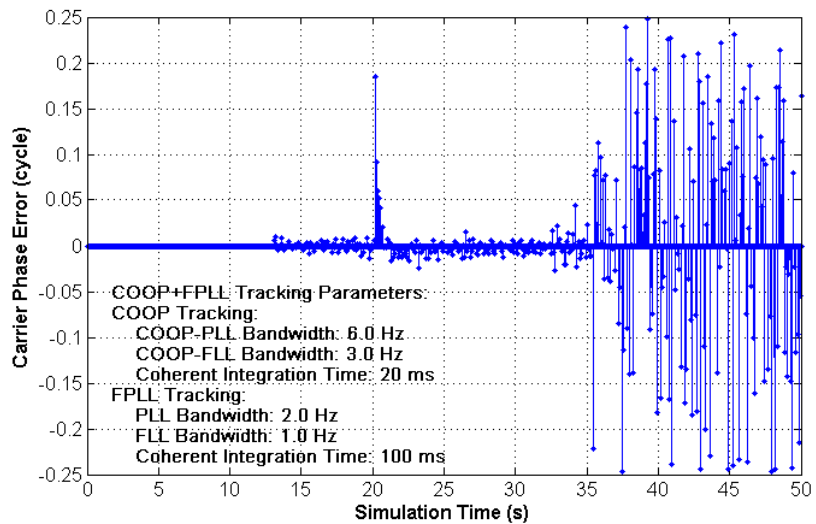


Figure 6.50 FPLL+COOP Carrier Phase Tracking Errors

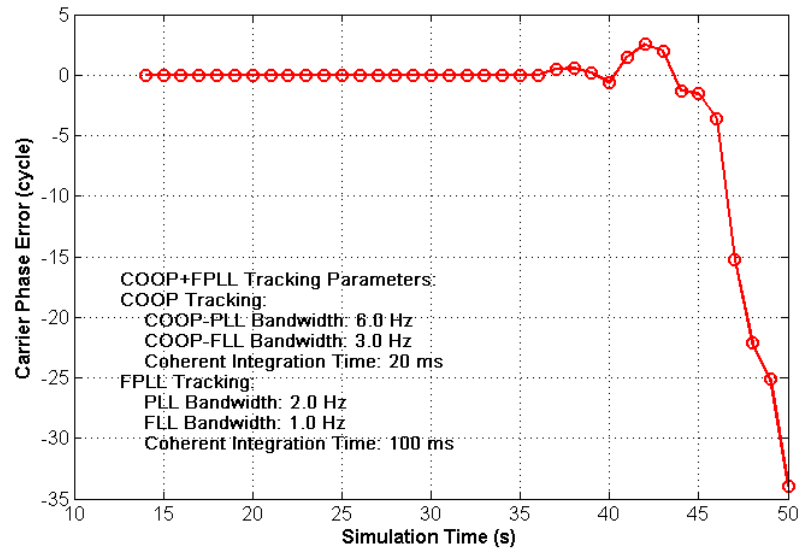


Figure 6.51 Total Carrier Phase Errors of FPLL+COOP Receiver with INS Aiding

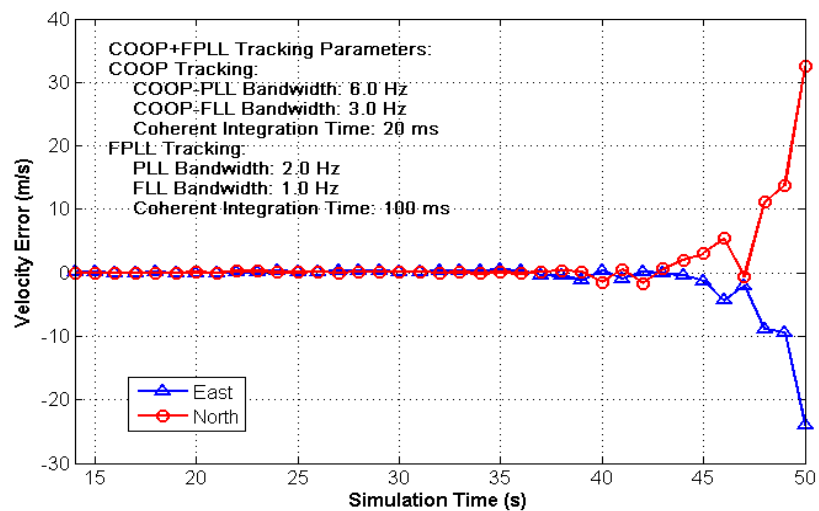


Figure 6.52 FPLL+COOP Tracking Horizontal Velocity Errors

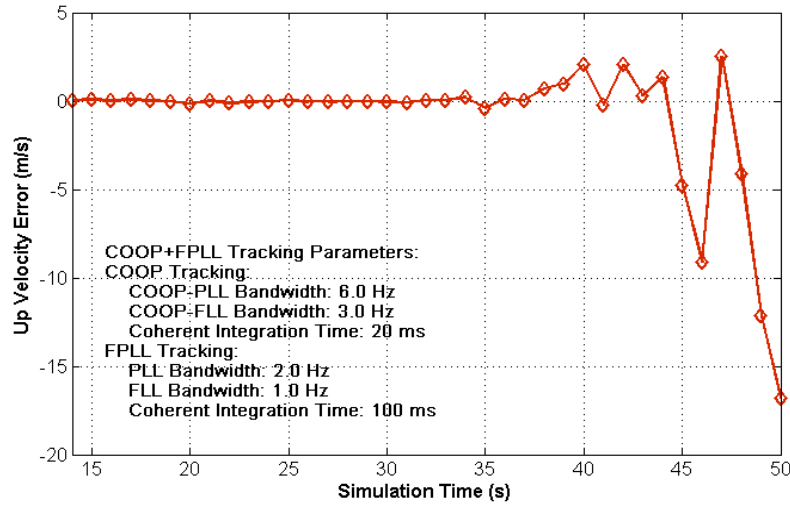


Figure 6.53 FPLL+COOP Tracking Vertical Velocity Errors

Figure 6.49 to Figure 6.51 show the tracking results of satellite PRN 07 for the FPLL+COOP receiver and Figure 6.52 and Figure 6.53 show the horizontal and vertical velocity errors of the FPLL+COOP receiver, respectively. The “true” reference carrier phase measurements are determined using the same methods as that used in dynamic test scenario 1.

When one compares the test results with those of static test scenario 2 (Figure 6.19 - Figure 6.24), one realizes that all conclusions arrived at in the static test are applicable to the dynamic test. As shown in Figure 6.52 and Figure 6.53, the velocity errors increase rapidly after the 47-s point, which implies that the receiver starts to lose lock on the carrier. This situation occurs because the INS velocity errors in Figure 6.48 change too rapidly. Since the signal is very weak (15 dB-Hz), the receiver cannot lock on the incoming carrier any more. However, considering that all signals have been held at 15

dB-Hz for 7 s before the receiver starts to lose lock on the carrier, the INS-assisted GPS receiver illustrates its superior tracking performance.

However, to respond these jerks, in this linear motion test, the optimal noise bandwidth of phase loop filter in FPLL jumps from around 1 Hz in static tests to 6 Hz, and the optimal noise bandwidth of position loop filter in COOP jumps from around 0.2 Hz in static tests to 2 Hz. This test illustrates that, although external INS aiding compensates most of receiver dynamics in signal tracking, the remaining effect on signal tracking ability due to jerks can be significant. In INS-assisted GPS receiver design, more attention should be paid to possible jerks in signal dynamics, since the Doppler error of the GPS signal is normally very small after INS aiding.

Furthermore, Figure 6.48 and Figure 6.50 show clearly that two strong jerks occur at the 20-s and 35-s points. Fortunately, these jerks do not affect signal tracking significantly. Since the receiver obtains satellite signals from different directions, a jerk that has the longest projection in one specific direction will reveal nothing in the perpendicular direction. Therefore, since the COOP method is adopted in this receiver, the impact of a strong jerk on vector-based signal tracking will be limited. This may be the reason why the receiver is not sensitive to jerks.

6.3.3 Dynamic Test Summary

In order to validate the conclusions deduced from the static tests, the two dynamic tests reported above were performed. A comparison of the results leads to the following conclusions:

1. Because INS aiding measures most of the receiver Doppler, high receiver dynamics does not significantly affect signal tracking in the INS-assisted GPS receiver, based on the test results performed herein. Therefore, all conclusions based on the static tests are also valid for the dynamic tests.
2. Furthermore, due the adoption of COOP tracking loops, the receiver is not sensitive to the effects of extreme dynamics on the incoming signals such as sharp jerks.

In real applications, because of the processing delay of GPS/INS Kalman filter (Petovello 2003) in the external INS loop, the aiding Doppler used in receiver signal tracking has to be extrapolated to the current time and thus lead to the prediction error. For a receiver with an acceleration of 100 m/s^2 (10 g), if the update rate of the involved INS is 200 Hz, the perdition error of INS aiding Doppler can be the maximum of $\frac{100}{200} = 0.5 \text{ m/s}$ in LOS direction. Therefore, in extremely-high dynamic applications,

Doppler error induced by the processing delay in GPS/INS Kalman filter should be considered. An INS with a higher data update rate is recommended in this case.

6.4 Comparison of INS-Assisted and Standard GPS Receivers

In the above sections, the performances of an INS-assisted HSGPS receiver were analyzed thoroughly. The roles of INS aiding loops, COOP loops, and FPLLs were investigated, and an effective tracking strategy was proposed. In this Section, the INS-assisted GPS receiver performances are compared to those of a standard GPS receiver.

The “standard” software GPS receiver GNSS_SoftRx without INS aiding was utilized in order to re-enact static scenario 4 and dynamic scenario 1. In both tests, a 10-Hz bandwidth and 10-ms coherent integration time were used in the standard GPS receiver.

6.4.1 Test Results and Analysis of Static Test

Figure 6.54 to 6.56 show performance comparisons of the two receivers. The tracking results for satellite PRN 07, namely C/N₀ density, carrier phase tracking errors, and carrier phase measurement errors are presented in the first three figures, while Figure 6.57 shows the position results from the two receivers.

Figure 6.54 to Figure 6.56 show that, although the signal power of satellite PRN 7 is attenuated from 45 dB-Hz to 15 dB-Hz during the last 30-s period, the INS-assisted GPS receiver can track the satellite with carrier phase locked. A standard GPS receiver without

INS aiding, however, cannot track the satellite when the signal power is lower than 30 dB-Hz. Figure 6.57 shows that, due to the large tracking errors on satellite PRN 7 around the 30-s point, there are two significant blunders at 31 s and 32 s. These are roughly 4 m/s and 11.5 m/s, respectively. These two blunders occur because an epoch-by-epoch least-squares based positioning approach is used to calculate receiver velocity. In this basic least-squares estimator, no blunder tests are performed. After the 32-s point, the standard receiver loses lock and the velocity error returns to a normal level.

Figure 6.54 and Figure 6.56 show that the signal tracking sensitivity of the INS-assisted GPS receiver is improved by at least 15 dB as compared to that of a standard GPS receiver, when multiple strong signals available. In this test, the standard GPS receiver loses lock on satellite 07 at the time point of 30 s, where the signal power is 30 dB-Hz. However, the INS-assisted HSGPS receiver can track the satellite 07 down to 15 dB-Hz and never lose lock in the entire test. This improvement can be attributed to two reasons:

1. Since INS aiding removes the Doppler signal and decreases the receiver dynamics uncertainty, a long coherent integration (100 ms in the present case) is used in weak signal tracking.

2. Since the COOP tracking method is utilized, the strong signals aid the weak ones.

In this test, the tracking of strong satellite signals is of considerable benefit to that of satellite PRN 7. This will be explained later in this section.

Figure 6.58 shows the carrier phase tracking error of satellite PRN 7 for the INS-assisted GPS receiver, with and without the use of the COOP loop. In the case without the COOP loop, the individual PLL parameters remain the same as those of the COOP loop, i.e. a 0.2-Hz bandwidth and a 100-ms coherent integration time. From Figure 6.58, it can be deduced that, although the coherent integration time is 100 ms, without the COOP loop, the tracking performance is even worse than that of a standalone GPS receiver where coherent integration time is only 10 ms. At the 26-s point, the PLL loses lock, and the carrier phase error drifts away rapidly. Based on the former discussion, it is evident that if the COOP method were not used, the individual PLL would have to track the INS aiding Doppler errors by itself. When the coherent integration time is very long, the INS aiding Doppler error will fail the pure PLL tracking.

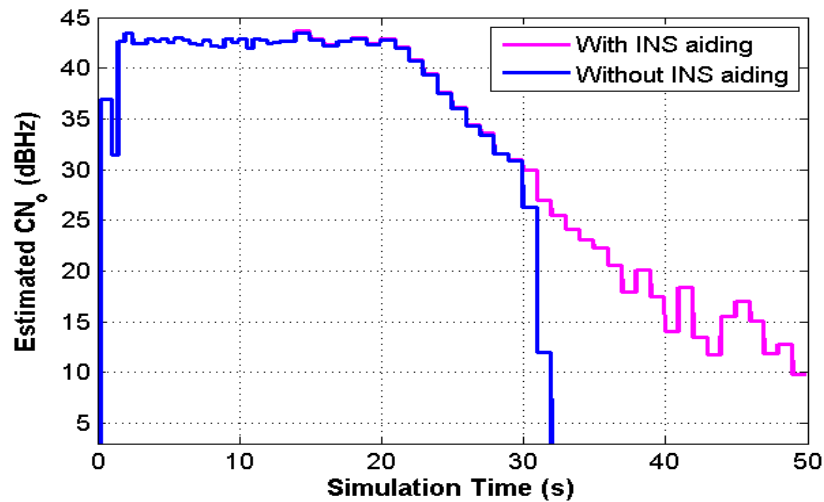


Figure 6.54 Satellite 07 C/N_0 During Static Test

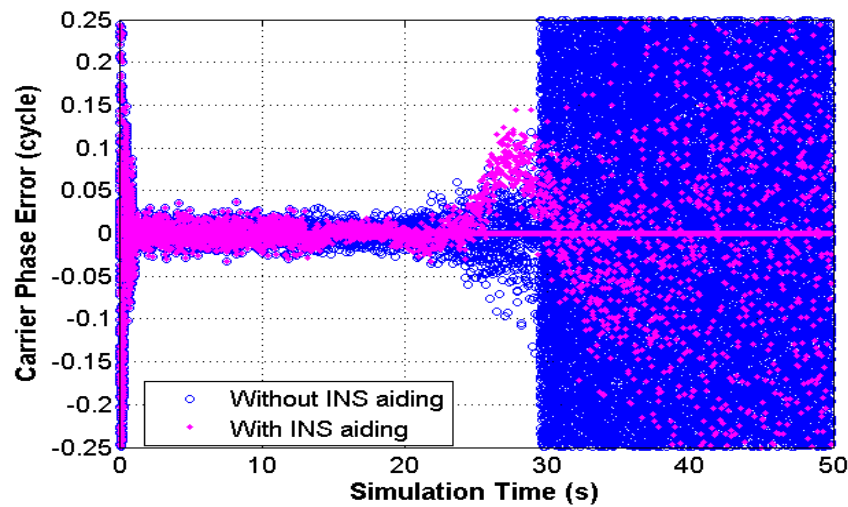


Figure 6.55 Satellite 07 PLL Carrier Phase Errors During Static Test

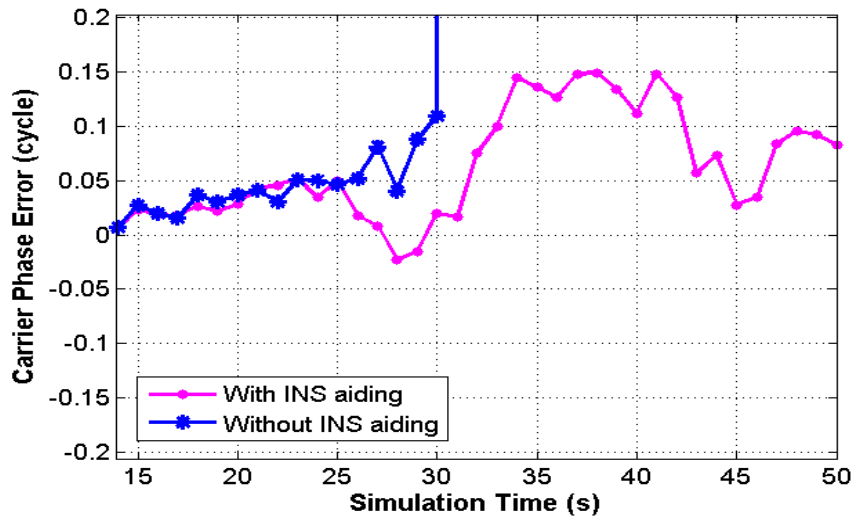


Figure 6.56 Satellite 07 Total Carrier Phase Errors During Static Test

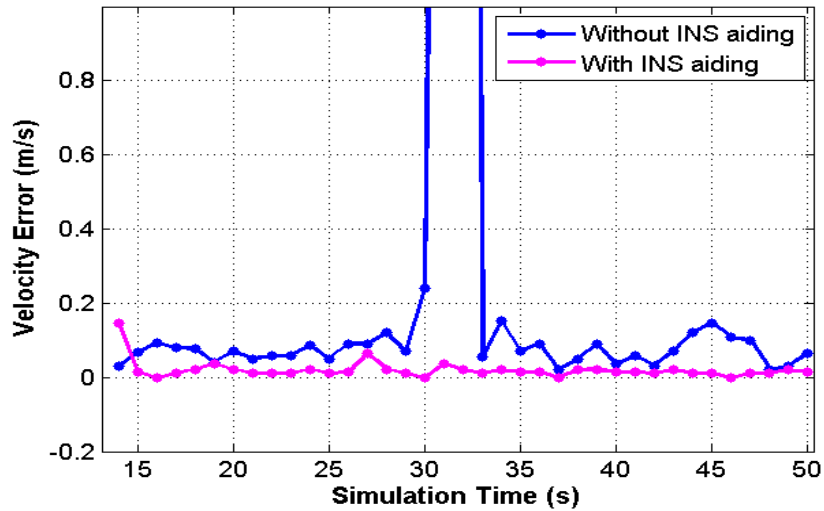


Figure 6.57 Horizontal Velocity Errors During Static Test

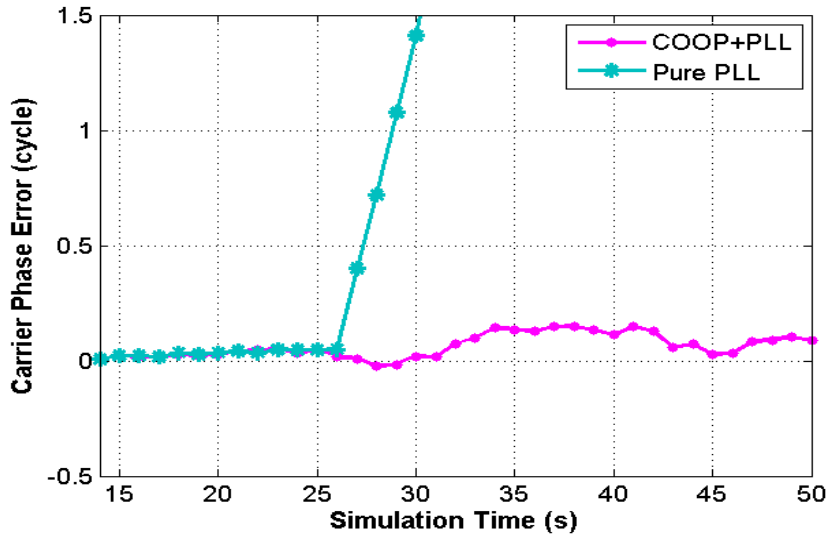


Figure 6.58 Satellite 07 Total Carrier Phase Errors of PLL-Only Receiver with INS Aiding in Static Test

6.4.2 Test Results and Analysis of Dynamic Test

Figure 6.59 to Figure 6.62 compare the performance of the standalone and INS-assisted GPS receivers. The tracking results of satellite 07, namely the C/N_0 density, carrier phase tracking error and carrier phase measurement error, are presented in Figure 6.59 to Figure 6.61. Figure 6.62 shows the position results from the two receivers.

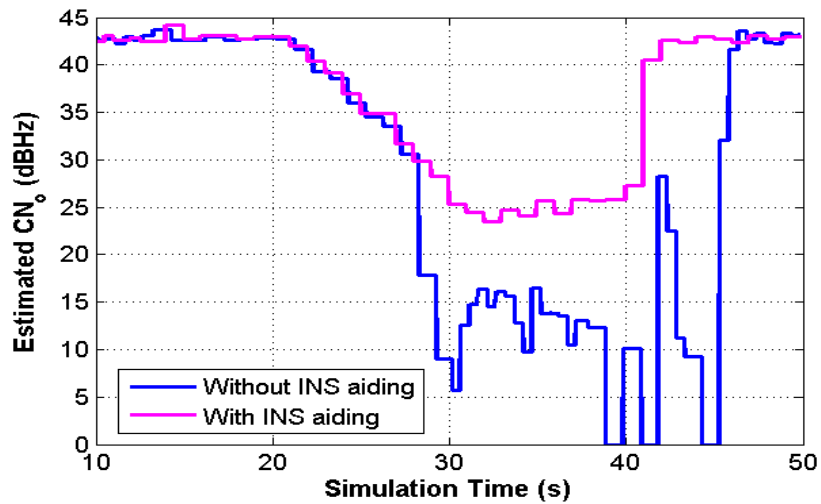


Figure 6.59 Satellite 07 C/N_0 in Dynamic Test

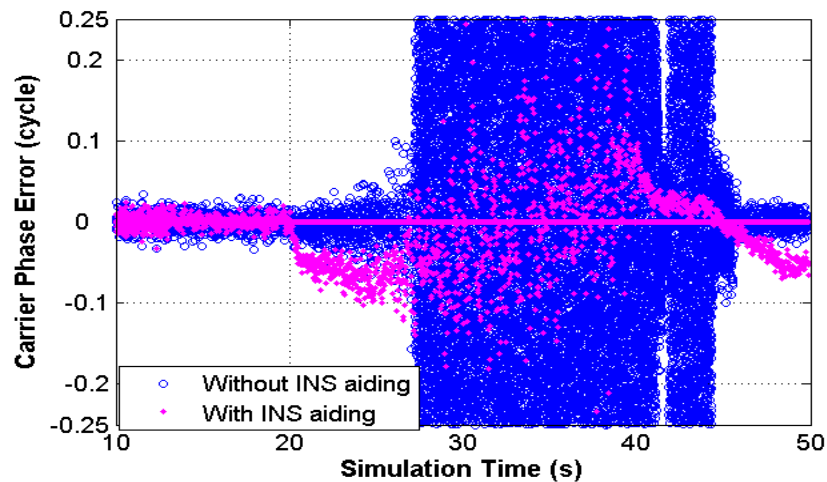


Figure 6.60 Satellite 07 PLL Carrier Phase Errors in Dynamic Test

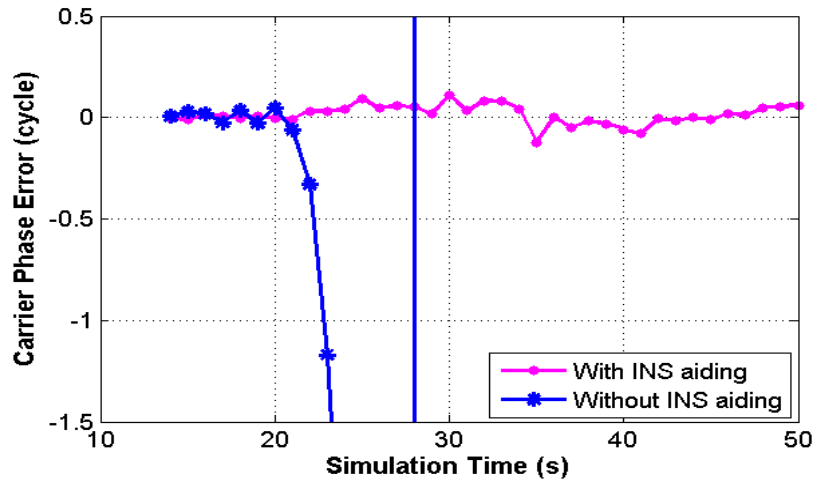


Figure 6.61 Satellite 07 Total Carrier Phase Errors in Dynamic Test

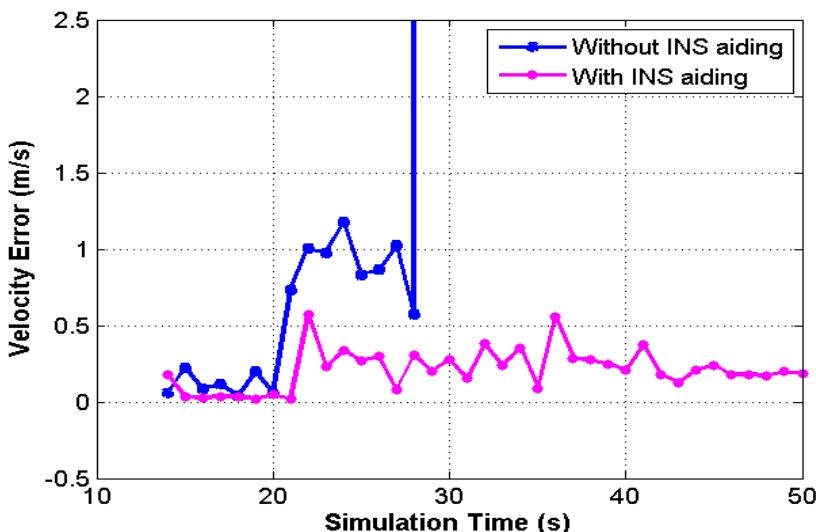


Figure 6.62 Satellite 07 Horizontal Velocity Errors in Dynamic Test

From the above figures, it can be seen that the tracking performance of the standard receiver is very poor in dynamic conditions as compared to the INS-assisted HSGPS receiver. Figure 6.61 and Figure 6.62 show clearly that the standard GPS receiver cannot

lock on the incoming carrier at all when the vehicle starts to make an “S” shaped trajectory. During the period between 20 s and 28 s, although the individual PLL in the standard receiver in Figure 6.60 displays lock on the incoming carrier, cycle slips occur due to vehicle dynamics as shown in Figure 6.61. From the 28-s point onward, the standard receiver stops outputting a GPS solution. In contrast, the INS-assisted HSGPS receiver can track incoming signals as low as 25 dB-Hz with carrier locked during the entire test period.

6.4.3 Summary

Compared with tracking results achieved by a standard GPS receiver without INS aiding, the INS-assisted GPS receiver proposed herein yields much better performance under both weak signal tracking and high dynamics signal tracking conditions. With INS aiding and adopting COOP tracking loops, very long coherent integration can be implemented safely in weak signal applications. There is little doubt that GPS/INS ultra-tight integration will provide an excellent technology for navigation and positioning in attenuated signal environments, such as vehicle navigation in urban canyons and personal positioning indoors.

Chapter Seven: Conclusions and Recommendations

GPS currently fulfills the positioning requirements of many applications intended for LOS environments. However, many location-based services (LBS) and navigation applications such as vehicular navigation and personal positioning require positioning capabilities in environments where LOS to satellites is not readily available, e.g., urban areas, indoors, and dense forests. Such environments either block the signals completely or attenuate them to a power level that is 10-30 dB lower than the nominal signal power. This renders it impractical for a standard receiver to acquire and maintain signal tracking, which causes discontinuous positioning in such environments.

In order to meet the positioning and navigation requirements under attenuated signal conditions, ultra-tight integration of GPS and inertial navigation systems has been investigated in this study. In general, an INS-assisted GPS receiver is far superior to a standalone receiver and offers the greatest potential for meeting positioning requirements under attenuated signal conditions. The extra cost associated with an INS-assisted GPS receiver is incurred not only from the INS hardware but also from the integration software.

As shown in these investigations, an INS-assisted GPS receiver provides full navigation capability including carrier phase output under attenuated signals. Accurate carrier phase measurements are deemed necessary for many high-accuracy applications.

In order to address the issue of GPS tracking and positioning in degraded signal environments, this research proposes a novel architecture for ultra-tight integration of a HSGPS receiver with an Inertial Navigation System. By enhancing signal tracking loops in receivers through the use of optimal controllers/estimators and an external source, the capabilities of the GPS receiver is improved to provide better availability and accuracy performance under a larger range of indoor environments. The proposed approach is distinct from the commonly used ultra-tightly coupled GPS/INS approaches, and makes use of different tracking enhancement technologies used in typical HSGPS receivers, multi-channel co-operated GPS receivers, and the current ultra-tightly coupled GPS/INS methods.

The method consists of sophisticated conventional Delay Lock Loops and Phase Lock Loops in individual signal tracking channels, external INS aiding loops, and multi-channel co-operated tracking loops, namely COOP loops. Specific attention was given to the role of COOP loops in the ultra-tightly coupled GPS/INS receiver. Furthermore, the effect of inertial measurement unit (IMU) quality and the effect of receiver oscillator noise and coherent integration time on weak signal tracking were also analyzed, from the theory point of view.

7.1 Conclusions

In order to perform ultra-tight integration, a GPS front end and an INS simulator were developed. Then, static and dynamic tests were conducted in order to analyze the system performance. An analysis of the results leads to the following conclusions:

1. INS aiding can effectively reduce the receiver dynamics uncertainty and, thus, improve tracking performance of a standard GPS receiver significantly in both weak signal and high dynamic signal applications.
2. When an INS solution is available, an effective signal tracking strategy can be summarized in three steps. First, the INS solution is implemented in order to remove most of receiver dynamics uncertainty. Therefore, the Doppler signal residual left for the COOP and FPLLs to track is close to zero. Next, a vector-tracking based COOP loop is designed to track the residual carrier Doppler effectively. Since six to 10 or more satellites are usually in view, COOP tracking yields much better performance than conventional FPLLs, especially in weak signal environments. Finally, FLL-assisted PLLs can be used to track the carrier. Since the Doppler signal is compensated by the INS+COOP aiding, for a digital FLL/PLL, the residual Doppler error is close to zero. This significantly decreases carrier phase tracking errors and, therefore, increases the FLL/PLL tracking sensitivity.

3. Although INS error increases rapidly with time during a GPS outage, the INS solution errors change smoothly. Smoothly increasing INS errors can be easily tracked by the COOP method and thus, will not affect signal tracking significantly. Therefore, even if the INS solution error is as large as 0.1 m/s, an INS-assisted GPS receiver can track a GPS signal that is 30 dB lower than LOS signals with acceptable positioning accuracy.
4. The combined tracking of the FPLL and COOP loops presented in this research have been shown to track signals as low as 15 dB-Hz. When the signal power is above 22-23 dB-Hz, this method can lock on the incoming carrier and provide accurate carrier phase measurements. When the signal is lower than 22 dB-Hz but higher than 15 dB-Hz, the method can track the incoming carrier most of the time, although cycle slips may occur. When there are several strong signals in view, the receiver can track the other weak signals as low as 15 dB-Hz with carrier tracking due to the assistance from the strong signals.
5. Because INS aiding provides most of the Doppler measurements, high receiver dynamics does not affect signal tracking significantly in INS-assisted GPS receivers. With INS aiding and by adopting COOP tracking, very long coherent integration can be implemented safely when necessary.

6. By adapting the COOP tracking method in an INS-assisted GPS receiver, the receiver can function more effectively in high dynamic applications and track much lower power signals with high dynamics such as strong jerks.
7. Compared to a standard GPS receiver without INS aiding, the INS-assisted GPS receiver proposed here yields much better performance in attenuated signal environments.

In this study, tests done in this study were limited. Many tests were only performed once with the responsible receiver parameters. Because the transition time in signal tracking is very short and this typical value is 0-2 seconds, the signal tracking process in most tests of this study can be regarded as wide-stationary process. For this reason, one test over a long time occupation can be performed to replace multiple tests over short time occupations. However, this doesn't happen in all tests. In future, more tests are preferred to validate the above conclusions.

7.2 Recommendations for Future Work

Two main tasks arise in GPS/INS ultra-tight integration, namely: 1) to provide the GPS receiver with the most accurate INS aiding information with an optimal estimator; 2) to utilize the INS aiding information fully in order to enhance GPS signal tracking in the receiver, especially in weak signal environments and/or high dynamic applications. This research focused on the latter task and presented an in-depth study of the issue. Although

some discussions of the former task is presented in Chapter 3, from the system design point of view, further studies of different Kalman filters and their applications in GPS/INS ultra-tight integration are needed.

In this study, the recommended loose/tightly coupled GPS/INS integration software package, namely SAINTTM, has not been fused into the prototype INS-assisted GPS receiver in order to form a complete ultra-tightly coupled GPS/INS system. In all tests discussed in this thesis, GPS does not correct INS. For this reason, the receiver prototype cannot be used in field tests: in real applications, the integration system would have to operate in a closed loop manner, where GPS is correcting INS when INS is assisting GPS. In future research, the performance of GPS/INS ultra-tight integration could be assessed when the system functions in a closed loop manner.

The position accuracy of MEMS-based IMU decreases rapidly as a function of time. If the performance of an ultra-tightly coupled MEMS-IMU/GPS is assessed when the system functions in a closed loop manner, the INS will be corrected by GPS online, and the INS errors will be limited. When a complete GPS/INS system is ready, the role of MEMS-based IMU in GPS/INS ultra-tight integration can be investigated. Furthermore, a system performance assessment is recommended for ultra-tightly integration with different grade IMUs.

The last recommendation for future work refers to GPS measurement blunders in ultra-tightly coupled GPS/INS systems. The GPS measurement blunders in urban canyon or indoor environments, such as those caused by multipath, degrade GPS signal tracking seriously. The impact of these measurement blunders on the ultra-tightly coupled GPS/INS system should be evaluated.

References

- Abdel-Hamid W., T. Abdelazim, N. El-Sheimy, and G. Lachapelle (2005) "Improvement of MEMS-IMU/GPS Performance using Fuzzy Modeling," *GPS Solutions*, July, Issue, DOI 10.1007/s10291-005-0146
- Alban S., D. M. Akos, S. M. Rock and D. Gebre-Egziabher (2003) "Performance Analysis and Architectures for INS-Aided GPS Tracking Loops," in *Proceedings of ION National Technical Meeting (NTM)*, 22-24 January, Anaheim CA, pp. 611-622, Institute of Navigation, Fairfax VA
- Beser J., S. Alexander, R. Crane, S. Rounds and J. Wyman (2002) "Trunavtm: A Low-Cost Guidance/Navigation Unit Integrating A SAASM-Based GPS And MEMS IMU In A Deeply Coupled Mechanization," in *Proceedings of ION GNSS*, 24-27 September, Portland, OR, pp. 545-555, Institute of Navigation, Fairfax VA
- Babu, R. and J. Wang (2005) "Ultra-tight GPS/INS/PLIntegration: A System Concept and PerformanceAnalysis," Submitted to GPS Solutions (available at http://www.gmat.unsw.edu.au/snap/publications/babu_etal2005c.pdf)
- Beser J., S. Alexander, R. Crane, S. Rounds and J. Wyman (2002) "Trunavtm: A Low-Cost Guidance/Navigation Unit Integrating A SAASM-Based GPS And MEMS IMU In A Deeply coupled Mechanization," in *Proceedings of ION GNSS*, 24-27 September, Portland OR, pp. 545-555, Institute of Navigation, Fairfax VA
- Brown R. G. and P. Y. C. Hwang (1992) *Introduction To Random Signals and Applied Kalman Filtering*, John Wiley & Sons, Toronto ON, second edition
- Chiou T. Y., S. Alban, S. Atwater, J. Gautier, S. Pullen, P. Enge, D. Akos, G. E. Demoz and B. S. Pervan (2004) "Performance Analysis and Experimental Validation of a Doppler-Aided GPS/INS Receiver for JPALS Applications," in *Proceedings of ION GNSS 17th International Technical Meeting of the Satellite Division*, 21-24 September, Long Beach, CA, pp. 1609-1618, Institute of Navigation, Fairfax VA
- Don K., S. Luis and R. B. Langley (2005) "Compensation of the Effects of Phase Wind-up for Improving the Performance of a GPS RTK-Based Vehicle Navigation System," in *Proceedings of ION GNSS 18th International Technical Meeting of the Satellite Division*, 13-16 September, Long Beach, CA, pp. 346-354, Institute of Navigation, Fairfax VA

Dong L., C. Ma and G. Lachapelle (2004) "Implementation and Verification of a Software-Based IF GPS Signal Simulator," in *Proceedings of ION National Technical Meeting (NTM)*, 26-28 January, San Diego CA, pp. 378-389, Institute of Navigation, Fairfax VA

Gao G. and G. Lachapelle (2006) "INS-Assisted High Sensitivity GPS Receivers For Degraded Signal Navigation", , in *Proceedings of ION GNSS*, 26-29 September, Forth Worth, TX, The Institute of Navigation, Fairfax VA

Gao. G. (2005) *Progress Report: Deeply integrated GPS/INS*, June 24, internal report of PLAN group, Department of Geomatics Engineering, University of Calgary, Canada

Gao G. (2004) *Realization and Testing of GPS IF Data Collecting System*, ENGO 699.19 special course, Department of Geomatics Engineering, University of Calgary, Canada

Gautier J. D. , B. W. Parkinson and D. Gebre-Egziabher (2003) "Using the GPS/INS Generalized evaluation Tool (GIGET) for the Comparison of Loosely Coupled, Tightly Coupled and Ultra-Tightly Coupled Integrated Navigation Systems," in *Proceedings of ION 59th Annual Meeting/CIGTF 22nd Guidance Test Symposium*, 23-25 June, Albuquerque, NM, pp. 65-76, Institute of Navigation, Fairfax VA

Godha S. and M. E. Cannon (2005) "Integration of DGPS with a Low Cost MEMS – Based Inertial Measurement Unit (IMU) for Land Vehicle Navigation Application," in *Proceedings of ION GNSS*, September13-16, Long Beach CA, pp. 333-345, Institute of Navigation, Fairfax VA

Gustafson D., J. Dowdle and K. Flueckiger (2000) "A High Anti-Jam GPS based Navigator," in *Proceedings of ION National Technical Meeting (NTM)*, 26-28 January, Anaheim CA, pp. 495-503, Institute of Navigation, Fairfax VA

Julien, O. (2005) *Design of Galileo L1F Receiver Tracking Loops*, PhD Thesis, published as Report No. 20227, Department of Geomatics Engineering, The University of Calgary, Canada (Available at <http://plan.geomatics.ucalgary.ca>)

Kaplan, E. D., ed. (1996) *Understanding GPS: Principles and Applications*, Artech House, Boston MA

Karunananayake, D., M.E. Cannon, G. Lachapelle, G. Cox (2004) "Evaluation of AGPS in Weak Signal Environments Using a Hardware Simulator," in *Proceedings of ION GNSS*, 21-24 September, Long Beach CA, pp. 2416-2426, Institute of Navigation, Fairfax, VA

Klukas, R. (1997) *A Superresolution Based Cellular Positioning System Using GPS Time Synchronization*. PhD Thesis, published as Report No. 20114, Department of Geomatics Engineering, The University of Calgary

Klukas, R., O. Julien, L. Dong, M.E. Cannon, and G. Lachapelle (2004) *Effects of Building Materials on UHF Ranging Signals*. GPS Solutions, 8, 1, 1-8

Klukas, R., G. Lachapelle, and M. Fattouche (1998) *Cellular Telephone Positioning Using GPS Time Synchronization*. GPS World Magazine, 9, 4, 49-54

Kreye C., B. Eissfeller and J. Ó. Winkel (2000) "Improvements of GNSS Receiver Performance Using Ultra-tightly coupled INS Measurements," in *Proceedings of ION GNSS*, 19-22 September, Salt Lake City UT, pp. 844-854, Institute of Navigation, Fairfax VA

Lachapelle G., H. Kuusniemi and D. T. H. Dao (2003) "HSGPS Signal Analysis and Performance under Various Indoor Conditions," in *Proceedings of ION GNSS*, 9-12 September, Portland OR, pp. 1171-1184, Institute of Navigation, Fairfax VA

Ma C. (2003) *Techniques to Improve Ground-Based Wireless Location Performance Using a Cellular Telephone Network*, PhD thesis, published as Report No. 20177, Department of Geomatics Engineering, University of Calgary, Canada (Available at <http://plan.geomatics.ucalgary.ca>)

Ma C., G. Lachapelle and M.E. Cannon (2004) "Implementation of a Software GPS Receiver," in *Proceedings of ION GNSS*, September 21-24, Long Beach CA, pp. 956-970, Institute of Navigation, Fairfax VA

MacGougan G. D. (2003) *High Sensitivity GPS Performance Analysis in Degraded Signal Environments*, Master thesis, published as Reports Number 20176, Department of Geomatics Engineering, University of Calgary, Canada (Available at <http://plan.geomatics.ucalgary.ca>)

Mitel Semiconductor (1998) *GP2000 - GPS Chipset Designer's Guide*, MS4395-2.3, April, Supersedes Issue 1.4 in August 1996, Global Positioning Products Handbook, HB3045-1.0

Nassar, S., X. Niu and N. El-Sheimy (2005) "Land-Vehicle INS/GPS Accurate Positioning During GPS Signal Blockage Periods," Journal of Surveying Engineering (JSE), The American Society of Civil Engineers (ASCE), USA

Niu, X., S. Nassar and N. El-Sheimy, (2005) "An Accurate Land-Vehicle MEMS IMU/GPS Navigation System Using 3D Auxiliary Velocity Updates," *Navigation, Journal of the Institute of Navigation, USA*

Parkinson B. W. and J. J. Spilker Jr (1996) *Global Positioning System: Theory and Applications*, Volume 1, 1996 (Chapter 7)

Petovello M. G. (2003) *Real-Time Integration of a Tactical-Grade IMU and GPS for High-Accuracy Positioning and Navigation*, PhD thesis, published as Reports Number 20173, Department of Geomatics Engineering, University of Calgary, Canada (Available at <http://plan.geomatics.ucalgary.ca>)

Petovello, M., and G. Lachapelle (2006) "Comparison of Vector-Based Software Receiver Implementations With Application to Ultra-Tight GPS/INS Integration." In *Proceedings of GNSS*, Setempter, Forth Worth, TX, The Institute of Navigation, Fairfax VA

Psiaki M. L. and H. Jung (2002) "Extended Kalman Filter Methods for Tracking Weak GPS Signals," In *Proceeding of ION GNSS*, 24-27 September, Portland, OR, pp. 2539-2553, The Institute of Navigation, Fairfax VA

Raquet J. F. (2004) *GPS Receiver Design*, ENGO 699.10 Course Notes, Department of Geomatics Engineering, University of Calgary, Canada

Scherzinger B. (2004) *Estimation with Applications to Navigation*, ENGO 699.11 Course Notes, Department of Geomatics Engineering, University of Calgary, Canada

Sennott J. (1997) "Robustness of Tightly Coupled Integrations for Real-Time Centimeter GPS Positioning," in *Proceedings of ION GPS*, 16-19 September, Kansas City KS, pp. 655-663, Institute of Navigation, Fairfax VA

Soloviev A., F. V. Graas and S. Gunawardena (2004) "Implementation of Deeply Integrated GPS/Low-Cost IMU for Acquisition and Tracking of Low CNR GPS Signals," in *Proceedings of ION National Technical Meeting (NTM)*, 26-28 January, San Diego CA, pp. 923-935, Institute of Navigation, Fairfax VA

Soloviev A., S. Gunawardena and F. V. Graas (2004) "Deeply Integrated GPS/Low-Cost IMU for Low CNR Signal Processing: Flight Test Results and Real Time Implementation," in *Proceedings of ION GNSS 17th International Technical Meeting of the Satellite Division*, 21-24 September, Long Beach CA, pp. 1598-1608, Institute of Navigation, Fairfax VA

Stephens S.A., and J. B. Thomas (1995) *Controlled-Root Formulation for Digital Phase-Locked Loops*, IEEE Transactions on Aerospace and Electronic Systems, Vol. 31, No. 1, pp. 78-95

Tetewsky, A. K. and F. E. Mullen (1996) "Carrier phase wrap-up induced by rotating GPS antennas," in *Proceedings of the Institute of Navigation ION AM-96*, Cambridge, MA, pp. 21-28, , Institute of Navigation, Fairfax VA

Van Diggelen F. and C. Abraham (2001) *Indoor GPS Technology*, CTIA Wireless-Agenda, Dallas, May

Watson R., (2005) *High-Sensitivity GPS L1 Signal Analysis for Indoor Channel Modelling*. MSc thesis, published as Report No. 20215, Department of Geomatics Engineering, The University of Calgary, Canada (Available at <http://plan.geomatics.ucalgary.ca>)

Zhodzishsky M., S. Yudanov, V. Veitsel and J. Ashjaee (1998) "COOP Tracking for Carrier Phase," in *Proceedings of ION GPS*, 15-18 september, Nashville, Tennessee, pp. 653-664, Institute of Navigation, Fairfax VA

Appendices

APPENDIX A: SIGNAL TRACKING LOOP TRANSFER FUNCTION

Figure A. 1 shows the basic architecture of a signal tracking loop, which includes a discriminator, a loop filter and a Numerically Control Oscillator (NCO).

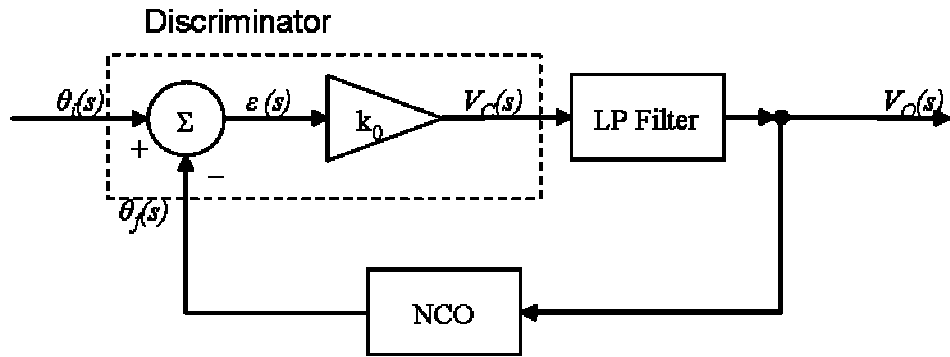


Figure A. 1 Architecture of Signal Tracking Loop

The open-loop transfer function of a second-order loop filter shown in Figure A. 1 can be written as (Mitel 1998)

$$G(s) = \frac{Y(s)}{X(s)} = \frac{T_2 s + 1}{T_1 s} , \quad (\text{A. 1})$$

where $X(s)$ is the input to the loop filter and is shown as $V_c(s)$ in Figure A. 1, $Y(s)$ is the output of the loop filter and is shown as $V_o(s)$, T_1 and T_2 are time coefficients and are subject to the inequality $T_1 > T_2 > 0$.

Rearranging Equation (A.1) yields

$$T_1 s \times Y(s) = T_2 s \times X(s) + X(s) . \quad (\text{A. 2})$$

Expressing Equation (A.2) in the time domain gives

$$T_1 \frac{dy}{dt} = T_2 \frac{dx}{dt} + x . \quad (\text{A. 3})$$

Over a sample interval ΔT :

$$\frac{dy}{dt} = \frac{y_i - y_{i-1}}{\Delta T}; \quad \frac{dx}{dt} = \frac{x_i - x_{i-1}}{\Delta T} . \quad (\text{A. 4})$$

Rearranging Equation (A.4) yields

$$T_1 \times (y_i - y_{i-1}) = T_2 \times (x_i - x_{i-1}) + x_i \times \Delta T \quad (\text{A. 5})$$

or more conveniently,

$$y_i = y_{i-1} + \left(\frac{T_2}{T_1} \right) \times (x_i - x_{i-1}) + \left(\frac{\Delta T}{T_1} \right) \times x_i . \quad (\text{A. 6})$$

The closed-loop transfer function of a second-order tracking loop can be expressed as (Mitel 1998)

$$\phi(s) = \frac{K_0 K_\phi G(s)}{S + K_0 K_\phi G(s)} = \frac{\omega_n^2 + 2\xi\omega_n S}{S^2 + 2\xi\omega_n S + \omega_n^2} , \quad (\text{A. 7})$$

Where, K_0 and K_ϕ are the discriminator gain and the code NCO conversion gain respectively.

With respect to Equation (A.6) and (A.7), the following important formulas related to the loop characteristics can be derived as follows (Mitel 1998):

$$\text{Closed-loop transfer function: } \phi(s) = \frac{K_0 K_\phi G(s)}{S + K_0 K_\phi G(s)} = \frac{\omega_n^2 + 2\xi\omega_n S}{S^2 + 2\xi\omega_n S + \omega_n^2} , \quad (\text{A. 8})$$

$$\text{Loop natural frequency: } \omega_n = \sqrt{\frac{K_\phi K_0}{T_1}} , \quad (\text{A. 9})$$

$$\text{Damping facto: } \xi = \frac{T_2 \omega_n}{2} , \quad (\text{A. 10})$$

$$\text{Pull-in range: } \Delta\omega_p = \begin{cases} \frac{4\sqrt{2\xi\omega_n K_\phi K_0 - \omega_n^2}}{\pi} & (\omega_n < K_\phi K_0) \\ \frac{4\sqrt{2\xi\omega_n K_\phi K_0}}{\pi} & (\omega_n \geq K_\phi K_0) \end{cases} , \quad (\text{A. 11})$$

$$\text{Pull-in time from: } \Delta\omega_0, T_p = \frac{\pi^2}{16} \times \frac{\Delta\omega_0^2}{\xi\omega_n^3} , \quad (\text{A. 12})$$

$$\text{Pull-out range: } \Delta\omega_{p0} = 1.8\omega_n(\xi + 1) , \quad (\text{A. 13})$$

$$\text{Hold range: } \Delta\omega_H = K_\phi K_0 , \quad (\text{A. 14})$$

$$\text{Lock range: } \Delta\omega_L \approx 2\xi\omega_n , \quad (\text{A. 15})$$

$$\text{Lock time: } T_L \approx \frac{2\pi}{\omega_n} , \quad (\text{A. 16})$$

$$\text{Closed-loop bandwidth: } B = \int_{-\infty}^{\infty} |G(j\omega)|^2 df = \frac{\omega_n(1+4\xi^2)}{8\xi} . \quad (\text{A. 17})$$

Equations (A.8) to (A.17) relating to receiver tracking loop design are used differently in hardware and software receivers.

In hardware receiver, the loop is designed so that the factors (T_2/T_1) and ($\Delta T /T_1$) are powers of 2 in order to reduce processor loading. In this manner, multiply/division operations can be performed by left/right shift operations. Since ΔT is the known integration time, after (T_2/T_1) and ($\Delta T /T_1$) are determined, T_1 , T_2 can be determined. At last, all other loop filter parameters, such as closed-loop bandwidth B and damping factor ξ , can be determined.

In a software receiver, the loop is designed for best performance. Therefore, the loop filter parameters such as closed-loop bandwidth B and damping factor ξ are first selected. Then, T_1 and T_2 are determined since ΔT is the known integration time. Finally (T_2/T_1) and ($\Delta T /T_1$) can be determined.

Here is an example of how to design a DLL for a software receiver with Equations (A.8) to (A.17).

Set the damping factor $\xi = 0.707$, which is the best tuning coefficient for a second-order tracking system. Also, assuming that a DLL discriminator described with Equation (2.17) in Chapter 2 is applied, the relationship between the closed-loop bandwidth B and loop natural frequency ω_n can be determined and the following relationships apply:

$$B = \frac{(1+4\xi^2)}{8\xi} \times \omega_n = 0.5303 \times \omega_n \text{ or } \omega_n = \frac{B}{0.5303} \quad (\text{A. 18})$$

$$T_2 = \frac{2\xi}{\omega_n} = \frac{1.414}{\omega_n} \quad (\text{A. 19})$$

$$T_1 = \frac{K_\phi K_0}{\omega_n^2} \quad (\text{A. 20})$$

$$K_0 = B'_{\text{norm}}(\delta\tau = 0) = 4 - 4\delta \quad (\text{A. 21})$$

$$K_\phi = 1 \text{ (the transfer function of code NCO is } \frac{1}{S} \text{).} \quad (\text{A. 22})$$

Equation (2.16) in Chapter 2 illustrates that the discriminator gain of the designed DLL here is $(4-4\delta)$. Dividing Equation (2.17) with $(4-4\delta)$ yields a new discriminator as follows:

$$B(\delta\tau) = \frac{(I_E^2 + Q_E^2) - (I_L^2 + Q_L^2)}{(I_P^2 + Q_P^2)(4 - 4\delta)}, \quad (\text{A. 23})$$

where δ is correlator spacing.

The new discriminator gain is

$$B'(\delta\tau = 0) = 1. \quad (\text{A. 24})$$

Therefore, one can write

$$K_0 = 1. \quad (\text{A. 25})$$

Furthermore, if set $\frac{T_2}{T_1} = a_2 \omega_n$, then the equations (A.8) to (A.17) can be rewritten

as

$$\text{Loop coefficient: } a_2 = \frac{T_2}{T_1 \omega_n} = 1.414, \quad (\text{A. 26})$$

$$\text{Closed-loop transfer function: } \phi(s) = \frac{G(s)}{S + G(s)} = \frac{\omega_n^2 + 1.414\omega_n S}{S^2 + 1.414\omega_n S + \omega_n^2}, \quad (\text{A. 27})$$

$$\text{Loop natural frequency: } \omega_n = \sqrt{\frac{1}{T_1}}, \quad (\text{A. 28})$$

$$\text{Damping factor: } \xi = \frac{T_2 \omega_n}{2}, \quad (\text{A. 29})$$

$$\text{Pull-in range: } \Delta\omega_p = \begin{cases} \frac{4\sqrt{1.414\omega_n - \omega_n^2}}{\pi} & (\omega_n < 1) \\ \frac{4\sqrt{1.414\omega_n}}{\pi} & (\omega_n \geq 1) \end{cases}, \quad (\text{A. 30})$$

$$\text{Pull-in time from: } \Delta\omega_0, T_p = \frac{\pi^2}{16} \times \frac{\Delta\omega_0^2}{0.707\omega_n^3}, \quad (\text{A. 31})$$

$$\text{Pull-out range: } \Delta\omega_{p0} = 3.07\omega_n, \quad (\text{A. 32})$$

$$\text{Hold range: } \Delta\omega_H = 1, \quad (\text{A. 33})$$

$$\text{Lock range: } \Delta\omega_L \approx 1.414\omega_n, \quad (\text{A. 34})$$

$$\text{Lock time: } T_L \approx \frac{2\pi}{\omega_n}. \quad (\text{A. 35})$$

Figure A. 2 shows the architecture of a second-order DLL.

Similarly,

Figure A. 3 and Figure A. 4 show the architectures of a first-order DLL and a third-order DLL respectively.

For a first-order DLL:

$$y_i = y_{i-1} + \omega_n T x_i. \quad (\text{A. 36})$$

For a third order DLL:

$$y_i = (2y_{i-1} - y_{i-2}) + (\omega_n^3 T^2 + a_3 \omega_n^2 T + b_3 \omega_n) x_i - (a_3 \omega_n^2 T + 2b_3 \omega_n) x_{i-1} + (b_3 \omega_n) x_{i-2}. \quad (\text{A. 37})$$

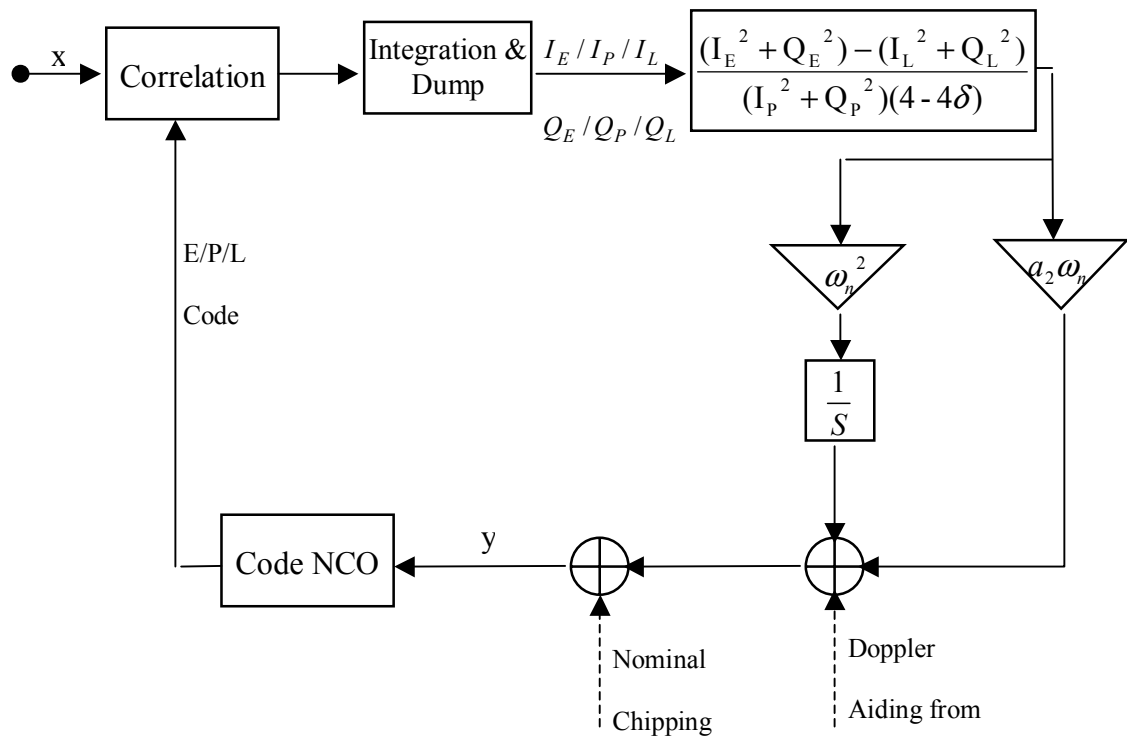


Figure A. 2 Architecture of A Second-Order Code Delay Locked Loop

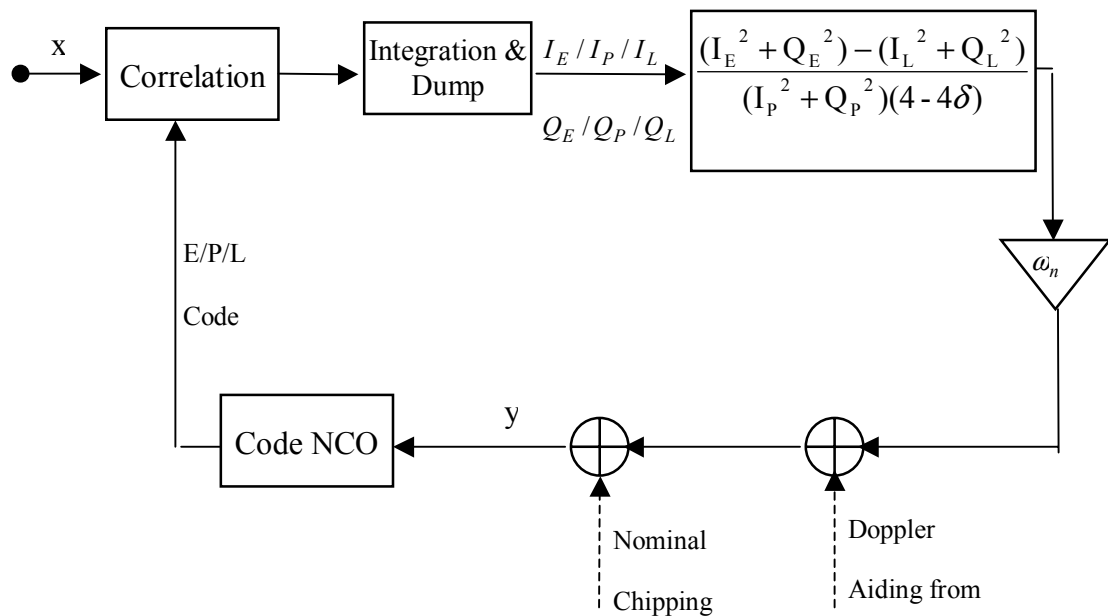


Figure A. 3 Architecture of A First-Order Code Delay Locked Loop

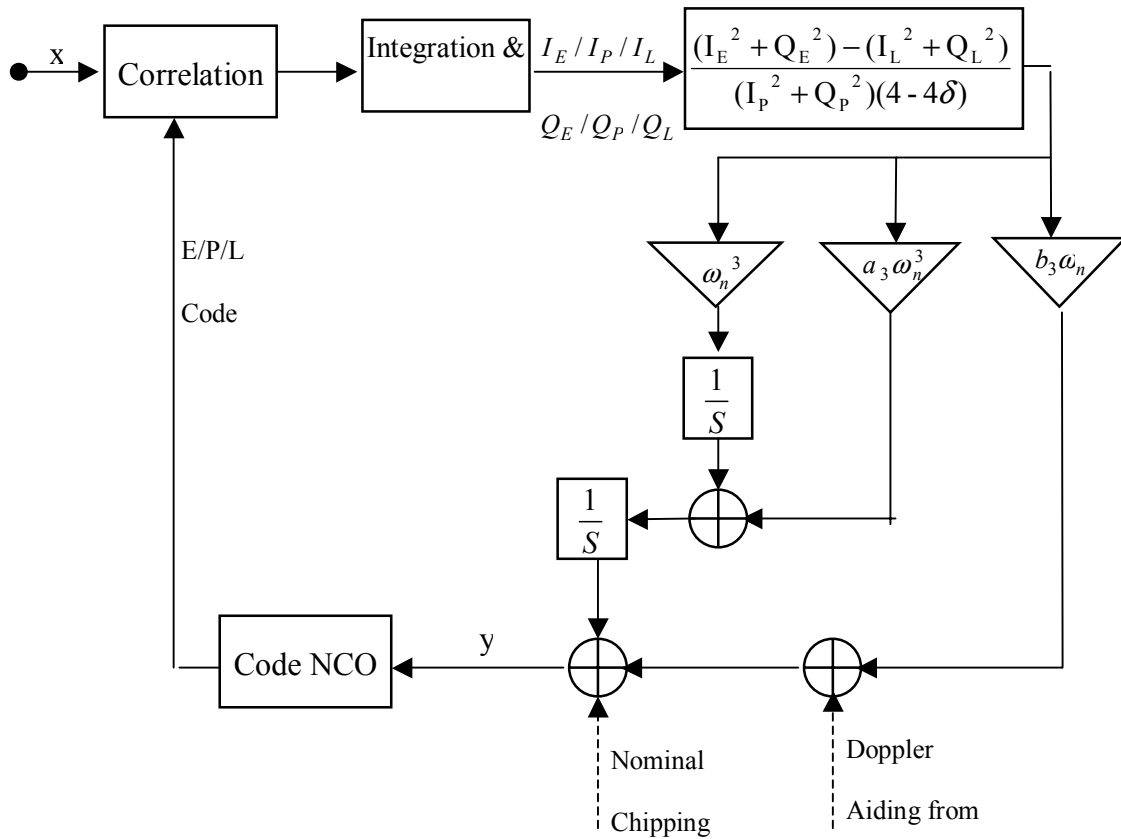


Figure A. 4 Architecture of A Third-Order Code Delay Locked Loop

Table A. 1 summarizes loop filter characteristics discussed above (Kaplan 1996).

For a second-order system, as expressed in Equations (A.11), (A.12) and (A1.3), the Pull-in range $\Delta\omega_p$, Pull-in time T_p (from $\Delta\omega_0$) and Pull-out range $\Delta\omega_{p0}$ are

$$\frac{4\sqrt{2\xi\omega_n K_\phi K_0 - \omega_n^2}}{\pi}, \frac{\pi^2 \Delta\omega_0^2}{16\xi\omega_n^3} \text{ and } 1.8\omega_n(\xi+1), \text{ respectively. So it is clear that in}$$

order to design a stable control system with wider pull-in/pull-out ranges and a shorter

pull-in time, a higher loop natural frequency ω_n is preferred. It is the same with a first order or third order system. From Table A. 1, it is clear that the same natural frequency ω_n will lead to different noise bandwidth B_n . When the natural frequency ω_n is the same, a first-order system will yield the narrowest noise bandwidth, and a third order system will yield the widest noise bandwidth. It is well known that the narrower noise bandwidth a DLL adopts, the less thermal noise the receiver will produce. So, in a loop filter design, although a higher order system normally provides better steady-state error performance, as shown in Table A. 1, a lower order system usually yields shorter response time, better system stability and less thermal noise.

Table A. 1 Characteristics of Different Loop Filters (Kaplan 1996)

Loop order	Noise Bandwidth	Typical filter values	Steady-state error
1	$\frac{\omega_n}{4}$	$B_n = 0.25\omega_n$	$R_e = \frac{dR}{\frac{dt}{\omega_n}}$
2	$\frac{\omega_n(1 + \alpha_2^2)}{4\alpha_2}$	$\alpha_2 = 1.414$ $B_n = 0.53\omega_n$	$R_e = \frac{dR^2}{\frac{dt^2}{\omega_n^2}}$
3	$\frac{\omega_n(\alpha_3 b_3^2 + \alpha_3^2 - b_3)}{4(\alpha_3 b_3 - 1)}$	$\alpha_3 = 1.1$ $b_3 = 2.4$ $B_n = 0.7845\omega_n$	$R_e = \frac{dR^3}{\frac{dt^3}{\omega_n^3}}$

**APPENDIX B: A THREE-STEP STRATEGY OF NAVIGATION DATA
DECODING BASED ON FLL MEASUREMENTS**

In order to decode the navigation data bit from a FLL directly when a PLL breaks down, a three-step strategy can be used, based on FLL measurements (Mitel 1998):

In step 1, calculate the I and Q components of the incoming signal tracked by the FLL as

$$\begin{aligned} I_i' &= \text{Norm}I_i \cdot \cos \theta_i + \text{Norm}Q_i \cdot \sin \theta_i, \\ Q_i' &= \text{Norm}Q_i \cdot \cos \theta_i - \text{Norm}I_i \cdot \sin \theta_i \end{aligned} \quad (\text{B. 1})$$

where $\text{Norm}I_i$, $\text{Norm}Q_i$ and θ_i are the normalized In-phase (I) component, Quadrature (Q) component and carrier phase of the incoming signal tracked by the FLL at epoch i , respectively.

In step 2, estimate the carrier phase at the epoch $(i+1)$ as

$$\theta_{i+1} = \arcsin(\text{sign}(I_i') \cdot Q_i') + \theta_i, \quad i = 1, 2, \dots, \quad (\text{B. 2})$$

where θ_{i+1} starts from $\theta_1 = 0$.

In step 3, the navigation data at epoch i can be decoded as follows:

$$D_i = \text{sign}(I_i') . \quad (\text{B. 3})$$

If one continues with Equations (B.1), (B.2) and (B.3), all navigation data bit can be decoded in sequence.

The mechanism of the three-step data decoding method is explained as follows:

In Equation (B.1), when $i=1$,

$$\begin{aligned} I_1' &= I_1 \cos(0) + Q_1 \sin(0) = D_1 \cos(\phi_1) \\ Q_1' &= Q_1 \cos(0) - I_1 \sin(0) = D_1 \sin(\phi_1) . \end{aligned}$$

Assuming $0 \leq \phi_1 \leq 90^\circ$,

$$\cos(\phi_1) \geq 0 ,$$

then,

$$\text{sign}(I_1') = \text{sign}(I_1 \cos(0) + Q_1 \sin(0)) = \text{sign}(D_1) ,$$

so,

$$\theta_2 = \arcsin(\text{sign}(I_1') \cdot Q_1') + \theta_1 = \phi_1 .$$

When $i=k$,

$$\begin{aligned} I_k' &= \text{Norm}I_k \cos(\theta_k) + \text{Norm}Q_k \sin(\theta_k) = D_k \cos(\phi_k - \theta_k) \\ Q_k' &= \text{Norm}Q_k \cos(\theta_k) - \text{Norm}I_k \sin(\theta_k) = D_k \sin(\phi_k - \theta_k) \end{aligned}$$

Assuming

$$-90^0 \leq \phi_k - \theta_k \leq 90^0, \quad (\text{B. 4})$$

then,

$$\text{sign}(I_k') = \text{sign}(D_k) \quad (\text{B. 5})$$

$$\theta_{k+1} = \arcsin(\text{sign}(I_k') \cdot Q_k') + \theta_k = \phi_k. \quad (\text{B. 6})$$

To obtain Equations (B.4) and (B.5), it is clear that $|\phi_k - \theta_k| = |\phi_k - \phi_{k-1}| \leq 90^0$.

Rearranging Equation (B.4) yields

$$|\phi_k - \phi_{k-1}| = |\pi(\Delta f_k - \Delta f_{k-1})T| \leq 90^0 \Rightarrow |\Delta f_k - \Delta f_{k-1}| \leq \frac{1}{2T} \quad (\text{B. 7})$$

If the pre-detection integration time $T = 10$ ms, then $|\Delta f_k - \Delta f_{k-1}| \leq \frac{1}{2 \times 0.01} = 50$ Hz. For a fine FLL discriminator after coarse frequency tracking, the condition described by Equation (B.7) is normally satisfied.

APPENDIX C: TWO POSSIBLE FLL DISCRIMINATORS FOR PURE CARRIER TRACKING

As discussed in Equation (2.20) in Chapter 2, the product from a Cross-Product FLL discriminator is:

$$\begin{aligned}
 \mathcal{D}_i &= (NormI_{i-1} \cdot NormQ_i - NormI_i \cdot NormQ_{i-1}) sign(NormI_{i-1} \cdot NormI_i + NormQ_i \cdot NormQ_{i-1}) \\
 &= D_{i-1} \cdot D_i \cdot \sin(\phi_i - \phi_{i-1}) \cdot sign(D_{i-1} \cdot D_i \cdot \cos(\phi_i - \phi_{i-1})) \\
 &= D_{i-1} \cdot D_i \cdot \sin(\phi_i - \phi_{i-1}) \cdot sign(D_{i-1} \cdot D_i) \\
 &= |D_{i-1} \cdot D_i| \cdot \sin(\phi_i - \phi_{i-1}) \propto (\phi_i - \phi_{i-1})
 \end{aligned} \tag{C. 1}$$

In Equation (C.1), $-90^\circ \leq \phi_i - \phi_{i-1} \leq 90^\circ$ is required to satisfy the following relationship suggested by Equation (C.1):

$$sign(D_{i-1} \cdot D_i \cdot \cos(\phi_i - \phi_{i-1})) = sign(D_{i-1} \cdot D_i) \tag{C. 2}$$

If the navigation data bit D_i is known and furthermore, assuming that $D_i = 1, i = 1, 2, \dots$, then

$$sign(D_{i-1} \cdot D_i \cdot \cos(\phi_i - \phi_{i-1})) = sign(\cos(\phi_i - \phi_{i-1})) \tag{C. 3}$$

Therefore, the products of the FLL discriminator in Equation (C.1) can be revised as follows:

revised FLL discriminator 1:

$$\begin{aligned}\delta f_{1,i} &= \text{Norm}I_{i-1} \cdot \text{Norm}Q_i - \text{Norm}I_i \cdot \text{Norm}Q_{i-1} \\ &= \sin(\phi_i - \phi_{i-1}) \propto (\phi_i - \phi_{i-1}) \quad (\text{when } -180^\circ \leq \phi_i - \phi_{i-1} \leq 180^\circ),\end{aligned}\quad (\text{C. 4})$$

revised FLL discriminator 2:

$$\delta f_{2,i} = \begin{cases} \text{Norm}I_{i-1} \cdot \text{Norm}Q_i - \text{Norm}I_i \cdot \text{Norm}Q_{i-1} \\ \quad \text{when } \text{sign}(\text{Norm}I_{i-1} \cdot \text{Norm}I_i + \text{Norm}Q_i \cdot \text{Norm}Q_{i-1}) \geq 0 \\ \text{sign}(\text{Norm}I_{i-1} \cdot \text{Norm}Q_i - \text{Norm}I_i \cdot \text{Norm}Q_{i-1}) \times 1, \\ \quad \text{when } \text{sign}(\text{Norm}I_{i-1} \cdot \text{Norm}I_i + \text{Norm}Q_i \cdot \text{Norm}Q_{i-1}) \leq 0 \end{cases}. \quad (\text{C. 5})$$

Figure C. 1 shows the products of these three FLL discriminators: original Cross-Product discriminator in Equation (C.1), revised discriminator 1 in Equation (C.4), and revised discriminator 2 expressed in Equation (C.5).

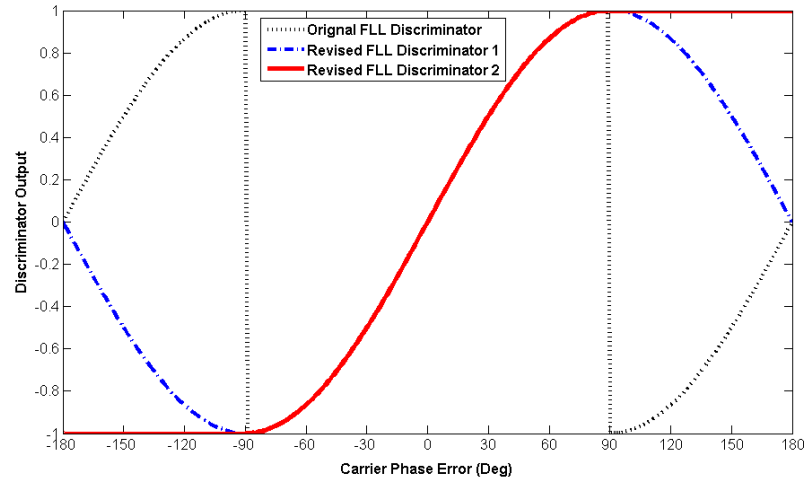


Figure C. 1 Products of different FLL discriminators

Figure C. 1 shows clearly that, although the products of the three discriminators are the same when $-90^\circ \leq \phi_i - \phi_{i-1} \leq 90^\circ$, the revised FLL discriminators for pure-carrier tracking yield much better performance when $|\phi_i - \phi_{i-1}| \geq 90^\circ$. It is clear that the tracking error range of the revised discriminators is from -180° to 180° , which is double the regular FLL discriminator.

It is well known that pure PLLs should replace Costas PLLs for carrier phase tracking when the incoming carrier signal is not modulated with navigation data bit, or the navigation data has been wiped off before doing carrier phase tracking. As with pure PLLs, revised FLL discriminators proposed herein achieve much more effective tracking performance than regular FLL discriminators in pure-carrier tracking.

The FLL tracking loop jitter due to thermal noise is (Kaplan 1996):

$$\sigma_{FLL,t} = \frac{1}{2\pi T} \sqrt{\frac{4FB_n}{C/N_o} \left(1 + \frac{1}{TC/N_o}\right)} \text{ (Hz).} \quad (\text{C. 6})$$

Therefore, the relationship between the FLL thermal noise and carrier-to-noise ratio is:

$$\sigma_{FLL,t} \propto \frac{1}{\sqrt{C/N_o}}. \quad (\text{C. 7})$$

Since the tracking threshold of the revised FLLs increased herein from 90° to 180° , the tolerant C/N_o can be 6 dB lower than before. In other words, using revised FLL discriminators, particularly the revised FLL discriminator 2, will achieve an additional 6 dB tracking sensitivity gain in theory in pure-carrier tracking, as compared to a regular FLL discriminator.

APPENDIX D: MATHEMATICAL MODEL FOR AN ULTRA-TIGHTLY COUPLED GPS/INS KALMAN FILTER

A model for an ultra-tightly coupled Kalman filter can be written in the following form:

$$\dot{X} = AX + W \quad (\text{D. 1})$$

$$Z = HX + V. \quad (\text{D. 2})$$

D.1. System Model for An Ultra-Tightly Coupled Kalman Filter

According to Scherzinger (2004), the system model is the same as that in a loosely coupled GPS/INS Kalman filter and is presented.

D.1.1. State Vector X

$$X = [X_{\text{INS}} \quad X_{\text{IMU_ERROR}} \quad X_{\text{GPS}}] \quad (\text{D. 3})$$

Equation (D.3) shows clearly that the state vector (X) includes three parts: INS states (X_{INS}), IMU sensor error states ($X_{\text{IMU_ERROR}}$) and GPS states (X_{GPS}). These states are:

$$X_{\text{INS}} = [\delta L \ \delta \lambda \ \delta H \ \delta V_E \ \delta V_N \ \delta V_U \ \phi_E \ \phi_N \ \phi_U] \quad (\text{D. 4})$$

where, δL $\delta \lambda$ δH are INS position errors in longitude, latitude and height, respectively. δV_E δV_N δV_U are INS velocity errors along the east, north and up directions in the local level frame, respectively. ϕ_E ϕ_N ϕ_U are INS attitude misalignments along the east, north and up directions in local level frame.

$$X_{GPS} = [T_{bias} \quad T_{drift}] \quad (\text{D. 5})$$

where T_{bias} is the GPS receiver clock bias and T_{drift} is the GPS receiver clock drift.

$$X_{IMU_ERROR} = [\varepsilon_x \quad \varepsilon_y \quad \varepsilon_z \quad S_{g_x} \quad S_{g_y} \quad S_{g_z} \quad \nabla_x \quad \nabla_y \quad \nabla_z \quad S_{a_x} \quad S_{a_y} \quad S_{a_z}] \quad (\text{D. 6})$$

where, ε_x ε_y ε_z are gyro drifts along X, Y, Z axes in the INS body frame. S_{g_x} S_{g_y} S_{g_z} are gyro scale factors along X, Y, Z axes in the INS body frame. ∇_x ∇_y ∇_z are accelerometer biases along X, Y, Z axes in the INS body frame and S_{a_x} S_{a_y} S_{a_z} are accelerometer scale factors along X, Y, Z axes in the INS body frame.

D.1.2. INS Modeling

$$\begin{aligned}
 \dot{\Phi}^n &= \delta\omega_{ie}^p + \omega_{en}^n - (\omega_{ie}^n + \omega_{en}^n) \times \phi^n + \varepsilon^p \\
 \dot{\delta v}^n &= f^n - (2\omega_{ie} + \omega_{en}) \times v^n + g^n \\
 \dot{\delta P}^n &= \left[\frac{\delta v_N^n}{R_m + H} \quad \frac{\delta v_E^n \sec(L)}{R_n + H} \quad \delta V_U^n \right]^T
 \end{aligned} \tag{D. 7}$$

where Φ is a vector of misalignment angles along each axis, f is the vector of errors in the measured specific force vector, and ω is the vector of errors in the measured angular rates. P is the position vector and v is the velocity vector. L is the latitude of the INS and H is the height of the INS. R_m and R_n are the longest and shortest radius of the earth, respectively. The super-script n and p represent the local level frame and earth centered earth fixed frame, respectively.

D.1.3. IMU Error Modeling

$$\begin{aligned}
 \delta f^b &= \nabla^b + f^b \times S_a^b + n_a^b \\
 \delta \omega^b &= \varepsilon^b + \omega^b \times S_g^b + n_g^b
 \end{aligned} \tag{D. 8}$$

where

∇^b, ε^b are accelerometer bias and gyro drift, respectively, and modeled as first-order Markov processes,

S_a^b, S_g^b are accelerometer scale factor and gyro scale factor respectively and modeled

as constant variables, f^b and ω^b are specific force and angular rotation rate of the IMU.

n_a^b, n_g^b are the noise of accelerometer and gyro respectively and modeled as Gaussian

white noise.

D.1.4. GPS Modeling

$$\begin{aligned} T_{BIAS} &= B_{clock} + n_{T_{BIAS}} \\ T_{DRIFT} &= D_{clock} + n_{T_{DRIFT}} \end{aligned} \quad (\text{D. 9})$$

where

B_{clock}, D_{clock} are clock bias and clock drift, respectively, and modeled as first-order Markov processes,

$n_{T_{BIAS}}, n_{T_{DRIFT}}$ are the noise of clock bias and clock drift and modeled as Gaussian white noise.

In the above models, the level-arm effect is ignored, since it is not the focus of this study.

D.2. Observation Model for an Ultra-Tightly Coupled Kalman Filter

As discussed in Chapter 3, the observation vector of an ultra-tightly coupled Kalman filter must contain I and Q errors in the WGS-84 frame between GPS and INS. So the observation model can be presented as:

$$Z_{Deep} = \begin{bmatrix} \delta I_1 & \delta Q_1 \\ \vdots & \vdots \\ \delta I_n & \delta Q_n \end{bmatrix} = \begin{bmatrix} I_{GPS,1} - I_{INS,1} & Q_{GPS,1} - Q_{INS,1} \\ \vdots & \vdots \\ I_{GPS,n} - I_{INS,n} & Q_{GPS,n} - Q_{INS,n} \end{bmatrix} = H_{\delta P, \delta V \rightarrow I, Q} X + V \quad (\text{D. 10})$$

where the subscript n is the number of satellites tracked by the receiver. Obviously, in the above equation, there are two questions that need to be answered, namely:

1. How to generate the $I_{INS,i}$ and $Q_{INS,i}$ data from INS observations, e.g., P_{INS} and V_{INS} ?
2. What is the transfer matrix $H_{\delta P, \delta V \rightarrow I, Q}$ that transfers observed information from the state vector P_{INS} and V_{INS} to the measurements $I_{INS,i}$ and $Q_{INS,i}$?

According to Babu & Wang (2005), the following derivation shows how to determine $I_{INS,i}$, $Q_{INS,i}$, and $H_{\delta P, \delta V \rightarrow I, Q}$.

D.2.1. Modeling I & Q Estimates

As discussed in Chapter 2, the I-phase (I) and Quadra-phase (Q) components of a GPS signal after correlation can be written as

$$\begin{aligned} I &= \int_{KT}^{(k+1)T} \{\cos(\hat{\omega}t + \hat{\phi}) [A \cos(\omega t + \phi) + n_0]\} dt \\ &= \frac{-A}{2\omega_e} [\sin(\omega_e(k+1)T + \phi_e) - \sin(\omega_e kT + \phi_e)] + n_I \end{aligned} \quad (\text{D. 11})$$

and

$$\begin{aligned} Q &= \int_{KT}^{(k+1)T} \{-\sin(\hat{\omega}t + \hat{\phi}) [A \cos(\omega t + \phi) + n_0]\} dt \\ &= \frac{-A}{2\omega_e} [\cos(\omega_e(k+1)T + \phi_e) - \cos(\omega_e kT + \phi_e)] + n_Q \end{aligned} \quad (\text{D. 12})$$

where $\omega_e = \hat{\omega} - \omega$ is the frequency error tracked by FLL, and $\phi_e = \hat{\phi} - \phi$ is the phase error tracked by PLL.

D.2.2. Received Phase and Frequency Estimates Modeling

Suppose that

$$\tau = \frac{|P_{satellite} - P_{receiver}|}{C} = \frac{|P_s - P_r|}{C}. \quad (\text{D. 13})$$

One then has

$$\begin{aligned} |P_s - P_r| &\approx |P_s(t) - P_r(t_0)| + \frac{d}{dt} |P_s - P_r| (t - t_0) \\ &= |P_{r0} - P_s| + |V_{s-r}|_{\text{Los}} (t - t_0) \end{aligned} \quad , \quad (\text{D. 14})$$

where t is a time point between the current epoch t_0 and the next epoch $t_0 + 1$. The operation $|V|_{\text{Los}}$ means taking the projection of V in the LOS direction, the result can be positive or negative

As Chapter 2 shows, the received GPS signal can be presented as

$$y(t) = A CA(t) D(t) \cos(\omega_0(t - \tau) + \phi_0) + n_0. \quad (\text{D. 15})$$

If one inserts Equation (D.14) into (D.15), one obtains

$$y(t) = A CA(t) D(t) \cos(\omega t + \phi) + n_0, \quad (\text{D. 16})$$

where

$$\begin{aligned} \omega &= \omega_0 \left(1 + \frac{|V_{s-r}|_{\text{Los}}}{C}\right) \\ \phi &= \phi_0 - \frac{\omega_0}{C} (|P_r(t_0) - P_s(t)|_{\text{Los}} + |V_{s-r}|_{\text{Los}} t_0) \end{aligned} \quad , \quad (\text{D. 17})$$

where, the operation $|X|_{\text{Los}}$ means taking the projection of X in the LOS direction.

D.2.3. Relationship between Phase, Frequency, Position, and Velocity

As shown in Equation (D.17), the estimates of α and ϕ are

$$\hat{\omega} = \omega_0 \left(1 + \frac{|\hat{V}_{s-r}|_{Los}}{C} \right) \quad (\text{D. 18})$$

and

$$\hat{\phi} = \phi_0 - \frac{\omega_0}{C} [|P_s(t) - \hat{P}_r(t_0)|_{Los} + |\hat{V}_{s-r}|_{Los} \cdot t_0]. \quad (\text{D. 19})$$

One then has

$$\omega_e = \hat{\omega} - \omega = \frac{\omega_0}{C} | \hat{V}_{s-r} - V_{s-r} |_{Los} = \frac{\omega_0}{C} | V_e |_{Los} \quad (\text{D. 20})$$

and

$$\phi_e = \hat{\phi} - \phi = \frac{-\omega_0}{C} [| P_r(t_0) - \hat{P}_r(t_0) |_{Los} + | V_{s-r} - \hat{V}_{s-r} |_{Los} \cdot t_0] = \frac{-\omega_0}{C} (| P_e(t_0) |_{Los} + | V_e |_{Los} \cdot t_0), \quad (\text{D. 21})$$

where $P_e = \hat{P}_r - P_r$ and $V_e = \hat{V}_r - V_r$ are the position and velocity errors of the GPS receiver, respectively.

D.2.4. Relationship between I and Q and Position and Velocity

Section D.2.1 illustrates the relationship between I and Q measurements and phase and frequency measurements. The relationship between phase and frequency measurements and position and velocity solutions is given in section D.2.3. Based on the above models, the following equation can be derived:

$$\begin{aligned}
I &= I(P_e, V_e) \\
&= \frac{-AC}{2\omega_0 |V_e|_{Los}} [\sin[\frac{\omega_0}{C} |V_e|_{Los} (k+1)T + \frac{-\omega_0}{C} (|P_e(t_0)|_{Los} + |V_e|_{Los} t_0)] \\
&\quad - \sin[\frac{\omega_0}{C} |V_e|_{Los} kT + \frac{-\omega_0}{C} (|P_e(t_0)|_{Los} + |V_e|_{Los} t_0)] + n_I]
\end{aligned} \tag{D. 22}$$

and

$$\begin{aligned}
Q &= Q(P_e, V_e) \\
&= \frac{-AC}{2\omega_0 |V_e|_{Los}} [\cos[\frac{\omega_0}{C} |V_e|_{Los} (k+1)T + \frac{-\omega_0}{C} (|P_e(t_0)|_{Los} + |V_e|_{Los} t_0)] \\
&\quad - \cos[\frac{\omega_0}{C} |V_e|_{Los} kT + \frac{-\omega_0}{C} (|P_e(t_0)|_{Los} + |V_e|_{Los} t_0)] + n_Q]
\end{aligned} \tag{D. 23}$$

where $P_e = \hat{P}_r - P_r$ and $V_e = \hat{V}_r - V_r$ are position error and velocity error of GPS receiver, respectively.

D.2.5. Observation Model for Ultra-tightly Coupled GPS/INS Kalman Filter

The in-phase (I) measurement equation can be rewritten as:

$$\begin{aligned}
I(P_e, V_e) &= I(P_r - P_{INS} + P_{INS} - P_{GPS}, V_r - V_{INS} + V_{INS} - V_{GPS}) \\
&\approx I(P_{INS} - P_{GPS}, V_{INS} - V_{GPS}) + \frac{\partial I}{\partial P}(P_r - P_{INS}) + \frac{\partial I}{\partial V}(V_r - V_{INS}). \\
&= I(P_{e0}, V_{e0}) + \frac{\partial I}{\partial P} \delta P + \frac{\partial I}{\partial V} \delta V
\end{aligned} \tag{D. 24}$$

Let

$$I(P_{e0}, V_{e0}) = I_{INS}, \tag{D. 25}$$

in which case

$$\delta I = I_{GPS} - I_{INS} = \frac{\partial I}{\partial P} \delta P + \frac{\partial I}{\partial V} \delta V. \quad (\text{D. 26})$$

Similarly, one has

$$Q(P_{e0}, V_{e0}) = Q_{INS} \quad (\text{D. 27})$$

and

$$\delta Q = Q_{GPS} - Q_{INS} = \frac{\partial Q}{\partial P} \delta P + \frac{\partial Q}{\partial V} \delta V. \quad (\text{D. 28})$$

As Equation (D.10) demonstrates, the observation model of the ultra-tightly GPS/INS coupled Kalman filter is given as follows:

$$[(I_{i,GPS} - I_{i,INS}) \quad (Q_{i,GPS} - Q_{i,INS})] = H_{\delta P, \delta V, \dots \rightarrow I, Q} X + V,$$

where

$$\begin{aligned} I_{INS,i} &= I_i(P_{INS} - P_{GPS}, V_{INS} - V_{GPS}) \\ &= \frac{-AC}{2\omega_{0,i} |V_{INS} - V_{GPS}|_{Los}} [\sin\left(\frac{\omega_{0,i}}{C}\right) |V_{INS} - V_{GPS}|_{Los} (k+1)T \\ &\quad + \frac{-\omega_{0,i}}{C} (|P_{INS} - P_{GPS}|_{t0, Los} + |V_{INS} - V_{GPS}|_{Los} \cdot t_0)] \quad , \\ &\quad - \sin\left(\frac{\omega_{0,i}}{C}\right) |V_{INS} - V_{GPS}|_{Los} kT + \frac{-\omega_{0,i}}{C} (|P_{INS} - P_{GPS}|_{t0, Los} \\ &\quad + |V_{INS} - V_{GPS}|_{Los} \cdot t_0)] \end{aligned} \quad (\text{D. 29})$$

$$\begin{aligned}
Q_{INS,i} &= Q_i(P_{INS} - P_{GPS}, V_{INS} - V_{GPS}) \\
&= \frac{-AC}{2\omega_{0,i} |V_{INS} - V_{GPS}|_{Los}} [\cos\left(\frac{\omega_{0,i}}{C} |V_{INS} - V_{GPS}|_{Los}\right) (k+1)T \\
&\quad + \frac{-\omega_{0,i}}{C} (|P_{INS} - P_{GPS}|_{t0,Los} + |V_{INS} - V_{GPS}|_{Los} \cdot t_0)] \quad , \\
&\quad - \cos\left(\frac{\omega_{0,i}}{C} |V_{INS} - V_{GPS}|_{Los}\right) kT + \frac{-\omega_{0,i}}{C} (|P_{INS} - P_{GPS}|_{t0,Los} \\
&\quad + |V_{INS} - V_{GPS}|_{Los} \cdot t_0)]
\end{aligned} \tag{D. 30}$$

$$\begin{aligned}
H_{\delta^P, \delta^V, \dots \rightarrow I, Q, i} &= \begin{bmatrix} \frac{\partial I_i}{\partial P} & \frac{\partial I_i}{\partial V} & 0 \\ \frac{\partial Q_i}{\partial P} & \frac{\partial Q_i}{\partial V} & 0 \\ 0 & 0 & 0 \end{bmatrix} \\
&= \begin{bmatrix} \frac{\partial I_i}{\partial \omega_e} \frac{\partial \omega_e}{\partial P} + \frac{\partial I_i}{\partial \phi_e} \frac{\partial \phi_e}{\partial P} & \frac{\partial I_i}{\partial \omega_e} \frac{\partial \omega_e}{\partial V} + \frac{\partial I_i}{\partial \phi_e} \frac{\partial \phi_e}{\partial V} & 0 \\ \frac{\partial Q_i}{\partial \omega_e} \frac{\partial \omega_e}{\partial P} + \frac{\partial Q_i}{\partial \phi_e} \frac{\partial \phi_e}{\partial P} & \frac{\partial Q_i}{\partial \omega_e} \frac{\partial \omega_e}{\partial V} + \frac{\partial Q_i}{\partial \phi_e} \frac{\partial \phi_e}{\partial V} & 0 \\ 0 & 0 & 0 \end{bmatrix}, \quad (\text{D. 31})
\end{aligned}$$

and

$$V_i = \begin{bmatrix} n_{I,i} \\ n_{Q,i} \end{bmatrix}. \tag{D. 32}$$

APPENDIX E: SOFTWARE RECEIVER VALIDATION WITH THE NEW GPS IF DATA COLLECTION SYSTEM

To collect live GPS IF data for software receiver testing and qualification, a GPS IF data collecting system, referred to as a front end, was implemented.

The GPS IF data collection system used a NovAtel AllstarTM receiver as its front end. Therefore, this system not only provides GPS IF data as the input signal for a software receiver, but also yields GPS measurements (e.g., pseudorange, carrier phase, etc.), and GPS solutions (e.g., position, velocity, etc.). During the software receiver testing and validation, these GPS measurements and solutions are used as reference. Figure E. 1 illustrates how the GPS IF data collection system is used for the software receiver testing and qualification in both simulation and field tests.

In this appendix, a brief introduction is presented on how to use the front end to collect GPS IF data, followed with the software receiver testing and validation with the collected GPS IF data.

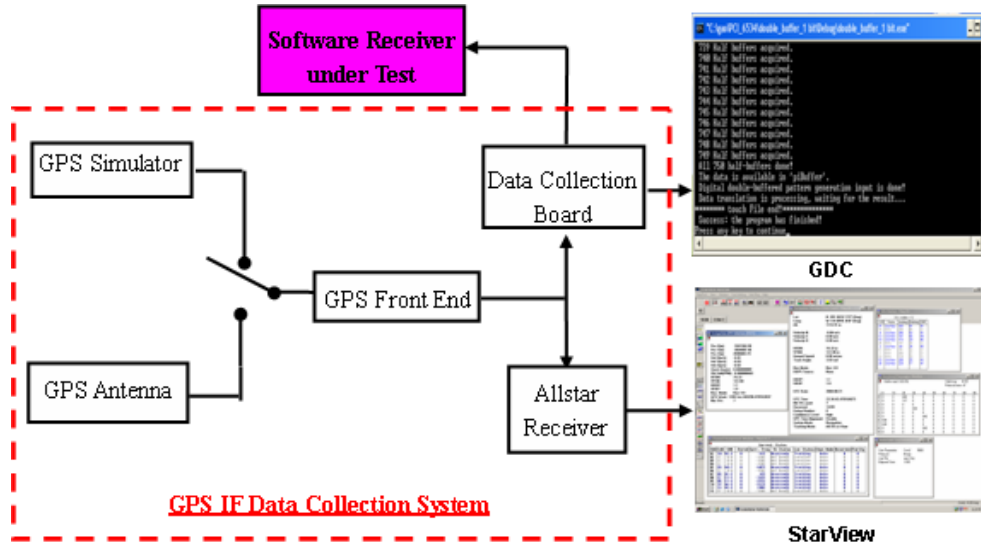


Figure E. 1 GPS IF Data Collection System Used for Software Receiver Testing & Validation during Both Simulation and Field Tests

E.1 Introduction of the GPS IF Data Collection System

Figure E. 2 shows the flow chart of a general GPS survey campaign, which includes the GPS IF data collection system, namely the GPS front end and the software receiver under test.

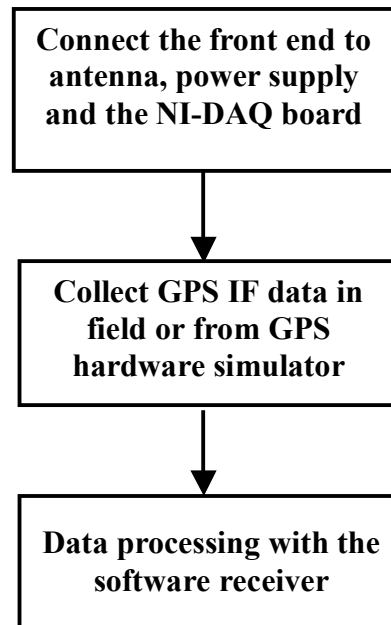


Figure E. 2 Flowchart of a General GPS Survey Campaign with the Front End and the Software Receiver

After the raw GPS IF data is collected in the field or from a GPS hardware simulator, the data is saved on the hard drive of a computer. In the computer, the format of the data file is then converted to an appropriate format for the data processing in the GPS software receiver. A GPS IF data collection software is developed in this study to perform the data collection. The software provides two data files after the collection and they are “File_RFdata.dat”, which records GPS IF data in binary in real-time, and “File_RFdata_for_GPSRx.dat”, which uses the format suitable for the software receiver under test. Besides the above two data files, the software also generates another data file

named “File_RFdata_Char.dat”. This file records GPS IF data in ASCII format for review purpose.

The processing scheme of the GPS IF data collection software is shown in Figure E. 3.

Figure E. 4 illustrates all connections of the GPS IF data collection system with peripheral equipments as the following:

1. connect the data collection system to a real antenna or a GPS hardware simulator,
2. connect the data collection system to a power supply,
3. connect the data collection system to a NI-DAQ board (e.g. PCI-6534),
4. connect the data collection system to COM1 or COM2 in the back of a common purpose computer and run software on the computer. starviewTM is commercial GPS software package provided by NovAtel. starviewTM can be used to monitor receiver states and load GPS measurements and positions.

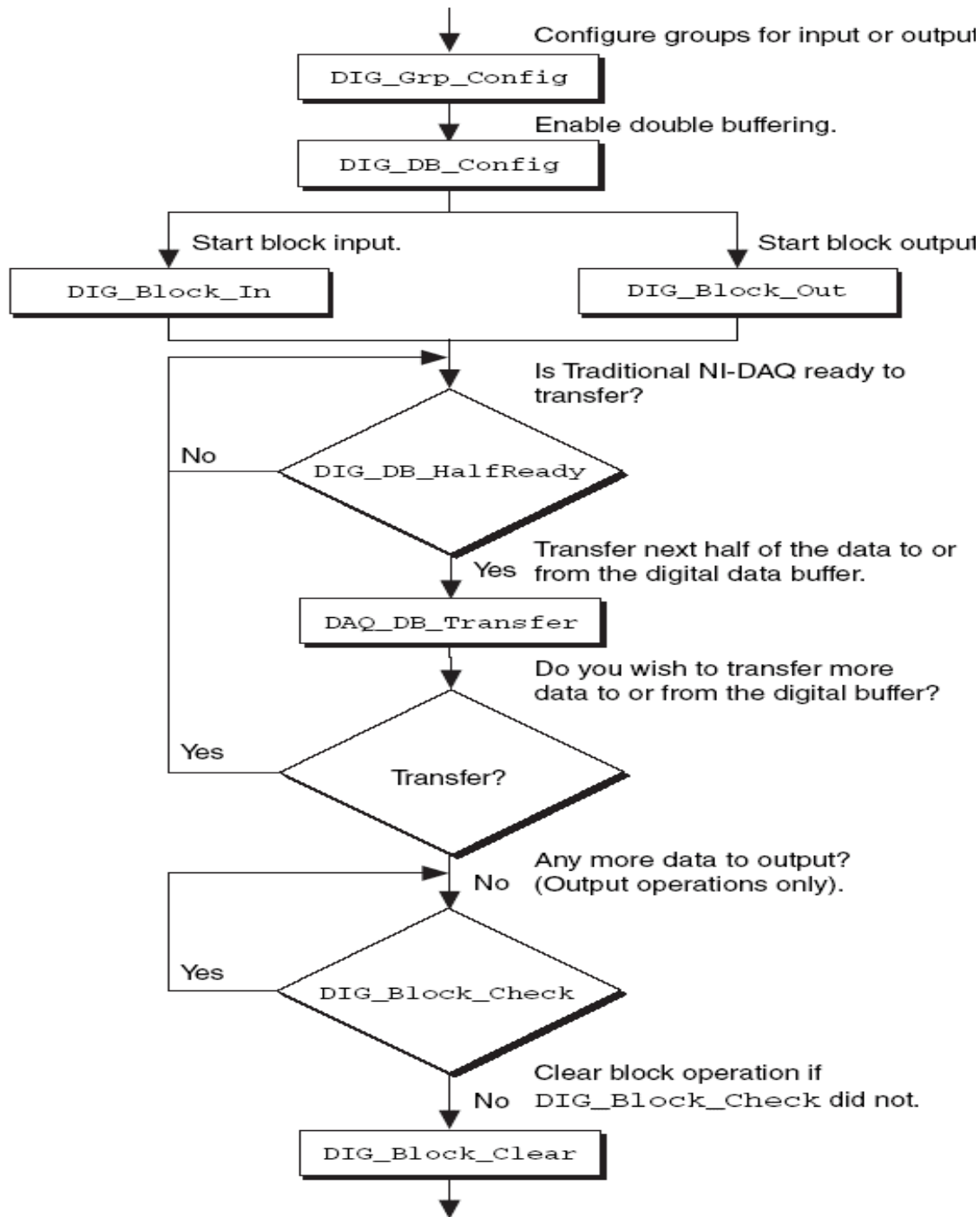


Figure E. 3 Processing Scheme of the GPS IF Data Collection Software

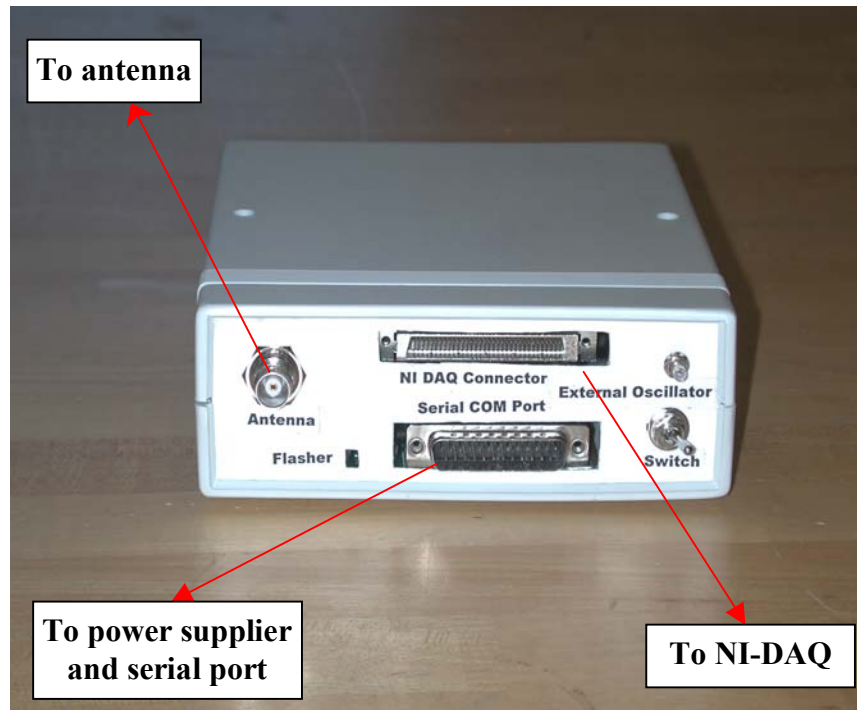


Figure E. 4 Connect the GPS IF Data Collection System with Peripheral Equipments

Using the GPS IF data collection system, it could then be assessed if the software receiver can correctly track the incoming signals and then yields the right positioning solution. For this purpose, several benchmark tests were conducted when the receiver was in stationary, medium dynamic and high dynamic situations. These benchmark tests validated that the receiver was designed properly, and its functions such as tracking and positioning operated correctly.

Figure E. 5 - Figure E.8 show the test results of a static field test. This test was done at 3:00 pm on August 9, 2004. The antenna was mounted at W1 survey point on the

roof of the CCIT building at the University of Calgary. The antenna position in WGS-84 frame was (-1641945.704, -3664805.609, 4940009.362). The data collection time in this test was 100 seconds and the bit quantization in the front end was one bit.

Figure E. 5 and Figure E. 6 show the tracking results of satellite PRN 1. Figure E. 5 illustrates estimated C/N_0 of satellite PRN 1 using the software receiver. It is clear that the software receiver can track the incoming signal very well. The navigation data modulated on satellite 1, which is shown in Figure E. 6, can be distinguished very easily.

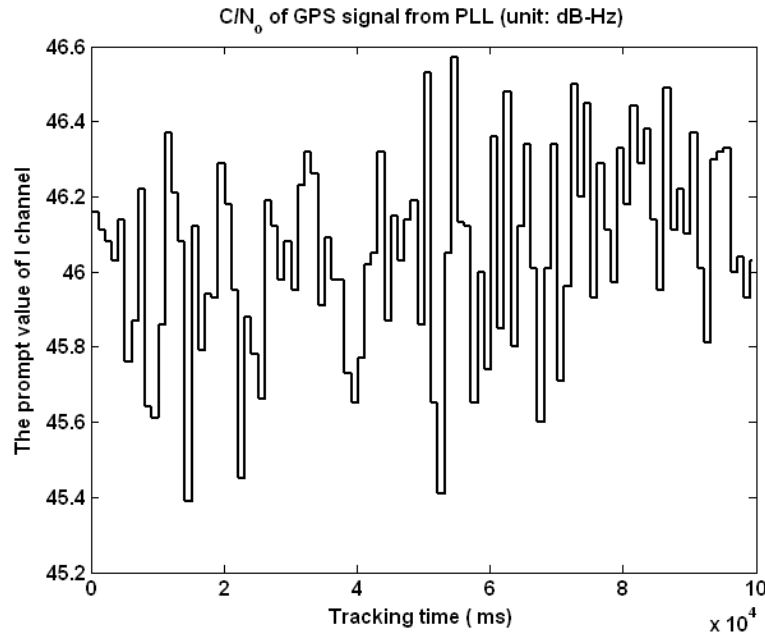


Figure E. 5 Estimated C/N_0 of Satellite PRN 1 by the Software receiver in Field

Static Test

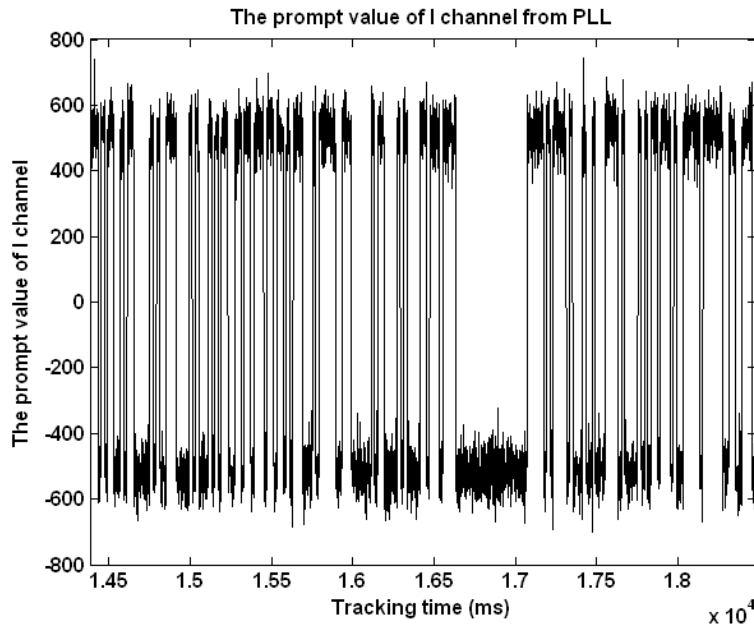


Figure E. 6 Prompt Values of I Channel (Satellite PRN 1) in the Software Receiver

Figure E.7 and Figure E.8 show the positioning results of the software receiver. Although there are biases presented in both horizontal and vertical position errors, the position precision is reasonable. The Root Mean Square (RMS) is under 5 m for the horizontal position error and under 15 m for the vertical position error. Comparing these position errors with the ones shown in simulation tests presented later in this appendix, the position biases are likely induced by atmospheric errors, e.g., tropospheric and ionospheric errors.

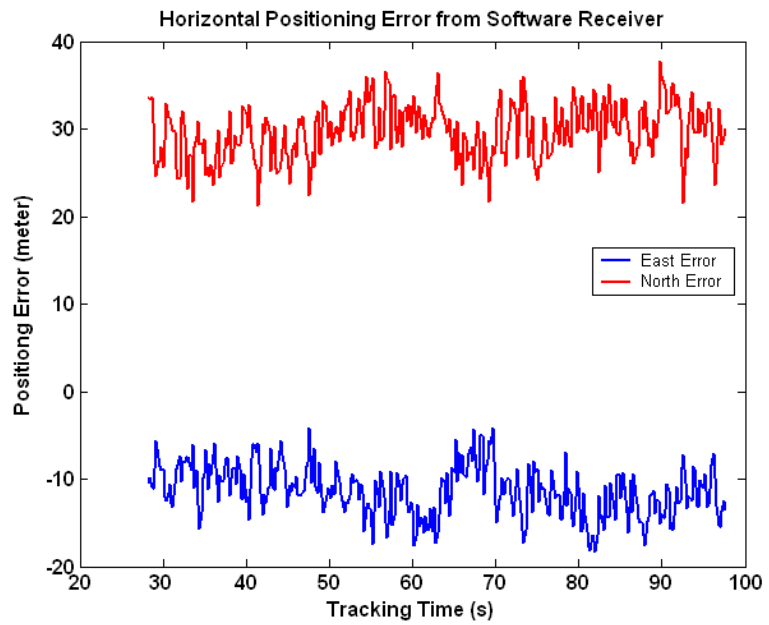


Figure E.7 Software Horizontal Position Errors

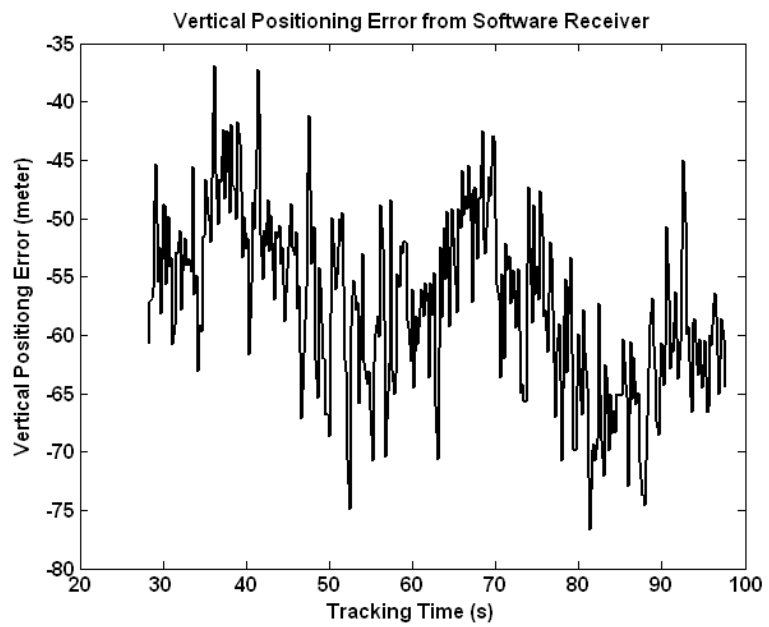


Figure E.8 Software Vertical Position Errors

To test and validate the performance of the software GPS receiver in dynamic situations, several simulation tests were done. In these tests, a GPS hardware simulator, namely the STR-6560 GPS Simulator from Spirent, was used as the GPS signal source.

Figure E.9 - Figure E. 12 show the test results of a simulation dynamic test. This test was done at 3:00 pm on August 16, 2004 and the start GPS time was 432000 s. Figure E.9 presents the trajectory of the software GPS receiver in the simulation test. The data collection time was 250 seconds and the bit quantization in the front end was one bit.

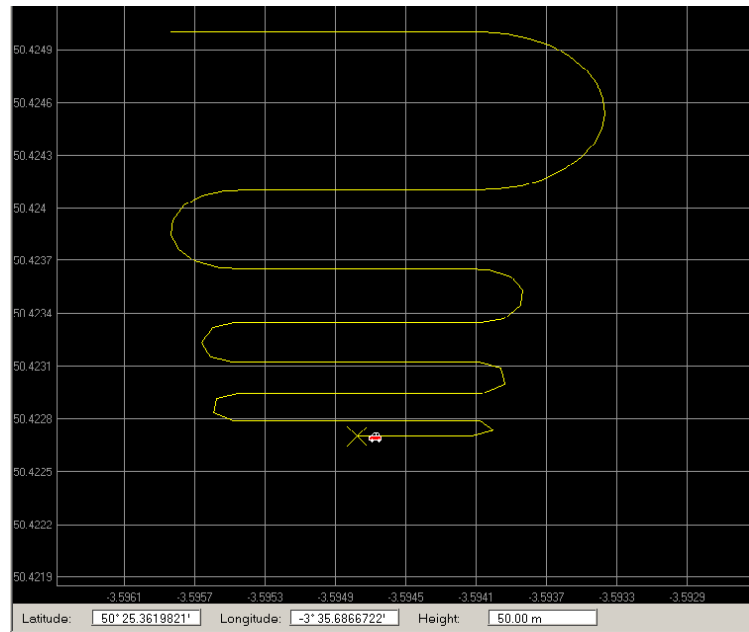


Figure E.9 Receiver Trajectory in Simulation Dynamic Test

Figure E.10 and Figure E.11 show the tracking results of satellite PRN 9 in this dynamic test. Figure E.10 shows the estimated C/N_0 of satellite PRN 9 using the

software receiver. It is clear that the software receiver can track the incoming signal very well. The navigation data modulated on PRN 9, which is shown in Figure E.11, can be distinguished very easily.

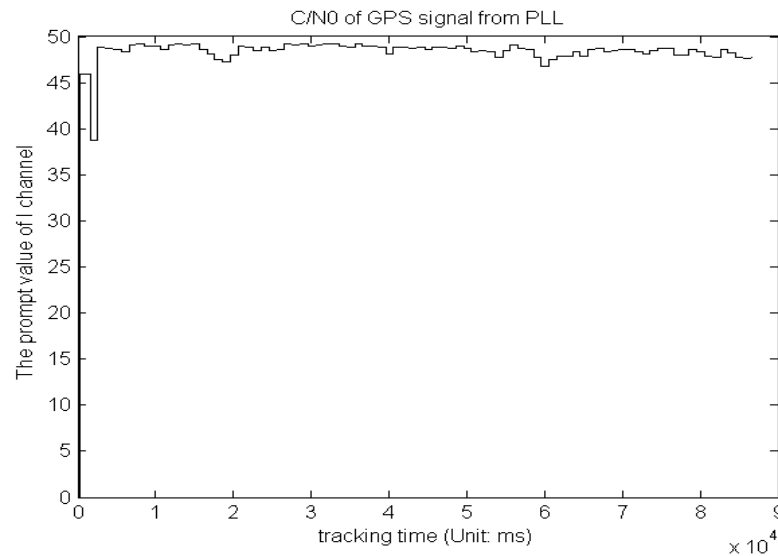


Figure E.10 Estimated C/N_0 of Satellite PRN 9 in the Software receiver

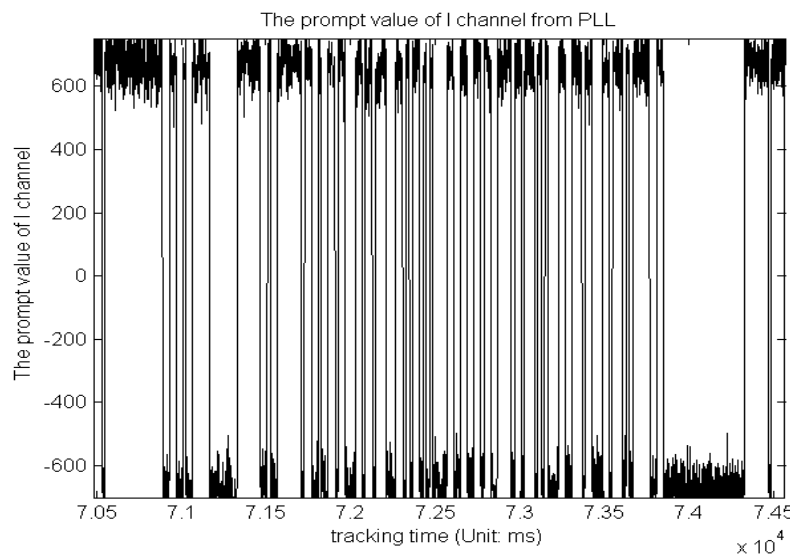


Figure E.11 Prompt Values of I Channel (Satellite PRN 9) in the Software Receiver

Figure E. 12 illustrates the positioning errors of the software receiver in the east, north and up dimensions. The receiver positions errors are bias-free errors and their STDs are less than 5 m for the horizon position error and less than 15 m for the vertical position error. Comparing these errors with the ones shown in Figure E.7 and Figure E.8 for the field test, it is evident that the position biases presented in the field test are induced by atmospheric errors.

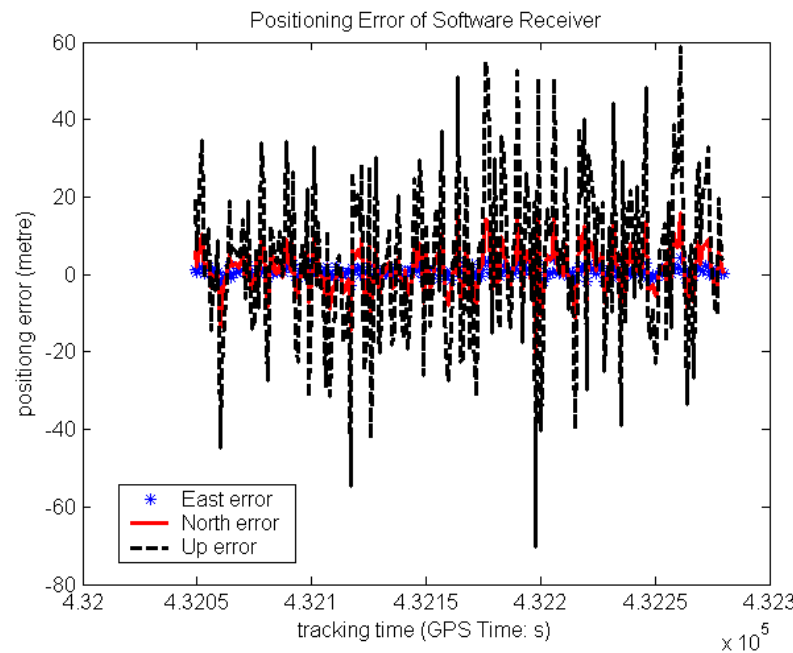


Figure E. 12 Software Receiver Position Errors

APPENDIX F: DEVELOPMENT OF AN INS SIMULATOR

In order to provide INS measurements for the simulation tests for the study of GPS/INS ultra-tight integration, an INS simulator called INS_Sim was also developed.

INS_Sim (INS Simulator) is an INS toolbox running in MatlabTM to simulate INS. It briefly includes a Trajectory Generator, IMU Simulator, an IMU Error Simulator, an Attitude Rotator and an INS Navigator. INS_Sim is an IBM PC compatible software package and uses of MATLABTM Version 3.0 or above.

This appendix presents specifics of the design and qualification of the INS simulator. The program structure of INS_Sim is outlined, followed with flow charts describing program execution. Contents and examples of the input and output needed for INS_Sim operation are also included in this appendix.

F.1 Architecture of INS Simulator

The architecture of the INS simulator (INS_Sim) is shown in Figure F.1.

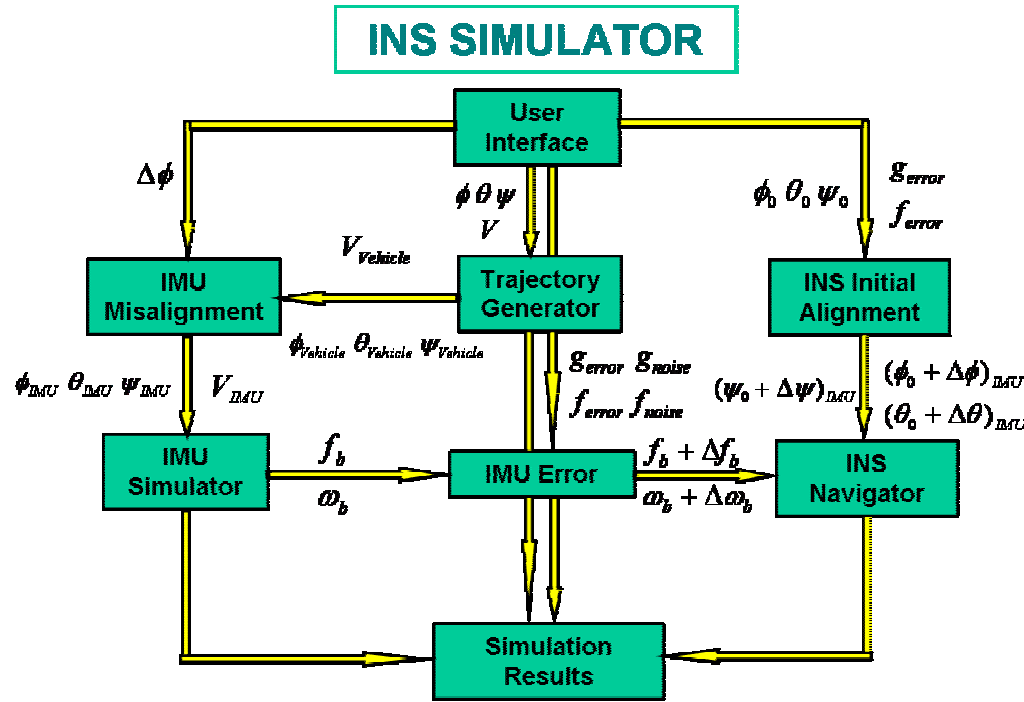


Figure F.1 INS Simulator Architecture

Figure F.1 shows that the INS_Sim includes eight modules. The functions of each module are as follows:

1. User Interface: This module is designed to input IMU and vehicle trajectory parameters for INS simulation.
2. Trajectory Generator: This module generates the vehicle trajectory over the specified simulation time with the required sampling rate.

3. IMU Simulator: This module simulates IMU and generates error-free IMU gyro and accelerometer measurements.
4. IMU Error Generator: This module simulates IMU errors and generates gyro and accelerometer measurements with errors.
5. IMU Misalignment: Because of INS mounting errors between the vehicle body frame and the IMU body frame, the vehicle attitude generated by the trajectory generator does not equal to the attitude of the IMU mounted in the vehicle. An attitude rotation is achieved to calculate the correct IMU attitude parameters.
6. INS Initial Alignment: In default mode, the INS is assumed to align in Zero velocity UPdaTe (ZUPT). Thus, the INS alignment errors can be determined based only on the simulated gyro drifts and accelerometer biases.
7. INS Navigator: Based on input IMU measurements, this module calculates the position and attitude of the vehicle by using mechanization equations in the wander angle frame.
8. Simulation Result demonstrator: In this module, all simulation results are presented in ten different windows or screens, as shown in Table 6.1.

Window No.	Window Name	Window Description
1	IMU Simulator: Vehicle Position	true position of the vehicle and used as the input of the IMU simulator
2	IMU Simulator: Vehicle Attitude	true attitude of the vehicle and used as the input of the IMU simulator
3	IMU Simulator: Vehicle Trajectory	true trajectory of the vehicle and used as the input of the IMU simulator
4	IMU Simulator: IMU Measurements	theoretical output of the IMU without measurement error
5	INS Navigator: Position	simulated position of the vehicle and computed by the INS navigator
6	INS Navigator: Attitude	simulated attitude of the vehicle and computed by the INS navigator
7	INS Navigator: Trajectory	simulated trajectory of the vehicle and computed by the INS navigator.
8	INS Navigator: Wander Angle	simulated wander angle of the vehicle in the wander angle frame, and computed by the INS navigator
9	INS Navigator: Wander Azimuth	wander azimuth of the vehicle in the wander angle frame and computed by the INS navigator
10	INS Navigator: IMU Measurements with Error	simulated field measurement of the IMU with measurement error

Table F.1 Output Windows of INS Simulator INS_Sim

F.2 Qualification of the INS Simulator

To validate the INS simulator, two testing strategies are used, as shown in Figure F. 2 and Figure F. 3.

In Figure F. 2, to test the consistency of the INS Simulator, the vehicle trajectory directly from the module “Trajectory Generator” (as shown in black arrow), and the one from the module “INS Navigator” (as shown in red arrow), are compared with each other at the module “simulation results” (shown as the red box). In such a consistency test, the IMU sensor error is set as zero. Therefore, the simulated trajectory from the module “Trajectory Generator” should be exactly the same as the one provided by the module “INS navigator”. If the two trajectories are not the same, then there must be something wrong in the link (shown in red arrow) from the module “Trajectory Generator” to the module “INS Navigator”.

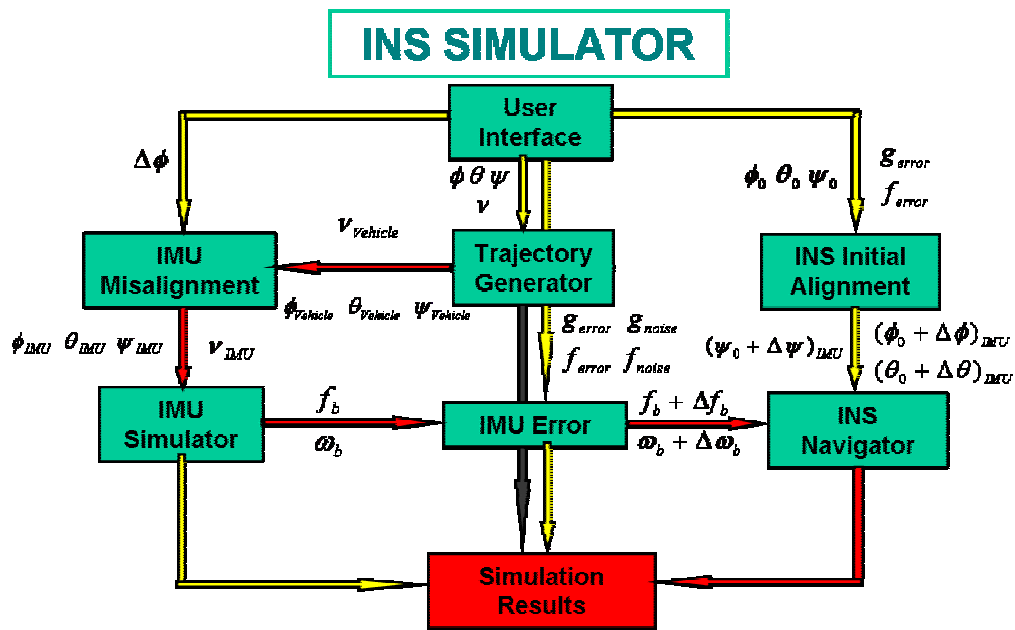


Figure F. 2 Consistency Test of the INS Simulator

Since the IMU sensor error is set as zero in a consistency test, the test can not verify the correctness of the module “IMU Error”. Therefore, some sample tests are applied to validate the module “IMU Error”.

As shown in Figure F. 3, the Observation generated by the module “IMU Error” is examined at the module “Simulation Results” (shown as the red box). Since we know the vehicle trajectory from the module “Trajectory Generator” and the IMU sensor errors, which are known simulation parameters, we can calculate the theoretical IMU observations and then compare these theoretical values with those from the module “IMU Error” and assess whether the modules “IMU Misalignment”, “IMU Simulator” and “IMU Error” linked with the red arrow are working properly or not.

To validate the INS Simulator, different trajectories were tested, including static point, straight line, circular movement and a "S" shaped trajectory. All tests showed that the INS simulator was designed properly, and its functions such as IMU simulation and INS navigation operated correctly.

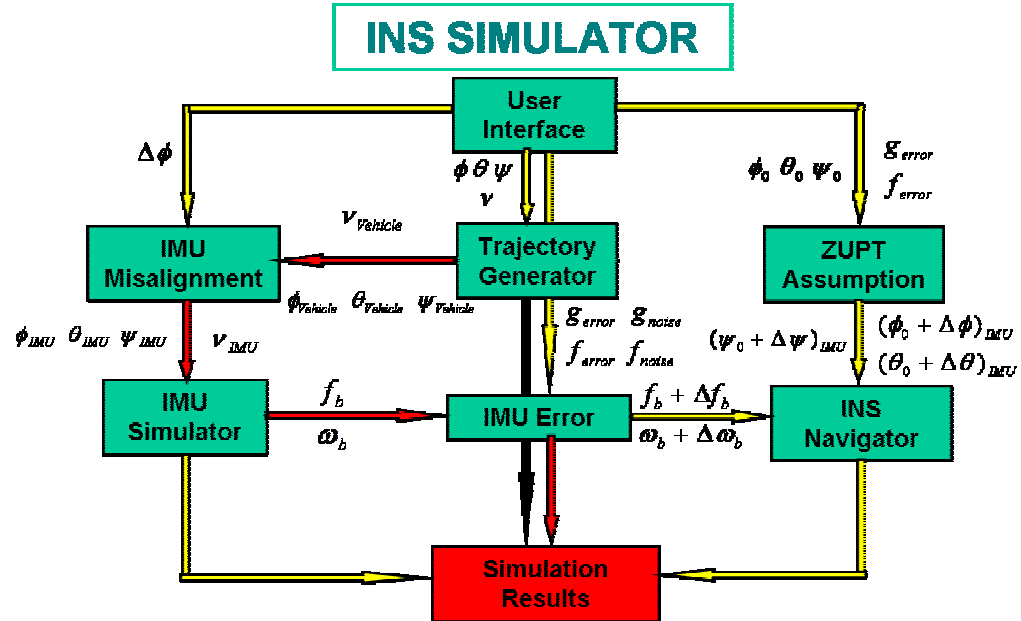


Figure F. 3 Sample Test of the INS Simulator

F.3 How to use INS_Sim to simulate a live INS

This section outlines what is contained in input option in MATLABTM command window and how to run INS_Sim program.

F.3.1 Run INS_Sim

- 1) Step one: In command window of MATLABTM, input

`K >> Auto_Run`

to run INS_Sim, as shown in Figure F. 4.

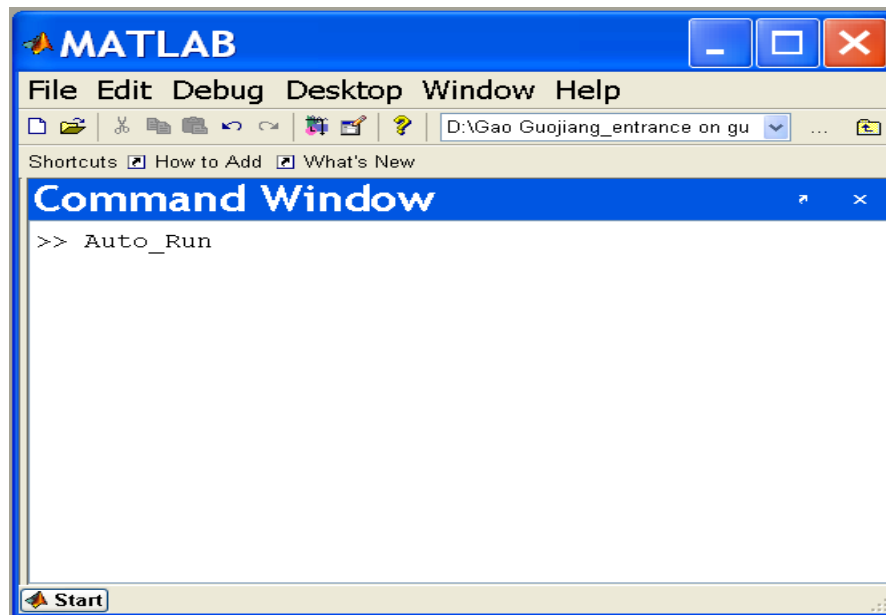


Figure F. 4 How to Start the INS Simulator

- 2) Step two: After the INS simulator runs, the user interface of INS Simulator will appear as Figure F. 5. Input vehicle trajectory parameters and IMU parameters for the deigned simulation through the INS simulator interface. Push on the “simulate” button to continue the simulation.

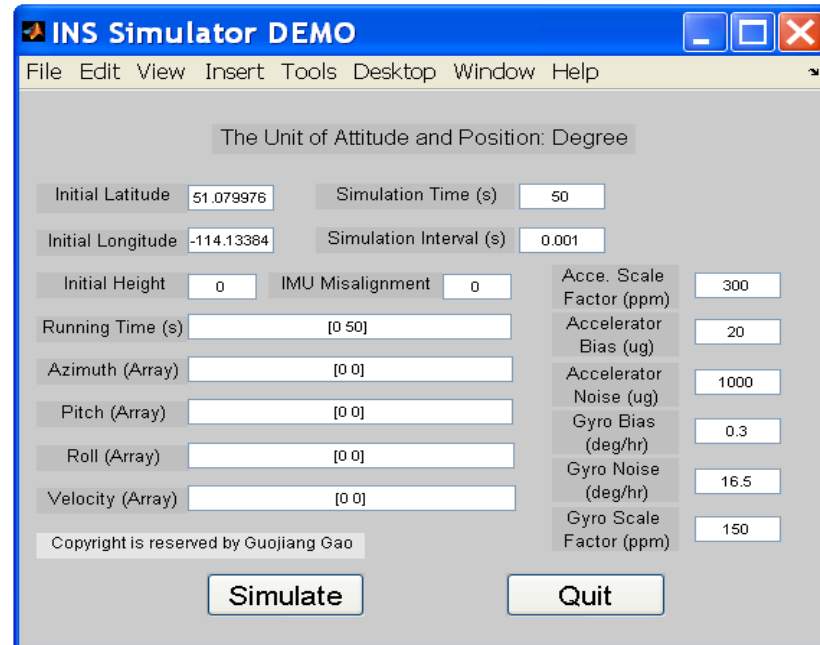


Figure F. 5 INS Simulator Interface

- 3) Step three: Follow the simulator wizard to finish the simulation, as shown in Figure F. 6 and Figure F. 7. Choose “YES” and “OK” in Figure F. 6 and Figure F. 7, respectively.
- 4) Step Four: all simulation results are presented in ten figures, as shown in Figure F. 8.

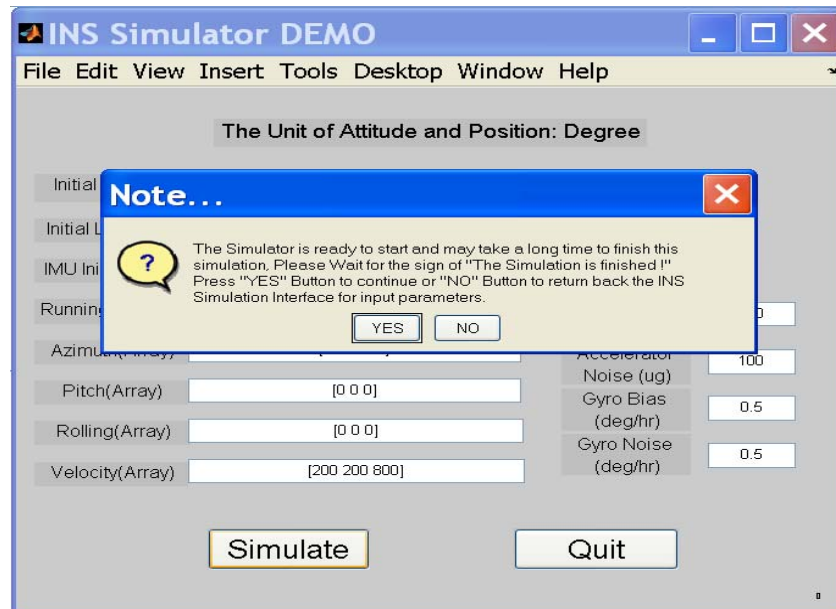


Figure F. 6 Sign one of the wizards

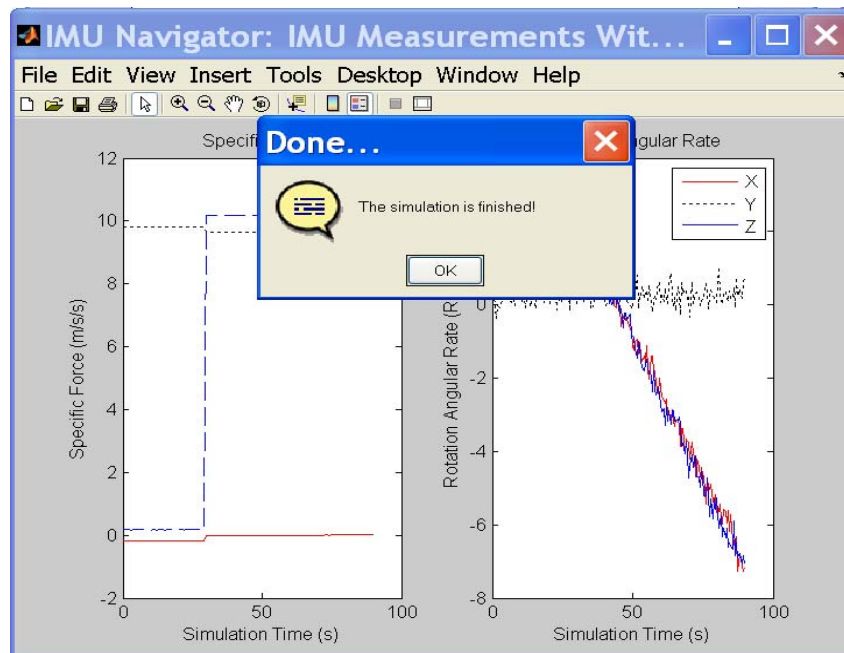


Figure F. 7 Sign two of the wizards

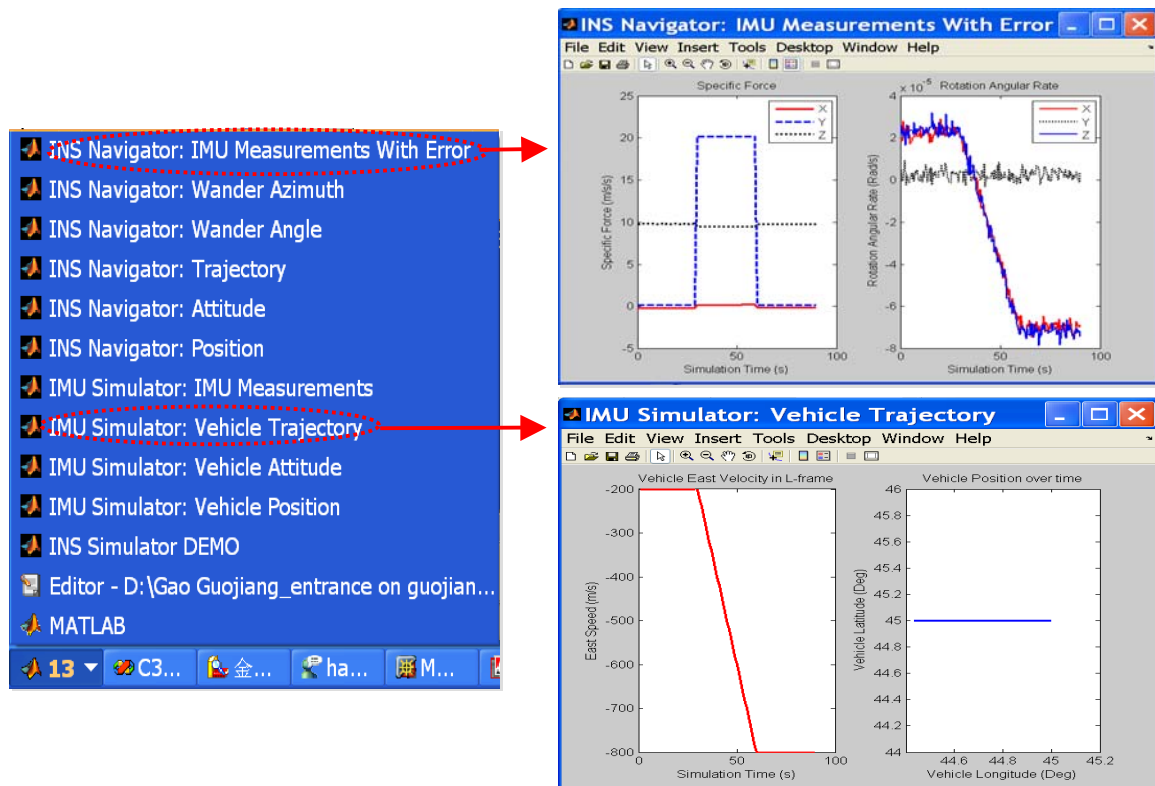


Figure F. 8 Simulation Results Available in an INS Simulator (INS_Sim)

F.3.2 On-line Help

In command window of MATLAB, input the name of the function you are interested in after HELP command, such as

```
K >> help INS_Navigator
```

the on-line help document is shown in MATLABTM command window, as shown in

Figure F. 9.

Command Window

```
>> help INS_Navigator
function[data,pusai,vt,fi,sita,gama]=INS_Navigator(f,wib,pusai0,data0,v0,fi0,sita0,gama0,tt,tmax)
-----
programed by:
    Mr. Guojiang Gao

Copyright is preserved by:
    Mr. Guojiang Gao and Plan group of Geomatics Eng. of UofC

Version: 1.0

Last Revised Date: June 1, 2005
-----

Name: INS Navigator

Task:
    By applying INS mechanization equations in azimuth wander frame, this function calculates the position
    of the vehicle with IMU outputs being the observations of Gyros and Accelerators.

The Input:
    f: Specific force in body frame over simulation time with sampling interval tt (unit: m/s/s)
    wib: Rotation angular Rate in body frame over simulation time with sampling interval tt (unit: Deg/s)
    pusai0/data0: Initial Vehicle Latitude/Longitude (unit: Degree)
    v0: Initial Vehicle Velocity in local-level frame (E-N-U frame, unit: m/s)
    fi0/sita0/gama0: Initial Vehicle Azimuth/Pitch/Rolling in local-level frame(E-N-U frame, unit: Degree)
    tt: the Simulation Interval (Unit: s)
    tmax: the Simulation Time (Unit: s)

The Output:
    data/pusai: Vehicle Longitude/Latitude over simulation time with sampling interval tt (Unit: degree)
    vt: Vehicle Velocity in local-level frame (E-N-U frame) over simulation time with sampling interval tt
    fi/sita/gama: Vehicle Azimuth/Pitch/Rolling in local-level frame(E-N-U frame, unit: Degree)over simulat
        time with sampling interval tt (unit: Deg)
    Figures: Some other simulation results are shown in given figures.
```

Figure F. 9 On-Line Help Document